The power stroke driven muscle contraction

Raman Sheshka

Thèse de doctorat de l'École Polytechnique

Spécialité : Mécanique

présentée par

Raman Sheshka

The power stroke driven muscle contraction

dirigée par **Lev Truskinovsky**

préparée

au Laboratoire de Mécanique des Solides (CNRS UMR 7649)

Soutenue publiquement le 21 Septembre 2012 devant le jury composé de

Abdul Barakat	Examinateur
Dominique Chapelle	Président
Tony Lelièvre	Rapporteur
Patrick Le Tallec	Examinateur
Pascal Martin	Rapporteur
Massimo Reconditi	Examinateur
Lev Truskinovsky	Directeur de thèse

Felix qui potuit rerum cognoscere causas

Remerciements

J'adresse me remerciements au Laboratoire de Mécanique des Solides ($UMR-7649$) pour m'avoir accueilli et particulièrement à son directeur Patrick Le Tallec, sans lequel ma dernière année de thèse n'aurait pas été tout simplement possible. Je voudrais adresser mes remerciements à l'École doctorale de l'École Polytechnique où j'ai effectué cette thèse sous d'excellentes conditions.

Je remercie chaleureusement mon directeur de thèse Lev Truskinovsky de m'avoir accompagné et m'avoir guidé durant ces années qui m'ont permis de poser mes premiers pas dans le domaine de la recherche scientifique. Je tiens à exprimer toute ma gratitude pour le constant partage de connaissances, son aimabilité et pour sa disponibilité et sa présence. Son apport scientifique m'a permis d'approfondir mes recherches et de m'améliorer en tant que personne. Je tiens également à remercier Jean-Marc Allain pour ses conseils précieux apportés á ce projet.

Le passage vers la recherche et la science en géneral aurait été impossible sans Pawel Pieranski dont la rencontre m'a fortement influencé. Je le remercie pour les nombreuses matinées passées ensemble durant l'étè 2007, et pour les connaissances variées qu'il m'a apporté.

Je remercie Pascal Martin pour le partage de sa grande connaissance dans le domaine des moteurs molléculaires et d'avoir accepté d'évaluer ce travail. Je souhaite également remercier Tony Lelièvre pour les longues heures qu'il a consacré et qui ont fortement contribué au bon déroulement de toutes mes simulations numériques. Un grand merci à vous deux pour le temps consacré à examiner ce travail. J'espère que nos conversations contribueront à un projet commun future.

Toutes mes sincères considérations à Dominique Chapelle, Abdul Barakat qui m'ont fait l'honneur de participer au jury. Je remercie aussi Massimo Reconditi d'avoir accepté de représenter l'équipe de Vincenzo Lombardi du Laboratoire de Physiologie de Florence. Les discussions sur le thème de la contraction musculaire ont eu un important impact sur le dévellopement des idées presentées dans ce travail.

A mes très estimés collègues de thèse, Matthieu Caruel et Pierre Recho. Je tiens à dire toute ma reconnaissance pour leur amitié et leur aide très stimulantes. J'espère que notre amitié et nos collaborations se poursuivront. Aussi je tiens à remercier mon collègue de bureau Paul pour nos pauses café. Et bien sûr je n'oublie pas LMS jazz band: Merci donc à Eva, Nicolas, Mathieu, Marc, Anders, Gérard, Matthieu, Gauthier et Camille. Je tiens également à remercier tous les thésards du LMS.

A toute l'équipe du LMS et en particulier Alexandra, Christiane et Christian j'adresse un grand Merci pour leurs compétences et leur soutien dans les diverses démarches administratives et les soucis informatiques.

Enfin, Je remercie ma famille pour leur soutien moral, leur encouragement et leur confiance ainsi qu'à mes amis et à mes proches et une très tendre Merci à Ghalia pour sa présence et d'avoir me supporter.

Contents

Introduction

Molecular motors perform various functions in life related processes: from cell division and eukariotic organelle transport to breathing and organismic motility. In this Thesis, we are focusing on the mechanical functioning of one of such motors, myosin II, responsible for active force generation in skeletal muscles.

The semi-phenomenological chemo-mechanical models of muscle contraction operate with kinetic constants depending on the elongation of an embedded spring, which allows the authors of these models to involve ad hoc fitting functions into their models. In an attempt to avoid this ambiguity we are proposing a set of models of a 'first principles' type where all constitutive elements are mechanical and can be in principle reproduced in a lab, perhaps at a larger scale than in reality. In this desire to understand the phenomenon of muscle contraction at a mechanical level we follow the approach developed by the Brownian ratchets community which replaced the conventional chemistry-based interpretation of active force generation (initiated by A. Huxley) by a study of Langevin dynamics of mechanical systems with well defined energy landscapes. In the classical theory of Brownian ratchets the motor is usually a system with one degree of freedom. In our PhD work we systematically study a slightly more complex mechanical system with two degrees of freedom. Bringing in an additional degree of freedom allows us to avoid the more conventional stimulation of myosin motors through actin fibers (rocking and fleshing ratchets) and instead concentrate on the ATP driven activity inside a single myosin head.

We recall that molecular motors convert chemical energy into mechanical work by catalyzing the hydrolysis of adenosin triphosphate (ATP) to the adenosine di-phosphate, freeing phosphate and using the released energy for generating motion against viscous forces and pulling cargos. Our main assumption is that the fundamental mechanism of chemo-mechanical transduction behind active force generation is basically the same in all molecular motors (myosins, kynesins, dyneines, etc.) and therefore while addressing specifically myosin II we obtain rather general results. To unify processive and nonprocessive motors, we focus on the role of the conformational change known as power stroke in the functioning of myosin II. Our interactions with V. Lombardi and other physiologists convinced us that the modeling of muscle contractions should be centered not around attachment-detachment as in the case of the existing motor models but on the power stroke which is usually neglected or under-represented in the ratchet based mechanical models.

By emphasizing the active role of the power stroke we are therefore building a bridge between processive and nonprocessive motors. Thus, in the current models the former are driven exclusively by the power stroke while the latter exclusively by attachment-detachment. In this Thesis we present first examples of a nonprocessive motors driven exclusively by the power stroke and exploiting the well known phenomenon of stochastic resonance. While we deal only with one cross bridge and neglect collective effects, our 'single-legged' nonprocessive motor has two degrees of freedom and therefore advances in

a way very similar to the 'double-legged' prosessive motor. This idea appears to be new in the field of muscle mechanics.

Despite the fact that Brownian motors can operate without the power stroke mechanism, most biologists perceive the power stroke as the major player in active force generation. Thus, according to the commonly accepted biochemical scheme, the myosin motors go through four steps of the Lymn-Taylor cycle while pulling actin filaments and producing a macroscopic force. Power stroke is involved in two out of the four stages of the Lymn-Taylor cycle so that both the biochemistry and the energetics of the cycle essentially depend on the power stroke related reactions. The mechanical role of the different stages in the Lymn-Taylor cycle is still poorly understood, in particular, the relative role of the power stroke in the activity of molecular motors has been ambiguous. In this Thesis we construct a simple purely mechanical model of the Lymn-Taylor cycle and identify the role of the power stroke as the main driver of contractility. The proposed perspective is different from most existing approaches where the power stroke is largely viewed as a mechanism of fast force recovery which does not require external fueling; at larger time scales, when ATP hydrolysis becomes crucial, the power stroke has been also perceived as playing only a secondary role. We question these basic tenets of the conventional mechanical models and assign to the power stroke the main role in both the force generation and the relative sliding of the actin and myosin filaments.

In our approach we abandon the phenomenological path of chemo-mechanical models and build the model of muscle contraction on the idea of continuous stochastic dynamics in multi-dimensional configuration space. The main outcome of our model is an interpretation of the power stoke as an element consuming the energy of ATP hydrolysis and playing active rather than passive role in force generation. We prescribe the energy landscape and represent the ATP activity by a correlated component of the external noise. The ensuing mechanical system can rectify random noise and produce mechanical work. We then study the average behavior of various arrangements of the power stroke (bi-stable potential) and the attachment/detachment element (periodic potential). To this end we either use direct simulations of the Langevin's system or compute the stationary probability distribution from the corresponding Fokker-Planck equations. We identify averaged trajectories with different stages of the Lymn-Taylor cycle and establish the energy balance by specifying consumed energy and produced mechanical work. We also study the efficiency of different proposed mechanical arrangements and show how it varies with the applied loading.

The attribution of active role to the power stroke reflects the biological reality imprinted in the Lymn-Taylor cycle. The appreciation of this fact allows one to unify the description of the power stroke and the process of attachment /detachment into a single mechanical framework. To find the optimal interplay between these two subsystems we study different arrangements of the power stroke and the attachment /detachment elements in the common framework of a stochastic model with coupled bi-stable and periodic potentials. We propose three main modeling archetypes with motor driven contraction, power stroke driven contraction and the synthetic model where power stroke not only drives the process but also controls the attachment/detachment mechanism. We show that all these mechanisms can partially reproduce the Lymn-Taylor cycle and we compare their mechanical efficiency. Finally we develop a synthetic model where the strength of the attachment/detachment mechanism depends on the state of the power stroke element. We show that such model reproduces all four stages of the Lymn-Taylor cycle if the coupling is hysteretic.

In this Thesis because of time limitations we could not make our model fully quantitative and did not attempt to match specific dependencies observed in experiment. Instead,

we focused exclusively on the development of a prototypical model reproducing all four stages of the Lymn Taylor cycle. It is important to remember that previous mechanical models could reproduce only two stages assuming that the other two stages are blended into the picture implicitly. In this sense we were able to reproduce the qualitative experimental picture more thoroughly than before. To match the observations quantitatively, one needs to consider a collective action of many units of the type proposed in this Thesis, which is the task we would like to pursue in the future.

In conclusion we mention that perhaps the most important new step in this work is the creation of a conceptual bridge between the processive molecular motors and the non-processive molecular motors. By associating the active role to the power stroke we can now apply the same modeling framework equally successfully for the description of a single kinesin motor and for the modeling of a large set of collectively operating myosin motors.

Chapter 1

Biological background

Before addressing the issue of mechanical modeling of molecular motors it is natural to discuss the biological side of the problem. In this section we present several examples of molecular motors which differ in both structure and function. We understand a motor as a device designed to convert non-mechanical energy into mechanical motion and to produce active force in static conditions. In the conventional internal combustion engines the fuel is burned and the mechanical power is generated by hot gases. Most of the molecular motors convert the chemical energy stored in adenosine triphosphate (ATP, or other nucleotide-triphosphate) into mechanical energy by activating large rotations inside protein molecules. In this way these nano-machines transform or transduce the input energy (chemical) into the output energy (mechanical). In view of the small scale of the protein molecules such engines are subjected to external thermal fluctuation that they cannot ignore and must instead rectify and harvest. This dependence of the operation cycle on fluctuations make molecular motors very different from the analogous macroscopic devices.

1.1 Main types of unidirectional motor proteins

Inside living cells one finds are large variety of motor proteins, each one playing a particular role in the cell's organization and functioning. All of them have the ability to transform a chemical energy into a mechanical motion. Different motors are responsible for different processes: from cell division and eukariotic organelle transport to cytoskeleton remodeling and muscle activity. Some molecular motors perform unidirectional motion and others are able to induce rotational motion. In this Thesis we limit our attention to unidirectional motors. Inside a cell a network of polar protein filaments plays the role of natural rails for the motion of unidirectional molecular motors.

Myosin, kinesin, dynein are the most important biological prototypes of unidirectional motors moving along specific tracks. The motors interact with the tracks through the heads known also as active motor domains. The protein motors are stereospecific and the biochemical composition of the motor domain depends on the nature of the rails. Thus, myosins moves along actin filaments in both directions, while kinesins and dyneins move along microtubules in different directions with kinesins moving toward the plus end and dyneins–toward a minus end.

Linear motors of this type can be classified into two groups by using the concept of the duty ratio: the fraction of time that each motors spends in the attached phase to the total time of a cyclic step. Suppose that during each cycle a molecular motor spends time

τ_{on} in the attached state where the conformation change leading to force generation takes place, and time τ_{off} while being detached from the filament, where the motor returns to its initial conformation, recharges the force generating mechanism and prepares for the next cycle. The duty ratio δ is then defined by the formula

$$\delta = \frac{\tau_{on}}{\tau_{on} + \tau_{off}}. \tag{1.1}$$

Motors with low duty ratio spend most of their enzymatic cycle in the detached state and are called nonprocessive motors. Nonprocessive motors are designed to act in a collective fashion. Motors with high duty ratio usually have the dimeric form with two legs/hands and move by shifting one leg/hand over the other. They perform a processive motion and are designed to act individually.

Kinesin is a standard example of a processive motor which moves continuously along the microtubule surface while performing hundreds of unitary steps. In contrast myosin II is a nonprocessive motor which is able to perform only a few unitary steps. Some myosins are however processive, for instance, myosin V, see [124, 11]. As in the case of myosin's family, some dyneins are processive and some are nonprocessive. Independently of the nature of the motor, its speed is about few nanometers per millisecond and the generated force is about few pikonewtons [42].

The main topic of this Thesis is myosin/actin interaction performed by nonprocessive motors. However, as we are planning to link different families of motor proteins we begin with a short description of kinesin which is a typical processive motor.

1.2 Kinesin

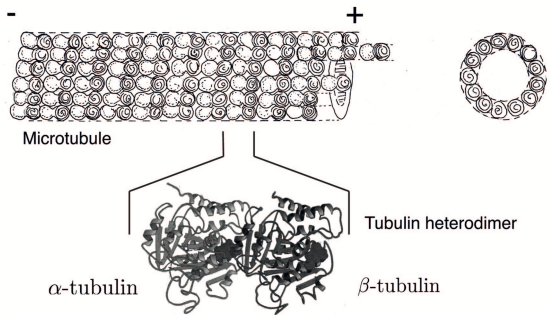

Figure 1.1. The schematic structure of one microtubule. Adapted from Alberts[4]

The microtubules, the natural tracks for the motion of kinesins, have a helical cylindrical structure with diameter $\approx 30nm$. The walls of the microtubule cylinder are made of $\approx$ 13 protofilaments which are in turn formed by dimers linked head-to-tail. These dimers are tubulin proteins composed of two similar subunits α-tubulin and β-tubulin. The microtubule, as well as actin filaments, are polar with all asymmetrical subunits of protofilaments oriented in the same direction. In most of the cells, microtubules are oriented with their minus ends towards the centrosome and their plus ends towards the cell periphery.

Kinesin was discovered during 1980's [115] and its structure is similar to that of myosin II. Most of the members of the kinesin family are dimetric molecules with two globular motor domains, a tail and a stalk, see Fig.1.2. The globular head is formed by two

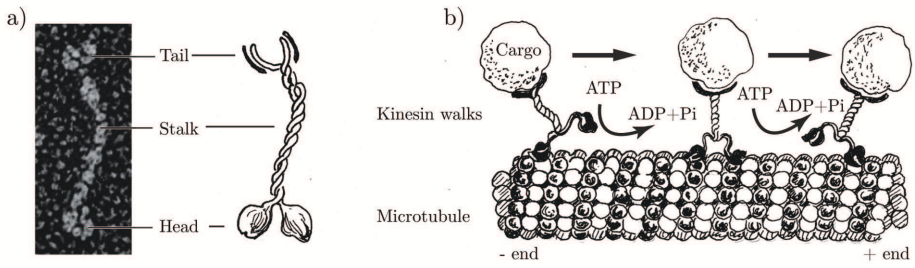

Figure 1.2. a) Schematic representation of the architecture of kinesin structure. b) The sketch of principals walk steps of kinesin along the microtubule in mechanochemical cycle. Adapted from http://www.uic.edu/classes/bios/bios100/summer2006/kinesin.jpg

heavy chains and two light chains; the tail may also include light chains and different tail configurations are specific for different transport functions [26, 27].

A significant difference between the conventional kinesin and the conventional myosin resides in the fact that the two kinesin motor domains work in the coordinated manner [132]. The mechanical and chemical cycles are coupled and both kinesin heads hydrolyse ATP (adenosine triphosphate) into ADP (adenosine diphosphate) and Pi (free phosphate). More precisely, the detachments from a microtubule require the hydrolysis of ATP, after a quick release of Pi, the attachment of one head is catalysed by the release the ADP. When one head in the dimer is attached to the microtubule (lead head), the other head (trailing) moves a distance of $16nm$ and binds the next open beta tubulin, so the center of mass of the dimeric kinesin moves through $8nm$. Once bound, the trailing head becomes the lead head and the process repeats. The correlated functioning of both heads distinguishes kinesin from myosin II where one of the heads appear to be always passive at least in the contraction phase of muscle activity. The particularity of kinesin family is in the fact that one kinesin moves to minus end of the microtubule and another one moves toward its plus end [35].

We now describe the kinesin cycle in more detail. Suppose that one head is attached to the microtubule and is without nucleotides while the detached head carries the products of the ATP hydrolysis. Then the bounding of ATP to the attached head catalyses the attachment of the trailing head and the release of bounded ADP. The release of ADP in turn catalyses the detachment of the first attached head, which hydrolyses the ATP into ADP and Pi. The unbounded head releases quickly the Pi.

The development of different single-molecule techniques offered an opportunity of direct characterisation of single processive motors in terms of force-velocity relations. The measured stall force for a kinesin motor is in the interval $4 - 8\ pN$; the maximal velocity is 800 nm/s, Fig.1.3. The efficiency of energy transduction by kinesin can reach $\approx 50\%$, estimated as $W_{mec}/\Delta G$, where W_{mec} is a mechanical work and ΔG is the chemical energy of the ATP hydrolysis.

We now turn to the main subject of the Thesis, the acto-myosin system.

1.3 Acto-myosin complex

1.3.1 Actin

Actin filaments (F-actin) play the fundamental role in muscle contraction and cell motility, moreover actin is one of the most present protein in the eukaryotic cells. Actin filaments

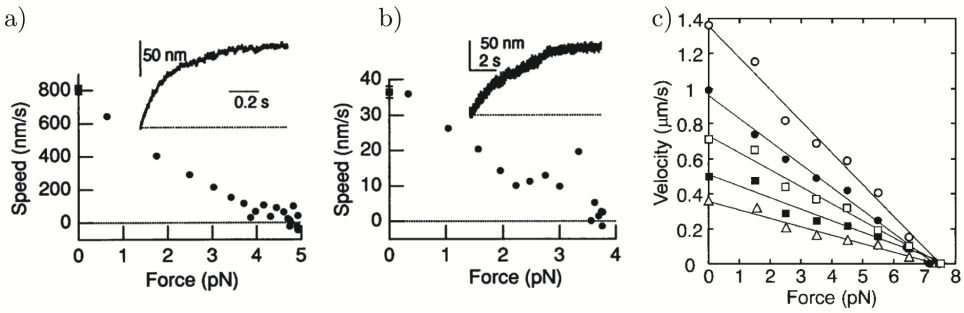

Figure 1.3. Force-velocity curves for kinesin. The speed as a function of load force, the dependence for the high ATP concentration a) and for the low ATP concentration b), the data provided by Meyhöfer and Howard. Adapted from [80]. c) Temperature dependence of force-velocity relation provided by Kawaguchi and Ishiwata. From bottom to top, open triangles, $15°C$; closed squares, $20°C$; open squares, $25°C$; closed circles, $30°C$; open circles, $35°C$. Adapted from [58].

are formed by polymerisation of monomers and this process is governed by ATP hydrolysis. Actin monomer protein is a globular molecule with weight of $\approx 43kDa$ (G-actin). The actin monomer is an asymmetric molecule which contains four subdomains and a binding site for ATP. Both F-actin monomer and G-actin are built from two similar parts. The resolved model of tertiary and quaternary structure based on X-ray fibre diffraction indicates the structural transition between two forms. This transition alternates the internal structure of G-actin during the polymerisation in filaments, transforming it into the monomers of F-actin[38, 84].

Because of the asymmetry of the monomers the actin polymer is polar. An actin filament formed by two parallel protofilaments oriented in the same direction. The filament can be described in a simplified way as a double helix with 13 monomers in 6 left-handed turns every $36nm$, Fig.1.4. The rise per subunit is $2.76nm$. Along morphological helices the actin monomers are spaced by $5.5nm$. As a consequence of polarity, the rate of elongation of the two ends of one filament are different. We call the "barbed end", the end where the elongation rate is faster and we call the "pointed end", where the elongation rate is slower. The two ends of a an actin filament have different affinities to the attachment of new components [15]. The essential role of actin filaments is to provide the binding sites for myosin heads. In skeletal sarcomere the actin filaments carry also other proteins that regulate the contraction. For example the attached tropomyosin troponin complex, Fig.1.4d), makes the actin/myosin interaction dependent on calcium concentration, [36].

1.3.2 Myosin

There is about 17 different classes of myosins [1]. Probably the most studied is the first discovered myosin II, myosin I and myosin V. All myosins except Myosin VI move toward the plus end of an actin filament.

The principal lines of the structure are the same in all myosins [102] and the study of the conventional myosin, myosin II, offers a good idea of the whole family. Myosin II is a very large protein. Its molecular weight is approximately $520kD$. The myosin consists of six polypeptides: two $220kD$ heavy chains and two pairs of $20kD$ light chains(essential light

[1]Information about different myosin classes and their role in activity of living systems can be found on:http://www.mrc-lmb.cam.ac.uk/myosin/Review/Reviewframeset.html

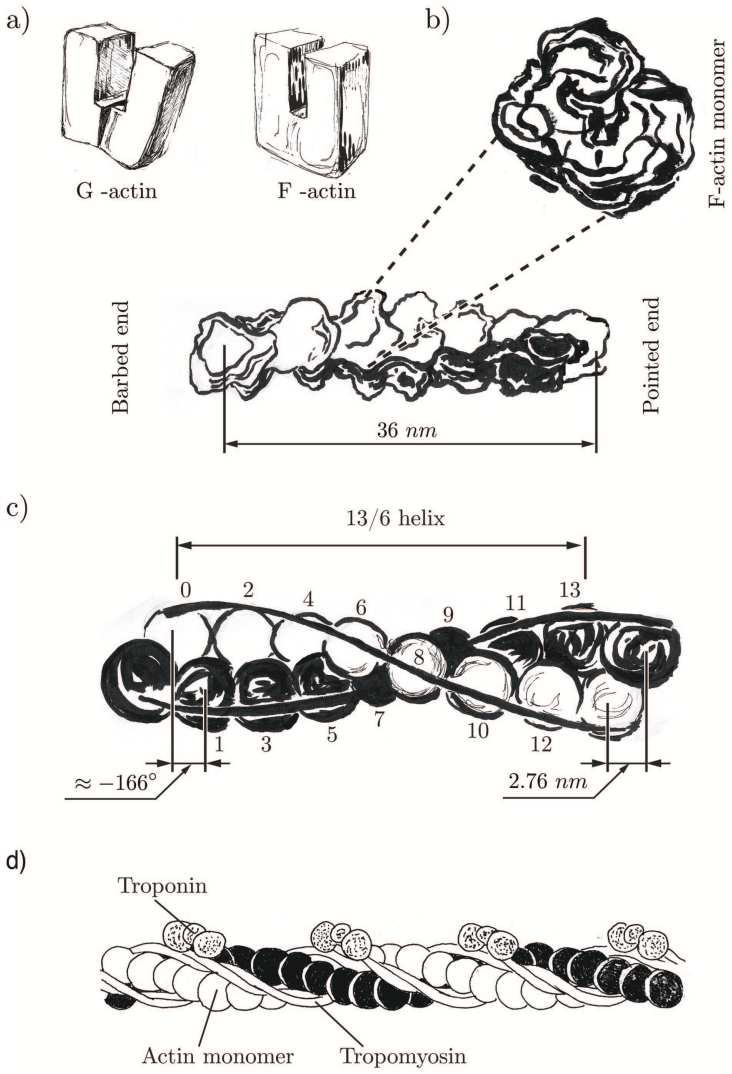

Figure 1.4. The structural basis of actin filament. Not drown at scale, the pictures based on research work of K.C.Holmes and T.Oda. a) The essential principle of the G-actin to F-actin transition is more flat configuration of the actin monomer in filament by a twist of two molecule domains. b) Sketch of a fundamental repeat of actin filament composed by F-monomers. c) The schematic representation of geometrical structure of actin helix. d) An actin double helix structure with bounded tropomyosin and troponin.

chain (ELC) and regulatory light chain (LCR)). The molecule is highly asymmetric. The heavy chains form two identical globular amino-terminal myosin heads. The intertwined α-helical carboxyl-terminal tails form the left-handed coil which is approximately $2nm$ in diameter and is $150nm$ long. The myosin heads are ATP active being the catalytic domains of the motor. The myosin cross-bridge may be decomposed in two parts: the heavy meromyosin HMM and the light meromyosin LMM, Fig.1.5. The HMM may be further decomposed into two fragments, the first one $S1$ ($\approx 120kD$) contains tree polypeptide chains, the second one, $S2$, is ATP inactive and is unable to interact with actin filaments.

The $S1$ fragment is the fully operational ATPase motor element and it is often used in the in vitro assays as a substitution for the full cross-bridge. It is also a basic unit for the X-ray diffraction study of the myosin motor head structure. Schematically, the myosin

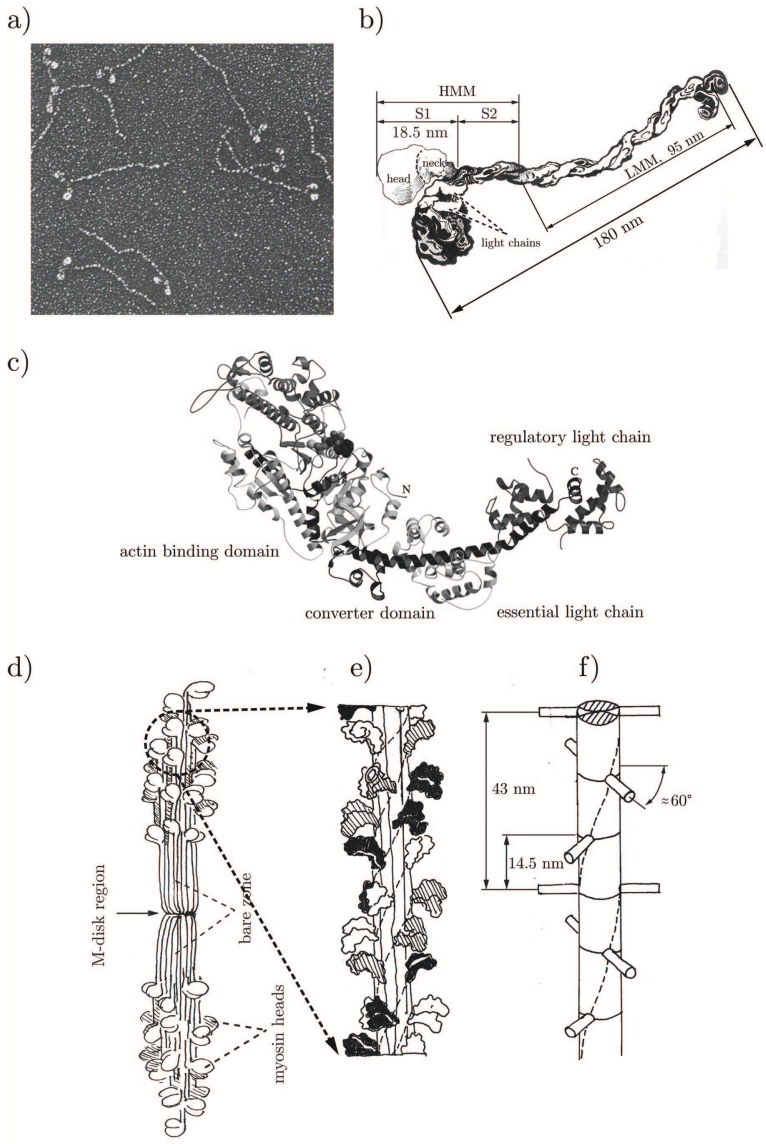

Figure 1.5. a) The electron micrograph two-headed myosin molecules with long tail. Adapted from [7]. b) Sketch of myosin protein structure. Not drown to scale. The myosin molecule can be cut in the short domain where α-helix is interrupted into several fragments: HMM which can be separate into S1-heads, S2-short part of tail and LMM- rest part of tail. c) The myosin molecule $S1$ from chicken skeletal muscle, [94]. The myosin $S1$ has an elongated head consisting of a 7-stranded β-sheet and a C-terminal tail or "neck" which carries two calmodulin-like (calmodulin is a calcium-binding protein) light chains: the regulatory light chain and the essential light chain. The motor head $50kDa$ fragment spans two domains: $50kDa$ upper domain and the $50kDa$ lower domain or an actin binding domain, which $S1$ head binds to actin monomer. The actin-binding domain has been colored grey. Reproduced from [39]. d)-e) The structure of myosin heads arrangement of the myosin filament, the three helices of myosin heads labeled : black, white and dashed. f) Scheme of one coaxial helix has with subunit translation about $14.3 - 14.5nm$ and unit repeat $42.9nm$, adapted from [106]. filament.

head, has an ATP binding pocket (formed by a particular helix of one of the light chains) and an actin binding interface, see Fig.1.5c). The head is linked to the neck region by a

"converter" domain which plays the role of "lever-arm", [93, 41]. Multiple crystallographic studies [93, 94, 37, 39, 40, 24] suggest that in the head of the myosin which is attached to actin, the binding of ATP molecule induces changes in the catalytic domain. These changes are transmitted to the lever-arm domain and cause an angular rotation of the lever-arm relative to the head (power stroke).

It's important to note that the core motor structure of the myosin is similar to the that of the kinesin. In fact, a common ATP dependent conformational change mechanism is used to generate motion in these seemingly so different motor proteins [114].

The myosin II molecules self assemble in bipolar or side polar filaments organized at a larger scale. In muscle sarcomere, the myosin filaments form thick filaments. The thick filaments have a constant size, each backbone is formed by packaging of myosin proteins with the tails oriented toward the center and the heads oriented toward the periphery. This organization forms the central region free of myosin heads projections known as the bare zone in the middle of the myosin filament where passive cross-linking takes place. The electron microscopy studies and the X-ray diffraction methods show that in $3\mathbb{D}$ the structure of the myosins head projections have an helicoidal arrangement, Fig.1.5d)-f). The heads emerge from the filament backbone with a regular step of $14.5nm$ [106].

In the absence of ATP, the myosin and actin form a stable complex (rigor) which is also formed by sub-fragment of myosin HMM and $S1$. In the presence of ATP complex interaction of myosin and actin is observed. Thus in solution with added ion of K^+ or Mg^{2+} the ATP molecule forms a complex with myosin and after the hydrolysis, the products of the reaction ADP and Pi are released and the rigor complex dissociates. The dissociation leads to a step-like motion of the myosin head along the actin filament. The interaction has a cyclic character which we discuss in more detail in the next section. The ATP activity in acto-myosin system is regulated by binding of the calcium [29].

1.4 Lymn-Taylor cycle

The first description of the force-producing mechanism in skeletal muscles based on acto-myosin interaction was proposed in 1954 in the papers of A.F. Huxley [45] and H.E. Huxley [33]. Both papers elucidated the striated structure of muscle myofibrils and introduced the sliding filament hypothesis of muscle contraction. In [48] the idea was proposed that the force is generated by the configuration changes inside cross-bridges. It was also conjectured that the cross-bridge/actin angle changes as a result of the chemical hydrolysis of ATP. In 1971 R.W. Lymn and E.W. Taylor proposed a chemo-mechanical scheme which linked more specifically the conformational changes in the myosin head and the ATP splitting reaction [70]. The proposed reaction cycle with four distinct chemical states remains a reference in the field. More complex descriptions involving many more chemical states have been proposed and used by the biochemical community between 1971 and now by e.g. Bagshaw and Trentham [5], Taylor [110], Kawai and Halvorson [59], Ishijima et al.[50], Smith et al., 2008[103, 104] to mention just a few.

Despite all these developments it remains commonly accepted based on spectroscopic and cryo-electron microscopy studies of the myosin cross-bridge structure that a myosin head always binds the actin site in a fixed configuration and that the relative movement of the filaments is produced by the angle change inside the "lever-arm" part of the cross bridge. In this sense the simplest lever-arm hypotheses has a solid foundation. After the crystal structure of the myosin at the end of the power stroke was resolved [93] it also became clear that the main movement indeed arrives as a result of a power stroke. Smaller changes in intrinsic myosin cross-bridge structure and the induced changes in conformation of the

myosin neck region may be happening as well but they are strongly correlated with the main chemical states which Lymn and Taylor linked to the fundamental ATP hydrolysis cycle.

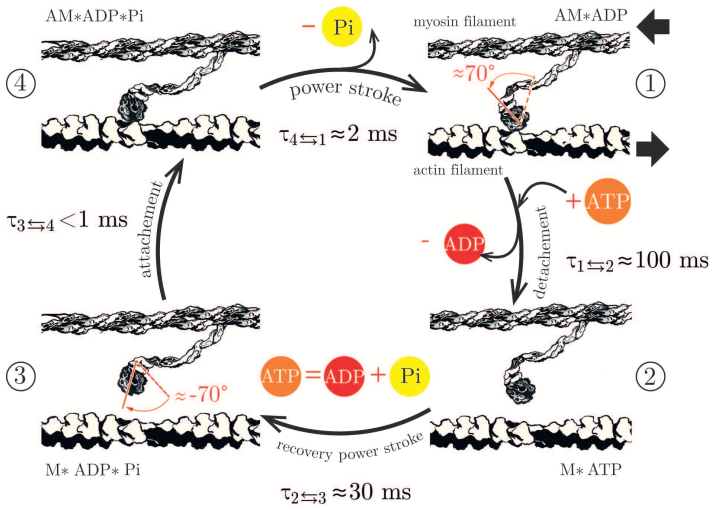

Figure 1.6. Representation of the Lymn-Taylor cycle.

The myosin ATP cycle can be viewed as a series of biochemical steps shown in Fig.1.6 and its mechanical interpretation is detailed below:

- ①→② In the absence of bounded nucleotide, the myosin head is strongly attached to actin. This is a rigor state or the post power stroke state. The ATP binding to active motor domain irreversibly dissociates the myosin cross-bridge from the actin filament forming the state known as $M * ATP$ with M as myosin.

- ②→③ The hydrolysis of ATP in the stable complex $ADP * Pi$ takes place next. This is relatively rapid reaction which lasts about few $msec$. The hydrolysis products, ADP and Pi, remain with myosin forming the complex $M * ADP * Pi$. During the ATP hydrolysis, the power stroke is recharged which requires energy of ultimately metabolic origin. This creates the pre power stroke state.

- ③→④ The affinity of myosin for actin depends on the bounded nucleotide in the ATPase pocket of the active domain and it is high in the pre power stroke state. The myosin head is reattached to the neighboring actin binding site, forming a new complex $AM * ADP * Pi$.

- ④→① The myosin-actin interaction in the attached state causes a change in the orientation of the neck region of the cross-bridge (the power stroke) which is accompanied by the dissociation of Pi from the complex $AM * ADP$. This conformational change stretches the elastic connection to the backbone, generating a force of a few pN, and advances the attached actin filament by $\approx 10nm$. Following such relative sliding of the filaments, ADP is released very quickly (within $2msec$) and is replaced within a $msec$ by the ATP. As the result the myosin head is dissociated again starting the next cycle.

In Fig.1.7 we show the crystal structures of myosin heads with bound nucleotides ATP and products ADP and Pi, which represents the states ④ and ①. This crystallographic

reconstruction illustrates the fact that the hydrolysis of ATP is indeed accompanied by a major conformational change (the power stroke).

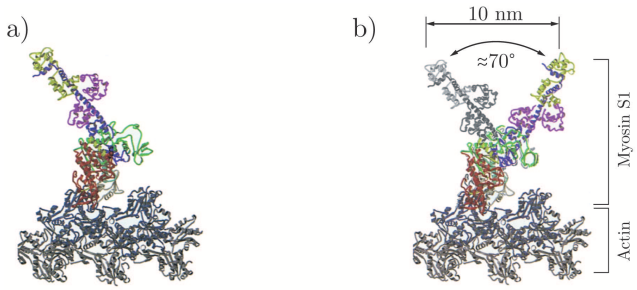

Figure 1.7. Power Stroke of Myosin $S1$. a) A model of the strongly bound $S1$ myosin in pre-power stroke configuration. b) The rigor state, the end of power stroke of $S1$ myosin. Upon binding to actin, the converter domain undergoes a conformational change, amplified by the lever arm that swings over 70° towards the Z-line. The rotation generate a linear displacement of $10nm$. Adapted from [24]

Experimental measurements show that different steps of the Lymn-Taylor cycle have different rates. The fastest steps of the cycle are the power stroke and the attachment process involving $M * ADP * Pi$. The typical time scale of the power stroke is about two milliseconds. The hydrolysis of ATP occurs on a much slower time scale in solution ($\approx 100ms$). These data must be interpreted with caution, because the time scales in a solution and in a fiber may be different. Thus in a solution, different molecular motors are not mechanically coupled to a loading device. Also, the presented cycle does not take into account the tree dimensional geometry of the system (steric effects). In solution, with a high concentration of actin, the attachment is a very fast step as soon as the myosin is in its hydrolyzed state $M*ADP*Pi$, in particular, the probability for the myosin to attach is sufficiently high. In the muscle, as the 'binding' cites on the actin filament are separated by a distance of $36nm$ [42], the hydrolyzed myosin heads may stay detached for a long time if there is no binding site near their location. The averaged attachment rate is then expected to be slower in the fiber than in a solution.

1.5 Single molecule experiments

In the previous section we presented a simple and commonly accepted chemo-mechanical interpretation of single working cycle of the acto-myosin system. Most of the data on myosin/actin interaction have been originally obtained from averaging the observations done on muscle fiber with a large number of cross bridges acting simultaneously. More recently, due to development of the techniques of single molecule manipulation, the direct measurements in vitro became possible by using microneedles, optical traps and optical sensors. Thus in the last decade the interaction of a single myosin molecule with actin filament have been characterized.

Single molecule experiments allow one to study individual ATPase of myosin motor domain [131, 130]. There are two typical experimental approaches in the single molecule measurements: the study of sliding actin filaments on the carpet of myosin sub-units and the measurement of steps of a single-myosin molecule 'walking' on the actin filament confined by laser traps, see Fig.1.8.

If we compare measurements in single molecule experiments with the data obtained on

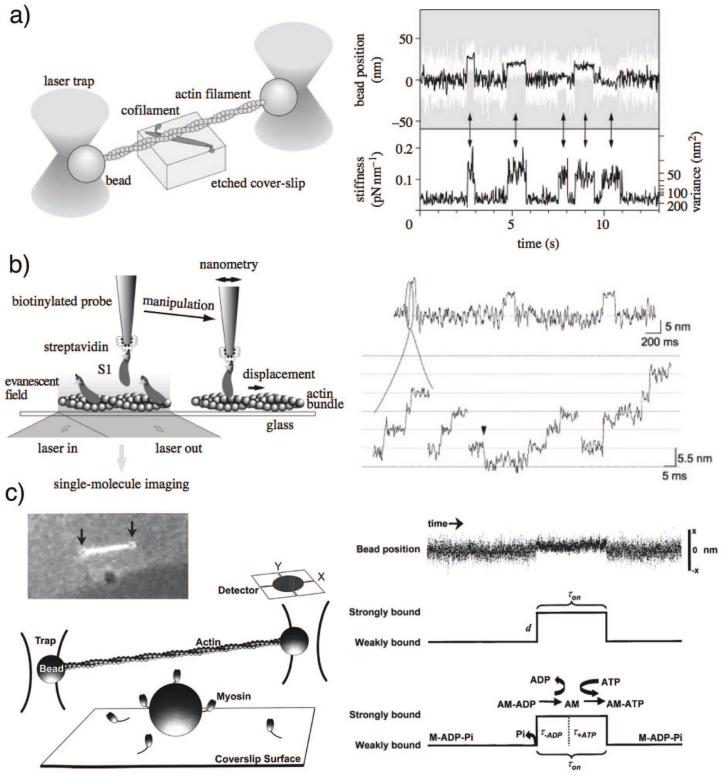

Figure 1.8. a) On the left, the scheme of the force measurement between single actin filaments and single myosin using laser trap. On the right, the time course of displacements by a single myosin molecule. White line represents raw data and black line represents the same data passed through a low pass filter of 20 Hz bandwidth. The changes in stiffness calculated from the variance of the displacement data as a monitor of the interaction of myosin with actin, adapted from [130]. b) Manipulation of single myosin molecules using a scanning probe and measurement of substeps of myosin. A technique developed by T.Yanagida group. On the right, we show the example of stepwise movements in the rising phase of the displacements. Some backward steps were observed as indicated by arrows. c) A schematic representation of most standard the three-bead optical trap assay. An actin filament is suspended between two refractile beads manipulated by independent optical traps. A third larger bead coated to surface and covered by myosin sub-fragments. Unitary events are recorded by photodetector, adapted from [113].

muscle fibers, we notice a large difference of reported values of the power stroke size. Thus, the power-stroke size inferred from muscle experiments is about $8-10nm$, while single molecule experiments suggest a $5-6nm$, which is close to the size of one actin monomer [82]. However some single molecule experiments produce values $> 10nm$,[129] which can be explained in part by the difficulty of such measurement and in part by geometrical arguments. In a single molecule in vitro measurements the movement of a myosin head is limited by a single actin protofilament and the fixation of the scanning support. Instead, in the sarcomere one myosin can interact with deferent actin filament because of $3\mathbb{D}$ nature of the actin myosin arrangement. Also in the muscle a large power stroke can be the consequence of a collective interaction of many attached cross-bridges [83, 113, 10].

Despite many single molecule experiments the intrinsic mechanism of step size of myosin motor power stroke during ATPase is not fully understood. Thus, Yanagida group reports that multiple step may be produced during each biochemical cycle (from one to five

steps for one ATP molecule), generating the displacements in the interval $5.3-30nm$. One interpretation of this result can be based on the idea of many rapid attachment/detachment cycles taking place in a diffusive mode. Or one can think that the power stroke takes place in multiple steps [61, 130]. An argument against single molecule experiments is that the orientation of the myosin motor cannot be controlled so it may attach in some sub-optimal way to the actin filament.

Finally in the Fig.1.9 we show some characteristic non-linear force-velocity curve obtained in the single molecule experiments. The conventional lever-arm theory predicts the characteristic shape of these curve which is a strong argument in favor of the simplest Lymn-Taylor type interpretation of the data.

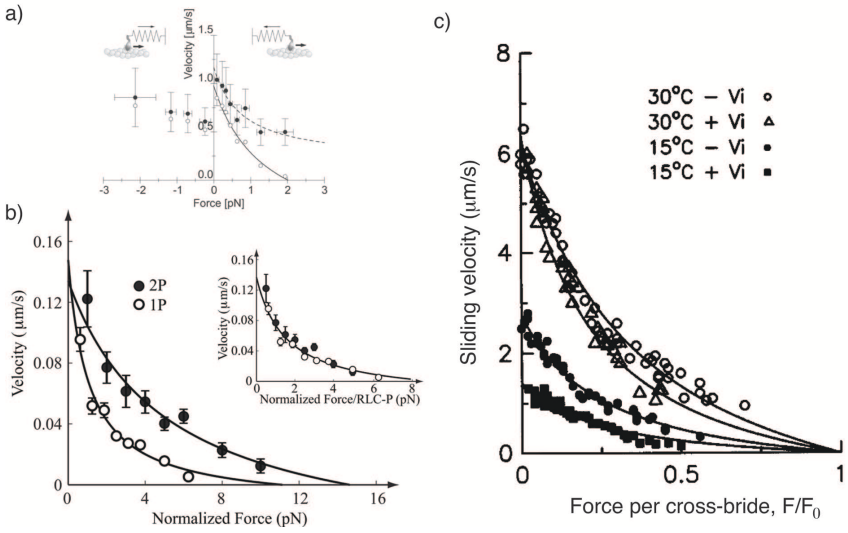

Figure 1.9. a) Force-velocity curve of individual S1 molecules. The velocity was obtained by dividing the step size, $5.5nm$, by the dwell time (filled circles). Bars indicate the standard deviations for $10-30$ steps. Open circles indicate the velocity corrected by the anisotropy of the stepping direction. The solid line shows the Hill's curve fitted to the corrected velocity. Adapted from [60]. b) The HMM-1P and -2P force-velocity relationships. The mechanical properties of an expressed heavy meromyosin (HMM) construct with only one of its RLCs phosphorylated (HMM-1P) and for fully phosphorylated myosin (HMM-2P). Adapted from [122]. c) Force-velocity curve for a myosin cross-bridge in rabbit psoas muscle, where orthovanadate, noted Vi, is analogue of free phosphate. Adapted from [87].

However from some contradictory observations, one can also conclude that the existing lever-arm theory is not sufficient to explain the actin/myosin interaction fully. Thus, a series of observations reported in [117, 99, 118] shows that the basic mechanism of force generation may be the same in all members of the myosin family due to the structure similarity of motor domains. Moreover, the authors argue that the results of their experimental observations could be interpreted as an evidence that the power stroke takes place in two steps. The duration of the first step depends on the amplitude of the load while the duration of the second step is affected only by the ATP concentration. The explanation of this observation in the framework of the lever-arm hypothesis is not easy.

The role played by the second head also remains a question. For instance in [112, 113] one can find the experimental force-displacement curves, which can be interpreted as a result of interaction between two heads. The authors offer two interpretation of their data: the successive attachment of two heads, one after on other very quickly, and production

by each head of $5nm$ independent displacement increments totaling $10nm$. The second explication agrees with [109] where the following scheme was proposed: the first head slides along the actin filament searching for the second head the optimal orientation in order produce the step of $10nm$. As a result, one head plays a passive role while the other head generates a full fledged power stroke. Interestingly, both explanations require simultaneous interaction of both motor heads with actin for a finite period of time. To our knowledge, there is no direct evidence of actin interaction with two-head myosin. Indirect evidence has been reported in [95] where the resolved X-ray interference data appear to be showing that both heads of one motor are strongly bound to the adjacent actin monomer. In view of uncertainty we account in our modeling for only one head and assume that all heads operate independently, [42].

Another issue that the classical interpretation neglects is that myosin heads interact with actin filaments stereo-specifically. Thus in [107] we find indications that a motor binds only to favorable oriented actin sites which explains that only 20% of myosin cross-bridges are bound in active muscle fiber.

1.6 Muscle contraction

As we have already mentioned, the issue of myosin II/actin interaction originally emerged from the study of muscle contraction. We recall that a skeletal muscle has a fibrous structure. The fibers, showing the striated structure, are very long multinucleate cells. In the heart striated muscles the cells are much shorter then in skeletal muscles and have a single nucleus. Smooth muscles , say visceral muscles, do not show striations at all.

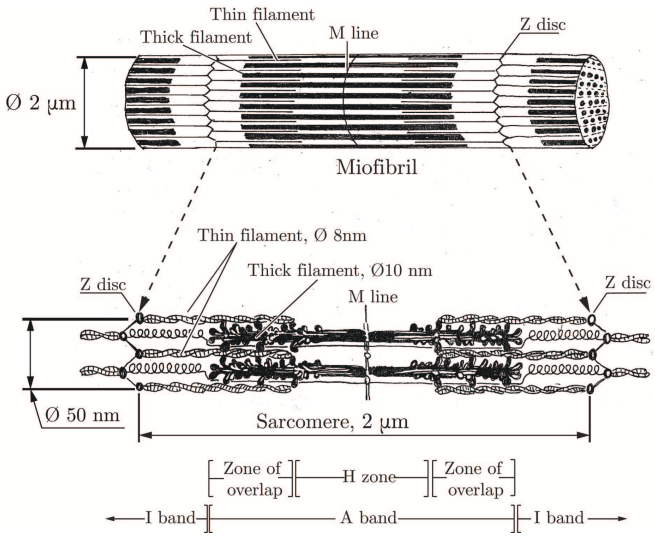

Figure 1.10. Schematic representation of a skeletal muscle sarcomere. Adapted from [111]

In skeletal muscles fibers are assembled in subunits known as myofibrils. Myofibrils have a cylindrical structure and are themselves cross-striated; the repeating contractile unit along their length is known as the muscle sarcomere, Fig.1.10. To describe fully muscle contraction we need to first study a single sarcomere [47]. Each sarcomere is located between two successive Z-discs. Large muscles are assemblies of millions of sarcomeres all working collectively in a correlated fashion.

Muscle sarcomere is a well ordered array of interacting filaments of myosin and actin. The actin filaments are oppositely oriented at the left and right sides of the sarcomere, the

plus ends are always oriented toward the Z-discs. The actin filaments interact with the myosins filaments. The shortening of a sarcomere takes place without change in length of neither actin nor myosin filaments, see Fig.1.11. The contraction is caused by sliding of myosin filaments along the actin tracks. It is a collective process with ($\approx$ 300) cross bridges active in every sarcomere [106]. Each sarcomere includes other proteins what we

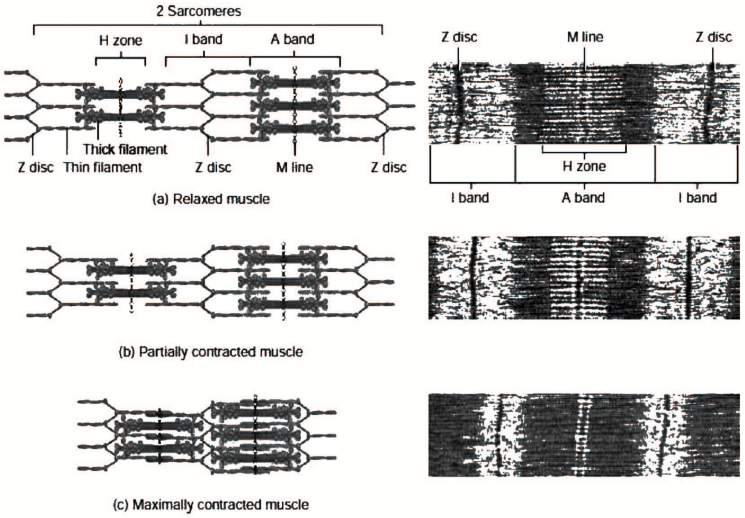

Figure 1.11. The scheme of sliding theory of muscle contraction at the scale of the sarcomere. On the left column: a cartoon representing the sliding of the filaments during contraction. On the left column: an electron micrograph of a contracting sarcomere. The width of the A band (dark) remains constant while the I band (white) shortens. Taken from [111].

did not mention yet but which play important role in regulating active force production: titin, tropomyosin, troponin, α-actin and $\beta - actinin$, M-protein, C-protein. The actual dynamic functioning of the chemo-mechanical regulation of myosin/actin interaction is a complex research field which is outside the scope of this manuscript.

In the cross-section sarcomere shows a hexagonal arrangements with the actin filaments at trigonal points of sub-lattice. The electron micrograph studies show two crystallographic arrangements of myosin filaments: the simple hexagonal lattice and the super hexagonal lattice, see the diagrammatic representation of the structure of striated muscle, showing overlapping arrays of actin-myosin containing filaments in Fig.1.12.

We now turn to different techniques of the mechanical characterization of a single muscle fiber. A stimulated muscle shortens and produces force. To study this force we can control the imposed force - then the contraction is called isotonic. Imposing different forces and measuring the speed of contraction we can obtain the force-velocity relation which one of the main characteristics of muscle contraction. The isometric force, measured in the hard loading device, varies with the imposed sarcomere length, Fig.1.13. Each point of the curve tension versus elongation corresponds to a tetanic stimulation at a given sarcomere length. The isometric force is directly linked to the degree of filaments overlap in each sarcomere. The maximal isometric tension is reached between point B and C, which is the main physiological range of the muscle. Such sarcomere length corresponds to the full overlap of the thin and thick filaments. At sarcomere length less than $2\mu m$, the ability of cross-bridges to develop tension decrease. When the sarcomere is too short,between D and E, the geometrical structure of the sarcomere is perturbed due to steric effects, (filament buckling, bad attachment conditions). At longer length, from B to A, the sarcomere length

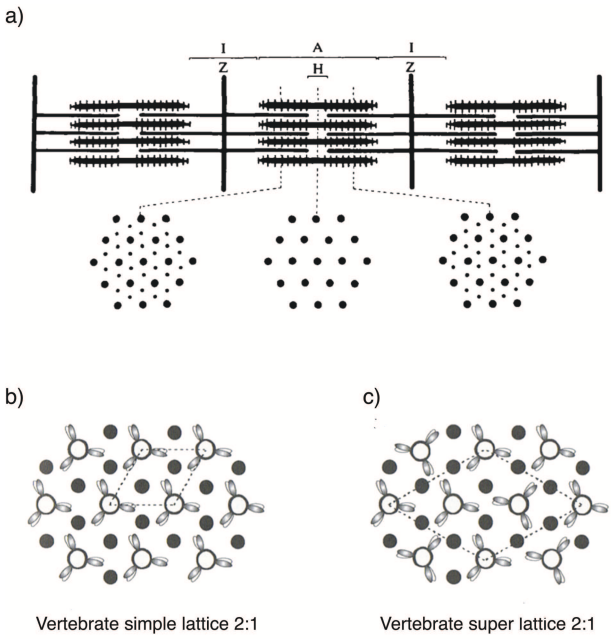

Figure 1.12. Cristallic structure of sarcomere. a) Scheme of filament organisation in the A-band of sarcomere, taken from [49]. b) The primitive vertebrate crystallographic lattice of thick myosins and thin actin filaments with the ration of actin to myosin filament mentioned. c) The structure lattice of higher organised vertebrate. The adjacent myosin filament are nor oriented in the same way. Adapted from [105].

increases beyond $2.5\mu m$, the degree of overlap decreases progressively and the tension reduces. An advance of experimental techniques created the possibility of the study of

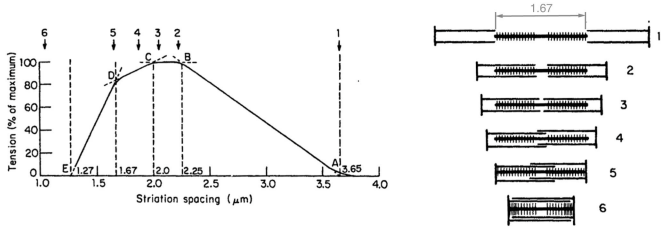

Figure 1.13. The isometric force is directly linked to the degree of filaments overlap in each sarcomere. Adapted from [28].

fast transients associated with quick recovery of tension which is usually performed on "in vitro" systems. These experiments were first performed by Huxley and Simmons in 1971 and have been since then considerably broadened and improved, most significantly by the group of V. Lombardi.

Different experiential techniques are used to characterize isometric and isotonic transients (length and force clam devices). In the length clam experiments, the activated fiber exerts after a transient period a constant isometric tension T_0, Fig.1.14. After this stationary state is reached, a fast length step δ is applied, which is measured traditionally in nanometers per half-sarcomere (nm/hs). In Fig.1.14a) we illustrate the evolution of the

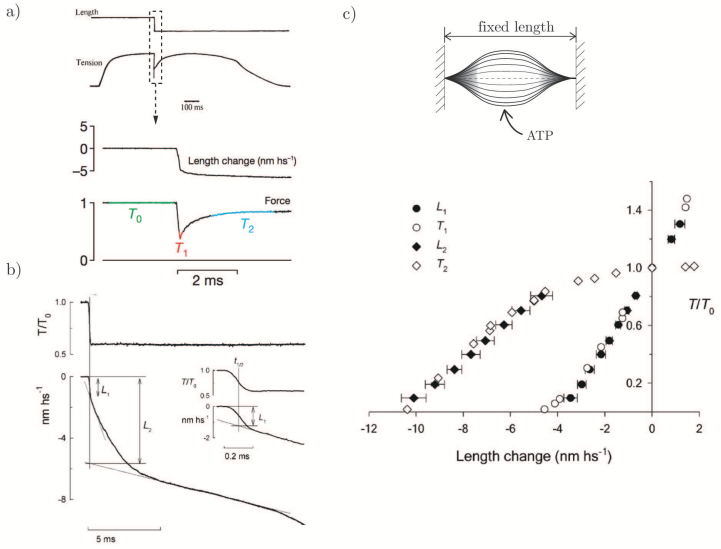

Figure 1.14. The results of fast transient responses. a) The length clamp experiments, after the step is applied, the tension progressively recovers up to its initial value with a time scale of about $100ms$, taken from [46]. On an expanded time scale, the tension first decays during the step up to T_1 (elastic response) and then partially recovers to a fraction of the initial tension, called T_2, within $\approx 2ms$ after the step. b) The force clam setting reporting the fast transients phases 1 and 2. The half-sarcomere first shortens elastically up to L_1 and phase 2 sees an additional shortening up to L_2. Measurement of L_2 is done by a linear extrapolation of phase 3 to the middle of the step (see the construction lines on T_1 and L_1 are the tension and half-sarcomere length attained at the end of the loading step. They correspond to the instant elastic response of the fiber. The $T_1 \to T_2$ and $L_1 \to L_2$ transitions are interpreted as the power-stroke events among the attached myosin heads. From [90, 91].

tension during such length clamp experiment. The tension generated by the fiber reaches the initial value in $\approx 100\mu s$. At shorter time scales the tension exhibits different phases. Thus, it first decays to T_1 which is interpreted as an elastic response and then partially recovers to a fraction of the initial tension T_2, within $\approx 2ms$ after the step length change. Such quick recovery to the T_2 level produces a plateau on Fig.1.14a). The time scale of fast transient response is the typical time of conformational change inside a single myosin motor. The length step associated with the tension T_1 is called L_1, and similarly the tension T_2 corresponds to the length step L_2.

In the force clam devices, the muscle fiber is first stimulated under isometric conditions reaching a tetanus force T_0. In this state the control device is switched to the force clamp mode and a force step is applied, see Fig.1.14b). The fiber shortens and after three transient phases, the steady state shortening regime is reached (phase 4 on Fig.1.15), where the shortening velocity can be measured. The intermediate phases 1 and 2 mirror some fast mechanical processes occurring at the scale of a cross-bridge before the attachment/detachment process gets involved (Huxley and Simmons, 1971) while phase 3 already reflects the onset of the attachment/detachment process [96]. In view of the similarity of the underlying physical process at the microscale one can try to extract the analogs of the isometric tension thresholds T_1, T_2 from the force clamp setting, see Fig.1.14.b). Indeed, one can see that a half-sarcomere first shortens elastically up reaching L_1 and then in phase 2 shortens additionally to L_2. Usually the measurement of L_2 is done by a linear extrapolation of phase 3 to the middle of the step. The summary of the data obtained in

two types of experiments is shown in Fig.1.14c). One can see that length and force clam devices produce essentially the same results regarding fast force/length recovery.

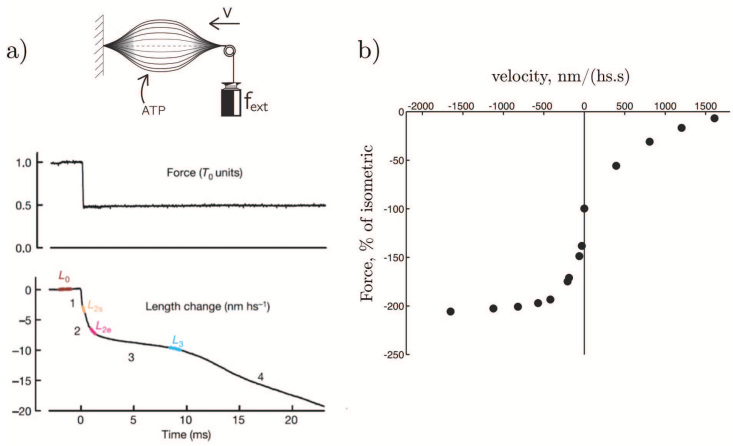

Figure 1.15. a) Force change normalised to the isometric tension T_0. Lower trace: length change in nm per half-sarcomere nm/hs. Transients phases 1 and 2 reveal the fast process occurring at the scale of the cross-bridges. Phase 3 represents the onset of attachment/detachment process and phase 4 is a steady state regime with shortening at constant velocity, taken from [96]. b)The constant velocity attained in steady state 4 versus the applied normalised force T/T_0. In shortening we observe the hyperbolic force-velocity relation described in (Hill, 1938). The force for which the velocity is equal to 0 is called the stall force. For low stretching, $T/T_0 < 120\%$, muscle resists the applied force before the velocity diverges at $T/T_0 > 120\%$. Data are taken from [21]–for shortening phase and from [69]–for lengthening phase. Adapted from [12]

In the right part of Fig.1.15 we show the force-velocity relation obtained for frog muscles [21, 69]. In the shortening regime (negative velocities), the muscle acts against the applied load and the dependence of the velocity on the force has a structure of a hyperbola (Hill, 1938). The shortening velocity progressively decreases as the force rises up to the stall force level where the velocity is equal to zero. In the stretching regime (positive velocities), the velocity remains close to 0 until the force reaches about 120% of the stall force and then diverges up to the point where the force reaches $\approx 200\%$ of isometric force leading to the destruction of the fibre. This asymmetry suggests that the functioning of a muscle may be very different in those two regimes. Shortening is a physiological regime where muscle pulls the load while stretching takes place only in accidental situations where the structural integrity of the muscle is threatened because the load is too high. For moderate stretching loads the muscle keeps velocity close to 0 and therefore plays the role of a damper.

The hyperbolic force-velocity relation is a crucial property observed at many scales. Thus hyperbolic force velocity behavior has been observed in a single molecule experiments performed on an isolated cross-bridge [60]. On the other side, the whole cell may also exhibit similar force-velocity relation in response to a fixed external traction [81].

1.7 Motor proteins and nanotechnology

Mathematical modeling of molecular motors is important not only for biology proper but will also play an important role in the future biomimetic engineering applications. Thus nanotechnology is presently mostly focused on imitating principles of cellular activity.

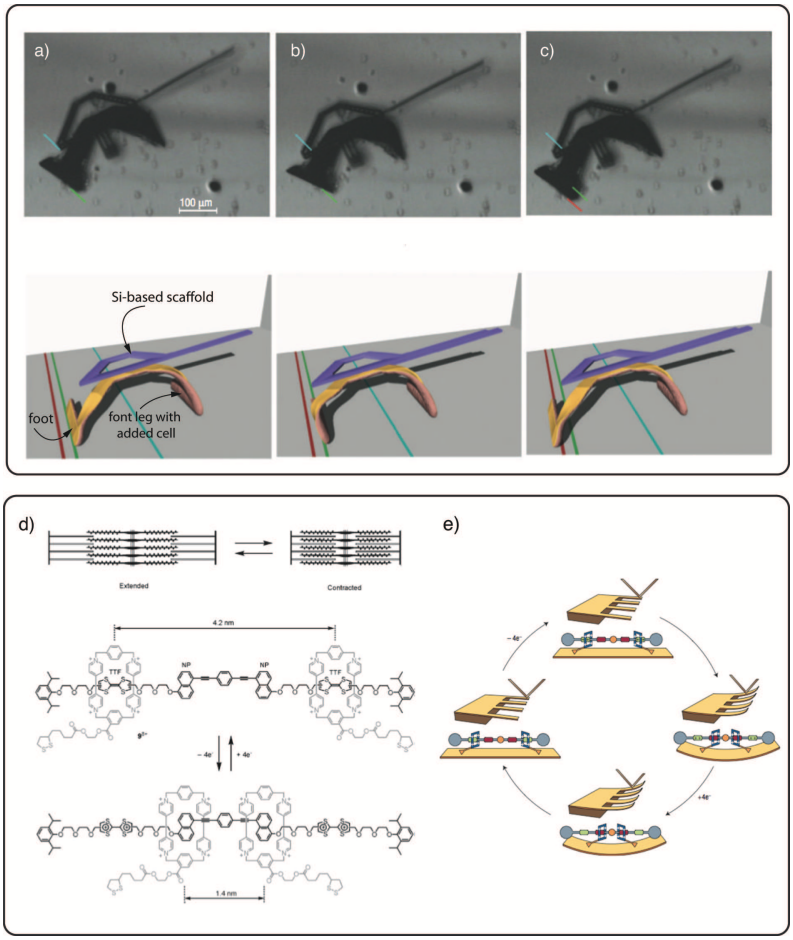

Figure 1.16. The top figure, a C.Montemagno's micro-mechanical device operated by muscle bundles, adapted from[128]. The images showing the sequential movement of the device during one step. a) Before contraction of the leg. b) During contraction of the leg. c) After relaxation of the leg. Blue, green and red bars mark the start positions of the inorganic scaffold and the motile leg, and the final position of the motile leg, respectively. d) Rotaxanes, the artificial structure in which the macrocycle is translocated from one position (station) on the thread to a second site through biased Brownian motion in response to an external trigger stimulation (light, electrons, reversible covalent bond formation). e) Cyclic bending of cantilever beams by the cooperative action of several rotaxane motors. The system based on bistable rotaxane structure in which each rotaxane has two positively charged rings and four stations. Two stations are redox active and can be switched between neutral and positively charged form. Adapted from [8]

Below we present a series of recent examples of the engineering research studying functional possibility associated with such motor proteins as myosin and kinesin [73, 116].

Molecular size motors are expected be used at the nanoscale as control devices and as devices carrying cargo. More specifically, they will be used as

- Smart sensing devices
- Devices for purification and separation
- Assembly devices participating in the construction of nanoelectronics
- Transport devices on a micro chip integrating multiple analyzing and delivery tasks.

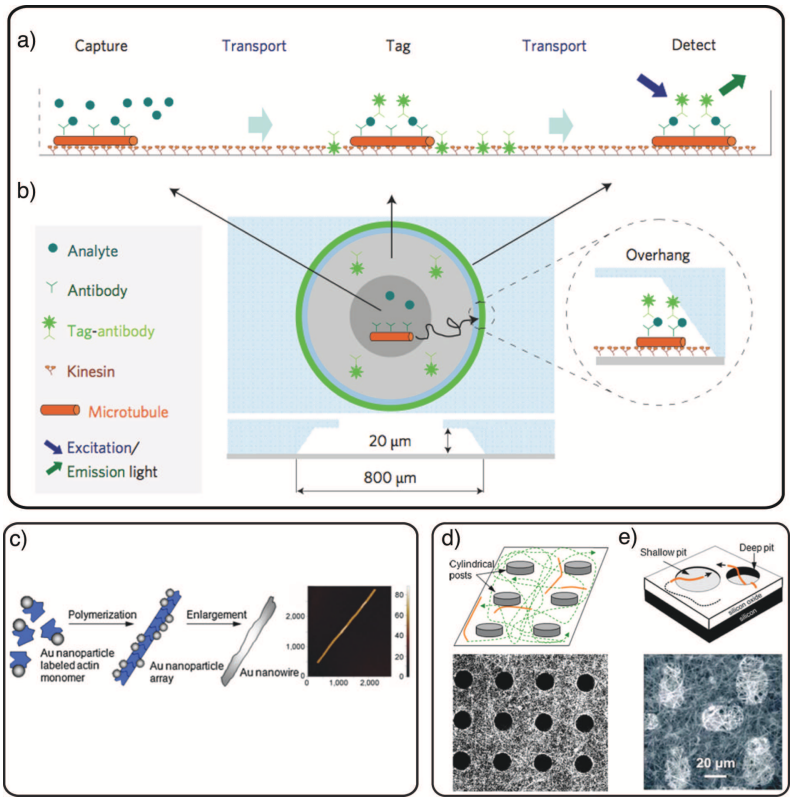

Figure 1.17. On the top figure, concept of a smart dust device using active transport by molecular shuttles. a),b) The capture-transport-tag-transport-detect functional cycle of the smart dust device, in which antibodies on microtubules capture antigens from solution. Kinesin motors are activated, and collisions of antigen-loaded, gliding microtubules with fluorescent particles functionalised with a second antibody lead to pick-up and transfer of the fluorescent tags to the detection zone, indicating the presence of antigen. Reproduced from[20]. c) Fabrication of gold nanowires using actin filaments as templates via polymerization of gold-labeled actin monomers and subsequent metalization. On right, the AFM image of a gold nanowire obtained by this procedure, all dimension are in nanometres, adapted from [88]. d) Investigation of surface properties using molecular shuttles. The Information about surface topography can be revealed in a time-integrated image of microtubules moving randomly on the surface. e) The height of the topographical features can also be quantitatively deduced by the utilization of fluorescence-interference contrast. Adapted form [1].

Resent engineering research in this field is focused on the development of optimal control of motion in specified direction. This includes control of directionality of the transport and the ability of the system to stop when it is necessary. Other tasks include pushing and pulling different filaments (cargo systems) by using a combination of topological (geometrical) and chemical control [25]. An example of the potential applications of myosin II transport capabilities in technology is the ATP-powered transportation of metallic nanowires [88], see Fig.1.17c).The use of kinesin motors as biosensors was proposed in [20]. The authors used the adhered kinesin molecules for biochemical detection and delivery of various components to the detection zone, see Fig.1.17a),b).

Individually myosin motors deliver only a minuscule mechanical work but in assembly of millions of units they can generate a significant response at a macroscopic scale. As an example of artificial devices powered by a collective functioning of a large number of myosin

molecules we can mention micro-mechanical devices operated by muscle bundles [128]. In Fig.1.16a),b),c) we show the step-like motion of a metallic leg attached to muscle tissue. A single working contractile artificial element was developed in [13], see Fig.1.16d). Another artificially generated system of macromolecules uses transitional metal-based templates for the formation of two-component interlocked molecules imitating an element of a muscle [43, 6]. The functional unit is translated from one position (station) on the thread to another position through biased Brownian motion in response to external stimulation. These systems are viewed as potential elements of molecular machinery able to perform a cyclic response to external stimulation Fig.1.16e).

Despite all these successes, broad industrial use of molecular motors is still limited by low stability of the biological components. For instance, biomolecular motors and filaments have to be maintained in a very specific chemical environment to prevent denaturation and other degradation effects [1].

1.8 Conclusions

In this section we reviewed a series of experimental observations regarding the functioning of molecular motors. We have shown how the motors work individually and in groups and how their activity can be used in artificial devices.

It is clear that the complexity behind the functioning and regulation of molecular motors is enormous and considerably surpasses complexity of analogous artificial devices developed by engineers of today. In this Thesis we obviously won't be able to deal with all this complexity and will instead focus on the development of simple and transparent mathematical models capturing only some of the observed phenomenology. More specifically, we shall use as a prototype an interacting acto/myosin complex involved in muscle contraction and shall try to reproduce only few biological details. In particular,

- We neglect the three dimensional structural organization of molecular motors and do not attempt to deal directly with steric effects. Instead we limit our description to $1\mathbb{D}$ by projecting all relevant physics on one dimension.
- We assume that the actin filament is polar, which defines the preferred direction of a walk along the filament. We assume the periodicity of the filament structure associating the period with the size of a monomer. We also neglect filament elasticity and assume that the filament (actin) is a rigid body.
- We neglect the full complexity of the full chemo - mechanical cycle involved in muscle contraction and focus exclusively on the simplest four states of Lymn-Taylor cycle. With each chemical state we associate a particular geometric/mechanical configuration and the aim of our modeling will be to translate the meaning of different states from the biochemical to mechanical language.
- We neglect the complex crystallographic structure of the cross-bridge, in particular we deal with only one myosin head. The power stroke is viewed as a conformational change causing either elongation or contraction of the cross bridge reference length.

In the next section we review several ingenious examples of the mechanical modeling of molecular motors which we used as a source of inspiration.

Chapter 2

Theoretical modeling of molecular motors

In this section we present several examples of the mathematical modeling of motor activity. The presented models will be of two types: chemo-mechanical models and mechanical models. The main difference is that in the case of chemo-mechanical models dynamics is modeled by a set of chemical reactions while in the case of mechanical models, actual stochastic dynamics of mechanical degrees of freedom is being considered. While the relation between these two types of models is rather delicate and is not fully understood, one can say that chemo-mechanical models can replace mechanical models when the Kramers approximation is applicable. This is in fact often the case but surely not always as we show in this work. We shall mostly focus on acto-myosin interaction but also review several approaches used in the description of kinesin. We begin with two famous chemo-mechanical models muscle contraction proposed by A.F.Huxley, one in 1957 focused on attachment detachment and another one in 1971 focused on the power stroke. Both of them strongly influenced the development of the research on myosin/actin interaction. We shall then turn to the models of Brownian ratchets and then consider several synthetic models.

2.1 Sliding filament model of A. Huxley (1957)

In 1957, the coupling mechanism of actin filament and myosin cross-bridges was still not fully understood. The existing mathematical description was based on the phenomenological model developed in 1938 by A.V. Hill which reproduced the hyperbolic dependence of the shortening velocity on applied force, by using very general energy balance considerations and some ad hoc phenomenological assumptions. A.F. Huxley [44] proposed the first mechanism based model which also reproduced the hyperbolic force-velocity curve which emerged as a solution of a differential rather than an algebraic equation. Most importantly Huxley's model produced the first link between the macroscopically measured relations and the microscopical picture of the attachment / detachment process. Interestingly, the power stroke which is a major element of the Lymn-Taylor cycle was not explicitly mentioned in this model. However, as we show below, it was surely implied.

In the Huxley model a myosin tail is modeled as a linear spring connected to a rigid backbone. It is assumed that the head M has an affinity to the specific binding site A on the rigid actin filament which is always displaced at a certain distance from the location of the relaxed head. Therefore when the head attaches, it always stretches the spring and

in this sense the attachment and the power stroke are combined into one event.

Suppose that x is the potential attachment site for the head M on the actin filament and that the spring is not stretched if $x = 0$. The myosin head is a subject to thermal fluctuations and the head M oscillates around its equilibrium position $x = 0$. To break the symmetry of thermal oscillations Huxley introduced a Markov rate functions $f(x)$ and $g(x)$ controlling the affinity of myosin for particular locations at the actin fiber and maintaining disequilibrium which is implicitly supported by the ATP hydrolysis. If $f(x)$ is the attachment rate and $g(x)$ is the detachment rate Huxley assumed that $f(x)$ is linear for positive x with a maximum at h and equal to zero beyond this point and for negative values of x. The detachment rate $g(x)$ was taken to be large for negative values of x and an increasing function for positive x. The rate function $f(x)$ exceeds the $g(x)$ on the interval $0 < x < h$ which creates a tendency for a cross-bridge to be attached in a state neat $x = h$ and generates positive tension. According to these assumptions a cross-bridge will be detached in the state of negative tension, see Fig.2.1.

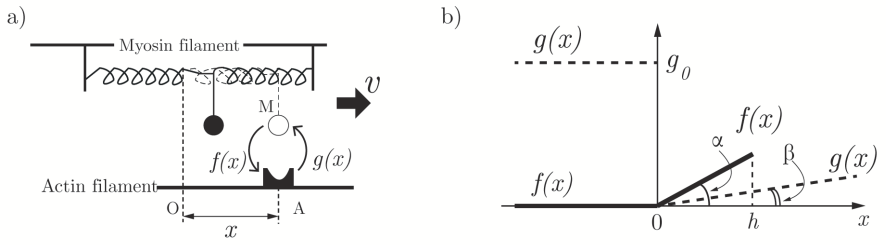

Figure 2.1. The mechanism proposed by A. F. Huxley in 1957. a) Sketch of the model. The part of system M modeled the myosin head is connected to the rigid backbone (thick filament) by the linear spring of stiffness k. The strain of myosin head is noted x. The myosin and actin filament are moving past each other at a velocity v. The symmetric Brownian motion is biased by two function $f(x)$ and $g(x)$, assumed model the chemical reaction of myosin/actin interaction. b) We shows how $f(x)$ and $g(x)$ depend on the binding site position x. Attachment is accelerated with rate $f(x)$, when M is displaced by Brownian motion in positive direction, $x > 0$. The detachment process is accelerated by rate $g(x)$ for $x < 0$.

If one attachment/detachment event associated with a particular cross-bridge does not influence the other similar events, one can model the system by a single particle distribution function $n(x, t)$ which can also be interpreted as a density of cross-bridge population with strain x at time t. We can write the Master equation describing the kinetics of the system:

$$\frac{\partial n}{\partial t} + v\frac{\partial n}{\partial x} = (1 - n(x))\, f(x) - n(x)g(x), \tag{2.1}$$

where v is the velocity of the thin filament with respect to the thick filament. Notice that we have here a continuum of chemical states labeled by x and that the relative sliding of actin and myosin filaments is explicitly present through the convective term which systematically shift the equilibrium for nonzero velocities. Interestingly, Huxley emphasized the kinetics and neglected the diffusion which in fact changes the results only slightly.

The detailed shape of the functions $f(x)$ and $g(x)$ is not important for us here, however, one can use the piece-wise linearity of the original model to obtain an explicit solution.

Therefore we assume that

$$\begin{aligned} f(x) =& 0,\ g(x) = g_0, \quad x < 0 \\ f(x) =& \alpha x,\ g(x) = \beta x, \quad 0 \le x \le h \\ f(x) =& 0,\ g(x) = \beta x, \quad x > h \end{aligned} \tag{2.2}$$

Under the assumption that the shortening takes place at constant speed $v = \frac{dx}{dt}$ the stationary distribution must solve the following ODE:

$$v\frac{\partial n}{\partial x} = f(x) - n(x)[f(x) + g(x)] \tag{2.3}$$

This equation can be solved explicitly and we obtain

$$n(x,v) = \begin{cases} \dfrac{\alpha}{\alpha+\beta}\left[1 - exp(\dfrac{\alpha+\beta}{2v}h^2)\right] exp(-\dfrac{g_0 x}{v}), & x < 0 \\ \dfrac{\alpha}{\alpha+\beta}\left[1 - exp(\dfrac{\alpha+\beta}{2v}[h^2 + x^2])\right], & 0 \le x \le h \\ 0, \quad \text{for } x > 0 \end{cases} \tag{2.4}$$

The tension generated by the system can be found from the formula

$$T(t) = k\int_{-\infty}^{+\infty} xn(t,x)dx \tag{2.5}$$

where k is the stiffness of a linear spring. Suppose that a muscle fiber has cross sectional area equal to A, that the length of one half-sarcomere is $s/2$, and that the number of participating cross-bridges is $mAs/2$, where m is number of cross-bridges per unit volume. Then the total force is

$$T(t) = \frac{mAs}{2}k\int_{-\infty}^{+\infty} xn(t,x)dx \tag{2.6}$$

By using (2.4) and (2.6) we can compute explicitly the total force for a given contraction speed

$$T(v) = \frac{mAsk}{2}\frac{\alpha}{\alpha+\beta}\left[\frac{1}{2}h^2 + \left[1 - exp(\frac{\alpha+\beta}{2v}h^2)\right]\left(\frac{v}{\alpha+\beta} - \frac{v^2}{g_0^2}\right)\right] \tag{2.7}$$

The isometric tetanic tension is the value of this tension at $v = 0$ which gives

$$T_0 = \frac{mAs(\alpha)}{2(\alpha+\beta)}\frac{kh^2}{2} \tag{2.8}$$

Finally, the energy consumption associated with shortening over the distance l per unit volume can be estimated as

$$E(t) = \frac{me}{l}\int_{-\infty}^{+\infty} f(x)(1 - n(t,x))dx \tag{2.9}$$

where e is the consumed energy per one functional cycle. It is clear that in this formulation the consumed energy can be viewed as fueling both attachment and the power stroke without clear indication of the difference between the two processes. The consumed energy partially dissipates as a heat and is partially transformed into mechanical work. In the isometric case, when the velocity is equal to zero, all consumed energy is dissipated as heat.

Under the appropriate choice of parameters Huxley's theory gave an adequate fit for both the force-velocity curve and the relation between the load and the rate of energy liberation found by A.V.Hill (1938). However this model cannot reproduce the characteristic phenomena accompanying force transients when the muscle is shortened rapidly. As we have seen, experimental observations suggest the presence of two mechanisms of force generation rather than one and two time scales rather than one, which is incompatible with the presented model.

2.2 Power stroke model of Huxley and Simmons (1971)

Observations of a peculiar muscle response to rapid length increments in the millisecond range made it necessary to formulate a new mathematical model taking into account explicitly the power stroke [46]. At these time scales one can ignore the attachment/detachment process and concentrate only on the force recovery by the attached myosin heads. Essentially, the 1971 model proposed the first mathematical description of the conformational change representing the power-stroke.

The model has two basic elements: a bi-stable element representing the $S1$ fragment and described by a discrete double welled energy potential $V(x)$ and a linear elastic element $V_m(x,y)$ representing the spring link between the $S1$ fragment and a thick filament, or in others words the $S2$ part of the cross-bridge. The internal degree of freedom x was interpreted as the angular position of the myosin head (or rather its projection), while the variable y can be viewed as the relative position of actin and myosin filaments. Each cross bridge is assumed to be independent of the rest at least in the hard device experiment, which makes the analysis rather straightforward.

In the original model each energy well was assumed to be infinitely steep and the power stroke was viewed as a chemical reaction representing a jump process between the two discrete state. The two wells are separated by a distance characterizing the power-stroke size – a, see Fig.2.2 a), the energy of the linear elastic element is taken in form: $V_m(x,y) = 1/2k(y+y_0+x)^2$. The transitions between the two well of the bistable potential can stretch or relax the elastic element which makes biasing of particular energy wells a mechanism of force generation.

The model describes the distribution of cross-bridges among the two energy wells. For instance, after a quick length change, the distribution first does not change and the tension T_1 varies exclusively due to the elastic deformation of the spring. Eventually the population of cross-bridges in both well starts to changes reaching the final steady state with which one can associate the plateau value T_2. It is clear that the system reaches the equilibrium plateau at a much slower rate than the time scale responsible for the elastic response T_1.

More specifically, Huxley and Simmons denoted by k_+ and k_- the transition rates from pre-power stroke to post-power stroke conformation and vice-versa. According to Kramers theory of chemical reactions, [32] the rate constant k_+ and k_- are inversely proportional to the exponential function of the size of the energy barriers which depend on the elastic energy stored in the linear spring V_m. For $\Delta V > 0$, see Fig.2.2a) the transition rates can be written as

$$\begin{aligned} k_+(y) &= \alpha exp\left[-\frac{1}{k_B T}B_1\right] = Const = k_+^0 \\ k_-(y) &= \alpha exp\left[-\frac{1}{k_B T}(B_0 + \Delta V(y))\right] \end{aligned} \tag{2.10}$$

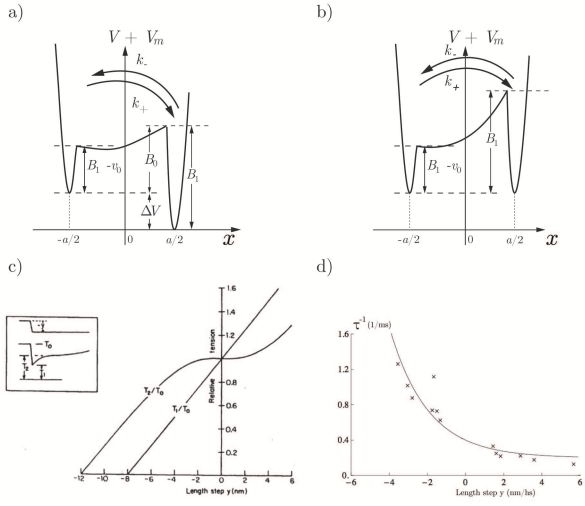

Figure 2.2. The original power stroke mechanism proposed by A.F. Huxley in 1971. a) Sketch of the potential associated with conformational change in cross-bridge. This is discrete potential composed by a potential with two wells separated by a distance a (the well at $x = -a/2$ has offset energy v_0) and the elastic part of system $V_m(x, y)$, modeled the elastic properties of myosin head. The barrier B_1 is constant, only ΔV is functions of y. b) Total potential energy when $y = 0$. This corresponds to the isometric initial condition. c) T_1 and T_2 curves obtained with Huxley and Simmons 1971 model for different value of length step y. d) The solid black line represent the rate following Huxley and Simmons paper, by a squatters we plot the experiments data. Adapted from [12].

where α is a fitting constant and $\Delta V(y)$ is the difference between the energies of state 2 and state 1

$$\Delta V(y) = \frac{1}{2}k(y_0 + \frac{a}{2} + y)^2 - \frac{1}{2}k(y_0 - \frac{a}{2} + y)^2 + v_0 = ka(y_0 + y) + v_0$$

. Considering the isometric tension where $\Delta V = 0$, for $y = 0$ we can express $v_0 = -kay_0$, see Fig.2.2b) which gives $\Delta V = kay$. Therefore the chemical rates depend on overall strain y. We can then rewrite k_+ as

$$k_-(y) = k_+^0 exp\left[-\frac{1}{k_B T}(kay)\right] \tag{2.11}$$

Now, introduce n_1 and $n_2 = 1 - n_1$ as the fractions of the total number of attached cross-bridges in states 1 and state 2. In the Kramers approximation the kinetics of the transition between the two conformation states is described by the following first order ODE

$$\frac{dn_2}{dt} = k_+ - (k_+ + k_-)n_2. \tag{2.12}$$

The system reaches the equilibrium with a rate τ

$$\tau^{-1} = k_+ + k_- = k_+^0(1 + exp\left[-\frac{kay}{k_B T}\right]) \tag{2.13}$$

In the case of isometric contraction we can assume that $n_2(0) = \frac{1}{2}$ which gives us an initial condition before the step application. Integrating the equation (2.12) with this initial condition we can find $n_2(t)$ in the form

$$n_2(t) = \frac{k_+}{k_+ + k_-} + \left(\frac{1}{2} - \frac{k_+}{k_+ + k_-}\right) exp(-\frac{t}{\tau}) \tag{2.14}$$

By computing the force per cross-bridge corresponding each configurational state $n_2(t)$, we obtain

$$\begin{aligned} T(y,t) &= n_1(t)k(y_0 + y - \frac{a}{2}) + n_2 k(y_0 + y + \frac{a}{2}) \\ &= k\left[y_0 + y - (n_2 - \frac{1}{2})a\right] \end{aligned} \tag{2.15}$$

The force plateau T_2 is found by considering the limit $T_2 = \lim_{t\to\infty} T(y,t)$ giving

$$T_2 = K\left(y_0 + y - \frac{a}{2} tanh[\frac{kay}{k_B T}]\right) \tag{2.16}$$

The T_1 tension can be simply defined as the force value corresponding to the fixed values of n_1 and n_2 which remain frozen in origin state 1/2:

$$T_1 = \frac{1}{2}k(y_0 + y - \frac{a}{2}) + \frac{1}{2}k(y_0 + y + \frac{a}{2}). \tag{2.17}$$

Fixing the constants from their own data Huxley and Simmons were able to obtain the functions T_1 and T_2 in accordance with experiment, see Fig.2.2c).

The above model of the power-stroke provides the first direct link between the rate constants and the mechanical state of the system. This approach is also consistent with the results of the crystallographic studies point to the rotation of the lever arm following the conformational change. One problem with the model is that the mechanical states of the system are interpreted as fixed chemical states and therefore the size of the power stroke does not depend on the magnitude of the shortening step. Another problem is that a more realistic choice of parameters makes the power stroke too slow and produces T_2 curve with a negative slope in the isometric contraction regime which is not supported by experiments. However, the Huxley-Simmons model has a clear mechanical origin and most of these problems can be removed if one takes into consideration interaction between different cross bridges (see below).

In this work we generalize the Huxley-Simmons model in a different way by first coupling the power stroke with attachment detachment machinery and second, by introducing active stimulation of the system through a correlated component of the environmental noise.

2.3 Recent chemo-mechanical models

In 1974 T.L. Hill made an attempt to formalize and unify the existing approaches by emphasize the necessity to link the kinetic constants, which in muscle mechanics become functions of the relative position of actin and myosin filament x, with the corresponding free energy landscape [34]. In 1978 E.Eisenberg and T.L. Hill proposed a model of muscle contraction where in addition to x the energy depended on a variable describing the degree of the conformational change $x - y$ [18]. This was a first attempt of a synthesis bringing together the approaches of Huxley 1975 where the only variable was x and of Huxley and Simmons 1971 where the only variable was $x - y$. The problem is that the model still treated the power stroke as a discrete transition and the authors studied jump dynamics instead of a continuous dynamics.

Similar assumptions were widely used in many subsequent chemo-mechanical models operating with more discrete states than in the Lymn-Taylor cycle. Usually in all these

models one solves a set of master equations with kinetic constants constrained by the detailed balance conditions. Still it leaves a lot of functional freedom in choosing how the rate functions depended on the strain. Such models contain fitting functions and allow the authors to reach an excellent agreement with excremental measurements.

A prominent example of such a theory is a three state model of Duke [16]. The model assumes that in each of the states the free energy varies quadratically with x. By the choice of the rate function one creates the preferred pathways allowing one to match the experimental data. The model is schematically represented in the Fig.2.3 together with the characteristic force velocity curve. Notice that the two detached states are represented

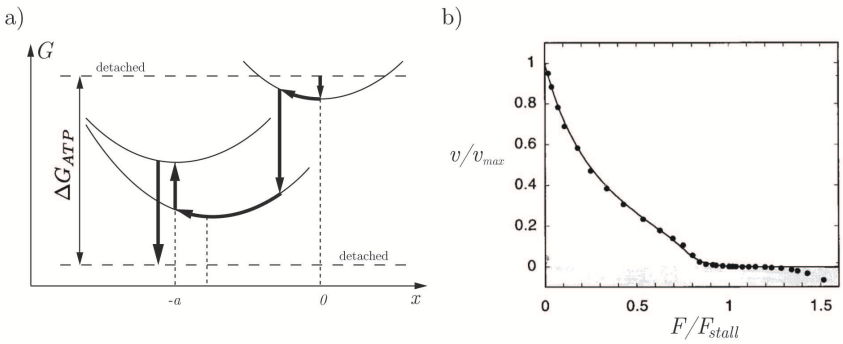

Figure 2.3. Duke 1999 description of muscle myosin kinetic cycle. a) The sketch of free energy profiles for Duke's chemo-mechanical model. The arrows indicate the typical reaction pathway of particle. b) The variation of sliding velocity v/v_{max} with external load F/F_{stall}, black line plots the estimations of Duke's theory and the black circles are experimental measurements of K.A.P. Edman, [17]. For more precisions see the Fig.3 of [16]

by strait lines. This model is characterized by a discrete set of parameters and is able to reproduce quantitatively most of the data describing isotonic velocity transients. However, the quick force recovery in isometric conditions is reproduced only qualitatively. A detailed theoretical study of collective effects in the three state model was performed by A. Vilfan and T.Duke in [119]. They observed instabilities in dynamics of a single half sarcomere and give a detailed investigation of dynamics of many elements in series.

A simplified two-states version of Duke's model was studied in [123]. The model has single detached states and single attached state, which blends the pre-power-stroke and the post-power-stroke chemical states into one state. The authors made an assumption what the two attached states are always in equilibrium, which is a correct assumption if we consider the attachment/detachment time scale. The attachment and detachment rate functions in this model are strain dependent and can be viewed as the fast time averaging of the rate functions proposed by Duke. The resulting model shows a good agreement with experimental measurements and is able to explain the presence of damped oscillations based on the study of the shape of the force-velocity curve. The model is also able to predict the inhomogeneity in sarcomere lengths during isometric contractions.

Another interesting generalization of the Huxley 1957 model was proposed by A. Vilfan, E. Frey and F. Shwabll [120]. This is a very flexible scheme allowing one to describe processive motors such as kinesin or myosin V as well as myosin II. The model is characterized by quadratic potential describing the deformation energy of a motor head $V(x) = \frac{1}{2}k_m x^2$ with $x = x_a - x_m - x_d$ where x_m–is the position of motor's tail on a rigid backbone, x_a the position of a motor head relatively the actin track, and x_d is the displacement due to a conformational change in the motor head. In the attached state $x_d = 0$ and in the

detached state $x_d = d_m$, see Fig. 2.4. The transition between the two states – attached and detached – is governed by the rate functions: f_a for attachment and f_d for detachment. The attachment rate t_a is considered to be constant while $f_d \equiv f(x)$ is a strain depended function. The binding sites along the actin filament are discrete and distributed

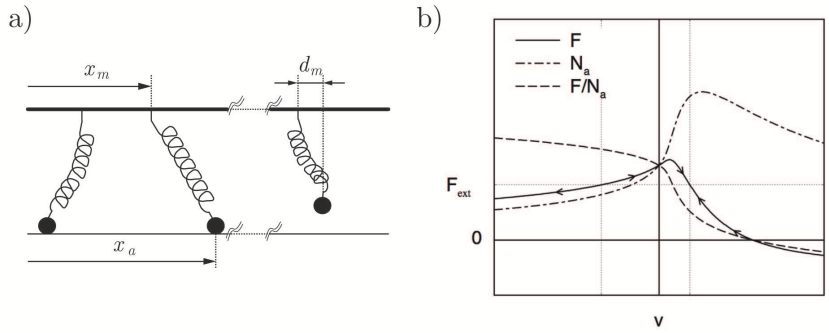

Figure 2.4. The 1999 two state model by A.Vilfan, E. Frey and F.Schwabl. a) The schematic picture of the motor with the rigid backbone distributed along a actin track with discrete binding sites. b) The force-velocity curve –the solid line, with dashed line we show the mean number of attached motors; dash-dotted line represents the mean force per attached motor head. From [121].

with period L. The function $n_a(x,t)$ describes the probability density for motor to be at time t attached at x and function $n_d(t)$ describe the probability density for motor to be detached at time t and free to diffuse. The dynamics of the probability densities is described by the Master equation:

$$\begin{aligned} \partial_t n_a(x,t) = &\quad f_a n_a(x,t)P(x) - f_d(x)n_d(x,t) + v\partial_x n_a(x,t) \\ \partial_t n_d(t) = &-f_a n_a(x,t) \qquad + \int dx f_d(x) n_d(x,t) \end{aligned} \tag{2.18}$$

The normalization condition for N motors take the form

$$n_d(t) + \int dx n_a(x,t) = N \tag{2.19}$$

The function $P(x)$ defines the probability for the motor to attach and is obtaining by the averaging of the Boltzmann type probability densities for single motor heads under the hypothesis of random distribution of positions x_m relatively the binding sites before the attachment process. The generated force by the N motors is then

$$F(x) = \int dx n_a(x,t)\partial_x V(x). \tag{2.20}$$

Depending on the definition of the symmetry breaking function $f_d(x)$ the model is able to generate two types of force-velocity behaviors: the standard monotonously decreasing velocity with increasing force and the hysteretic behavior around the point $v = 0$. In the hysteretic regime one obtains two different values of velocity at one value of the force. In particular, this model explains the possibility of spontaneous oscillations in cross-bridge systems which were observed in acto-myosin systems [121].

A detailed study of chemical reactions associated with ATPase activity shows many more chemical states than in the simple 4-state Lymn-Taylor cycle and by incorporating some of these states one can achieve better agreement with experiment. However, the price

is the complexity of the model and the increasing number of fitting functions. An important step in the direction of a minimal extension of the Lymn-Taylor model was proposed by V. Lombardi group. The proposed model has three attached states (noted $A1$,$A2$ and $A3$) , two detached states (noted $D1$ and $D2$) and requires six forward rate functions. Elementary force-generating step of a cross-bridge (power stroke) is now represented by a set of transitions $A_1 \rightleftharpoons A_2$ and $A_2 \rightleftharpoons A_3$. To illustrate the complexity of the ensuing model we show the rate functions, used in [89] on Fig.2.5. The variable x represents the relative axial position of the myosin/actin filaments. The forward and reverse rates functions for

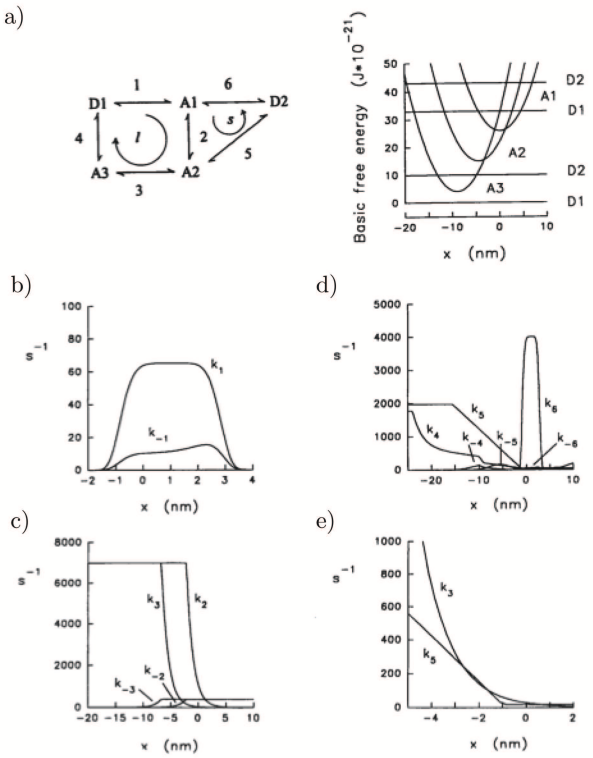

Figure 2.5. Chemo-mechanical G.Piazzesi and V.Lombardi model, adapted from [89]. a) On the left, the ensemble of possible reactions between the chemical states: the three attached states A_1, A_2, A_3 and the two detached states D_1, D_2. On the right, the presentation of free energy level associated to the chemical states of cross-bridge, the attached states are harmonic with the same stiffness and the detached states have a fixed energy. b)–e) Shows the rates transitions functions between the states.

the neighboring states with free energy level $G_i(x)$ and $G_j(x)$ $(i = 1, 6$) are related by the detailed balance relations

$$\frac{k_{ij}}{k_{ji}} = e^{-\frac{\Delta G_{i,j}}{k_B T}}. \tag{2.21}$$

In the model the free energy profiles are fit in order a to produce the curves obtained in experiment. The system of five differential equations governing the dynamics of the distribution functions in each state (three attached and two detached) has the form

$$\partial_t n_i = -v\partial_x n_i(x,t) + \sum_{i,j} n_j k_{ji} - n_i \sum_i k_{ij} \tag{2.22}$$

with normalization condition:

$$\sum_{i=1}^{5} n_i(x,t) = 1. \tag{2.23}$$

The model shows a good agreement with the experimental observations if six fitting functions are selected appropriately which is by itself a formidable task.

Probably the most complete model of collective acto-myosin interaction in skeletal muscles was proposed by D.A.Smith [103, 104]. This model is able to reproduce almost all known experimental observations related to isotonic and isometric contractions of skeletal muscles. Moreover, it is the attempt to produce a comprehensive theory with a complete description of mechanochemical cycle of one cross bridge, and incorporating also the description of three-dimensional myosin-actin filaments lattices. The cross-bridge cycle adopted in this model includes intermediate states between the pre-power stroke state and the post-power stroke state. Again, the rate constants for the attachment and detachment processes depend on the pre-power stroke strain in a phenomenological, semi-empirical way. The resulting model is analytically opaque and can be viewed only as a numerical tool.

2.4 Purely mechanical models of the power stroke

Despite the efficiency of chemo-mechanical models in fitting experimental data they are not very satisfactory from mechanical point of view because it is not clear how the corresponding force generating devices can be reproduced in the mechanical laboratory. It is therefore of interest to propose an alternative, purely mechanical description of the mechanism of muscle contraction. So far all the advances in this direction were focused on the modeling of the power stroke which is conventionally viewed as a purely mechanical element. The proposed models were aimed at reproducing the behavior of the system at small time scales corresponded to quick force-recovery by power-stroke mechanism. In particular, the existing models of this type do not incorporate the description of the attachment-detachment process. In contrast to the Huxley Simmons model, the mechanical models of the power stroke operate with continuous variable describing the conformational change. In this sense these models can be viewed as a development of the ideas suggested by E. Eisenberg and T.L. Hill in [18].

The first model of this type, proposed by Marcucci and Truskinovsky [74], generalizes the Huxley and Simmons model by replacing the discrete degree of freedom accounting for the conformation of the myosin head by a continuous variable x. This degree of freedom can be interpreted as the projected angle between the sub-fragment $S1$ of the myosin head and the actin filament. Since the structure of the half-sarcomeres is essentially one dimensional, the authors choose to work with elongations instead of angles, by assuming that there is a direct relation with the orientation of the myosin head. The introduction of a continuous variable eliminates the necessity to deal with multiple discrete configurations for the head domain, see Fig.2.6. The model takes into account two most important mechanical characteristics of the myosin head: the head has at least two distinct conformations, pre- and post-power-stroke which suggests the bistable potential shape; the head has a series elasticity unit which is necessary to reproduce the mechanical response T_1 after a length step in isometric contraction.

The bi-stable potential $V(x)$, a mechanical energy associated with $S1$ structure, was modeled as a piecewise quadratic function. This rather simple form can be explained by the intention to make the computations analytically doable. In addition to this non convex

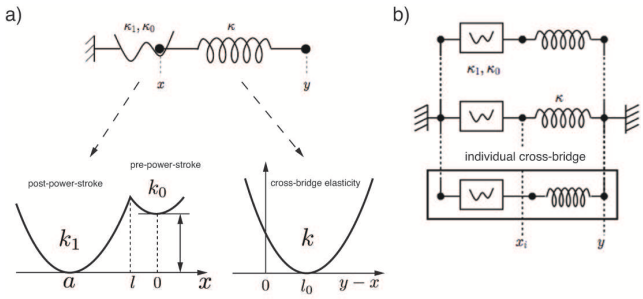

Figure 2.6. Each myosin $S1$ sub-fragment is associated with a bi-stable energy v modeled as a piecewise quadratic function of the rotational degree of freedom x. In addition to this non convex energy, we associate with $S1$ a series linear elastic element (with stiffness k) that models the stretching of the lever arm. Adapted from [12].

energy, a series linear elastic element with stiffness k has been added:

$$V(x,y) = V(x) + \frac{1}{2}(y - x - l_0) \tag{2.24}$$

where the bistable element $V(x)$ is:

$$V(x) = \begin{cases} \frac{1}{2}k_0x^2 + V_0 & if\ x > l \\ \frac{1}{2}k_1(x-a)^2 & if\ x \leq l \end{cases} \tag{2.25}$$

Here l is the location of the barrier, the point of intersection of the two parabolas in the interval $[-a, 0]$. The well at $x = 0$ and the well $x = 1$ represent the states of pre- and post-power-stroke conformations respectively. The value a is interpreted as the characteristic length of the conformational change rather than the unique size of the power-stroke. The parameter V_0 is the energy difference between the pre-power-stroke and the post-power-stroke configurations. To ensure the continuity of the potential $V(x)$ the following relation at $x = l$ was imposed:

$$\frac{1}{2}k_0l^2 + V_0 = \frac{1}{2}k_1(l+a)^2 \tag{2.26}$$

One can see that this cross-bridge model is fully described by set of four parameters: k_0,k_1,l and a. The use of the series quadratic element $\frac{1}{2}k(y - x - l_0)^2$ plays an important role in this model providing metastability and allowing the authors to avoid multiple intermediate states in the description of the power stroke mechanism. When the position y is moved, the energy landscape changes. Eventually one of the minima can disappear which questions the validity of the Kramers approximation. Interestingly, the use of continuous landscape allowed the authors to propose simple and natural explanation of the force dependence of the power stroke size.

The above model was generalized in the work of Caruel and Truskinovsky who considering the simplest elastic interaction between individual cross-bridges inside a half-sarcomere, see Fig. 2.7. As a result the authors obtained a fully quantitative model of a half-sarcomere which they were able to build in full agreement with experiments. Once again, the attached myosin heads were represented as a set of parallel bi-stable springs described by a piecewise quadratic potential. In addition, a linear elasticity of myofilaments (actin and myosin filaments) was incorporated into the model which introduced a mean-field type interaction between the cross-bridges and generated interesting collective effects [12] The proposed model produced the first explanation of the observed difference in time

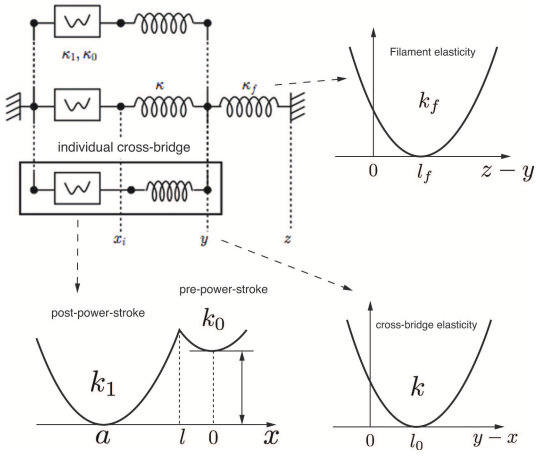

Figure 2.7. The sketch of mechanical model proposed by Caruel and Truskinovsky. Adapted from [12]

scales between fast force/length recovery in soft and hard device. Moreover, the model has shown that the power-stroke mechanism operates in an unstable regime opening the way to the explanation of the inhomogeneous response in multi-sarcomere chains representing myofibrils.

2.5 Brownian ratchets models

Another type of mechanical modeling relevant for muscle contraction and acto-myosin interaction can be associated with the Brownian ratchet framework which was developed in the last 20 years. The concept of Brownian ratchet gave an explanation of how motor proteins can rectify thermal fluctuations and produce useful work. In this type of models the description is stochastic because thermal fluctuations can no more be neglected and on the contrary, play the crucial role in motor functionality.

In this type of models the energy liberated in a chemical reaction acts to rectify the fluctuations produced by the thermal bath which allows the system to move in one particular direction. The simplest idea can be illustrated by the evolution of a dynamical system with one degree of freedom x. With this degree of freedom we can associated a particular free energy landscape $V(x,t)$. The system interacts with a thermal bath, which we model by the Langevin equation [68]. For a single particle of finite mass m we obtain

$$\begin{cases} v = \dfrac{dx}{dt} \\ m\dfrac{d^2x}{dt^2} = -\dfrac{\partial V(x,t)}{\partial x} - \eta\dfrac{dx}{dt} + \sqrt{2\eta k_B T}\ \xi(t) \end{cases} \tag{2.27}$$

Usually the motor motion is dominated by viscous friction, due to the small size of the motor and the inertial terms can be neglected. Then the motion of the particle is described by the overdamped Langevin equation:

$$\eta\frac{dx}{dt} = -\frac{\partial V(x,t)}{\partial x} + \sqrt{2\eta k_B T}\ \xi(t) \tag{2.28}$$

where η is the viscous drag coefficient and $\sqrt{2\eta k_B T}\xi(t)$ is the random Langevin force which is prescribed by the following two moments in accordance with the fluctuation dissipation

theorem:

$$\begin{aligned} \langle \xi(t) \rangle &= 0 \\ \langle \xi(t)\xi(s) \rangle &= 2\eta k_B T \delta(t-s) \end{aligned} \tag{2.29}$$

Here $\langle \bullet \rangle$ denote the ensemble average and $\delta(t)$ is the Dirac function. What makes this system Brownian ratchet is a particular time dependence of the energy landscape. In particular, the potential $V(x,t)$ must brake the phase space symmetry of the system which is a necessary condition of generating a non-zero probability flux. More specifically, the potential $V(x,t)$ can be chosen in the following form:

- $V(x,t) = V(x) - xf(t)$, where the correlated noise signal $f(t)$ is an additive time depended force. We call such a model the tilting or rocking ratchet. The space depended part $V(x)$ is space periodic with period L. The function $f(t)$, or the colored noise, describes the external source of energy and it is often chosen to be time periodic. If we want the system to be able to generate a net directional flux, then one of the two: the space periodic potential $V(x)$ or the time periodic signal $f(t)$ must be chosen asymmetric. The simplest example of the rocked thermal ratchet was proposed by Magnasco [72]

- $V(x,t) = \Psi(t)V(x)$, where the colored noise is $\Psi(t)$. We call such a model the flashing ratchet. The space depended potential $V(x)$ is periodic with period L. We can interpret the function $\Psi(t)$, as the switch which modifies the amplitude of the potential $V(x)$. The simplest form of the function $\Psi(t)$ is "on-off" flashing, when $\Psi(t)$ takes only two value 1 and 0 and switches between them with a fixed time rate. Once again to obtain a net directional flux, one of the two: space periodic potential $V(x)$ or time periodic excitation $\Psi(t)$ must be chosen asymmetric. The simplest example of the flashing ratchet was proposed by Ajdari and Prost [3]

Instead of using the colored noise one can consider the system with multiple thermal baths as was originally proposed by Feynman. A simple example of such Brownian ratchet is the motor driven by the position dependent temperature as in the model of Büttiker and Landauer [9, 66]. In this model a Brownian particle is in contact with different reservoirs at different positions, and is driven by the following Langevin equation:

$$\begin{cases} v = \dfrac{dx}{dt} \\ m\dfrac{d^2x}{dt^2} = -\dfrac{\partial V(x)}{\partial x} - \eta\dfrac{dx}{dt} + \sqrt{2\eta k_B T(x)}\ \xi(t) \end{cases} \tag{2.30}$$

The model describes the motion of a Brownian particle with mass m and drag coefficient η in a potential $V(x)$; x denotes the position of the particle and $\xi(t)$ is a Gaussian white noise. The potential $V(x)$ is a space periodic with space period L. The temperature function $T(x)$ varies along the potential with values T_1 and T_2, where $T_1 > T_2$, and is also periodic with period L. The energetics of this model was studied in [**?**, 2].

A Brownian ratchet model with direct relevance to muscle contraction was proposed by Ajdari, Jülicher and Prost [3, 52, 55]. It is a flashing ratchet where the colored component of the noise is used as a multiplicative term in the energy modifying the amplitude of the potentials barriers. To explain the functioning of this ratchet we can instead of using the Langevin representation pass directly to the Fokker-Planck description.

Suppose that we have two energy landscapes W_1 and W_2 and in this sense it is a two-state model, see Fig.2.8a). Different energy landscapes correspond to different chemical

states, for example, attached and detached states of the myosin head may have different interaction with an actin filament. Generally, the potentials are L periodic $W_i(x+L) = W_i(x)$ and are asymmetric $W_i(x) \neq W_i(-x)$.

The evolution of the probability density functions describing each of the states is governed by the coupled equations:

$$\begin{aligned} \partial_t P_1(x,t) + \partial_x J_1(x,t) &= -P_1(x,t)\omega_{12} + P_2(x,t)\omega_{21} \\ \partial_t P_2(x,t) + \partial_x J_2(x,t) &= -P_2(x,t)\omega_{21} + P_1(x,t)\omega_{12} \end{aligned} \tag{2.31}$$

where ω_{12} and ω_{21} are transition rate functions with period L, see Fig.2.8.a). As in chemo-

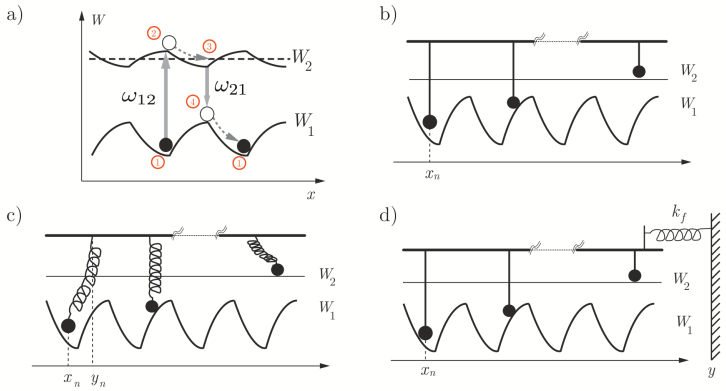

Figure 2.8. Flashing ratchet model of molecular motors developed by J.Prost, F.Jülicher, A.Ajdari. a) The sketch of general two state model with two space periodic potential W_1 and W_2, both potentials are space periodic asymmetric function. W_1 and W_2 define attached and detached state. For myosin II description, W_2 is usually flat, dashed black line. The detachment activated in the minima of well of potential W_1. At the unbound state W_2 particle excited to jump in the maxima of potential W_1, where the potential slop imitate the power-stroke force generation. b) The schematic presentation of collective model of rigid motors based on "on-off ratchet", where W_1 is space periodic potential presented the attached state and $W_2 = 0$ – it is detached state. The motions obtain by switching between this two state. c) the picture with collective soft motors taking in account the individual elasticity of motor. d) The sketch of collective model with added quadratic potential, presented by k_f.

mechanical models, the transition rates between the two states need to be prescribed. The necessary condition to obtain a directed motion is to break the detailed balance. To this end the transition functions ω_{12} and ω_{21} are related as follows:

$$\Omega(x) = \omega_{12}(x) + \omega_{21} e^{-\frac{W_1(x) - W_2(x)}{k_B T}} \tag{2.32}$$

where $\omega_{12}(x)$ is a function which controls the local deviation from thermal equilibrium [54, 92, 85, 51]. The two-state model is consistent with the observed behavior of biological motors and reproduces the typical force-velocity relation. In order to model the cooperative effects in muscle fibers, N motors can be fixed on a rigid backbone, [53] or a quadratic potential can be added to take into account the elasticity of the backbone, Fig.2.8c). Such system shows dynamical instability around the stall force regime and can exhibit bi-directional motion,[30, 31].

One can say that the models of Brownian ratchets incorporate the idea of the power stroke implicitly. More specifically, in those models the power-stroke is not associated with a conformational change occurring without net displacement along the molecular

track, but is viewed as any motion down the energy well which generates elongation of the linear spring. One of the goals of our work will be to extend the Brownian ratchet models in the direction of accounting for the conformational change more explicitly. Another limitation which we try to overcome is the assignment of activity exclusively to the actin filament through either rocking or flashing terms in the energy. Instead, we shall attempt to interpret the power stroke as the driving force of the process which is stimulated directly by the ATP hydrolysis.

2.5.1 Kinesin models

As an inspiration of our approach, we discuss here a different type of Brownian ratchets which have been so far applied exclusively for the description of dimeric motors such as Kinesin . In this class of models each motors are represented as two particles rather than one with each particle moving along the same periodic potential. This potential is asymmetric and has periodic wells which represented the binding sites. The particles are connected by a bi-stable spring representing a conformational change responsible for the advance of the motor.

The simplest model of this type [14] is governed by the following system of overdamped Langevin equations:

$$\begin{aligned} \gamma\frac{dx_1}{dt} &= -\frac{\partial V(x_1)}{\partial x_1} - f_{load} - k\left[x_1 - x_2 - l(t)\right] + \sqrt{2k_BT\gamma}\xi_1(t) \\ \gamma\frac{dx_2}{dt} &= -\frac{\partial V(x_2)}{\partial x_2} - f_{load} + k\left[x_1 - x_2 - l(t)\right] + \sqrt{2k_BT\gamma}\xi_2(t) \end{aligned} \tag{2.33}$$

where $x_{1,2}$ denote positions of the particles, γ is the frictional drag coefficient and $V(x)$ is the ratchet potential with a periodically placed piecewise linear wells and flat barriers; it is essential that the well slope in backward direction is steeper when in the forward direction see Fig.2.9. The parameter k denotes the stiffness of the bi-stable unit and $l(t)$ is the rest length which can take two values. Finally, $\xi_{1,2}(t)$ is again the Gaussian white noise with autocorrelation function $\langle\xi_i(t)\xi_j(s)\rangle = 2k_BT\gamma\delta_{i,j}\delta(t-s)$ for $i,j = 1,2$. The external load force f_{load} can be applied as well.

The bi-stability of the system rests in the fact that the parameter $l(t)$ takes alternatively two values $-l_{min}$ and l_{max}. The switch between the two quadratic wells is governed by a stochastic process which plays the role of the source of disequilibrium. Indeed, the ATP induced switches of the rest length push the system out of thermal equilibrium and provide the driving force to pull the cargo. The motor proceeds in a step by step fashion in one direction, and shows different velocities at different external loads; the two limiting values, l_{min} and l_{max}, can be designed to produce realistic size of the power stroke. To illustrate the working of this ratchet suppose that $l_{min} = 0$ and the two particles start from the same reference position. The change of the rest length, initiated by a stochastic process, pushes the two heads in the opposite directions. Because of the asymmetry of the potential, only one head makes a forward step of $8nm$ relaxing the spring. This unstrained configuration is again perturbed by the sudden change of the reference length that comes back to zero. Now the two heads are pulled together and end up again in the same well because the asymmetry of the potential facilitates the forward step of the second head.

The model shows good agreement with kinesin experiments, see Fig.2.9, and can be considered as rather realistic. Notice that the periodic potential in this model is passive and all activity is concentrated in the bi-stable element. However, the model can also be modified to move the activity into the periodic potential describing the (track) filament.

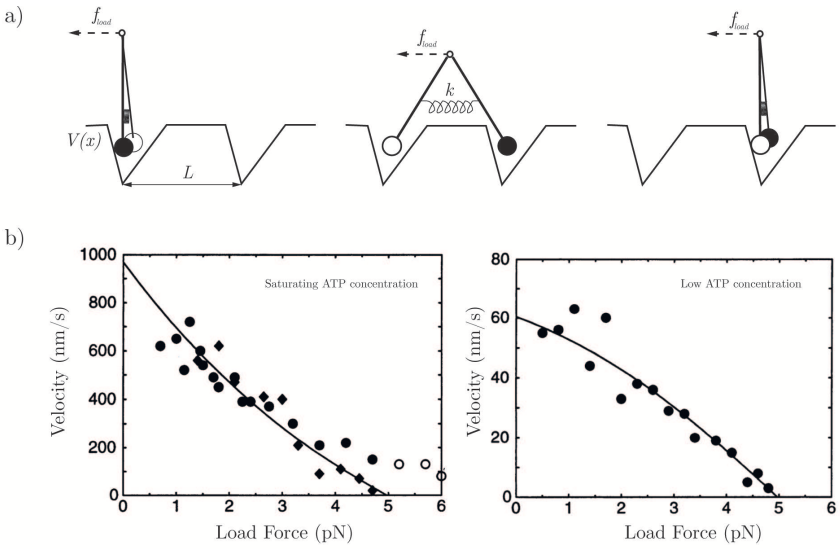

Figure 2.9. The I.Derényi and T. Vicsek model. a) Sketch of the potential shape $V(x)$ and the subsequent steps of the motor cycle, from left to right. b) The force-velocity curves for an individual motor at saturating ATP concentration, on the left part; and force-velocity at low ATP concentration. From [14]

Thus, in [79] the authors study the motion of two Brownian particles coupled by a bistable snap-spring on a periodically rocked landscape. Each of the particles is a Brownian ratchet in the sense defined above and the role of the bistable potential is to synchronize their motion. The corresponding system of overdamped Langevin equation can be written in the form

$$\begin{cases} \dfrac{dx}{dt} = -\dfrac{\partial[\Phi(x) + V(x-y)]}{\partial x} + f_{tilt}(t) + \sqrt{2D}\ \xi_x(t) \\ \dfrac{dy}{dt} = -\dfrac{\partial[\Phi(y) + V(x-y)]}{\partial y} + f_{tilt}(t) + \sqrt{2D}\ \xi_y(t) \end{cases} \tag{2.34}$$

where $\Phi(x)$ and $\Phi(y)$ are two identical dimensionless ratchet potentials submitted to time periodic rocking with intensity $f_{tilt}(t)$ which has zero average. The x and y are positions of two legs and the rocking term act simultaneously on both positions.The bistable potential $V(x-y)$ describes the interaction between the two legs. The parameter D is the intensity of the zero-mean statistically independent Gaussian white noises $\xi_x(t)$ and $\xi_y(t)$ acting on particles x and y. The periodic rocking places the system out of thermal equilibrium. The asymmetry of the ratchet potential ensures that this system can move directionally and generate force if constrained.

2.6 Conclusions

Several models reviewed in this section represent different aspects of muscle contraction and acto-myosin interaction. Each one emphasizes a particular physical aspect of the problem and can be viewed as prototypical. None can be considered as fully comprehensive which is not surprising in view of the enormous complexity of the underlying problem.

Most of the models are able to reproduce some experimental measurements at the expense of introducing various phenomenological elements and bringing in fitting functions and dependencies. The freedom to introduce intermediate power-stroke states and the

multiplicity of the ways to break the detailed balance creates undesirable ambiguity. On the other hand, the schematic models blend different states of the minimal Lymn-Taylor cycle and do not allow to distinguish the power stroke from the attachment process. In general, the most sophisticated fitting schemes mix mechanical and chemical description and bring together jump and continuous stochastic processes. Different groups of researchers disagree on where the ATP activity resides: in the attachment phenomenon, in the power stroke or in both.

In this Thesis we attempt to formulate a set of simple toy-models which bring together the ideas of Brownian ratchets focusing on attachment detachment and the ideas of Huxley and Simmons regarding the functioning of the power stroke element. We try to remain in the purely mechanical framework and keep the description fully transparent mathematically. Interestingly, to achieve such synthesis we need to overcome the distinction between processive and non-processive motors making our model applicable for the description of both a single-legged non-processive molecular motor Myosin II and a double-legged processive motor kinesin. In the following sections we introduce our techniques step by step, and then study systematically several model archetypes in the attempt to finally provide a definitive mechanical interpretation of the Lymn-Taylor cycle.

Chapter 3

Ratchet element

In the large family of known Brownian ratchets, one model stands out as truly mechanical in the sense that it is quite clear how the corresponding device can be built and reproduced in the lab. This is a model of Magnasco [72] which we first tried to generalize in order to accommodate for the conformational change and then ended up completely rewriting. In this section we present an extended discussion of the original model which incorporates later contributions as well [56]. In addition to the known results this section contains new studies of the Magnasco ratchet placed in a mixed/hard device regime and offers a comparison of the efficiency of the energy transduction in this system under different loading conditions. Most importantly we systematically study the validity of the adiabatic approximation adopted unconditionally by Magnasco and his followers and compare the analytical results available in this approximation with the results of direct numerical simulation of the stochastic Langevin equation.

3.1 Formulation of the model

The goal of the modeling is to ensure directed motion of a randomly walking particle in a periodically rocked asymmetric potential. The associated one dimensional overdamped Langevin equation reads

$$\eta\frac{dx}{dt} = -\partial_x V(x) + f_{tilt}(t) + \sqrt{2\eta k_B T}\ \xi(t) \tag{3.1}$$

where dx/dt is the velocity of the particle, η is the drag coefficient, k_B is the Boltzmann constant and T– the absolute temperature. The random environment is represented by the white noise $\xi(t)$, while the ATP activity is modeled by the time periodic force $f_{tilt}(t)$, which rocks the infinitely periodic energy landscape $V(x)$.

It is convenient to rewrite (3.1) in dimensionless form. We use the following definitions of the nondimensional variables:

$$\begin{aligned}
\tilde{x}\left(\tilde{t}\right) &\equiv \frac{1}{L}x\left(t=\tau\tilde{t}\right)\\
\tilde{V}\left(\tilde{x}\right) &\equiv \frac{1}{V_{max}}V\left(x=L\tilde{x}\right)\\
\tilde{f}_{tilt}\left(\tilde{t}=\frac{t}{\tau}\right) &\equiv \frac{L}{V_{max}}f_{tilt}(t)\\
\tilde{\xi}(\tilde{t}) &\equiv \xi(t)\tau^{-1/2}
\end{aligned} \tag{3.2}$$

where the time scale is chosen as follows

$$\tau = \frac{\eta L^2}{V_{\max}} \tag{3.3}$$

Here L the typical length inside the model, and $V_{\max}$ is the energy scale. Applying the transformation we obtain a new dimensionless parameter $D = \frac{k_B T}{V_{max}}$ and rewrite (3.1) in the form

$$\frac{dx}{dt} = -\partial_x V(x) + f_{ext} + f_{tilt}(t) + \sqrt{2D}\ \xi(t) \tag{3.4}$$

Here we added an external force f_{ext} representing the cargo which was absent in the original model of Magnasco. We assume that the ratchet potential $V(x)$ is periodic with period L, see Fig.3.1. The time periodic driving force $f_{tilt}(t)$ is a symmetric square wave-like function with amplitude A, see Fig.3.1. Obviously the time averaged effect of the rocking force $f_{tilt}(t)$ must be equal to zero because otherwise we are dealing with a standard mechanical ratchet. It is easy to show that in the absence of the tilting force the system reaches

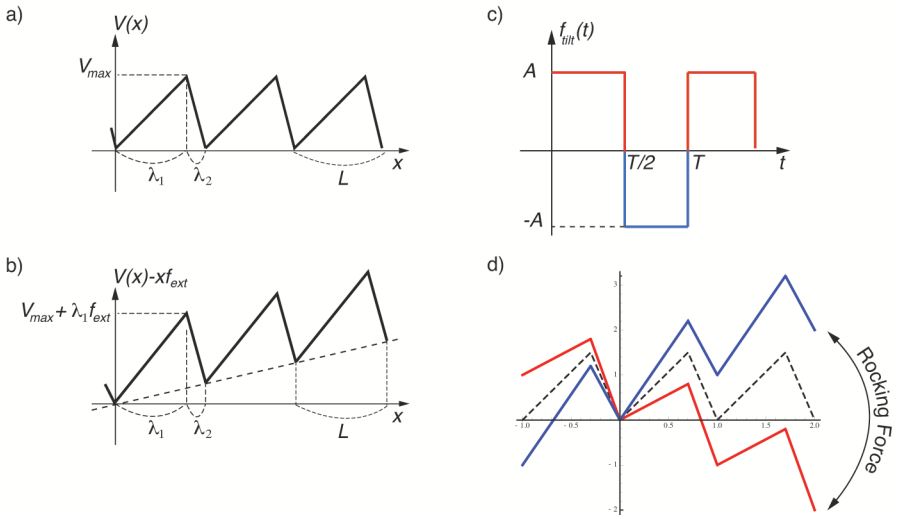

Figure 3.1. a) Scheme of sawtooth ratchets potential $V(x)$ with space period $L = \lambda_1 + \lambda_2$ and asymmetry $\Delta = \lambda_1 - \lambda_2$. b) Scheme of sawtooth ratchets potential with conservative load $V(x) - xf_{ext}$. c) Scheme of a slow square wave time periodic function $f_{tilt}(t)$ of amplitude A and time period T. d) Action of rocking force on saw-tooth potential.

thermal equilibrium with zero net current. However, as we show below the interplay between asymmetry and out-of-equilibrium (meaning correlated) fluctuations is able to produce the systematic net motion.

In addition to Langevin equation (3.4) we'll be also using the corresponding Fokker-Planck equation

$$\frac{\partial P(x,t)}{\partial t} = \frac{\partial}{\partial x}\left[\left(-\frac{\partial V(x)}{\partial x} + f_{ext} + f_{tilt}(t)\right) P(x,t)\right] - D\frac{\partial^2 P(x,t)}{\partial x^2} \tag{3.5}$$

where $P(x,t)$ is the distribution function for the mechanical variable x indicating the probability for particle to be at point with coordinate x at time t.

3.2 Adiabatic limit

In general the linear equation (3.5) with time dependent coefficients can be solved only numerically. However, if the rocking combines slow and fast stages, one can search for piece wise stationary solutions. Indeed, when the potential changes shape it takes some time for the system to relax to equilibrium and if the rocking is much slower than the time of relaxation, the piece wise equilibrium approximation known also as adiabatic approximation, may be adequate. To find stationary solution we need to fix the tilting force and solve the Fokker-Planck equation with $\partial_t P(x,t) = 0$. Moreover, in the case of tilted periodic potential such stationary distributions can be obtained in quadratures [98].

Suppose for determinacy that the periodic rocking force is taken in the form of a square wave signal with period T and amplitude A.

$$f_{tilt}(t) = \begin{cases} +A & \text{for } n\dfrac{T}{2} \le t \le (n+1)\dfrac{T}{2}, \\ -A & \text{for } (n+1)\dfrac{T}{2} \le t \le nT,\ n \in \mathbb{N} \end{cases} \tag{3.6}$$

. In the adiabatic approximation we assume that the period T is sufficiently large. To obtain stationary solutions of (3.5) with $f_{tilt}(t) = f = \pm A$ it is convenient to define the potential $\Phi(x) = V(x) - xf - xf_{ext}$. B y using the fact that the flux

$$J = [\partial_x V(x) - f - f_{ext}]P(x) - D\partial_x P(x) \tag{3.7}$$

is constant we obtain the following stationary distribution

$$P_{st}(x) = P_0 \exp(-\frac{\Phi(x)}{D}) - \frac{J}{D}\exp(-\frac{\Phi(x)}{D}) \int_0^x \exp(\frac{\Phi(x)}{D})dx. \tag{3.8}$$

To find the integration constants P_0 and J we recall that the stationary probability distribution $P_{st}(x)$ must be periodic with period L. By using the fact that $\Phi(x + nL) = \Phi(x) - nL(f + f_{ext})$ we can then write

$$J\int_0^L \exp(\frac{\Phi(x)}{D})dx - P_0 D\left[1 - \exp(-\frac{L(f+f_{ext})}{D})\right] = 0 \tag{3.9}$$

To find the second condition we can use the normalization of the probability density $\int_0^L P(x)dx = 1$. We obtain

$$P_0 \int_0^L \exp(-\frac{\Phi(x)}{D})dx - \frac{J}{D}\int_0^L \exp(-\frac{\Phi(x)}{D}) \int_0^x \exp(\frac{\Phi(x')}{D})dx'dx = 1 \tag{3.10}$$

We can now eliminate P_0 and obtain the following expression for J as a function of f and f_{ext}:

$$J(f, f_{ext}) = \frac{D\left(1 - e^{-\frac{L(f+f_{ext})}{D}}\right)}{\int_0^L e^{\frac{\Phi(x)}{D}}dx \int_0^L e^{-\frac{\Phi(x)}{D}}dx - \left(1 - e^{-\frac{L(f+f_{ext})}{D}}\right)\int_0^L e^{-\frac{\Phi(x)}{D}} \int_0^x e^{\frac{\Phi(x')}{D}}dx'dx} \tag{3.11}$$

Notice that the stationary current carries information about the time scale of the system, because it is proportional to the inverse of the time necessary for the particle to cross the length of one spacial period.

To be more specific consider the following expression for the asymmetric saw-tooth L-periodic potential

$$V(x) = \begin{cases} \frac{2V_{max}}{L}(x - nL) \quad for \quad nL \leq x < nL + \frac{L}{F}, \\ \frac{2V_{max}}{L}((n+1)L - x) \quad for \quad nL + \frac{L}{2} \leq x < (n+1)L, \ n \in \mathbb{N} \end{cases} \tag{3.12}$$

The shape of the potential is chosen to be asymmetric with the asymmetry factor $\Delta = \lambda_1 - \lambda_2$ defining the direction of the motion. In this case the integrals can be computed explicitly and we obtain

$$J(f, f_{ext}) = \frac{{P_2}^2 \sinh(\frac{L(f+f_{ext})}{D})}{\frac{DL^2}{V_{max}^2}\left(\cosh(\frac{V_{max} - \Delta\frac{f+f_{ext}}{2}}{D}) - \cosh(\frac{L(f+f_{ext})}{2D})\right) - \frac{2LP_1P_2}{V_{max}}\sinh(\frac{L(f-f_{ext})}{2D})} \tag{3.13}$$

where

$$P_1 = \Delta + \frac{(f - f_{ext})(L^2 - \Delta^2)}{4V_{max}}, \quad \text{and} \quad P_2 = \left(1 - \frac{\Delta(f - f_{ext})}{2V_{max}}\right)^2 - \left(\frac{L(f - f_{ext})}{2V_{max}}\right)^2 \tag{3.14}$$

For the square wave rocking the tilting force takes the value A during one half of the period and $-A$ during the second half of the period. Therefore the parameter f in (3.13) takes two value A and $-A$. To obtain the average value of the current we need to compute

$$\langle J(f, f_{ext})\rangle_t = \frac{1}{T}\int_0^T J(f_{tilt}(t), f_{ext})dt \tag{3.15}$$

When T is sufficiently large we can approximate this integral by the following expression

$$J_{avg} = \frac{1}{2}[J(A, f_{ext}) + J(-A, f_{ext})] \tag{3.16}$$

The mean drift velocity $\langle v\rangle$ is then given by the expression

$$\langle v\rangle = LJ_{avg} \tag{3.17}$$

We can now apply our analytical results to study the parametric dependence of the model. In our subsequent discussions we make the following selection of the secondary parameters: $V_{max} = 1.5$, $\lambda_1 = 0.7$, $\lambda_2 = 0.3$ and $L = 1$.

The main object of study is the particle current, or the average velocity, as a function of the amplitude A. We first assume that the temperature is fixed and that $f_{ext} = 0$, meaning that there is no cargo in the system.

Our formula (3.13) with a positive value of parameter f gives the behavior of system tilted to the right, while with negative f we obtain the behavior of the system tilted to the left. In Fig.3.2a) we show the behavior of both positive and negative branches as functions of the tilt magnitude A. Since the two branches are not symmetric the average probability flux in the adiabatic limit defined in (3.16) is different from zero, see Fig.3.2b). The particle moves in forward direction along the x axis following the forward asymmetry of the ratchet potential $\lambda_1 > \lambda_2$.

In Fig.3.2c) we show the region of low amplitude forcing, where the temperature increase helps to increase the current. In this region of parameters the particle extracts

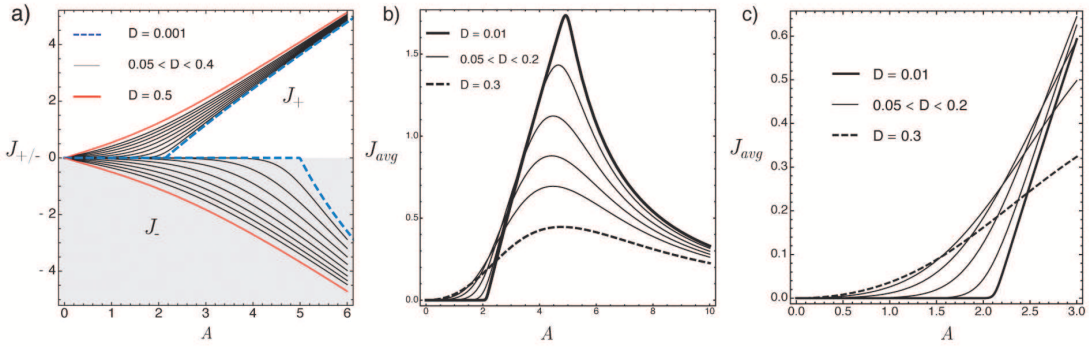

Figure 3.2. The adiabatic probability flux J_{avg} (average velocity) as function of amplitude A for increasing temperatures D in soft device with $f_{ext} = 0$. a) The behavior of positive and negative branches $J_{\pm}$ as functions of the tilt magnitude A. Note, the two branches are not symmetric. b) We show the J_{avg} for increasing values of D from bottom to down, the thick solid line $-D = 0.03$, the dashed line – $D = 0.3$. As we see the probability current vanishes with increasing of temperature and amplitude. c) The region of low amplitude forcing, where the temperature increase helps to increase the probability current.

energy form the thermal bath in order to cross the potential barriers. Interestingly, that here it is not the average tilt but its dispersion that drives the motion.

In Fig.3.2b) and Fig.3.2c) we show the dependence of J_{avg} on temperature (diffusion coefficient). As we see for small values of D there is a threshold in the forcing amplitude A, below which the probability current has almost zero value. For the moderate value of forcing, J_{avg} is an increasing function of A and we observe the maximum at A close to 5. For high amplitudes of the forcing J_{avg} decreases again. The hight level of the correlated input signal destroys the ratchet functionality. The high level of temperature has the same effect, see Fig.3.2. One can use these data to optimize the ratchet's output velocity.

The same analysis can be performed in the presence of external load f_{ext}. Thus, in Fig.3.3 we show the results of the computations performed for same model parameters as in Fig.3.2, but at the fixed value of external load $f_{ext} = 0.3$. The general trends do not

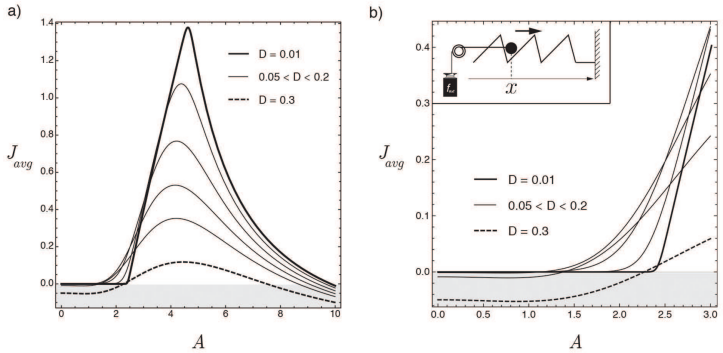

Figure 3.3. The adiabatic probability flux J_{avg} (average velocity) as function of amplitude A for increasing temperatures D in soft device with $f_{ext} = 0.3$. a) The J_{avg} for increasing value of D from bottom to down, the thick solid line $-D = 0.03$, the dashed line – $D = 0.3$. Note the emergence on the negative values of the current in the regimes with small forcing amplitude and high temperature. b) The region of low amplitude tilting, the presence of thermal fluctuations is crucial.

change however we observe the emergence on the negative values of the current in the regimes with small forcing amplitude and high temperature. The probability flux in this domain of parameters changes its direction, meaning that the external input of energy is not sufficient for the particle to carry the load and it is instead being dragged by the load. However, for sufficient large amplitude of forcing we observe that the system can perform the mechanical work against the external load. As in the case with no load the presence of thermal fluctuations is crucial in the regime with small amplitude of forcing. It

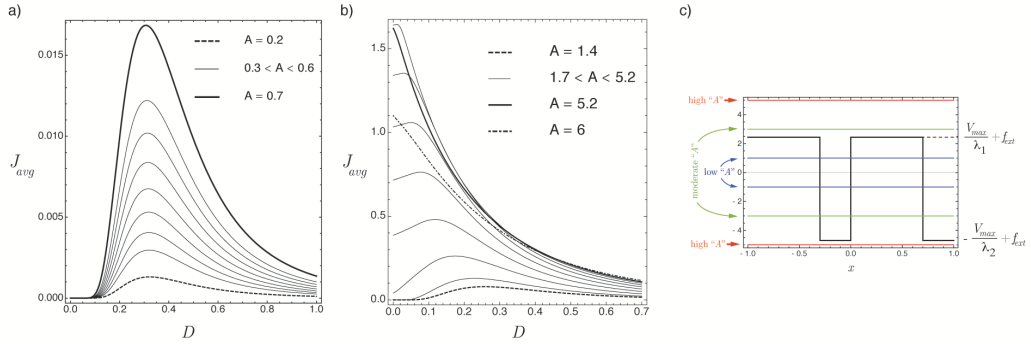

Figure 3.4. The behavior of the probability flux J_{avg} as function of temperature D at different amplitude A in soft device with $f_{ext} = 0$. a) The probability flux is maximized at a finite value of temperature. The amplitude A increases from bottom to top, we show the flux behavior at lowest A with black dashed line and at highest A – with solid thick line. b) The plot of probability flux in the three different regimes of rocking: for low, intermediate and hight amplitude A. c) The three different regimes of rocking force. With black solid lines we show the derivative $\partial_x[V(x) - xf_{ext}]$, with blue line we show the low amplitude range, with green lines - the intermediate range, and with red line - the high amplitude range

is instructive to study the behavior of the probability flux as a function of temperature at different amplitudes of forcing, see Fig.3.4. One can see that at low amplitudes of tilting, see Fig.3.4a), the probability flux is maximized at a finite value of temperature where the ratchet uses the thermal energy to generate the motion in the optimal way.

In general, we can distinguish three regimes where the behavior of the probability flux J_{avg} as function of temperature is radically different:

- the low amplitude regime, $A < \frac{V_{max}}{\lambda_1} - f_{ext} < \frac{V_{max}}{\lambda_2} + f_{ext}$
- the moderate amplitude regime, $\frac{V_{max}}{\lambda_1} - f_{ext} < A < \frac{V_{max}}{\lambda_2} + f_{ext}$,
- the high amplitude regime, $\frac{V_{max}}{\lambda_1} - f_{ext} < \frac{V_{max}}{\lambda_2} + f_{ext} < A$

In Fig.3.4c) we show the simple illustration of these three regimes. With black solid lines we show the derivative $\partial_x[V(x) - xf_{ext}]$, with blue line we show the low amplitude range, with green lines - the intermediate range, and with red line - the high amplitude range. In Fig.3.4b) we display all three regimes. We notice that the flux shows a local maximum at finite temperature in the range of low values of A. With increasing A the maximum vanishes progressively by transforming into the plateau-like region. At large amplitudes of the rocking force the system reaches the mechanical regime, where the flux becomes a monotonically decreasing function of temperature. However, as we show later in this section, one has to be careful in making conclusions from the adiabatic approximation at low temperatures where the internal time scale may diverge.

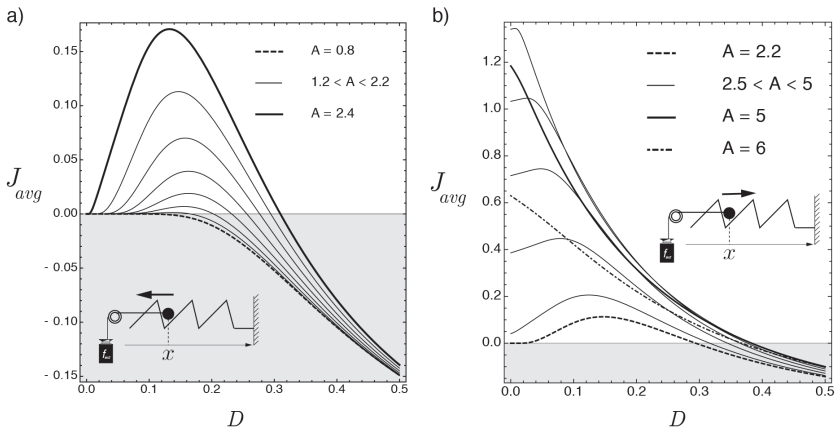

Figure 3.5. The behavior of the probability flux J_{avg} as function of temperature D at different amplitude A in soft device with $f_{ext} = 0.3$. a) The J_{avg} plotted for increasing value of A, from down to bottom, the lowest value with black dashed line and the highest – with solid thick line. The function is maximised at finite temperature in regime of low forcing. We observe the interval where the functions take a negative value, the system does not perform any work. b) The plot of probability current in three different regime: for low, intermediate and hight amplitude forcing. The flux shows a local maximum at finite temperature in the range of low values of A. At large amplitudes of the rocking force the system reaches the mechanical regime, where the flux becomes a monotonically decreasing function of temperature.

The system exhibits almost the same behavior in the presence of an external load $f_{ext} = 0.3$, see Fig.3.5. Thus in Fig.3.5b), we see a maximum of the flux at finite temperature and low A. With increasing A the maximum vanishes progressively. One again finds that J_{avg} may become negative in the high temperature regime which means that the ratchet effect disappears. In this regime the system is carried by the load and the motor is unable to perform useful mechanical work.

3.3 Validity of the adiabatic approximation

The above theoretical analysis and the corresponding simulations were based on the assumption that the forcing frequency is much lower than the internal frequencies of the system. To check the validity of this assumption we now compare the result obtained in adiabatic approximation with direct numerical simulation of the Langevin equation (3.4). In our numerical simulations we use the standard Euler scheme which is largely sufficient to obtain the stable results considering the simple form of the potential. To ensure numerical stability of the dynamics we take the time step to be sufficiently small $\Delta t = 10^{-3}$. The total time of observation is about 100 times the period of rocking force. At $t = 0$ we assume that the particle is at $x = 0$ with zero velocity, however, since we search for the steady state regime we also tried uniform distribution of initial conditions over one period of the potential. The ensemble averaging was performed over 10^4 trajectories.

Below we present the results of a series of numerical experiments which confirm the consistency of our adiabatic approach and also reveal the parameter ranges where it fails. The numerical results are juxtaposed with our analytical results representing stationary solution of the Fokker-Planck equation in the adiabatic approximation. In Fig.3.6 we show by the solid lines the analytically computed results and by the skaters we depict

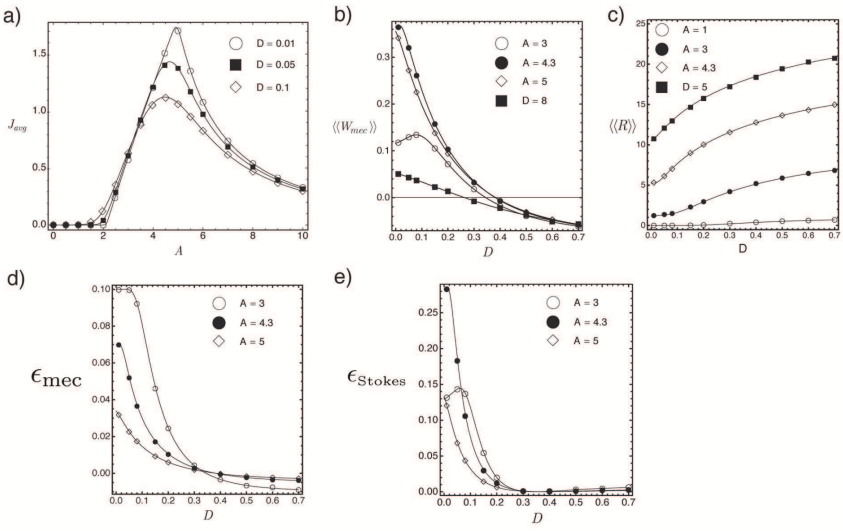

Figure 3.6. We show by the solid lines the analytically computed results and by the skaters we depict the corresponding results of the direct numerical simulation of the Langevin equation performed at a finite value of the time period $T = 120$ of the rocking force $f_{tilt}(t)$. a) The particle current versus amplitude A. b) The mechanical work W_{mec} versus temperature D. c) The average input of energy R versus temperature D. d) The mechanical efficiency versus D. e) The Stokes efficiency versus D. See the detailed definitions for efficiency functions below.

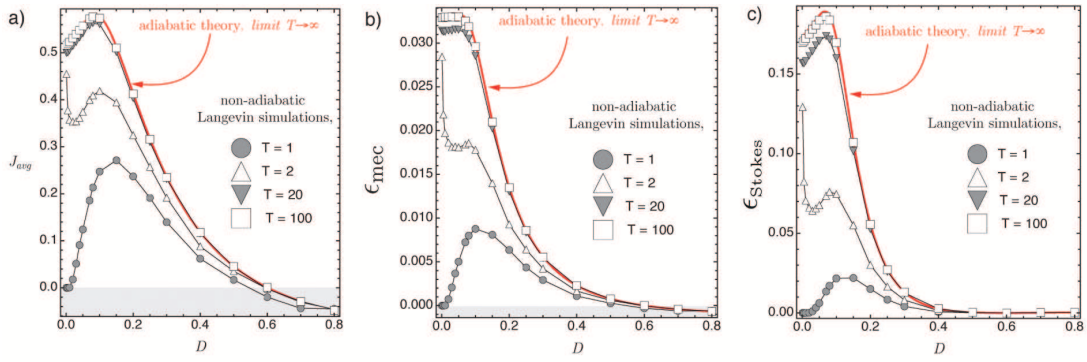

Figure 3.7. Comparison of the adiabatic theory and the direct numerical simulations. a) The probability flux versus D provided by the direct numerical simulation of the Langevin equation performed at a finite value of the time period T of the rocking force $f_{tilt}(t)$. b) The mechanical efficiency versus D provided by the direct numerical simulation of the Langevin equation performed at a finite value of the time period of the rocking force. c) The Stokes efficiency versus D provided by the direct numerical simulation of the Langevin equation performed at a finite value of the time period of the rocking force.

the corresponding results of the direct numerical simulation of the Langevin equation performed at a finite value of the time period of the rocking force. In order to reproduce the adiabatic regime in numerical simulations we take the tilting force $f_{tilt}(t)$ with a finite but sufficiently large value of the period T. Interestingly, in the regime of slow time variation of tilting force, sufficiently high precision can be obtained even for a stochastic ensemble characterized by rather low number of averaged trajectories, say 10^2. the reason

is that in regime of slow time variation of tilting force we are rather close to adiabatic behavior of the motor system.

One can see that our numeric computations reproduce the analytic results almost perfectly in a broad range of regimes. Here we used the standard scheme with constant time-step Δt in each numerical simulation however to capture the regimes with low amplitude of rocking while maintaining sufficient resolution we had to use much smaller time steps.

To summarize our results, for sufficiently large values of T, the numerical results are in full agreement with the adiabatic limit. For instance, we always observe three different regimes identified in the previous section in agreement with the adiabatic theory. For instance, in the regimes with low and moderate amplitude of rocking it is always possible to identify a finite temperature where the current is optimized before it decrease with increasing D (kind of adiabatic stochastic resonance) . At high amplitudes of the forcing, the current decreases monotonically as a function of temperature, because the ratchet effect becomes progressively unimportant in this regime.

The agreement between the adiabatic theory and the direct numerical simulations are not always perfect. Consider for instance a finite time period of rocking force, $T = 1$ and low value of the amplitude A. At low temperatures the behavior of the mechanical efficiency in this system (see the detailed definitions for this case below) can be different from the predictions of the adiabatic theory, see Fig.3.7b). Thus, in the direct numerical simulations we observe that the mechanical efficiency attains its maximum at a finite temperature. Instead, in the adiabatic theory we find that the efficiency is optimized at zero temperature. We explain the difference with the adiabatic theory by the fact, what at low temperature the internal time scale diverges and the adiabatic approximation becomes invalid.

3.3.1 Force velocity relation

The introduction of the external load f_{ext} in the motor potential function (which represents cargo) opens a possibility to study the efficiency of the energy transduction in our motor. By varying the value of the external force we can also recover the force-velocity relation, which furnishes a usual characterization of a motor. In our simulations we adopt a physical rather than physiological definition of the external load and plot the response in the axis $[\langle v \rangle,\ f_{ext}]$. In this case the motor performs useful work moving against an external forces. The negative sign of f_{ext} indicates the external load acts against the direction of the motion of the motor.

In the absence of the input energy provided by $f_{tilt}(t)$, the system quickly reaches the state of thermal equilibrium. In this state a non zero velocity indicates the action of an external force f_{ext}. The direction of the motion is fully determined by the sign of f_{ext}. In Fig.3.8a) we showed by the dashed line the behavior of the "force-velocity" relation in the limit of $A = 0,\ D = 0$, by solid black line we presented the behavior of the system for progressively increasing value of D, while keeping $A = 0$. One can see that in this passive system we obtain the classical features of the frictional behavior when the sign of the velocity is the same as the sign of the force.

In Fig.3.8b) we show the force-velocity curve for a similar system but in the presence of the active force $f_{tilt}(t)$, i.e. $A \neq 0$. The dashed line corresponds to the lowest value of D, the thick solid line–to the highest value of D. We observe that the emergence of the active region with $\langle v \rangle > 0, f_{ext} < 0$. In this domain the motor is able to perform the mechanical work against the imposed load. Different modes of operation of the motor can

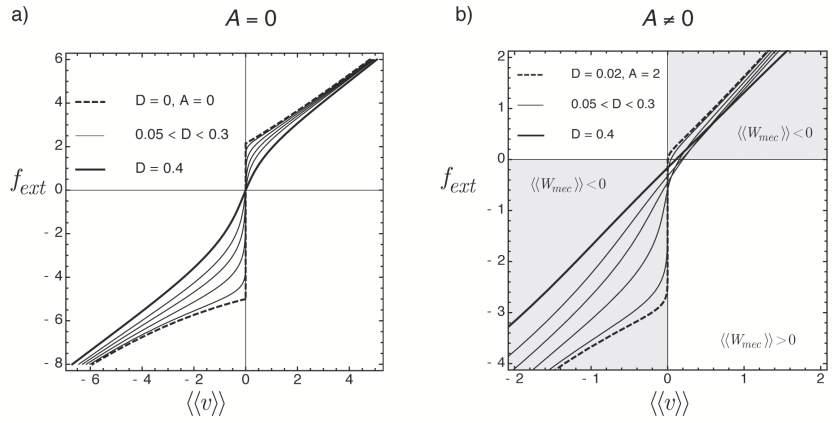

Figure 3.8. The plot of force-velocity relation for increasing temperature D. a) The plot of prediction adiabatic theory in absent of input of energy for $A = 0$ for increasing D; the dashed line –the pure mechanical behavior, $A = 0$ and $D = 0$, the thick line– the highest value D. b) The plot of prediction of adiabatic theory in presence of input energy, $A = 2$, for same increasing values of D.

be distinguished by looking at the sign of the energy dissipation produced by the system. Passive regimes correspond to the cases where the dissipation is positive meaning that $\langle v \rangle$ and f_{ext} have the same direction: both positive or both negative. That means that input energy is dissipated as in the classical nonequilibrium thermodynamics. More interesting are the active regimes where the motor can transform the input energy into mechanical work, i.e. the system anti-dissipates. In our representation such active regimes exist in the region where $\langle v \rangle > 0, f_{ext} < 0$. The motor uses the chemical energy of the ATP as the input and performs the mechanical work by moving with a positive velocity $\langle v \rangle$ against the negative force f_{ext}.

In Fig.3.9 we study the variation of the force-velocity relation with the amplitude of rocking at fixed temperature (constant D). The dashed line corresponds to the lowest value of A and the thick solid line–to the highest value of A. For small amplitudes of rocking the particle follows closely the external force and performs almost no mechanical work against the load. We need to surpass a threshold in the amplitude in order to generate significant active transport. The increase of A increases the associated maximum value of velocity at zero external load, which corresponds to the intersection of the force-velocity curve with the axis $f_{ext} = 0$. Also we observe the increase of the value of the stall force defined as the value of the load associated with zero average velocity of the motor. In other words it is the maximum load that the motor system is able to support without moving. Notice also that the probability current shows a maximum at a particular value of the amplitude A. Overall, the force velocity relation is nonlinear passing from concave to convex shape as the magnitude of the rocking force increases.

In Fig.3.10 we show the variation of the force-velocity relation with the temperature D for a fixed value of the rocking amplitude A. At zero temperatures the system follows the purely mechanical behavior without the stochastic term in the Langevin equation. The dashed line corresponds to the smallest value of D and the thick solid line–to the largest value of D. The increase of temperature (or diffusion coefficient) D progressively increases the area between the force-velocity curve and the axes $f_{ext} = 0$ and $\langle v \rangle = 0$. After the threshold in D, as we have seen in the study of a free particle, the ratchet phenomenon gets progressively lost, and the motor loses the ability to perform the mechanical work against

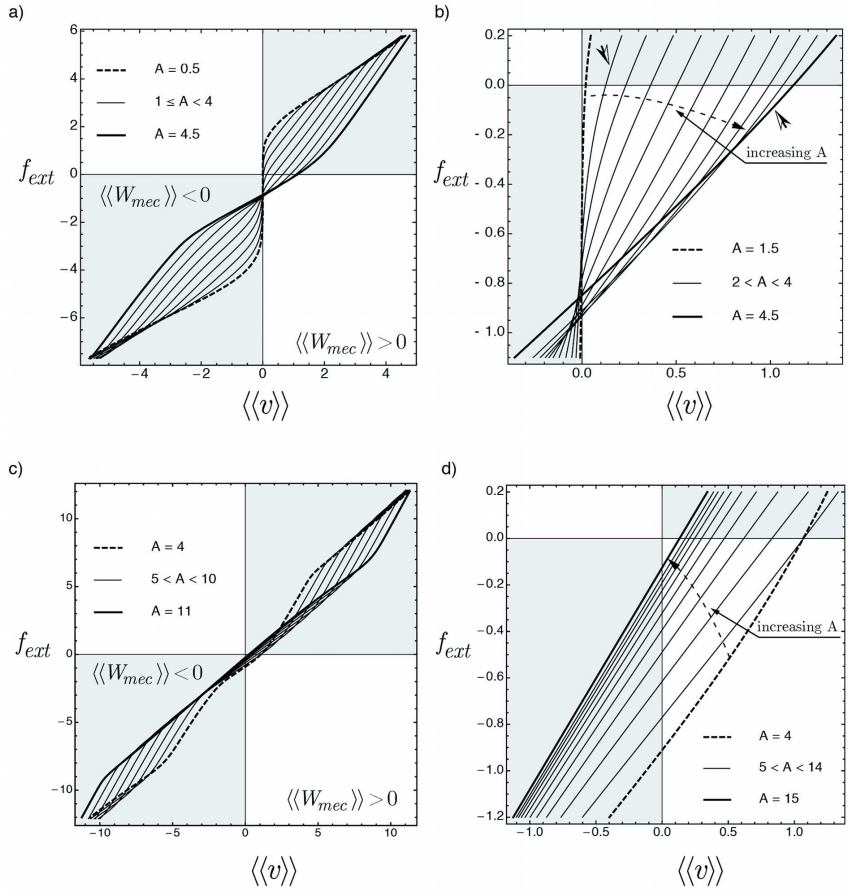

Figure 3.9. The variation of the force-velocity relation with the amplitude A of rocking at fixed temperature $D = 0.01$ in adiabatic theory. a) The force velocity response with variation of A in interval $0.5 < A < 4.5$, the dashed line corresponded to $A = 0.5$, solid line to $A = 4.5$. On the b) we show only the region of positive mechanical work, we notice the non-linear characteristics of force-velocity curves the note the convex and concave force-velocity relation indicating by arrows. c) The force velocity response with variation of A in interval of hight amplitude value of rocking force A, $A > 5$, the dashed line corresponded to $A = 4$, solid line to $A = 11$. d) We show only the region of positive mechanical work. The non-linearity vanished for linear behavior in region of positive mechanical work.

the external load. We notice the pronounced concave character of the force-velocity curve at low value of the rocking amplitude A and low temperatures, see Fig.3.10a); the convex force-velocity curve is obtained at intermediate values of A and low temperatures, see Fig.3.10c).

3.3.2 Hard/mixed device

So far we have been studying the behavior of the Magnasco ratchet in a soft device which implied that we applied external conservative load. In particular we associated the (maximal) force developed by the motor at zero average velocity with the stall force. Another way to measure this force is to introduce the hard/mixed device by attaching to the motor a fixed spring and measuring the developed average displacement.

Consider a coupled system where the ratchet is attached to a linear spring with the fixed stiffness k_m. We impose the constant elongation to the free end of the spring $z = Const.$

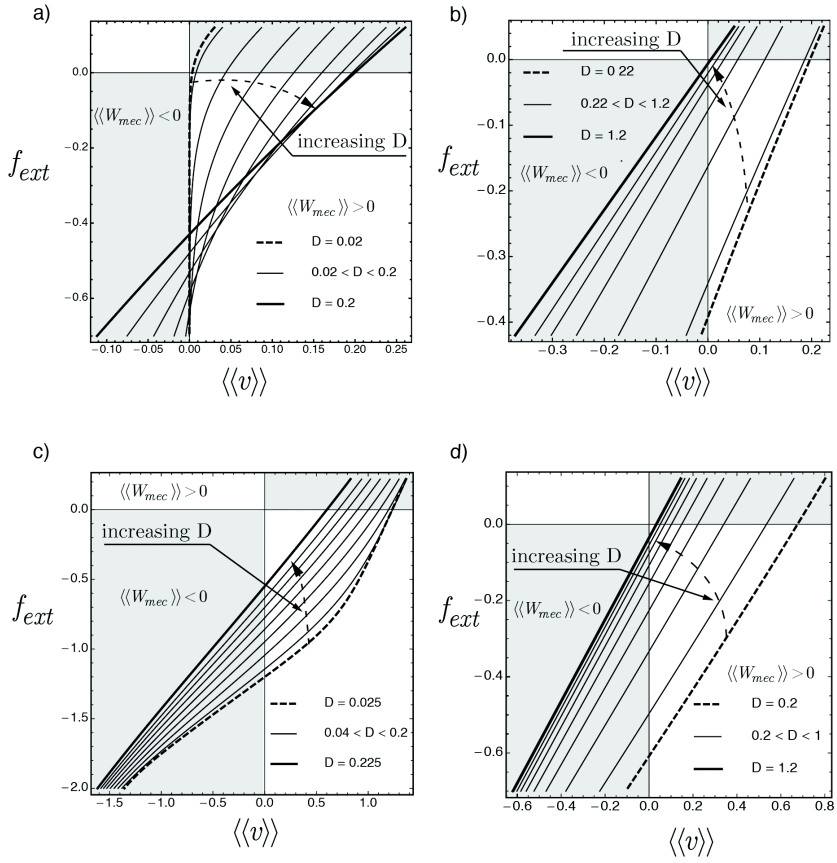

Figure 3.10. The variation of the force-velocity relation with the temperature D at fixed amplitude of rocking A. On a) and b), we show the behavior of system for relatively low amplitude characterised by concave force-velocity curve $A = 2$, see a) we loose the non linearity and the ratchet mechanism with increase of D see b). On the figure c) and d), we show the behavior of the system at medium value of A for which the force-velocity response characterised by convex form, which is loosed with increase of temperature D.

The force developed by the motor is proportional to the elongation of the linear spring. The corresponded stochastic differential equation can be written as

$$d_t x = -\partial_x V(x) - k_m(x - z) + f_{tilt}(t) + \sqrt{2D}\ \xi(t) \tag{3.18}$$

To simplify the model we incorporated the reference spring length into the definition of the coordinate z. In computation we chose the $z = 0$, the computation of the average value of the motor coordinate x was done done in the steady state. The study was performed by direct numerical simulations because the analytic evaluation of the integrals in the adiabatic approximation does not appear feasible. In Fig.3.11b) we show the sketch of our hard device for Magnasco thermal ratchet. Interestingly, this system can also be interpreted as elementary experimental setup for the isometric test in muscle mechanics.

In Fig.3.11b) we plot the function $\langle x\rangle$ versus D for different values of the amplitude of tilting force, A. We see that in this system the diffusion plays an important role. At low forcing amplitude A, the curve show a maximum at finite value D which means that that system produces optimal force at finite temperature (stochastic resonance).

We also notice that the force generated in the hard device is in the same range as the stall force obtained from the adiabatic force-velocity curve in the soft device. For

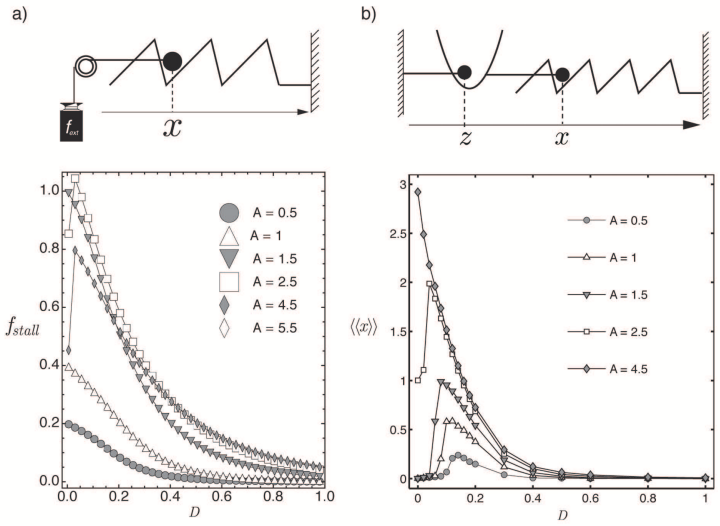

Figure 3.11. The Magnasco thermal ratchet force generation in hard and soft device configurations. a) We show the plot of adiabatic theory prediction of stall force as function of D for increasing values of amplitude A. b) We characterize the force generated in hard device by motor average position x at fixed z. We show the plot of average motor position versus D for increasing amplitude A of rocking.

comparison we need to multiply the average value of x by the value of k_m, and in our simulations we used the value $k_m = 0.5$. We observe, however, a systematic difference between the behavior of the stall force in the soft device and in the hard device. We can explain it by the different nature of the motion in these two force generation devices. Thus, in the soft device the force is fixed and is a deterministic parameter f_{ext}. Instead, in the hard device we obtain the force by averaging of the stochastic variable x_t which means that this force fluctuates and the stall force is just the average. We will developed this idea much deeper by using a simpler example of a bistable system in the next chapter.

The difference between the plots for the force generated in soft and hard devices can also be explained by the limited validity of the adiabatic theory in the case of temperatures close to zero. The values were obtained by finding numerically the roots of the adiabatic equation $J_{avg}(f_{ext}, A) = 0$. For more definitive quantitative comparison a finite element solution of the Fokker-Plank equation in both hard and soft devices is required which we leave outside the scope of this Thesis.

3.3.3 Efficiency

In this section we present a study of the energetics for the Magnasco model at the fixed value of the external load f_{ext}. Here we use the same ratchet parameters as in the previous section, and throughout this section adopt the value $f_{ext} = 0.3$. In particular, we study the average mechanical work and the average dissipation as functions of D. In this way we can understand the role of the temperature in ratchet dynamics by using the energetic terms. The main question is whether the temperature helps the motor to perform the useful work against an externally imposed load or is it an obstacle?

In the adiabatic approximation of the Magnasco model the average probability current J_{avg}, (3.16), is the function of the amplitude A and temperature D. Notice first that because of the cyclic nature of the motor the variation of the internal energy over one

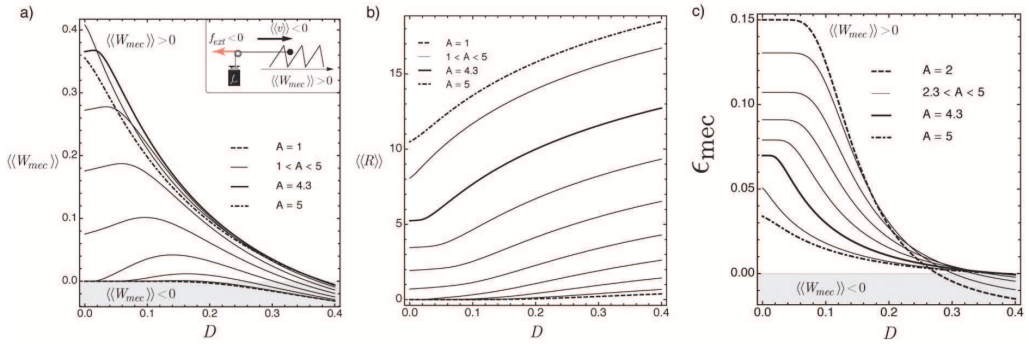

Figure 3.12. a) The variation of the mechanical work W_{mec} with the temperature D. b) The variation of the input energy R with the temperature D. c) The variation of the mechanical efficiency ϵ_{mec} with temperature D.

cycle T is equal to zero.

By using the known analytical expression for J_{avg} we can compute the mechanical work by the formula:

$$\langle W_{mec}\rangle = \frac{1}{t_f - t_i}(-f_{ext}\langle v\rangle) = \frac{f_{ext}L}{2}(J(A,D) + J(-A,D)) \tag{3.19}$$

In Fig.3.12a) we show the dependence of W_{mec} on D As the applied force remains constant W_{mec} follows the behavior of J_{avg}, see the previous section.

We can also compute the energy provided by the active source by using the definition,

$$\langle R\rangle = \left\langle \frac{1}{t_f - t_i}\int_{t=t_i}^{t=t_f} \partial_t V(x,t)dt \right\rangle = \frac{1}{T}\int_0^T dt \int_0^\lambda dx\,(\partial_t V(x,t)P(x,t)) =$$
$$= \frac{1}{T}\int_0^T dt \int_0^\lambda dx F(t)J(F) = \frac{LA}{2}(J(A,D) - J(-A,D)) \tag{3.20}$$

The dissipation during the period T can now be extracted from the energy balance equation $\langle Q\rangle = -\langle R\rangle + \langle W_{mec}\rangle$. In Fig.3.12b) we show the input energy R. At zero load f_{ext}, we can have $\langle R\rangle = -\langle Q\rangle$. The heat is negative by definition which indicates that the energy is being dissipated.

Next we can compute the efficiency of the energy transduction ϵ_{mec} defined as ratio of the produced mechanical work and the consumed input energy,

$$\epsilon_{mec} = \frac{\langle W_{mec}\rangle}{\langle R\rangle} = \frac{f_{ext}}{A}\frac{J(A) + J(-A)}{J(A) - J(-A)} \tag{3.21}$$

In (3.21) the numerator W_{mec} is proportional to the generated particle current J_{avg}. As we have shown in the previous section, J_{avg} is maximized at finite temperature in first two first regimes that we have identified for Magnasco ratchet, while in the high amplitude regime J_{avg} is a monotonically decreasing function of the temperature. However, the denominator in (3.21) also varies with temperature. To better understand the behavior of the ratio, it is convenient to rewrite the equation (3.21) in the form:

$$\epsilon_{mec} = \frac{f_{ext}}{A}\left(1 - \frac{2\left|\frac{J(-A)}{J(A)}\right|}{1 + \left|\frac{J(-A)}{J(A)}\right|}\right) \tag{3.22}$$

from this expression we can see that the mechanical efficiency is not simply proportional to the particle current. In fact, the efficiency is a monotonically decreasing function of temperature in all three regimes, because the fraction $\left|\frac{J(-A)}{J(A)}\right|$ is a monotonically increasing function of temperature, [56].

One can see that somewhat counterintuitively, the state of a maximum current does not correspond to maximum efficiency, see Fig.3.12c). As the efficiency does not show a maximum at finite temperature, one can question whether the presence of thermal fluctuation really helps the efficient energy transduction by the ratchet. Here we also need to take in account the limitations of the adiabatic theory. However, one must first consider the Stokes efficiency

$$\epsilon_{Stokes} = \frac{\eta\langle v\rangle^2}{\langle R\rangle} \tag{3.23}$$

as well as the rectifying efficiency

$$\epsilon_{rec} = \frac{\eta\langle v\rangle^2 + f_{ext}\langle v\rangle}{\langle R\rangle} \tag{3.24}$$

In Fig. 3.13 we show these measures of efficiency are indeed maximized at finite temperature.

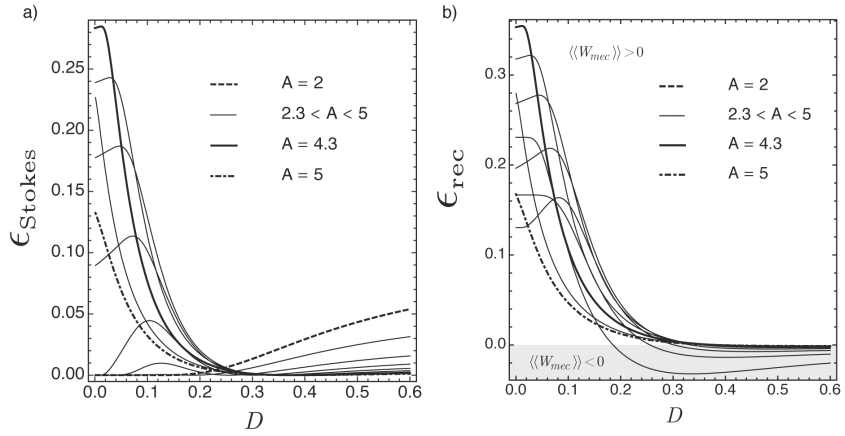

Figure 3.13. a) We show the variation of the Stokes efficiency ϵ_{Stokes} with temperature D. b) We show the rectifying efficiency ϵ_{rec} with temperature D.

3.4 Rocking ratchet with temporal asymmetry

As we remarked one can use the asymmetry in both space and time to generate directional current. In this section we extend the adiabatic theory for Magnasco ratchet to illustrate the effect of time-asymmetry.

Consider again a Brownian particle in the space periodic potential which is tilted in time. Suppose now that the potential is symmetric but the tilting is asymmetric : a larger force acts for a shorter time while smaller force acts for a longer time (in the opposite direction). The force field are chosen in such way that areas in Fig.3.14 are equal, $S_1 = S_2$. This ensures that there is no systematic directed force and $\int_t^{t+T} dt f_{tilt}(t) = 0$. Other results on tilted ratchets with time asymmetry can be found in [64, 63]. In this section we apply these ideas to the study of the Magnasco ratchet.

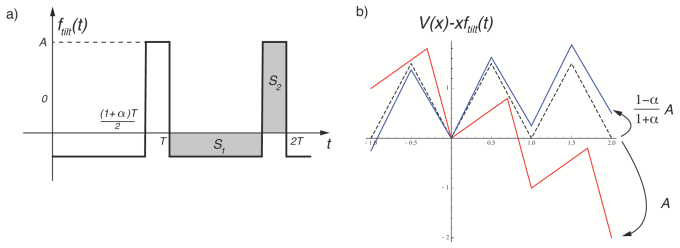

Figure 3.14. a)The time asymmetric rocking signal $f_{tilt}(t)$. The force field are chosen in such way that areas of each segments, S_1 and S_2, are equal. b) The action of asymmetric rocking $f_{tilt}(t)$ on the symmetric ratchet potential $V(x)$.

The Langevin equation in this case is (3.4). We consider again the general piecewise linear ratchet potential shown in Fig.3.1a). We can also study the adiabatic problem by solving the corresponding Fokker-Planck equation with the constant tilting term. The current in the stationary regime must be averaged over the period T of the driving force $f_{tilt}(t)$. We assume that

$$f_{tilt}(t) = \begin{cases} -\dfrac{1-\alpha}{1+\alpha}A, & for \quad , nT \le t < nT + \dfrac{1+\alpha}{2}T \\ A, & for \quad , nT + \dfrac{1+\alpha}{2}T \le t < (n+1)T, \quad n \in \mathbb{N} \end{cases} \tag{3.25}$$

Here α is used as a parameter measuring temporal asymmetry. In the adiabatic limit the averaged current J_{avg} can be computed as

$$\begin{aligned} J_{avg} = \langle J(f_{ext}, f^T_{tilt}(t))\rangle_t &= \frac{1}{T}\left(\int_0^{\frac{1+\alpha}{2}T} \dots dt + \int_{\frac{1+\alpha}{2}T}^{T} \dots dt \right) \\ &= \frac{1+\alpha}{2} J(f_{ext}, -\frac{1-\alpha}{1+\alpha}A) + \frac{1-\alpha}{2} J(f_{ext}, A) \end{aligned} \tag{3.26}$$

We recall that here we consider symmetric saw-tooth potential, i.e. $\Delta = 0$; the phase space symmetry is broken by time asymmetry parameter $\alpha = 0.7$.

In Fig.3.16.a). b) we plot the behavior of J_{avg} versus A and D without conservative external load. We notice the similarity in behavior between the Magnasco thermal ratchet and the time asymmetric thermal ratchet defined in this section.

On the Fig.3.16 we show the behavior of force-velocity curves for the ratchet model with broken time symmetry, i.e. $\Delta = 0$ and $\alpha \neq 0$, and we show the force-velocity curves of the ratchet model with both broken time and space symmetry, i.e. $\Delta \neq 0$ and $\alpha \neq 0$.

We notice same new interesting features by tuning the parameter Δ and α. Notice first that in the adiabatic limit the ratchet system with either space, or time asymmetry, can not exhibit the reversal of the current at finite temperature. However, in the ratchet system with $\alpha \neq 0$ and $\Delta \neq 0$ one can obtain current reversals in the adiabatic regime. To obtain such regimes we need to chose the parameters of the asymmetry in such a way that the directions of the current in the cases of pure spatial and temporal asymmetries are in opposite directions. For example, in Fig.3.17 the current is in the positive direction when $\Delta = 0.9$ and $\alpha = 0$, and in the negative direction when $\Delta = 0$ and $\alpha = 0.9$. By tuning the combination of these two parameter to $\alpha = 0.8$ and $\Delta = 0.9$ we obtain the phenomenon of current reversal with the increase of temperature D . It should be noted

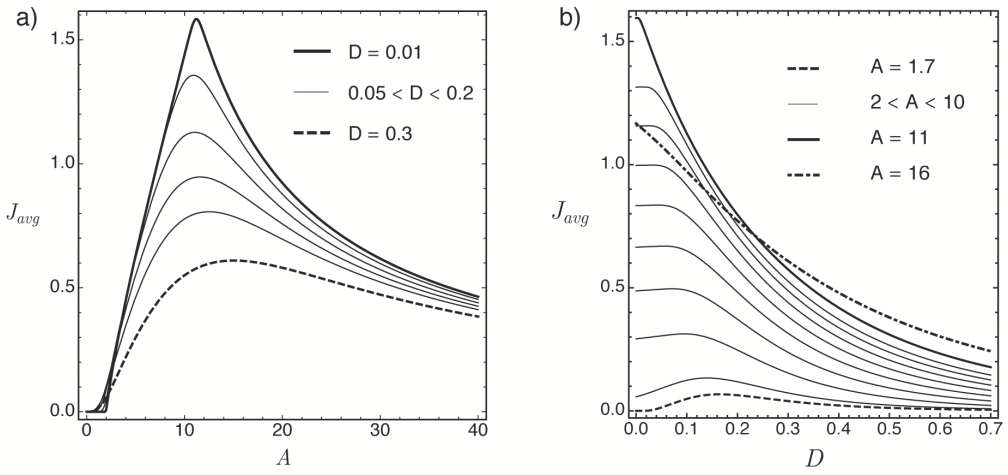

Figure 3.15. The typical characteristics of time asymmetric rocked ratchet with parameters $\Delta = 0$ and $\alpha = 0.7$. a) The variation of the average current with amplitude A at different temperature D. b) The variation of the average current with temperature D at different regimes of amplitude A.

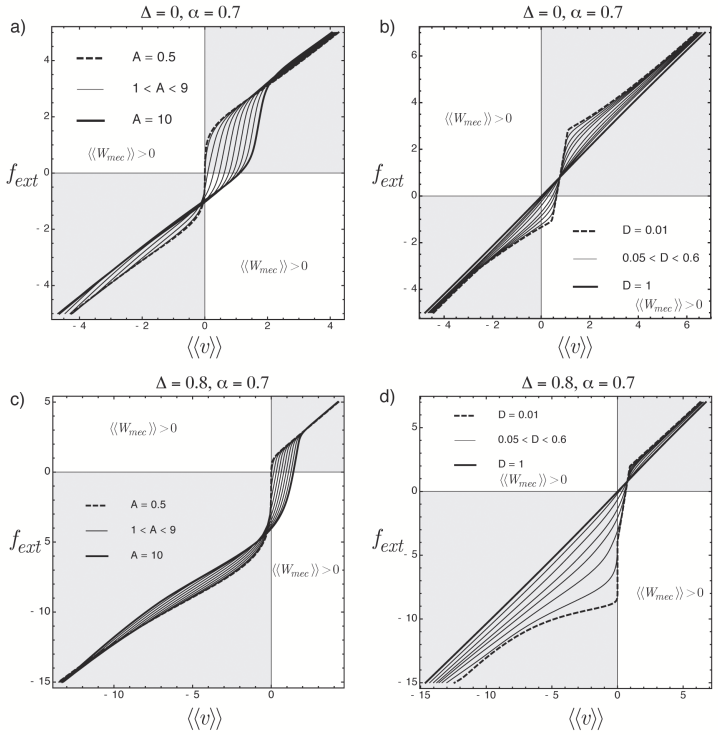

Figure 3.16. a) The variation of force-velocity curve with temperature D, for $\Delta = 0$ and $\alpha = 0.7$. b) The variation of force-velocity curve with amplitude A, for $\Delta = 0$ and $\alpha = 0.4$. c) We plot for example the force-velocity curve for ratchet motor with $\Delta = 0.8$ and $\alpha = 0.7$ for different amplitude A, the both space and time symmetry are broken. d) We plot for example the force-velocity curve for ratchet motor with $\Delta = 0.8$ and $\alpha = 0.7$ for different temperature value D.

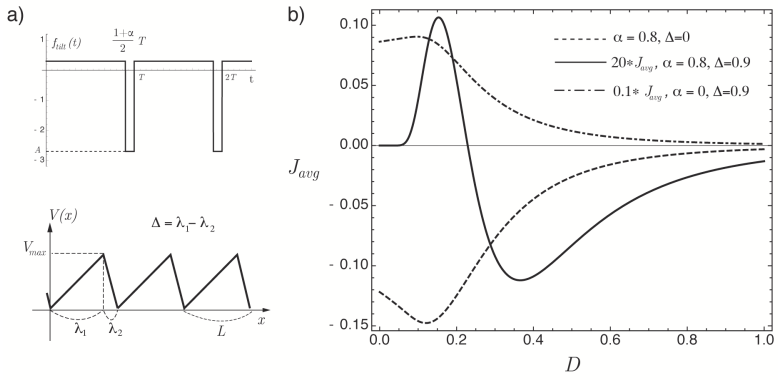

Figure 3.17. a) On the left, the time asymmetric forcing $f_{tilt}(t)$ with amplitude $A = -2.7$. On the right, we recall the definition of saw-tooth potential. b) The variation of the average current with the temperature D for the tuned parameter Δ and α. With solid black line we plot the average current for $\Delta = 0.9$ and $\alpha = 0.8$, with dashed line we plot the average current for $\Delta = 0$ and $\alpha = 0.8$, and with dot-dashed line –the average current for $\Delta = 0.9$ and $\alpha = 0$.

that this is not an additive effect separately arising from α and Δ. The current reversal arises due to complex interplay of these two ratchet mechanisms. By using the known

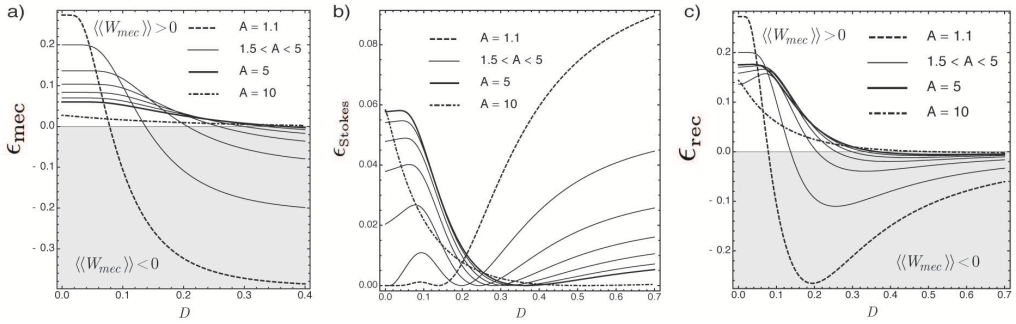

Figure 3.18. The energetics of time asymmetric rocked ratchet model, the model parameters $\Delta = 0$ and $\alpha = 0.7$ and $f_{ext} = 0.3$. a) The variation of the mechanical efficiency with temperature for increasing amplitude A. b) The variation of Stokes efficiency with the temperature for increasing amplitude A. c) The variation of rectification efficiency with temperature for increasing amplitude A.

expressions for the average current we can now compute the corresponding energetics quantities: mechanical work W_{mec}, the heat $\langle Q \rangle$ dissipated by the system, the input of energy $\langle R \rangle$, and the work performed against the viscous media W_{Stokes}. We can then plot the corresponded ratios ϵ_{mec}, ϵ_{Stokes} and ϵ_{rec}, see Fig.3.18 a),b),c).

In the case of pure time asymmetry the computed energetic measures exhibit the same behavior as in the case of spatial asymmetry in the original Magnasco ratchet. We may again conclude that the thermal bath does not facilitate the energy transfer, as mechanical efficiency does not show a maximum at a particular temperature, however we again recall what the adiabatic theory may be incorrect at small values of D. The other two measures of efficiency show such a maximum at the same value of the asymmetry parameters even in the adiabatic limit.

Notice that by fine tuning of the asymmetry parameters $\alpha \neq 0$ and $\Delta \neq 0$ one can

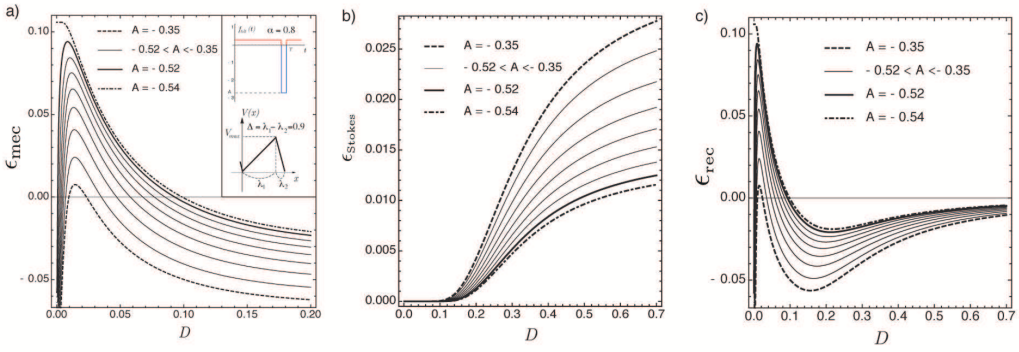

Figure 3.19. The energetics of time asymmetric ratchet model with the fine tuned parameters $\alpha = 0.8$ and $\Delta = 0.9$ at load $f_{ext} = 0.03$. a) The variation of the mechanical efficiency with temperature for increasing amplitude A. b) The variation of Stokes efficiency with the temperature for increasing amplitude A. c) The variation of rectification efficiency with temperature for increasing amplitude A.

obtain the regimes in which even in the adiabatic theory the mechanical efficiency ϵ_{mec} has a maximum at a finite temperature D. For example, we find such a regime at $f_{ext} = 0.03$, $\alpha = 0.8$ and $\Delta = 0.9$, see Fig.3.19a),b),c).

3.5 Conclusions

In this section we studied a prototypical ratchet model first proposed by Magnasco which we generalized in several directions. This model describes the overdamped motion of a Brownian particle in a space periodic potential driven by a periodic tilting force. The resulting motion shows high degree of complexity in the presence of a thermal noise however we show that the averaged motion can be directional and steady. We discussed this one-dimensional ratchet model mostly in terms of the adiabatic approximation where analytical solutions for the stationary regime are readily available. We compared these analytical results with the results of direct numerical simulations performed on the original Langevin equation and used this relatively transparent case to test and verify our numerical procedures.

The presented model can be used to describe a molecular motor capable to carry cargo and exert forces. The periodic tilting of the spatial potential can be interpreted as an action of the ATP where we interpret correlations in the external signal as the sign of non-equilibrium. The spatial potential can be viewed as describing an actin filament with periodically positioned binding sites, and the transition from one minimum to the other as attachment /detachment step of the molecular motor.

The main problem with the application of this description to acto-myosin interaction is that it completely ignores the phenomenon of power stroke. One can say that the advance of the motor is driven by the activity in actin filament expressed through the periodic tilting of the actin potential. This effect is global and can hardly be viewed as a realistic description of the energetically localized interaction between a cross bridge and a binding site. In addition, we observe that our Magnasco type myosin is advancing by using a mechanism which is principally different from the mechanism known to be used by kinesin which is strange in view of their fundamental configurational similarity.

To address these concerns we develop in the next sections an alternative idea that the

activity is concentrated not in a filament but in the additional structure capable of undergoing a conformational transition. The incorporation of this additional structure requires us to introduce additional internal variable making the minimal relevant Langevin equation two dimensional. We study several successively more elaborate working arrangements for such a power stroke driven system, first completely abandoning the periodic potential and then reinstating it again.

Chapter 4

Power stroke element

In this chapter we study the possibility of active force generation by an asymmetric snap-spring placed in a Brownian environment. The model describes Brownian motor activated by a periodic (correlated) tilting of the bi-stable potential. In the biological perspective the model can be viewed as describing an isolated attached myosin cross bridge represented as a linear spring in series with a bi-stable element (snap-spring). Usually such cross bridges are considered to be passive elements in rigor state. Here we propose to view this system as an ATP consuming device which can produce active force. While this model does not allow one to represent isotonic contractions outside the stall force regime it can be used to obtained surprisingly rich description of isometric contractions. In the next chapters we further extend this model making it finally capable to capture isotonic contractions. This is done at a price of an additional degree of freedom 'living' in a passive periodic potential. The advantage of the minimal model presented in this section is its complete analytical transparency which is lost as the model becomes more realistic.

4.1 Snap-spring as a motor

Active element consumes input energy and in return generates force. Here we show that a simple snap-spring with a double well energy may serve as a force generating device if placed in a Brownian environment and subjected to additional correlated tilting with zero average. The bi-stable potential must be asymmetric and for simplicity we choose it to be piecewise quadratic. The our goal is to characterize the efficiency of the force generation by such a system placed in either hard or soft experimental setup. The difference between the two protocols is detailed below:

- To imitate the isometric setup we couple a bi-stable system with a linear spring fixed at one end. By varying the reference length of the linear spring we can obtain different force levels in the case of rocking input. This system will be referred to as a hard device configuration.
- To imitate isotonic stall force set up we study a particle in a rocking bistable potential subjected to the action of a fixed external force. Such system will be referred to as a soft device.

Both system are shown in Fig.4.1.

As in the previous section we consider an over-damped Langevin equation

$$\frac{dy}{dt} = -\partial_y G(y,t) + \sqrt{2D}\,\xi(t) \tag{4.1}$$

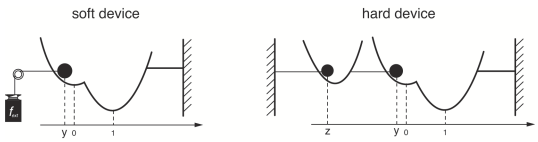

Figure 4.1. The graphic scheme of bistable system in two experimental setup: soft and hard device.

The form of the energy $G(\mathbf{X}, t)$ depends on the protocol:

- In the hard device the potential is:

$$G_{h.d.}(y, t|z) = V(y) - y f_{tilt}(t) + \frac{1}{2} k_m (y - z - z_0)^2 \tag{4.2}$$

  The fixed parameter z can always be chosen to absorb the reference length z_0 of the linear spring with stiffness k_m.

- In the soft device the energy potential is:

$$G_{s.d.}(y, t|f_{ext}) = V(y) - y f_{tilt}(t) - y f_{ext} \tag{4.3}$$

  Here the fixed parameter is the conservative load f_{ext}.

The potential $V(y)$ describing the snap-spring (power stroke element) is a non-convex function with two local minima. It is asymmetric with one global minimum biased by choice in order to distinguish between the pre-power stroke state and to post-power stroke state. The particular shape of this potential does not affect our main conclusions.

To be specific we model $V(y)$ by a piecewise quadratic function with minima in the points $y = 0$ and $y = a$ and a (singular) barrier at $y = l$. We could also remove this singularity by considering a smoother transition between the two local minima by inserting a third inverted parabola in the segment $[l - \delta_1, l + \delta_2]$ representing the spinodal interval, however it will not affect our conclusions. We therefore define:

$$V(y) = \begin{cases} \frac{1}{2} k_0 \, (y)^2 + \varepsilon_0(l), & y \leqslant l \\ \\ \frac{1}{2} k_1 \, (y - a)^2 \, , & y \geqslant l \end{cases} \tag{4.4}$$

The location of the spinodal point controls the value of the energy barrier $\varepsilon_0(l)$ through,

$$\varepsilon_0 = \frac{1}{2} \left(k_1 (l - 1)^2 - k_0 l^2 \right) \tag{4.5}$$

The ATP activity is modeled again by the periodic external force $f_{tilt}(t)$ with zero average.

To obtain dimensionless formulations we introduce the following definitions

$$\begin{aligned} \tilde{X}_{\tilde{t}} &= \frac{1}{a} X_{\tau \tilde{t}} \\ \tilde{V}(\tilde{y}, \tilde{z}) &= \frac{1}{k_m a^2} V(a\tilde{y}, a\tilde{z}) \\ \tilde{f}^{\tilde{T}}_{tilt}(\tilde{t}) &= \frac{1}{k_m a} f^{T}_{tilt}\left(\frac{t}{\tau}\right) \\ \tilde{\xi}_i(\tilde{t}) &= \xi_i(t) \tau^{-1/2} \end{aligned} \tag{4.6}$$

where $\tau = \frac{\eta_y}{k_m}$ is the main time scale. The main nondimensional parameter of the problem is

$$\tilde{D} = \frac{k_B T}{k_m a^2} \tag{4.7}$$

In what follows we omit tildas and work exclusively with nondimensional equations. In the hard device setting we need to compute the average generated force

$$f = \langle\langle y \rangle\rangle - z \tag{4.8}$$

while in the soft device we need to compute the mean displacement $\langle\langle y \rangle\rangle$. In both cases by $\langle\langle \bullet \rangle\rangle$ we imply averaging over both the ensemble and the period of the external force.

Observe that in the absence of the white noise, $D = 0$, the trajectory $y(t)$ is fully determined by the potential shape and the input signal f_{tilt}. In Fig.4.2 we show two responses of the system: without a thermal bath and with a thermal bath. Suppose that the amplitude of the correlated noise f_{tilt} is small so that without thermal noise the system always remains in the same energy well. In the figure we show two types of rocking force: a square-wave signal and sinusoidal signal plotted by blue solid lines. One can see that in the presence of the thermal noise the particle visits both potential wells with the barrier crossing being correlated with the rocking. This shows that the noise can considerably amplify the effect of the rocking which is known as the phenomenon of stochastic resonance [22]. In other words, the system in contact with a thermal bath may

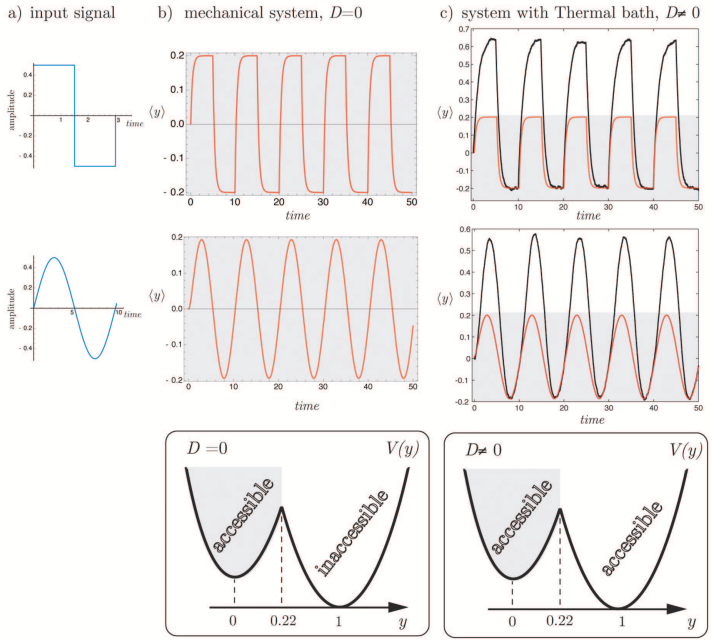

Figure 4.2. Two responses of the system: without a thermal bath $D = 0$ and with a thermal bath $D = 0.02$. The corresponded equations solved with initial condition $y(t_0) = 0$. The values of parameters: $k_0 = 1.5, k_1 = 0.43, l = 0.22$.

need much weaker rocking signal to cross the potential barrier between the two well. This effect is most probably used by the molecular motor systems operating in the environment where the correlated signal is weak and the uncorrelated signal is strong.

Before we move to numerical experiments, we need to specify the values of parameters. The bistable dimensionless potential $V(y)$ in both, hard and soft devices will be of the

form:

$$V(y) = \begin{cases} \frac{1}{2}k_0 \left(y\right)^2 + \varepsilon_0(l) & y \leqslant l \\ \\ \frac{1}{2}k_1 \left(y-1\right)^2 & y \geqslant l \end{cases} \tag{4.9}$$

with

$$k_0 = 1.5,\ k_1 = 0.43,\ l = 0.22 \tag{4.10}$$

. We define $f_{tilt}(t)$ as a symmetrical square wave function

$$f_{tilt}(t) = \begin{cases} +A & \text{for } n\dfrac{T}{2} \leq t \leq (n+1)\dfrac{T}{2} \\ \\ -A & \text{for } (n+1)\dfrac{T}{2} \leq t \leq nT,\ n \in \mathbb{N} \end{cases} \tag{4.11}$$

where we shall systematically vary T - the time period of rocking and A - the amplitude of the driving force. The particular choice of the numerical parameters is not crucial for the physical interpretation of our results. What is crucial, however, is the asymmetry of the bi-stable potential shape. Our choice of the asymmetry was motivated by numerical values for muscle power stroke in acto-myosin system fitted from experimental measurements by M.Caruel. However, our main goal is not the reproduction of particular curves but rather qualitative understanding of the feasibility of muscle contractions being driven by the power stroke element.

4.2 Adiabatic approximation

We begin by writing the Fokker-Planck equation for our system

$$\partial_t P(y,t) = D\partial_y \left[\frac{P(y,t)}{D}\partial_x G(y,t) + \partial_y P(y,t)\right] \tag{4.12}$$

where $G(y,t)$ is one of the energies (4.2) or (4.3). We deal with a stationary loading in confining potential and are interested in studying the mean displacement of our particle $\langle\langle y \rangle\rangle$ defined by the integral:

$$\langle\langle y \rangle\rangle = \int_t dt \int_y y P(y,t) dy \tag{4.13}$$

To study the dependence of this displacement on various parameters of the system we need to find first the associated periodic solution of the Fokker-Planck equation 4.12. When the period of the rocking T is sufficiently large, one can expect that the adiabatic approximation which we have successfully used and justified in the previous section will also work in this case. Later we shall again check the validity of this analytical tool by solving numerically the corresponding Langevin equation and independently by solving the time dependent Fokker-Planck equation by the finite element method.

Let us replace the time depended periodic signal $f_{tilt}(t)$, by a constant term with amplitude A. We then search for the corresponding stationary solution of the Fokker-Planck equation (4.12) with constant coefficients. We obtain

$$P_{st}(y|A) = N^{-1} \exp\left(-\frac{G(y|A)}{D}\right) \tag{4.14}$$

where $N = \int_y dy \exp\left(-\frac{G_s(y|A)}{D}\right)$ is the normalization constant. The notation $P_{st}(y|A)$ indicate that the probability density is computed for the given value of the amplitude A. We define the ensemble averaged displacement as

$$\langle y(A)\rangle = \int_{-\infty}^{+\infty} y P_{st}(y|A) dy \tag{4.15}$$

Now we recall that during one half of the period the function $f_{tilt}(t)$ takes the value $+A$ and during the other one half of the period - the value $-A$. We can then compute two probability densities $P_{st}(y|+A)$ and $P_{st}(y|-A)$, defined by (4.14) for positive and negative values of the rocking amplitude A. The averaging over the period can then be performed according to the rule

$$\langle\langle y(A)\rangle\rangle = \frac{1}{T}\int_0^T dt \int_{-\infty}^{+\infty} y P_{st}(y|A) dy = \frac{1}{2}[\langle y(+A)\rangle + \langle y(-A)\rangle] \tag{4.16}$$

The computed average displacement depends not only on A but also on the temperature D, however we do not explicitly mention this dependence.

To perform the calculation of the integrals in (4.14) in the case of hard device we take advantage of the piecewise nature of the potential $V(y)$. First, we develop the expression for the normalization constant N:

$$N_{h.d.}(A,z) = \int_{-\infty}^{+\infty} \exp\left(-\frac{G_{h.d.}(y|A,z)}{D}\right) dy = \int_{-\infty}^{l} \ldots dy + \int_{l}^{+\infty} \ldots dy \tag{4.17}$$

where l is the barrier point in the bistable potential. We continue

$$\int_{-\infty}^{+\infty} \exp\left(-\frac{G_{h.d.}(y|A,z)}{D}\right) dy = \int_{-\infty}^{l} \exp\left(-\frac{\frac{1}{2}k_0 y^2 + \frac{1}{2}k_m(y-z)^2 + \varepsilon_0 - yA}{D}\right) dy + \int_{l}^{+\infty} \exp\left(-\frac{\frac{1}{2}k_1(y-1)^2 + \frac{1}{2}k_m(y-z)^2 - yA}{D}\right) dy$$

Similar expression can be obtained for the $\int_{-\infty}^{+\infty} y \exp(-G_{h.d.}(y|A,z)/D) dy$. At the end we can write an explicit expression for $\langle y(A,z)\rangle_{h.d.}$

$$\begin{aligned}\langle y(A,z)\rangle_{h.d.} = {} & N_{h.d.}^{-1} \frac{P_0^{h.d.}}{k_0+k_m}\left[-D\exp\left(-u_0^2\right) + \frac{A+k_m z}{2}\sqrt{\frac{2D\pi}{k_0+k_m}}\ erfc\left[-u_0\right]\right] \\ & + N_{h.d.}^{-1} \frac{P_1^{h.d.}}{k_1+k_m}\left[D\exp\left(-u_1^2\right) + \frac{k_1+A+k_m z}{2}\sqrt{\frac{2D\pi}{k_1+k_m}}\ erfc\left[u_1\right]\right]\end{aligned} \tag{4.18}$$

where [1]

$$N_{h.d.}(A,z) = P_0^{h.d.}\sqrt{\frac{2D\pi}{k_0+k_m}}\ \frac{1}{2}\ erfc\left[-u_0\right] + P_1^{h.d.}\sqrt{\frac{2D\pi}{k_0+k_m}}\ \frac{1}{2}\ erfc\left[u_1\right] \tag{4.19}$$

[1] we use the special complementary error function noted $erfc(x) = \frac{2}{\sqrt{\pi}}\int_x^\infty e^{-t^2} dt$

and

$$\begin{aligned} P_0^{h.d.} &= \exp\left[-\frac{1}{2D}\left(2\varepsilon_0 + k_m z^2 - \frac{(A+k_m z)^2}{k_0+k_m}\right)\right] \\ P_1^{h.d.} &= \exp\left[-\frac{1}{2D}\left(k_1 + k_m z^2 - \frac{(A+k_1+k_m z)^2}{k_1+k_m}\right)\right] \\ u_0 &= \sqrt{\frac{k_0+k_m}{2D}}\left(l - \frac{A+k_m z}{k_0+k_m}\right) \\ u_1 &= \sqrt{\frac{k_1+k_m}{2D}}\left(l + \frac{A+k_1+k_m z}{k_1+k_m}\right) \end{aligned} \tag{4.20}$$

We can now express the mean value of the displacement (4.16) by using (4.18):

$$\langle\langle y(A,z)\rangle\rangle_{h.d.} = \frac{1}{2}[\langle y(+A,z)\rangle_{h.d.} + \langle y(-A,z)\rangle_{h.d.}] \tag{4.21}$$

The force generated by the system can then be written as

$$f_{h.d.}(A,z) = k_m[\langle\langle y(A,z)\rangle\rangle_{h.d.} - z]. \tag{4.22}$$

Knowing the explicit form of the solution in the hard device configuration we can now easily find the corresponding expressions in the soft device configuration. To this end we need to replace in (4.19) and (4.18) the ATP induced force A by the total force $A' = A + f_{ext}$ and take the limit $k_m \to 0$. As a result we obtain

$$\text{Hard device} \xrightarrow[\lim\limits_{k_m\to 0}]{A\equiv A'} \text{Soft device} \tag{4.23}$$

After taking the limit we find :

$$N_{s.d.}(A, f_{ext}) = P_0^{s.d}\sqrt{\frac{2D\pi}{k_0}}\,\frac{1}{2}\,erfc\,[-w_0] + P_1^{s.d.}\sqrt{\frac{2D\pi}{k_0}}\,\frac{1}{2}\,erfc\,[w_1] \tag{4.24}$$

and

$$\begin{aligned} \langle y(A,f_{ext})\rangle_{s.d.} = \;& N_{s.d.}^{-1}\frac{P_0^{s.d.}}{k_0}\left[-D\exp\left(-w_0^2\right) + \frac{A}{2}\sqrt{\frac{2D\pi}{k_0}}\;\;erfc\,[-w_0]\right] \\ & + N_{s.d.}^{-1}\frac{P_1^{s.d.}}{k_1}\left[D\exp\left(-w_1^2\right) + \frac{k_1+A}{2}\sqrt{\frac{2D\pi}{k_1}}\;\;erfc\,[w_1]\right] \end{aligned} \tag{4.25}$$

where

$$\begin{aligned} P_0^{s.d.} &= \exp\left[-\frac{1}{2D}\left(2\varepsilon_0 - \frac{(A+f_{ext})^2}{k_0}\right)\right] \\ P_1^{s.d.} &= \exp\left[-\frac{1}{2D}\left(k_1 - \frac{(A+f_{ext}+k_1)^2}{k_1}\right)\right] \\ w_0 &= \sqrt{\frac{k_0}{2D}}\left(l - \frac{A+f_{ext}}{k_0}\right) \\ w_1 &= \sqrt{\frac{k_1}{2D}}\left(l + \frac{A+f_{ext}+k_1}{k_1}\right) \end{aligned} \tag{4.26}$$

By using these expressions we can compute the average displacement

$$\langle\langle y(A, f_{ext})\rangle\rangle_{s.d.} = \frac{1}{2}[\langle y(+A, f_{ext})\rangle_{s.d.} + \langle y(-A, f_{ext})\rangle_{s.d.}] \tag{4.27}$$

To summarize, in the soft device we fix the value of the external load f_{ext} and measure the average value of the mean displacement $\langle\langle y(A, f_{ext})\rangle\rangle_{s.d.}$. Here the force is a know deterministic parameter while the displacement is a fluctuation variable. In the hard device, we define the force through the average displacement of the particle (4.22), so we end up measuring the average value of the force. Therefore in the hard device both the force and the displacement are fluctuating parameters. Now, the stall force can be determined by using both protocols and an interesting question is how the stall forces defined through these two types of measurements are related.

4.3 Computational results

In Fig.4.3 we show the average displacement versus amplitude of rocking in the hard device configuration with $z = 0$, and $k_m = 1$.

To understand these results we notice that at $D = 0$ and small rocking amplitude A the system remains in the first energy well and since it is quadratic, the average displacement (together with the corresponding force) remains zero till the amplitude reaches the threshold allowing the system to escape to the second energy well. At this threshold (in A) the displacement jumps since the system now reaches the bottom of the second well. Subsequent increase in the amplitude leads to oscillations in an asymmetric potential and the average displacement gradually increases with A. In physical terms one can say that in this 'large displacement regime' the system produces force because it periodically preforms the power stroke which is then continuously recharged due to the energy influx from the rocking device. Since thermal diffusion is absent, the system behaves as a mechanical ratchet. Interestingly this system can be used as a very sensitive indicator detecting the strength of the correlated component of the noise. When temperature is different from

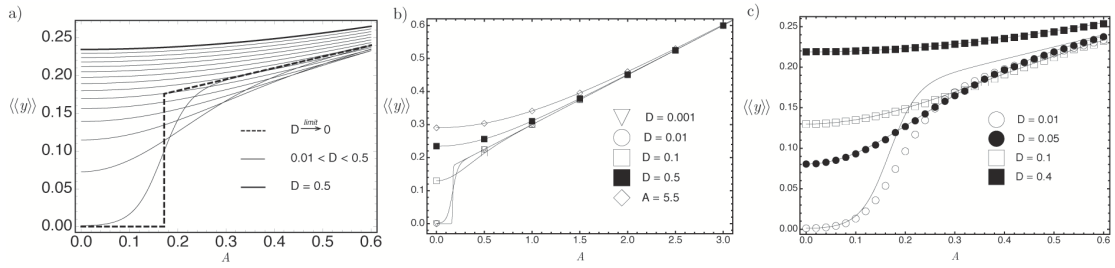

Figure 4.3. The average displacement versus amplitude A of rocking $f_{tilt}(t)$ in the hard device with $z = 0$. Solid lines represent predictions of the adiabatic theory and the results of direct numerical simulation of the Langevin equation plotted by scatters. The values of parameters: $k_0 = 1.5, k_1 = 0.43, l = 0.22$.

zero $D > 0$, the system is in both wells even when the rocking amplitude is vanishingly small because of thermally induced barrier crossing. That is why we see small thermal expansion even at small values of A. At large temperature thermal diffusion completely dominates rocking and thermal expansion is the only thing we see. At the intermediate levels of thermal noise one can expect a stochastic resonance phenomenon when in some

interval of rocking amplitudes the generated force (displacement) reaches its maximum at finite temperature.

The analytical formulas presented in the previous section are obtained in the adiabatic approximation under the assumptions that the period of rocking is large comparing to the characteristic time of the thermal crossing of the barrier. The latter depend on D and the adiabatic approximation clearly breaks as $D \to 0$. Therefore the computations based on the adiabatic assumption may misrepresent the fine detailed of the stochastic resonance. In particular, the limit $D \to 0$ in adiabatic approximation, is different from the actual mechanical response at zero temperature. Therefore in addition to analytical computations based on the adiabatic approximation, we also performed here direct numerical simulation of the Langevin equation plotted in Fig. 4.3 by scatters, while solid lines represent predications of the adiabatic theory. One can see that at large D the results are perfectly consistent however at small D the agreement is only qualitative. For instance, we see a small disagreement at $D = 0.01$ in the intermediate range of amplitudes A. In Fig.4.4 we

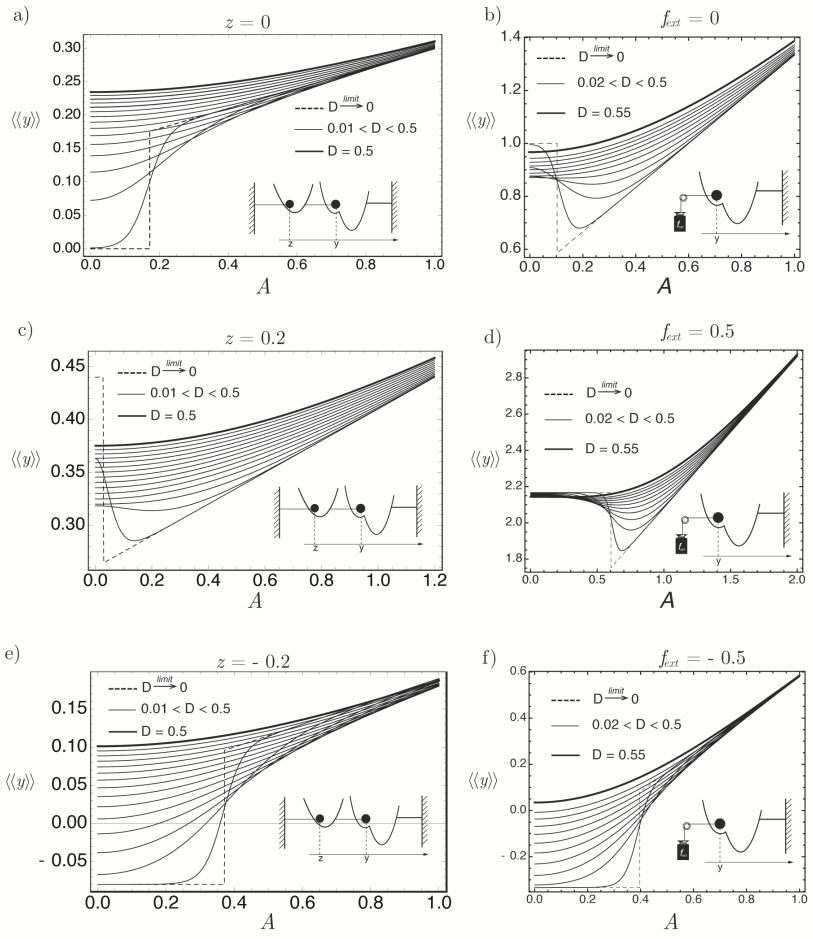

Figure 4.4. The adiabatic dependence of average displacement $\langle\langle y\rangle\rangle$, denoted y, versus amplitude A in hard device and soft devices with increasing temperature D. With black dashed lines we plot the limit $D \to 0$ in the adiabatic approximation and with solid thick black lines we plot the dependence for highest temperature D. The values of parameters: $k_0 = 1.5, k_1 = 0.43, l = 0.22$.

compare the adiabatic dependence of the average displacement $\langle\langle y\rangle\rangle$ on rocking amplitude

A in hard device and soft devices. If the applied force f_{ext} and the prestress z are appropriately adjusted the overall behavior of the two systems is rather similar. We observe two major regimes. One regime, which we have already seen in Fig. 4.3 corresponds to the negative values of both f_{ext} and z when the system starts in the pre power stroke state and the force/displacement increases when rocking allows the system to cross the barrier. Another regime corresponds to positive f_{ext} and z when the system starts in the post power stroke and the periodic rocking leads to the (initial) drop in the force/displacement as the system starts to escape into the pre power stroke state. As the amplitude A increases, the system oscillates between the wells and the asymmetry of the potential leads to eventual gradual increase of the average displacement/force and the response becomes linear in A.

The temperature dependence of the passive force generated in hard and soft devices can be studied already at $A = 0$. In Fig.4.5a). and Fig.4.5b). we show that the thermal expansion in this system can be both positive and negative. Negative thermal expansion takes place when the system is originally in the post power stroke state and diffusion facilities crossing of the barrier and recharging the system into the pre power stroke state. As temperature increases further the double well structure of the potential becomes progressively less important and the thermal expansion first becomes linear and then eventually saturates. In Fig.4.6 we subtract the passive thermal expansion at $A = 0$ from the av-

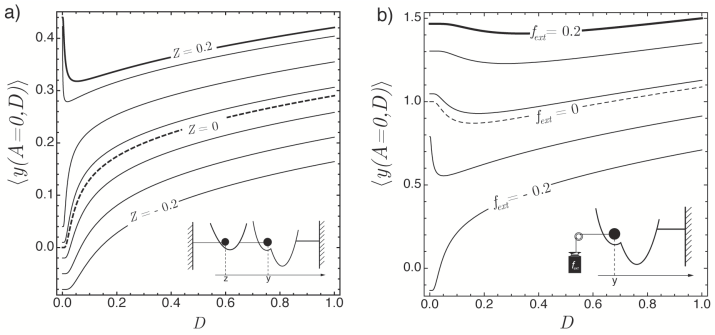

Figure 4.5. a) The variation of thermal expansion $\langle y(A = 0, D)\rangle_{h.d.}$ with the temperature D in hard device for the positive and negative z. b) The variation of thermal expansion $\langle y(A = 0, D)\rangle_{h.d.}$ with the temperature D in soft device for the positive and negative external load f_{ext}.

erage displacement to study the temperature dependence of the active component of the displacement $\langle\langle y(A, z)\rangle\rangle_{h.d.} - \langle y(A = 0, z)\rangle_{h.d.}$ in the hard device setting. One can see that the active contribution to the displacement is strongly temperature dependent exhibiting an extremum at a particular value of D which can be interpreted as the effect of stochastic resonance (in a distorted adiabatic approximation). In particular the active component is minimized if $z > 0$ and the system is originally in the post power stroke state and is maximized if $z < 0$ and the system was originally in the pre power stroke state.

We now turn to more systematic comparison of the magnitude of the active forces generated in soft and hard devices and in Fig.4.7, we show the resulting force - average displacement curves.

We recall what the force generated in the hard device is defined as follows:

$$f_{h.d.}(z, A) = k_m \left[\langle\langle y(z, A)\rangle\rangle_{h.d.} - z\right] \tag{4.28}$$

If the whole system is viewed as a linear spring with the total displacement z, the active force plays a role of a prestress equal to the average value of the displacement y.

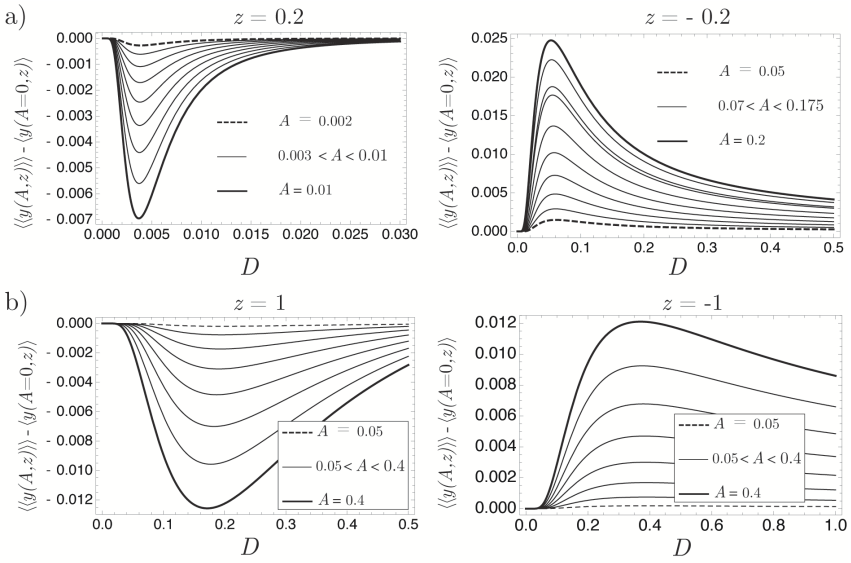

Figure 4.6. The adiabatic variation of the active component $\langle\langle y(A,z)\rangle\rangle_{h.d.} - \langle y(A=0,z)\rangle_{h.d.}$ in hard device with the temperature D for the different values of z. The values of parameters: $k_0 = 1.5, k_1 = 0.43, l = 0.22$.

Instead we can study the dependence of the force $f_{h.d.}$ on $\langle\langle y\rangle\rangle_{h.d.}$ by choosing different values of the prestress z. The resulting parametric relation $\mathcal{F}[\langle\langle y\rangle\rangle_{h.d.}, f_{h.d.}]$ becomes nonlinear and even non-monotone so that several values of $\langle\langle y\rangle\rangle_{h.d.}$ may correspond to the same value of $f_{h.d.}$. In this case we obtain a family of values for the stall force parameterized by z implicitly representing location of the attachment site. In reality the range of available values of the stall force is rather small because the attachment mechanism has a limited strength. However, this effect will be studied in the next chapters and for now we consider the attachment as infinitely strong.

What is important here is that the model suggests that we have a finite interval of 'stall forces'. Only one value is selected by the process that involves also attachment detachment. The rest of the 'stall forces curve' is revealed in experiments on fast force recovery originated by Huxley and Simmons who called it the T_2 curve.

We observe that in the force displacement relation obtained in the hard device at low temperatures the left linear branch corresponds to strongly negative values of the variable z and the right branch to the strongly positive value of z. In both cases the system is practically confined to one of the energy wells. For the intermediate values of z the system is close to the spinodal state and one can see that this passively unstable state can be partially stabilized by active rocking. Interestingly, this stabilized region contains the location of the physiological stall force know also as the isometric contraction force T_0

In the soft device, the generated force again depends on the active prestress which is here represented by $\langle\langle y\rangle\rangle_{s.d.}$. Characteristically in this case the $\mathcal{F}[\langle\langle y\rangle\rangle_{s.d.}, f_{ext}]$ relations are strictly one-to-one for $D > 0$ which agrees with experiments on half force recovery capturing only part of the T_2 curve.

To make connection between the responses in hard and soft device we can consider the limit $k_m \to 0$ in the hard device configuration, see Fig.4.8. One can see that progressive lowering the spring stiffness k_m, we can continuously go from the hard device setting to the soft setting. Our next goal is to isolate the pure active component of the force. We define the "the active force" as a difference between the total generated force due to active

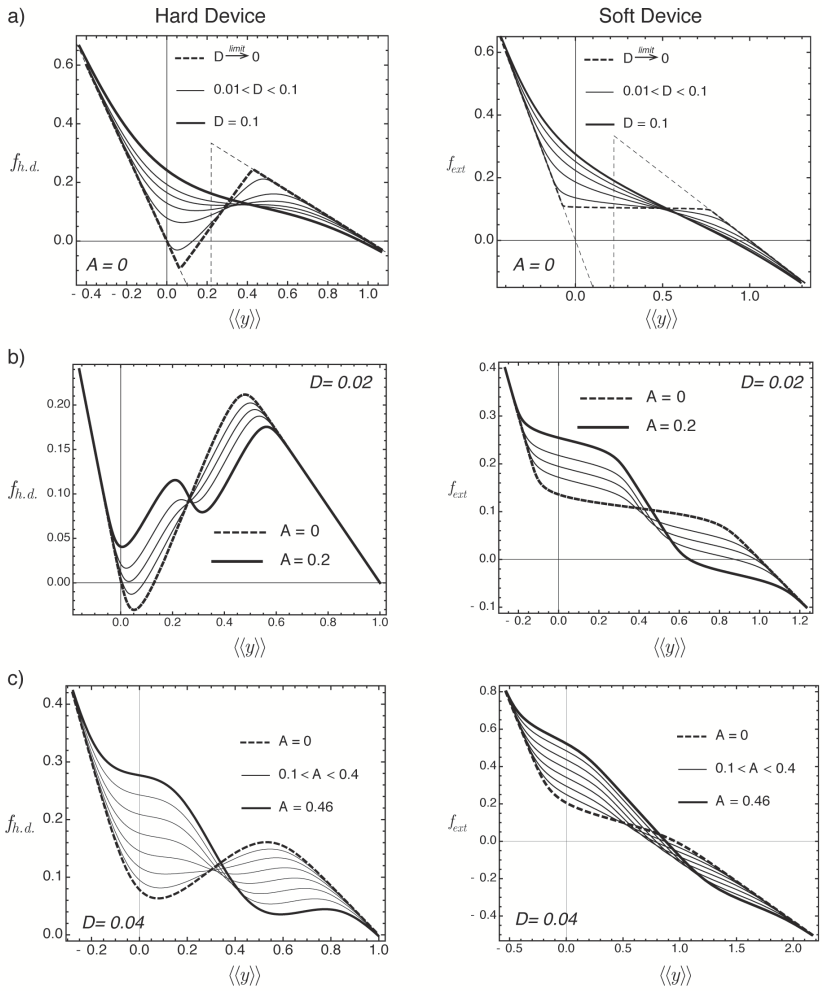

Figure 4.7. The comparison of force-displacement dependence in hard and soft device configurations in the adiabatic limit. a) The variation of the force-displacement with the increasing temperature D, without the active tilting mechanism, $A = 0$. b) The variation of the force-displacement in the presence of the active tilting mechanism at the fixed temperature $D = 0.02$. Note the second local minima which is formed in the presence of rocking. c) The variation of the force-displacement curve with the increasing amplitude A at the fixed temperature $D = 0.04$. The parameters: $k_0 = 1.5, k_1 = 0.43, l = 0.22$.

rocking $f_{tilt}(t)$ and the passive force due to thermal expansion without rocking. To this end we need to subtract from the total force the value of the passive at a given average displacement. In the soft device we define:

$$\mathcal{F}\left[\langle\langle y(A, f_{ext})\rangle\rangle_{s.d.}, f_{ext}\right] - \mathcal{F}\left[\langle y(A = 0, f_{ext})\rangle_{s.d.}, f_{ext}\right]. \tag{4.29}$$

Similarly, in the hard device:

$$\mathcal{F}\left[\langle\langle y(A, z)\rangle\rangle_{h.d.}, f_{h.d.}(A, z)\right] - \mathcal{F}\left[\langle y(A = 0, D, z)\rangle_{h.d.}, f_{h.d.}(A = 0, z)\right] \tag{4.30}$$

where $\mathcal{F}[\bullet, f(\bullet)]$ is the parametric response curve in the coordinate plane $f(\bullet)$ versus $\bullet$. In Fig.4.9 and Fig.4.10 we illustrated our results.

First in Fig.4.9 we show the active component of the force at different values of the amplitude A and fixed temperature. Notice the similarity between the responses in two devices showing that active force is practically the same in both cases.

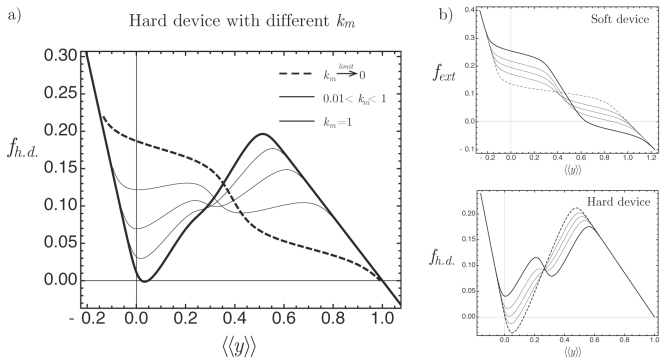

Figure 4.8. The graphic illustration of the limit $k_m \to 0$. a) The variation of the curve force-displacement in the hard device with the progressive lowering the spring stiffness k_m. b) We recall the typical curves force-displacement in hard and soft device configurations.

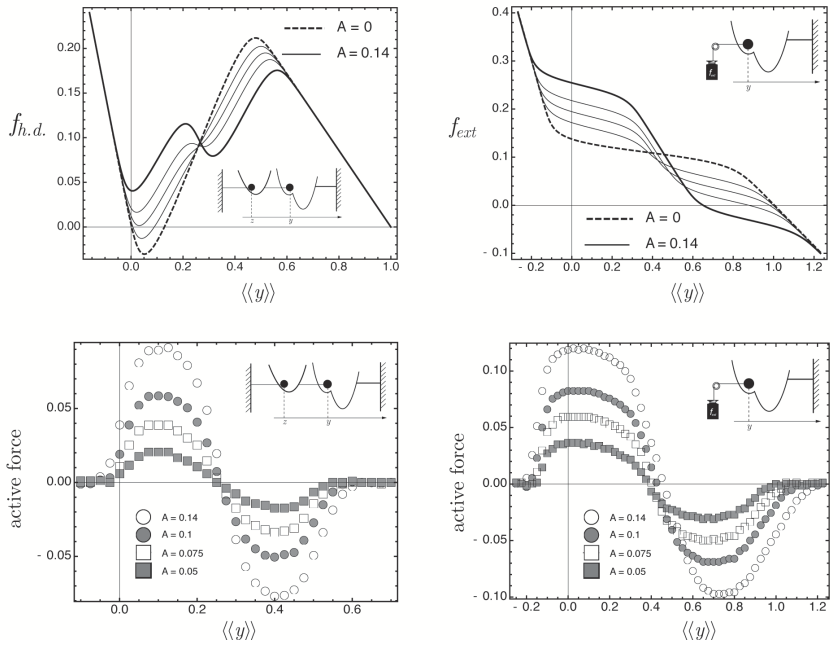

Figure 4.9. The plot of the isolated pure active component of the force in hard and soft device obtained at the fixed temperature $D = 0.01$ for the increasing amplitude A of rocking. On the top sketches we recall the force-displacement curves, the solid black lines corresponded to the system with the rocking and the dashed black line corresponded to the system without the rocking. The computation done in the adiabatic limit with the parameters: $k_0 = 1.5, k_1 = 0.43, l = 0.22$.

In Fig.4.10 we show the dependence of the active force on the temperature D at the fixed value of the rocking amplitude A. Once again we notice that the behavior of the active component is qualitatively similar in soft and hard devices. The common feature of both figures is that the active component of force is positive when the system is in the pre power stroke state and is directed towards the power stroke while it is negative when the system is in the post power stroke state and is directed towards the recharging of the power stroke mechanism. This response indicates ultimate stability of the state of isometric contractions.

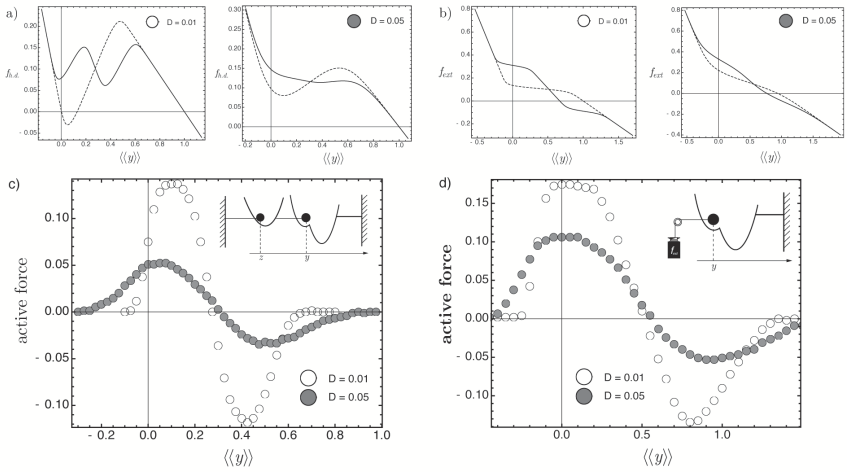

Figure 4.10. The plot of the isolated pure active component of the force in hard and soft device at the fixed amplitude $A = 0.1$ for two different temperatures. On the top sketches we recall the force-displacement curves, the solid black lines corresponded to the system with the rocking and the dashed black line corresponded to the system without the rocking. The computation done in the adiabatic limit with the parameters: $k_0 = 1.5, k_1 = 0.43, l = 0.22$.

4.4 Tension-length curve

In this section we make another interesting observation regarding the obtained curves. Suppose that we are in the hard device setting and we fix the prestress at $z = 0$. Then the generated force is simply $f_{h.d.} = k_m \langle\langle y \rangle\rangle_{h.d.}$. This gives us a parametric function $\mathcal{F}[\langle\langle y \rangle\rangle_{h.d.}, f_{h.d.}]$ obtained after the elimination of k_m. This function is different from the parametric function $\mathcal{F}[\langle\langle y \rangle\rangle_{h.d.}, f_{h.d.}]$ studied above, see Fig.4.9 and Fig.4.10, where the eliminated/varied parameter was z and k_m was fixed. Now, on the contrary, z is fixed while k_m is varied. We interpret the ensuing relation as a tension-length curve for a muscle where the number of attached cross bridges changes due, for instance, to varying overlap between actin and myosin filaments. The corresponding prestress, however, remains the same. In this section we explore the resulting curves while always using the simplest adiabatic theory.

In Fig.4.11a) we show the implied parametric plot in the interval $[0, k_m = k_{max}]$. The maximum elongation is obtained for $k_m = 0$ and we also obtain $y \to 0$ as $k_m \to \infty$ (pure soft and hard devices). We show the parametric curves for increasing value of the amplitude A while the temperature is fixed at $D = 0.01$. For hight amplitude A the temperature does not plays a big role and we can interpret our system as mechanical. Instead, for low amplitudes where we must interpret our system as a thermal engine, we observe an apparent plateau, see $A = 0.045$ in Fig.4.11b). Along the curve $A = 0.045$ the stiffness of the linear spring varies in the interval $k_m \in [0, 1]$. Moreover we observe that when $k_m \sim 0$ the system explores only the well 1 of the bi-stable potential (post power stroke state), why the average displacement is close to $y = 1$. As k_m is increasing the shape of the bistable potential changes progressively biasing more the well 0 of the bi-stable potential (pre power stroke state), As a result the system explore only the are around the bottom of the well 0 of the bistable potential,and the average displacement is close to 0. At larger values of the rocking amplitude A and low k_m (close to zero), the the system visits both local minima of the bistable potential. With increasing k_m the system gets locked in the well 0 and the average displacement becomes close to zero.

In Fig.1.13 we illustrate the implied analogy between the variation of the isometric force with the imposed sarcomere length (see the first chapter) and the behavior of our simple system in the hard device with varying stiffness of the linear spring.

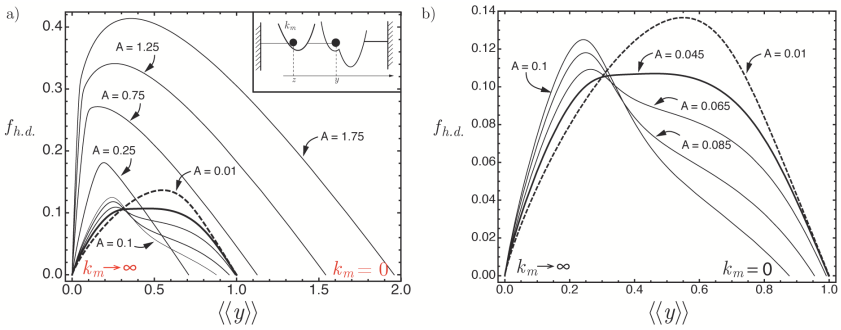

Figure 4.11. The implied parametric plot force-displacement in the interval $[0, k_m = k_{max}]$, the maximum elongation is obtained for $k_m = 0$ and we also obtain $y \to 0$ as $k_m \to \infty$ (pure soft and hard devices). a) We show the parametric curves for increasing value of the amplitude A while the temperature is fixed at $D = 0.01$. With the black dot-dashed line we plot the graph corresponded to lowest value of A and with the solid thick black line–the graph for highest amplitude A. b) The implied parametric plot force-displacement in the interval $k_m \in [0, 1]$ for the regime of low amplitude. Note, we observe an apparent plateau at $A = 0.045$. The computation done in the adiabatic limit with the parameters: $k_0 = 1.5, k_1 = 0.43, l = 0.22$.

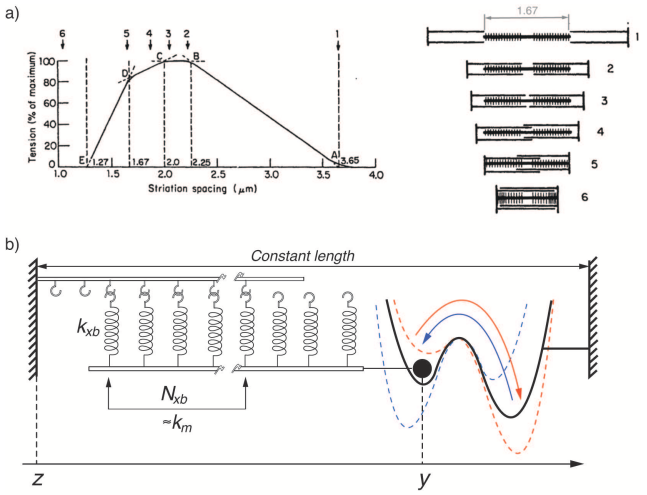

Figure 4.12. The illustration of the analogy between the variation of the isometric force with the imposed sarcomere length and the behavior of our simple system in the hard device with varying stiffness of the linear spring. a) We recall the form of developed tension versus length for single fiber [28]. b) The isometric force is directly linked to the degree of filaments overlap between thin and thick filament in each sarcomere. We link the variation of k_m with variation of the number N_{xb} of cross-bridge involved in tension generation, the stiffness k_m increases with the number of cross-bridges involved in the process.

Each point on the experimental curve tension versus elongation in Fig.4.12a), corresponds to a different state of tetanic stimulation with varying initial sarcomere length. As shown by the scheme, the isometric force is directly linked to the degree of filaments

overlap between thin and thick filament in each sarcomere. The physiological regime of the muscle is characterized by a plateau. The isometric tension starts to eventually decrease with sarcomere length even though filaments are in full overlap. Let us interpret the overlap as a number of cross-bridges interacting with actin. In isometric contraction we shall neglect the role of attachment/detachment and attribute the active role only to the power stroke mechanism and link the level of the force with the number of cross-bridges involved in process, see Fig.4.12.b). In the hard device we may view the bistable potential $V(y)$ as a primitive model of the "collective power stroke" involving certain number N_{xb} of cross-bridges. It is known that the motors consume ATP during isometric contraction, which we model by the rocking action of $f_{tilt}(t)$. The rocking effectively changes the shape of the bi-stable potential modeling. We link the variation of k_m with variation of the number N_{xb} of cross-bridge involved in tension generation. More specifically, the stiffness k_m increases with the number of cross-bridges involved in the process, however, it is not important for our discussion, how exactly N_{xb} is related to k_m. In our lump model the stiffness k_m describes the ensemble of N_{xb} cross-bridges with identical stiffnesses k_{xb}.

The presented prototypical model can be viewed as a primitive mechanical attempt to understand the tension-length curve in a sarcomere. The emergence of a characteristic plateau, observed, for instance, in the regime with $A = 0.045$, is the consequence of an asymmetric nature of the rocked bi-stable element. Usually, the plateau regime on experimental tension-length curve is linked to the fact that the number of the interacting cross-bridge remains the same. Here we argue that the plateau can also be obtained under the assumption that the number of interacting cross bridges varies to ensure that the total length of a sarcomere remains the same. This assumption may have its origin in the steric effects.

4.5 Conclusions

In this chapter we studied a simple toy-model of a single bi-stable element rocked by a time dependent periodic force at a finite temperature. The bistable potential is interpreted as describing a power-stroke in a cross-bridge. In this sense we proposed a simple mechanical interpretation of the power stroke based mechanism of active force generation in muscles due to ATP hydrolysis. We investigated two typical experimental protocols: hard and soft device, and presented some interesting manifestations of stochastic dynamics in both system. We have shown that active force generated in both devices at small amplitude of activation gets amplified by the thermal noise with the maximum effect at a particular temperature. The system can actively either increase or decrease the force and shows the effect of the dynamic stabilization of at least some spinodal states. The obtained T_2 curves agree with experiment in both soft and hard device and show that active contribution is practically the same under both protocols. Based on the hard device configuration and applying the idea of variable stiffness we were able to present a simple mechanical interpretation of the plateau type variation of the isometric force with the imposed sarcomere length.

In the next chapters we remove the constraint that the cross bridge is always attached and consider much more complex stochastic dynamics involving at least two variables: one leaving in a bi-stable potential and another one living in a periodic potential.

Chapter 5

Power stroke driven ratchets

In this chapter we combine the periodic and bi-stable potentials and propose a set of integrative models which can describe both: the fast force recovery due to power stroke (associated with the bi-stable potential) and the force velocity relations involving attachment/detachment (associated with the periodic potential). Our goal is to reinterpret the conventional bio-chemical cycle of muscle contraction in terms of a simple mechanical model of the myosin/actin interaction where we can identify relative mechanical roles of the power stroke and of the attachment/detachment process. The novelty of our approach is in shifting the activity function from the periodic potential as in the conventional models of Brownian ratchets to the bi-stable potential. In this way we explore a possibility that the power stroke machinery is not only crucial for passive fast force recovery but is also essential for the active functioning of the main motor behind muscle contraction. In a slightly different terms, we propose a new model of a Brownian ratchet with internal degree of freedom which is driven by an internal rather than external flashing.

5.1 Introduction

We begin by recalling the bio-chemical scheme of muscle contraction based on the hydrolysis of the ATP. We adopt the four-step Lymn-Taylor model for the myosin enzymatic cycle [70]. In very general terms, this cycle implies two coordinates. Along one of them there are two states, associated with two positions of the lever-arm corresponding to two conformational states of the myosin head. Along the other one there are also two states describing attached and detached configurations of the acto-myosin system. In $2\mathbb{D}$ the ensuing $2x2 = 4$ configurations as usually represented as 4 vertices of a square. The biochemical description of these four vertices goes as follows.

Upon binding of an ATP molecule, myosin detaches from actin in a very fast process (detached, post power stroke). In the detached state myosin hydrolyzes ATP into stable products: ADP and phosphate Pi and this reaction pushes the swing the level arm while charging the power stroke mechanism (detached pre power stroke). Without the ATP the myosin head reattaches to a neighbouring actin site (attached pre power stroke). In the attached state the conformational change takes place which moves the actin filament by $6 - 10nm$ (attached, post power stroke). During the power stroke first the release of Pi molecule takes place and at the end of the power stroke, ADP is also released. The new ATP molecule can now bind to the myosin, and the cycle starts again. One can see that on one side ATP facilitates detachment and on the other side its hydrolysis recharges the power stroke element. The challenge is to translate this description into the language of a

specific mechanical action of an external energy reservoir on a mechanical system with few degrees of freedom. Below we list some physical effect that our prototypical model must capture:

- The motor moves in a fluid medium and is subjected to random thermal fluctuations. It can also receive indirected energy from an external reservoir.
- The received energy is converted/transduced into mechanical work with certain efficiency.
- The unidirectional motion along the actin filament is due to the conformational changes in the myosin head.
- The mechanical cycle of force generation includes four clearly distinguished stages that can be associated with four steps of the biochemical cycle.

While the first two items in this list are standard, the last two items are new. Indeed, usually the power stroke plays only a passive role in the models of non-processive motors and the Lymn-Taylor cycle is usually lumped into two or at most three steps. Below we discuss several specific mechanical set ups which can be potentially used as the mechanical analogs of the Lymn-Taylor cycle. None of them can be dismissed without a detailed quantitative study.

5.2 General formalism

The chemo-mechanical Lymn-Taylor cycle offers a highly organized vision of acto-myosin interaction, and we need to map this "order" into space and time, using the language of mechanics. Denote by A the attached state in the pre-power stroke configuration, by B the attached state in the post-power-stroke configuration, by C the detached state in the post-power stroke configuration and finally by D the detached state in the pre-power-stroke configuration, see Fig. 5.1a. The progressing motor passes through different replicas of the main four configurations as shown in Fig.5.1b. In Fig.5.1c we sketch a prototypical energy landscape in the configurational space $\mathbf{X}$ where the replicas of the original four states are represented by equivalent wells of the potential $G(\mathbf{X}, t)$. One can see that the mechanical system must be at least two dimensional to reproduce the energy landscape with this complexity. In real space the model can still be one dimensional with two internal variables if different wells can be projected on a single spatial dimension. For instance, we can interpret the attached configurations as the energy minimum states for one of the internal variables along a space-periodic potential and the detached configurations as the maxima/plateaus as it is illustrated in Fig.5.1d. The second variable, coupled to the first one, may live in a double well potential which can also be projected into the same spatial coordinate.

Inspired by the work of Magnasco [72] we represent the chemical activity of the highly non equilibrium ATP hydrolysis by the action of a mechanical force with zero average. If this mechanical action is not correlated, the underlying chemical reaction is in equilibrium. Therefore we must present the mechanical action of the ATP hydrolysis as a correlated noise. By grossly exaggerating the strength of the correlations, we shall be using a simple periodic signal as the source of external energy. The internal mechanical device must work as a ratchet. Being exposed to a correlated noise such ratchet should be able to consume the indirected energy and transform it into the work or motion.

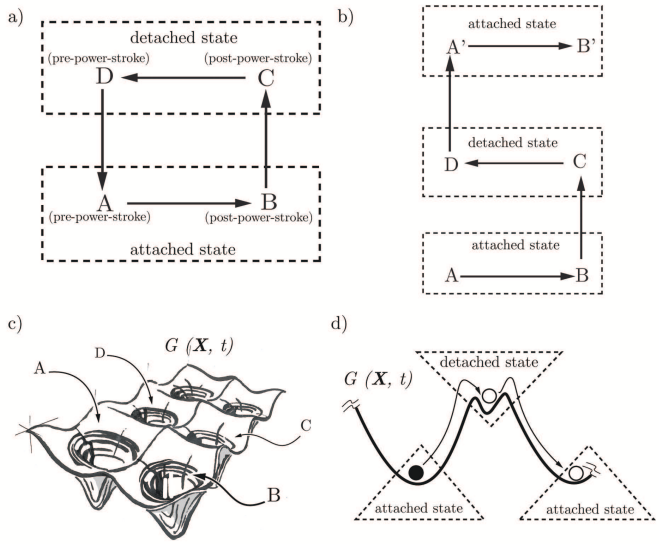

Figure 5.1. a) The simple graphic representation of four-state Lymn-Taylor cycle. b) The progressing motor passes through different replicas of the four configurations. c) The prototypical energy landscape in the configurational space $\mathbf{X}$ where the replicas of the original four states are represented by equivalent wells of the potential $G(\mathbf{X}, t)$. d) We interpret the attached configurations as the energy minimum states for one of the internal variables along a space-periodic potential and the detached configurations as the maxima/plateaus.

More specifically, our mechanical model will be dealing with three stochastic variables x, y, z see the Fig.5.2. The motor head position is represented by x and the connection point of a cross-bridge with a myosin filament is represented by z. The precise interpretation of y is more delicate, because this variable describes the configuration of the lever-arm inside the cross-bridge.

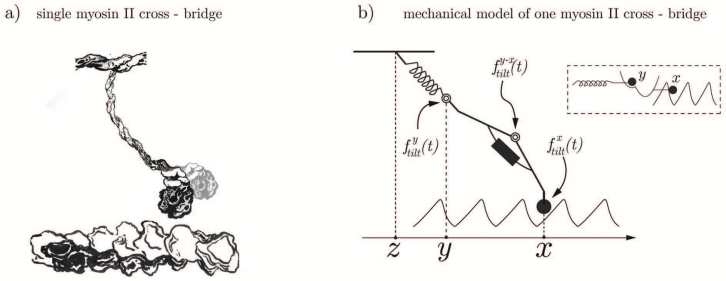

Figure 5.2. a) One myosin II protein projected from the myosin in the detached configuration, not drown to scale. b) The mechanical model of one cross-bridge. The motor head position is represented by x variable and the connection point of a cross-bridge with a myosin filament is represented by z variable. The y variable describes the configuration of the lever-arm inside the cross-bridge.

We assume that the connection between the motor head and the motor tail attached to the myosin filament can be modeled as a bi-stable spring. Inside the tail we introduce a linear spring imitating the cross bridge stiffness. The interaction between the myosin head and the actin filament is represented by a space periodic potential. This potential provides

a very simplified description of the different bound configurations available in acto-myosin system.

The energy provided by the ATP hydrolysis affects on one side the actin/myosin bound states and on the other side - the conformational state of the lever-arm. This means that the corresponding correlated force signal can affect coordinate either x or coordinate y or even both. The coordinate z is assumed to be far away from the ATP source and will be used to specify the external loading (soft or hard device).

To model the ensuing system we write the corresponding system of overdamped Langevin equations:

$$\boldsymbol{\eta}\frac{d\mathbf{X}}{dt} = -\nabla G(\mathbf{X},t) + \boldsymbol{\sigma}\boldsymbol{\xi}(t) \tag{5.1}$$

with

$$\boldsymbol{\eta} = \begin{pmatrix} \eta_x & 0 & 0 \\ 0 & \eta_y & 0 \\ 0 & 0 & \eta_z \end{pmatrix}, \qquad \mathbf{X} = \begin{pmatrix} x(t) \\ y(t) \\ z(t) \end{pmatrix}, \qquad \boldsymbol{\xi}(t) = \begin{pmatrix} \xi_x(t) \\ \xi_y(t) \\ \xi_z(t) \end{pmatrix} \tag{5.2}$$

Here σ is constant diagonal matrix:

$$\boldsymbol{\sigma} = \begin{pmatrix} \sqrt{2\eta_x D} & 0 & 0 \\ 0 & \sqrt{2\eta_y D} & 0 \\ 0 & 0 & \sqrt{2\eta_z D} \end{pmatrix} \tag{5.3}$$

while $\boldsymbol{\xi}(t)$ is the vector Gaussian random variable with zero mean $\langle \xi_i(t) \rangle = 0$, and with correlations given by

$$\langle \xi_i(t)\xi_j(s) \rangle = \delta_{ij}\delta(t-s), \qquad t > s, \quad i,j = x,y,z. \tag{5.4}$$

The function $G(\mathbf{X},t)$ introduces the complex energy landscape of the motor device coupling the space periodic potential, the bi-stable potential and the quadratic potential describing the linear spring

$$G(\mathbf{X},t) = G(x,y,z,t) = \Phi(x) + V(y-x) - xf^x_{tilt}(t) - yf^y_{tilt}(t) + \frac{1}{2}k_m(y-z)^2 - zf_{ext} \tag{5.5}$$

Here, the bi-stable potential $V(y-x)$ describes two conformational states of the power stroke mechanism. We used $y-x$ as the argument (instead of $x-y$), because it describes the experimental situation better, see Fig.5.2b and c. The power stroke variable $y-x$ can be in two energy wells: "0" and "1". We identify well "0" with the pre-power-stroke state and well "1" with the the post-power-stroke state. The potential $\Phi(x)$ describes the (typically) asymmetric ratchet-like potential: it is periodic function with period L so that $\Phi(x+L) = \Phi(x)$. We define the force term $f^i_{tilt}(t)$ imitating the ATP activity as a periodic function with zero average over the period T_i; in general the function $f^i_{tilt}(t)$ does not have to be the same for $i = x$ and $i = y$ as the corresponding time periods T_i may be different. Finally the terms $\eta_i\dot{x}_i$ describe frictional forces and the drag coefficients are assumed to be constants. The external cargo is represented by the force f_{ext} acting on the z coordinate.

In fact, as in the previous chapter, we can build two archetypal experimental device –hard and soft. On the Fig.5.3 we illustrate two representations of the system depending on whether we use $y-x$ or $x-y$ as a power stroke variable. In our computations we usually use $y-x$, however to simplify the figures we will often use the configuration shown in Fig.5.3a).

Notice that in the Fig.5.3 we present a model of a single cross-bridge described by three internal variables. However, the third coordinate z is important only when we consider

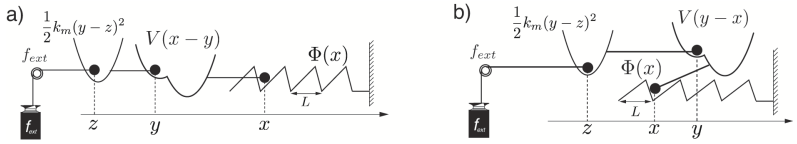

Figure 5.3. An illustration of two representations of the system in soft device configuration depending on whether we use $x - y$ a) or $y - x$ b) as a power stroke variable.

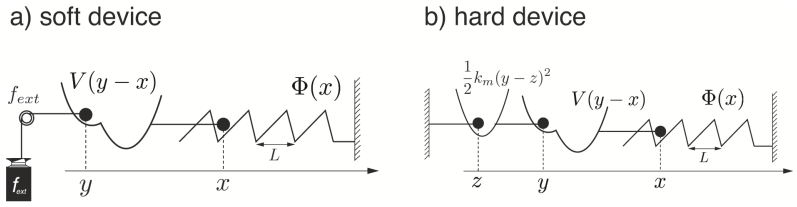

Figure 5.4. The sketch of hard and soft device corresponded to the model of one single cross-bridge.

interaction of several cross-bridges. For the description of a single cross bridge we will often us two parametric model with coordinates x, y as it is shown in Fig.5.4a). This model is sufficient in the case of soft device. The the case of hard device the model requires three variables, however the variable z must be treated as fixed external parameter. In this case the system can be again described by a system of two coupled overdamped Langevin equations.

5.2.1 Energy landscape

Our equations (5.1) and (5.5) contain the bistable potential $V(y-x)$ and the periodic potential $\Phi(x)$. The sum of the potentials $V(y-x)$ and $\Phi(x)$ defines the intrinsic energy landscape of the motor.

To be specific, we define the double-well potential as a minimum of two parabolas with stiffness k_0 and k_1. The bottoms of the energy wells are located in the points 0 and a;the degenerate barrier is located at l:

$$V(y-x) = \begin{cases} \frac{1}{2}k_0\,(y-x)^2 + \varepsilon_0 & (y-x) \leqslant l \\ \\ \frac{1}{2}k_1\,(y-x-a)^2 & (y-x) \geqslant l \end{cases} \tag{5.6}$$

As $k_0 \neq k_1$ and $l \neq a/2$ the bistable potential is asymmetric with $\varepsilon_0 = 1/2\left(k_1(l-a)^2 - k_0 l^2\right)$. We associate with the well "0" stiffness k_0 and with the well "1" – stiffness k_1. To model asymmetric periodic potential $\Phi(x)$ we can use a combination of two trigonometric functions, say

$$\Phi(x) = \frac{V_{max}}{2\pi}\left(b_0 \sin(\frac{2\pi(x-x_0)}{L}) + b_1 \sin(\frac{4\pi(x-x_0)}{L})\right) \tag{5.7}$$

where b_0 and b_1 control the asymmetry of the potential and L is the period. The parameter x_0 prescribes the origin of the coordinate system and does not influence any of the results.

The tilting force, $f_{tilt}(t)$, imitating the ATP activity can also be defined as a trigonometric function with amplitude A and period T. By construction, the average force over

the period must be equal to zero, $\int_0^T dt f_{tilt}(t) = 0$. For instance, we can consider:

$$f_{tilt}(t) = A\cos(\frac{2\pi t}{T}) \tag{5.8}$$

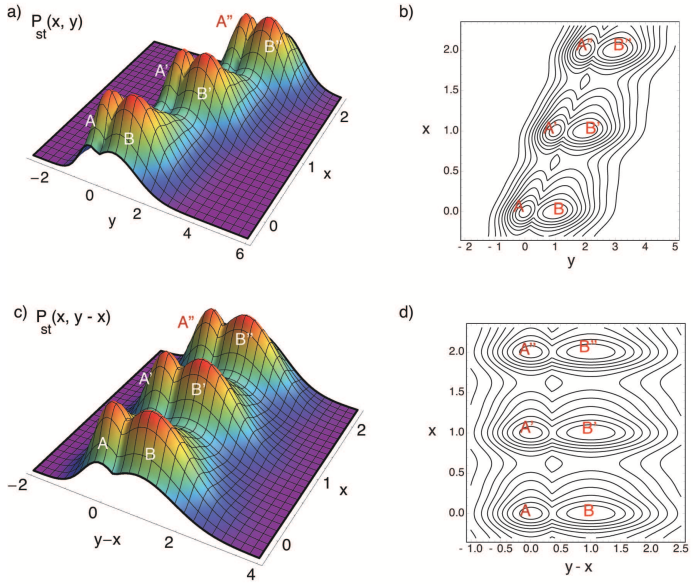

Figure 5.5. The stationary probability distribution associated with energy $G_0(x, y) = \Phi(x) + V(y - x)$. Each maximum is a particular 'bound' state that our system may occupy. a) We present the system in orthogonal coordinates $[y, x]$. b) We present the system in coordinates $[y - x, x]$.

Consider now the intrinsic energy landscape

$$G_0(x, y) = \Phi(x) + V(y - x) \tag{5.9}$$

in more detail. We recall that the energy minima in this landscape can be associated with particular (chemical) states of the motor. In addition to the direct plot the energy landscape we can also consider the stationary probability distribution:

$$P_{st}(x, y) = Z^{-1} \exp\left(-\frac{G_0(x, y)}{D}\right) \tag{5.10}$$

where Z is normalization constant. It is clear that the minima of the energy landscape are associated with the maxima of the probability distribution at fixed temperature, measured by $D = k_B T$.

In Fig.5.5 we show the stationary probability distribution associated with energy,(5.9). It has a periodic structure along x axes due to the periodicity of the ratchet potential defined in (5.7). The asymmetric probability maxima along y axes reflect the well of the bi-stable potential (5.6). Each maximum is a particular 'bound' state that our system may occupy. In the figure we labeled the well "0" as A and the well "1" as B. The replica wells are label as $[A', A'', \dots]$.

In Fig.5.5a) we present the system in orthogonal coordinates $[y, x]$ while in Fig.5.5b) we show the same system in coordinates $[y - x, x]$. The latter coordinates can be used for the identification of the mechanical states with the bio-chemical states of the Lymn-Taylor

cycle. In what follows all computations will be performed in orthogonal coordinates x, y while all the plots will be presented in coordinates $[y - x, x]$. In Fig.5.5 we presented the typical view of untitled landscape $\Phi(x) + V(y - x)$, this is also the landscape in the soft device with zero load f_{ext}. The introduction of additional linear spring $1/2k_m(y - z)^2$ in the hard device modifies the probability distribution because it changes the shape of the effective bi-stable potential. Note that hard device configuration usually biases considerably the landscape privileging the pre-power stroke configuration.

We can now discuss mechanical equivalents of the Lymn-Taylor states. Consider, for instance, a cross-bridge in the soft device shown in 5.5. Under the action of the noise which has thermal and correlated components the motor moves cyclically through different states performing mechanic work. The question that we can ask is what will be the averaged behavior and whether we can interpret particular dynamic configurations in the motor cycle with the four states of the biochemical Lymn-Taylor cycle. In our two-dimensional energy landscape we can identify the pre-power-stroke and the post-power-stroke configurations with the two wells of the bistable potential. The minima of the periodic potential can be viewed as the attached states. Regarding the detached states we shall consider three possible interpretations:

- We can interpret the detached states as the maxima of our periodic potential $\Phi(x)$. In this way we capture the fact that in the detached state the interaction force between actin and myosin is equal to zero but essentially neglect the time spent by the motor in the detached state. Doing so we misrepresent the duty ratio–the fraction of time spent in the attached state. This makes it difficult to differentiate between the processive and non-processive motors. However, in this way we obtain a unifying description and develop a general framework allowing one to describe both kinesin, an example of processive protein motor, and myosin II, the typical non-processive motor.

- We can interpret the detached states as the special minima of the periodic potential $\Phi(x)$. To this end we would need to change the definition of $\Phi(x)$ given in (5.7) and introduce additional wells or plateau around each maximum while preserving the periodicity $\Phi(x + L) = \Phi(x)$ and the asymmetry. In this setting, the motor still moves along the x coordinate only but can spend longer time in the special 'detached' energy wells that may be very flat.

- Finally, we can take into account the steric effects and assume that in the detached state the acto myosin interaction is weakened independently on the position of the motor inside the periodic potential. This idea, taken from the theory of flashing ratchets, will be pursued in the very last section of the Thesis and for now we focus on the first two options.

In Fig.5.6 we illustrate two alternative representations of the cycle shown in Fig.5.1b) based on the first representation of the detached state. The both shown cases the system goes through four mechanical configurations which can be associated with the bio-chemical states described by the Lymn-Taylor cycle. The question now is whether our mechanical model can indeed exhibit such highly organized behavior.

5.3 The basic designs

The system (5.1) with potential (5.5) is very general and now we specify several archetypal problem set ups which we later study in full detail. Our main idea is that the external

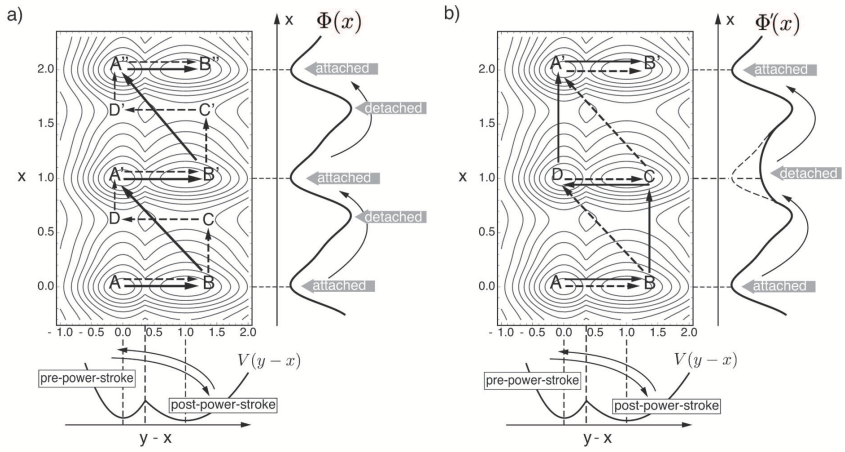

Figure 5.6. An illustration of two alternative representations of the Lymn-Taylor cycle. a) The detached states is the maxima of our periodic potential $\Phi(x)$. With the arrows we show the possible motor cycles, we can interpret the transition $A \to B$ as a motor power-stroke. b) The detached states is the special minima of the periodic potential $\Phi'(x)$. With the arrows we show the possible motor cycles.

stimulation representing mechanical manifestation of the ATP hydrolysis is associated mainly with the power-stroke rather than with actin filament. the power stroke in our model is described by coordinate $y - x$ and therefore we can model external correlated signal by forces acting on coordinate x, coordinate y or even their difference $x - y$. We define these three sub-family of motor devices below and formulate in each case a closed two parametric stochastic description.

5.3.1 X-tilted model

Consider a system characterized in a soft device configuration by the potential $G(\mathbf{X}, t)$:

$$G(x, y, t) = \Phi(x) + V(y - x) - x f_{tilt}(t) - y f_{ext} \tag{5.11}$$

The corresponding stochastic system with two degrees of freedom is described by the following overdamped Langevin equations:

$$\begin{cases} \eta_x \dfrac{dx}{dt} = -\partial_x \Phi(x) - \partial_x V(y - x) + f_{tilt}(t) + \sqrt{2\eta_x D}\ \xi_x(t) \\ \eta_y \dfrac{dy}{dt} = -\partial_y V(y - x) + f_{ext} + \sqrt{2\eta_y D}\ \xi_y(t). \end{cases} \tag{5.12}$$

In X-tilted model, which was first introduced in [75], the correlated noise acts only on x variable which can be interpreted as tilting of the periodic potential. To illustrate the role of the correlated noise $f_{tilt}(t)$ on this model we can replace the time dependent force $f_{tilt}(t)$ by a constant, which can be either positive $+A$ and negative $-A$. We obtain time independent potentials of the form

$$G(x, y, A) = \begin{cases} \Phi(x) + V(y - x) - xA - y f_{ext} & for \quad f_{tilt}(t) > 0 \\ \Phi(x) + V(y - x) + xA - y f_{ext} & for \quad f_{tilt}(t) < 0 \end{cases} \tag{5.13}$$

With each of these potentials we can associate the stationary probability distribution $P_{st}(x, y-x, A)$ which can be written as:

$$P_{st}(x, y-x, A) = \begin{cases} Z_+^{-1} \exp\left(-\dfrac{\Phi(x) + V(y-x) - xA - yf_{ext}}{D}\right) & \text{for} \quad f_{tilt}(t) > 0 \\ Z_-^{-1} \exp\left(-\dfrac{\Phi(x) + V(y-x) + xA - yf_{ext}}{D}\right) & \text{for} \quad f_{tilt}(t) < 0 \end{cases} \tag{5.14}$$

where Z_+ and Z_- are the corresponding normalization factors. In Fig.5.7a),b) we show the probability distributions and the corresponding surface contour plot for the case when $f_{ext} = 0$. As the tilting force $f_{tilt}(t)$ changes periodically from positive to negative value

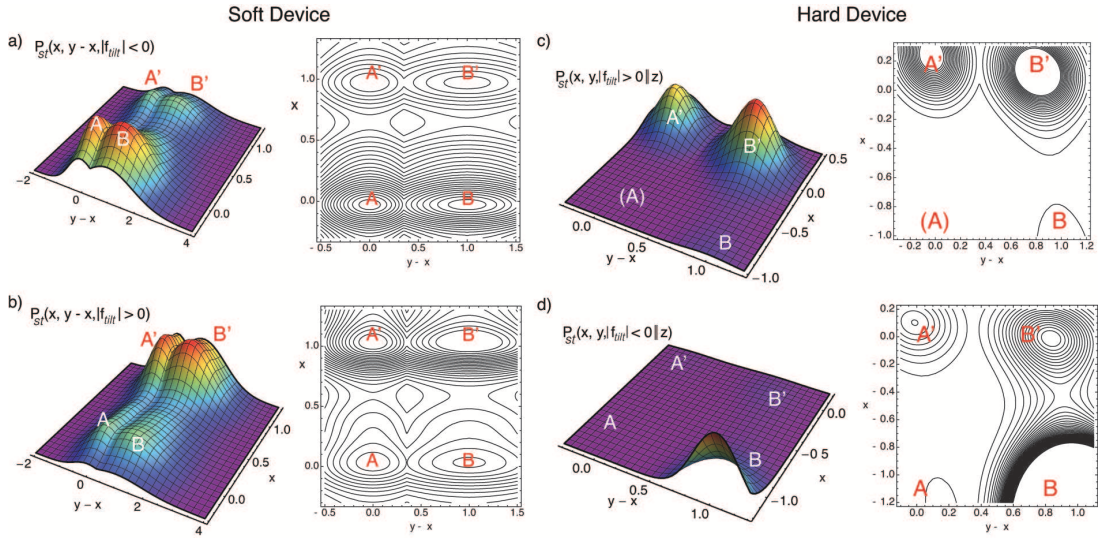

Figure 5.7. X-tilted model in soft and hard device configuration. a) The stationary probability distribution and the corresponded surface contour plot in the positive phase of rocking in soft device configuration with $f_{ext} = 0$. b) The stationary probability distribution and the corresponded surface contour plot in the negative phase of rocking in soft device configuration with $f_{ext} = 0$. c) The stationary probability distribution and the corresponded surface contour plot in the positive phase of rocking in hard device configuration with $z = 0$. d) The stationary probability distribution and the corresponded surface contour plot in the negative phase of rocking in hard device configuration with $z = 0$. We decided change the landscape parameters in hard device configuration in order to obtain the representative illustration.

the rocking biases different energy wells in the periodic potential associated with the x axes: when $f_{tilt}(t) > 0$ the probability density has maxima at A', B' and when $f_{tilt}(t) < 0$ the probability density has maxima at A, B.

To describe the hard device setting we use the potential $G(\mathbf{X}, t)$:

$$G(x, y, t) = \Phi(x) + V(y-x) + \frac{1}{2}k_m(y-z)^2 - xf_{tilt}(t) \tag{5.15}$$

where z is now a parameter. The corresponding system of the overdamped Langevin equations reads

$$\begin{cases} \eta_x \dfrac{dx}{dt} = -\partial_x \Phi(x) - \partial_x V(y-x) + f_{tilt}(t) + \sqrt{2\eta_x D}\ \xi_x(t) \\ \eta_y \dfrac{dy}{dt} = -\partial_y V(y-x) - k_m(y-z) + \sqrt{2\eta_y D}\ \xi_y(t) \end{cases} \tag{5.16}$$

We can again define the stationary probability distribution in the adiabatic approximation by considering two types of forces $f_{tilt}(t)$: positive and negative.

$$P_{st}(x, y-x, A \parallel z) = \begin{cases} Z_+^{-1} \exp\left(-\dfrac{G_{h.d.}(x,y,z,A>0)}{D}\right) & \text{for} \quad f_{tilt}(t) > 0 \\ Z_-^{-1} \exp\left(-\dfrac{G_{h.d.}(x,y,z,A<0)}{D}\right) & \text{for} \quad f_{tilt}(t) < 0 \end{cases} \tag{5.17}$$

where Z_+ and Z_- are the corresponding normalization factors. For determinacy we take $z = 0$ in (5.17) and obtain

$$G_{h.d}(x, y-x, z, A) = \begin{cases} \Phi(x) + V(y-x) + \dfrac{1}{2}k_m(y-z)^2 - xA & \text{for} \quad f_{tilt}(t) > 0 \\ \Phi(x) + V(y-x) + \dfrac{1}{2}k_m(y-z)^2 + xA & \text{for} \quad f_{tilt}(t) < 0 \end{cases} \tag{5.18}$$

In Fig.5.7c),d) we show the probability distributions defined by (5.17) and the corresponding surface contour plot for the case when $z = 0$. Note what we changed the numeric values of geometric parameter of energy landscape in order better to illustrate the characteristic motor behavior of hard device configuration.

Notice that in soft device the tilting does not differentiate clearly between the pre and post power stroke configurations while in the hard device the post power stroke configurations is obviously biased.

In summary, the model with X-tilting attributes active role to the actin fiber described by the periodic potential. Active interaction of the myosin head with this filament produces a (Brownian) ratchet which is the main driving force behind the motor activity. The motor is then expected to periodically recharge the power stroke element creating the cycling process and ensuring the constant force generation. The power stroke is passive in this scheme and in the next section we show that gives rise to the cycle reproducing only few of the expected biochemical states.

5.3.2 Y-tilted model

In this setting we assume that the system characterized by the potential

$$G(x, y, t) = \Phi(x) + V(y-x) - yf_{tilt}(t) - yf_{ext} \tag{5.19}$$

where the rocking action is now applied only to y variable. The corresponding system of the overdamped Langevin equations take the form

$$\begin{cases} \eta_x \dfrac{dx}{dt} = -\partial_x \Phi(x) - \partial_x V(y-x) + \sqrt{2\eta_x D}\ \xi_x(t) \\ \eta_y \dfrac{dy}{dt} = -\partial_y V(y-x) + f_{ext} + f_{tilt}(t) + \sqrt{2\eta_y D}\ \xi_y(t) \end{cases} \tag{5.20}$$

Once again, to illustrate the role of the correlated noise $f_{tilt}(t)$ on the motor dynamics we consider an adiabatic setting and replace the variable force $f_{tilt}(t)$ by the constant force, which can be positive $+A$ and negative $-A$. We will then write

$$G(x, y, A) = \begin{cases} \Phi(x) + V(y-x) - yA - yf_{ext} & \text{for} \quad f_{tilt}(t) > 0 \\ \Phi(x) + V(y-x) + yA - yf_{ext} & \text{for} \quad f_{tilt}(t) < 0 \end{cases} \tag{5.21}$$

Define again the stationary probability distribution $P_{st}(x, y-x, A)$

$$P_{st}(x, y-x, A) = \begin{cases} Z_+^{-1} \exp\left(\dfrac{\Phi(x) + V(y-x) - yA - yf_{ext}}{D}\right) & \text{for} \quad f_{tilt}(t) > 0 \\ Z_-^{-1} \exp\left(\dfrac{\Phi(x) + V(y-x) + yA - yf_{ext}}{D}\right) & \text{for} \quad f_{tilt}(t) < 0 \end{cases} \tag{5.22}$$

where Z_+ and Z_- are the corresponding normalization factors. To make the action of the driving force more transparent we take $f_{ext} = 0$ and show in Fig.5.8 the energy landscape and the and the corresponding probability distribution function in the soft device. One can

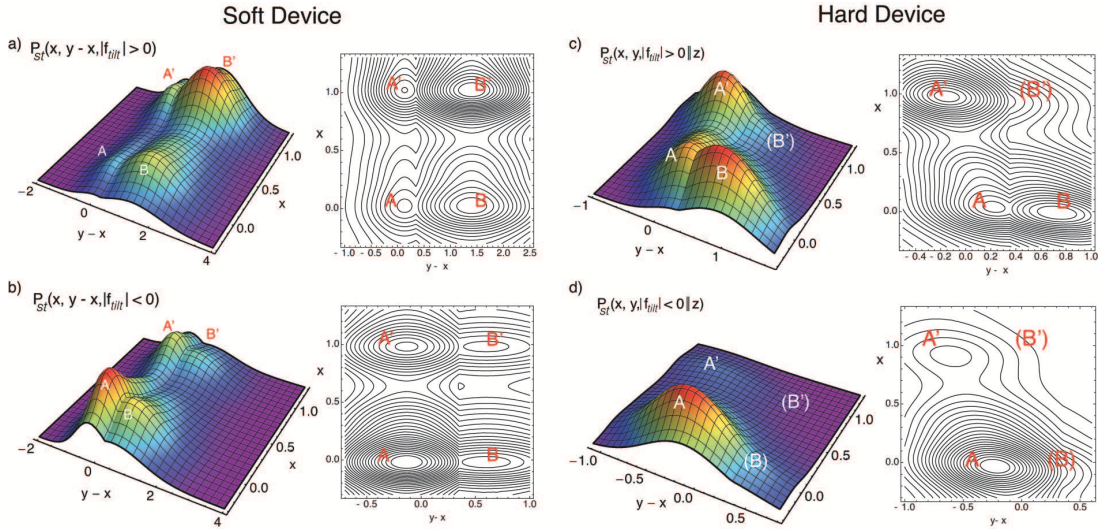

Figure 5.8. Y-tilted model in soft and hard device configuration. a) The stationary probability distribution and the corresponded surface contour plot in the positive phase of rocking in soft device configuration with $f_{ext} = 0$. b) The stationary probability distribution and the corresponded surface contour plot in the negative phase of rocking in soft device configuration with $f_{ext} = 0$. c) The stationary probability distribution and the corresponded surface contour plot in the positive phase of rocking in hard device configuration with $z = 0$. d) The stationary probability distribution and the corresponded surface contour plot in the negative phase of rocking in hard device configuration with $z = 0$.

see that now the action of the tilting produces more complex biasing action. In particular, in two subsequent attached states two different states of the power stroke mechanism may be biased. Thus, at $f_{tilt}(t) > 0$ the highest peak of the probability density is in B' while at $f_{tilt}(t) < 0$, the highest peak is at A. This means that the advance of the motor in this model is automatically accompanied with the power stroke making the two phenomena practically indistinguishable.

In the hard device configuration we use the potential

$$G(x, y, t) = \Phi(x) + V(y-x) + \frac{1}{2}k_m(y-z)^2 - yf_{tilt}(t) \tag{5.23}$$

where z is now a fixed parameter. The corresponding system of overdamped Langevin equations takes the form

$$\begin{cases} \eta_x \dfrac{dx}{dt} = -\partial_x \Phi(x) - \partial_x V(y-x) + \sqrt{2\eta_x D}\ \xi_x(t) \\ \eta_y \dfrac{dy}{dt} = -\partial_y V(y-x) - k_m(y-z) + f_{tilt}(t) + \sqrt{2\eta_y D}\ \xi_y(t) \end{cases} \tag{5.24}$$

As we see from Fig. 5.8c),d) the probability distribution is again strongly influenced by the type of the loading device. In particular, one may have different states of the power stroke mechanism biased in different phases of the external loading without the advance of the motor along the actin filament. This opens the way of describing two attached states, pre and post power stroke, shifting activity from actin filament to the power stroke itself. In reality we do not know exactly with which degrees of freedom to associate the activity of the ATP hydrolysis because all these effective variables characterizing a complex of large number of molecules are geometrically very close and the mechanical action of the reaction may even affect several degrees of freedom simultaneously. For instance, the variable Y couples the attachment mechanism and the power stroke mechanism and therefore the Y-tilted model may be considered as an intermediate between the X-tilted model making the filament active and XY-tilted model assuming that activity is fully localized in the power stroke element.

5.3.3 XY-tilted model

The XY-tilted model is characterized by the following potential

$$G(x,y,t) = \Phi(x) + V(y-x) - (y-x)f_{tilt}(t) - yf_{ext} \tag{5.25}$$

In this model the external force tilts directly the bi-stable potential why the actin filament remains fully passive. The potential (5.25) can be obtained from (5.5) by choosing $T_x = T_y$ and $f^y_{tilt}(t) = -f^x_{tilt}(t)$. The corresponding system of the overdamped Langevin equations takes the form

$$\begin{cases} \eta_x \dfrac{dx}{dt} = -\partial_x \Phi(x) - \partial_x V(y-x) - f_{tilt}(t) + \sqrt{2\eta_x D}\,\xi_x(t) \\ \eta_y \dfrac{dy}{dt} = -\partial_y V(y-x) + f_{ext} + f_{tilt}(t) + \sqrt{2\eta_y D}\,\xi_y(t) \end{cases} \tag{5.26}$$

As in the other two cases we illustrate the role of the correlated component of the noise f_{tilt} which now acts in a coherent manner on variables x and y by replacing $f_{tilt}(t)$ with a constant term which can be either positive $+A$ or negative $-A$. We can write the corresponding tilted potentials in the form

$$G(x,y,A) = \begin{cases} \Phi(x) + V(y-x) - A - (y-x)f_{ext} & \text{for} \quad f_{tilt}(t) > 0 \\ \Phi(x) + V(y-x) + A - (y-x)f_{ext} & \text{for} \quad f_{tilt}(t) < 0 \end{cases} \tag{5.27}$$

We can now compute the stationary probability distribution associated with different degree of tilting

$$P_{st}(x,y,A) = \begin{cases} Z_+^{-1} \exp\left(\dfrac{\Phi(x) + V(y-x) - A - (y-x)f_{ext}}{D}\right) & \text{for} \quad f_{tilt}(t) > 0 \\ Z_-^{-1} \exp\left(\dfrac{\Phi(x) + V(y-x) + A - (y-x)f_{ext}}{D}\right) & \text{for} \quad f_{tilt}(t) < 0 \end{cases} \tag{5.28}$$

where Z_+ and Z_- are the corresponding normalization factors; to simplify the picture we again take $f_{ext} = 0$. In Fig.5.9a),b) we show the stationary probability and corresponded surface contour plot in the case of soft device.

From Fig.5.9a),b) one can see that XY tilting can now bias the post power stroke in the neighboring sites of the periodic potential which we could not achieve in any of the previously considered models. This means that attachment detachment can take place

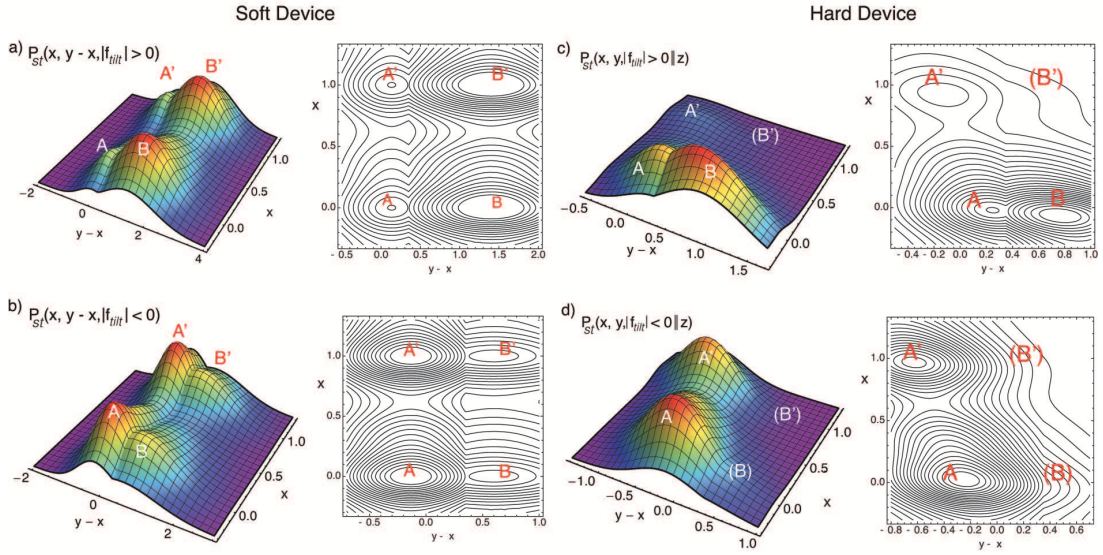

Figure 5.9. XY-tilted model in soft and hard device configuration. a) The stationary probability distribution and the corresponded surface contour plot in the positive phase of rocking in soft device configuration with $f_{ext} = 0$. b) The stationary probability distribution and the corresponded surface contour plot in the negative phase of rocking in soft device configuration with $f_{ext} = 0$. c) The stationary probability distribution and the corresponded surface contour plot in the positive phase of rocking in hard device configuration with $z = 0$. d) The stationary probability distribution and the corresponded surface contour plot in the negative phase of rocking in hard device configuration with $z = 0$.

without changing of the state of the power stroke element which opens additional ways of reproducing the whole variety of chemical states constituting the Lymn-Taylor cycle.

In the hard device setting the potential takes the form:

$$G(x, y, t) = \Phi(x) + V(y - x) + \frac{1}{2}k_m(y - z)^2 - (y - x)f_{tilt}(t) \tag{5.29}$$

where z is again a fixed parameter. The corresponding system of the overdamped Langevin equations reads

$$\begin{cases} \eta_x \dfrac{dx}{dt} = -\partial_x \Phi(x) - \partial_x V(y - x) - f_{tilt}(t) + \sqrt{2\eta_x D}\ \xi_x(t) \\ \eta_y \dfrac{dy}{dt} = -\partial_y V(y - x) - k_m(y - z) + f_{tilt}(t) + \sqrt{2\eta_y D}\ \xi_y(t) \end{cases} \tag{5.30}$$

The energy landscape corresponding to different levels of tilt and the associated stationary probability distribution are shown in Fig. 5.9c),d). This model shows a very reach behavior which will be fully explored in the special chapter dedicated to the XY tilted model.

5.4 Conclusions

In this chapter we identified two crucial degrees of freedom which can be mechanically associated with the power stroke and with the attachment detachment process in a single cross bridge. We then proposed a series of models which are based on different interpretations of the mechanical role of the ATP activity expressed in terms of these two internal

degrees of freedom. Since our goal is to consider models with active power stroke we will not treat the most general case, where $f^y_{tilt}(t)$ and $f^x_{tilt}(t)$ are independent and focus on three specific models:

- in X-tilted model when $f_{tilt}(t)$ acts on variable x, is
- in Y-tilted-model when $f_{tilt}(t)$ acts on variable y and
- in XY-tilted model when $f_{tilt}(t)$ acts on the difference $y - x$.

In Fig.5.10 we show the schematic picture illustrating these three different rocking mechanisms: notice that tilting about the Y axis provides nontrivial coupling between the periodic and the bi-stable potentials. Each of our toy-models is a thermal ratchet exposed

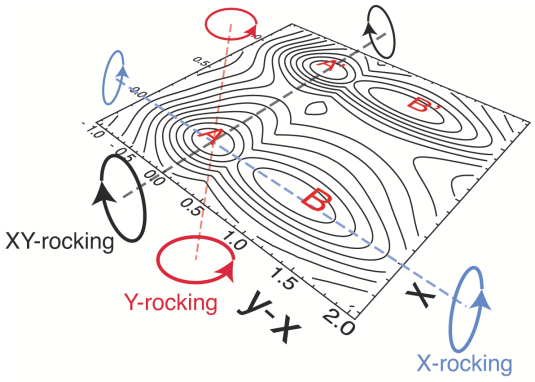

Figure 5.10. The scheme illustrating three different rocking mechanism: X-tilted ratchet , Y-tilted ratchet model and XY-tilted ratchet.

to a colored noise with uncorrelated and correlated components of force having zero averages. While all degrees of freedom are equally exposed to the white noise, only one of them in each of the models is subjected to a correlated noise. By localizing the effect of the tilting in these three different settings on a single internal degree of freedom, we can study separately the possibilities that either only the actin filament is active (X tilted model), or only the power stroke is active (X-Y tilted model). Finally, only the coupling between the attachment and the power stroke elements may be active while both of them can remain passive (Y tilted model).

The final selection of the adequate ac driving mode in this setting will come from the better understanding of the microscopic, molecular scale phenomena taking place during non-equilibrium enzymatic action of the ATP hydrolysis. However, another way to narrow the class of acceptable models is to simulate different protocols and to compare the ensuing macroscopic mechanical manifestations with what is known about the biochemical nature of the underlying processes. Thus, an adequate model must be able to reproduce all four stages of the minimal Lymn Taylor cycle and associate with the corresponding chemical states specific mechanical configurations. As we show in the next chapters, each of the discussed model imposes very restrictive constraints on stochastic dynamics of our two parametric system and as a result the three proposed models are very different in regard to their ability to reproduce the fine structure of the accepted biochemical cycle. We examine each of the proposed protocols and obtain not only qualitative but also quantitative characterization of their adequacy. In particular, we compute the corresponding force-velocity relations and study the parametric dependence for the mechanical efficiency of the associated energy transduction mechanisms.

Chapter 6

X-tilted thermal ratchet

In this chapter we discuss the X-tilted ratchet model. This model was introduced in [75] and here we present the first detailed analysis. In this model the power stroke is a passive mechanism, and the ATP activity is represented by a correlated component of the noise which acts directly on the periodic ratchet potential as in Magnasco model. We explore the structure of the motor cycle in the ensuing system in soft in hard devices, establish the force-velocity relation and study the energetics of the system.

6.1 Preliminaries

In this section we recall the main definitions for the X-tilted ratchet model. The main feature of this model is that the correlated noise $f_{tilt}(t)$ with zero time average is applied to the x variable. In Fig.6.1 we present a schematic illustration of the corresponding energy landscape in coordinates $[y-x, x]$. This landscape is tilted periodically and biases the

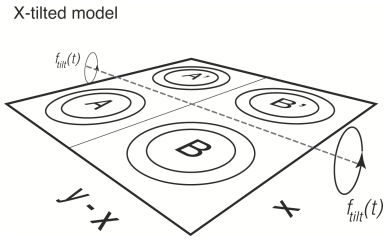

Figure 6.1. X-tilted ratchet model the energy landscape biased by f_{tilt} around one fictive axe, we sketch of energy landscape with a fictive axe where rocking is applying.

states A', B' during the first half of the period and the states A, B during the second half of the period.

We study this model in two regimes: isometric case or hard device regime (when we fix the length) and isotonic case or soft device regime (when we fix the applied force). In the soft device configuration the model is described by the system of coupled overdamped Langevin equations:

$$\begin{cases} \eta_x \dfrac{dx}{dt} = -\partial_x \Phi(x) - \partial_x V(y-x) + f_{tilt}(t) + \sqrt{2\eta_x D}\ \xi_x(t) \\ \eta_y \dfrac{dy}{dt} = -\partial_y V(y-x) + f_{ext} + \sqrt{2\eta_y D}\ \xi_y(t) \end{cases} \tag{6.1}$$

where η_x and η_y are viscous drag coefficients and $D = k_B T$. The term f_{ext} describes external conservative load. In the hard device the X-tilted ratchet is described by the system:

$$\begin{cases} \eta_x \dfrac{dx}{dt} = -\partial_x \Phi(x) - \partial_x V(y-x) + f_{tilt}(t) + \sqrt{2\eta_x D}\,\xi_x(t) \\ \eta_y \dfrac{dy}{dt} = -\partial_y V(y-x) - k_m(y-z) + \sqrt{2\eta_y D}\,\xi_y(t) \end{cases} \tag{6.2}$$

where again η_x and η_y are viscous drag coefficients and $D = k_B T$. The parameter z plays the role of the control parameter, and corresponds to the length of the linear spring with stiffness k_m. The $\xi_i(t)$ is the Gaussian random variable with zero mean and with correlation

$$\langle \xi_i(t) \rangle = 0, \quad \langle \xi_i(t)\xi_j(s) \rangle = \delta_{ij}\delta(t-s), \;\; t > s, \; i,j = x,y$$

It is convenient to rewrite the equations (6.1) and (6.2) in the dimensionless form. We use the following definitions of the nondimensional variables:

$$\begin{aligned} \tilde{X}\left(\tilde{t}\right) &\equiv \frac{1}{a} X\left(t = \tau\tilde{t}\right) \\ \tilde{V}\left(\tilde{x},\tilde{y}\right) &\equiv \frac{1}{k_m a^2} V\left(x = a\tilde{x}, y = a\tilde{y}\right) \\ \tilde{f}_{tilt}\left(\tilde{t} = \frac{t}{\tau}\right) &\equiv \frac{1}{k_m a} f_{tilt}(t) \\ \tilde{\xi}_i(\tilde{t}) &\equiv \xi_i(t)\tau^{-1/2} \end{aligned} \tag{6.3}$$

Here τ is the main time scale of the problem

$$\tau = \frac{\eta_y}{k_m} \tag{6.4}$$

The distance a between two minima of the potential $V(y-x)$ introduces the characteristic length scale, while the natural energy scale is $k_m a^2$. The remaining nondimensional parameters are now $\tilde{D} \equiv \frac{D}{k_m a^2}$ and $\alpha = \eta_y/\eta_x$.

In the soft device the dimensionless system (6.1) takes the form:

$$\begin{cases} \dfrac{dx}{dt} = -\alpha\left(\partial_x \Phi(x) + \partial_x V(y-x) - f_{tilt}(t)\right) + \sqrt{2\alpha D}\,\xi_x(t) \\ \dfrac{dy}{dt} = -\partial_y V(y-x) + f_{\text{ext}} + \sqrt{2D}\,\xi_y(t) \end{cases} \tag{6.5}$$

In the hard device configuration we obtain

$$\begin{cases} \dfrac{dx}{dt} = -\alpha\left(\partial_x \Phi(x) + \partial_x V(y-x) - f_{tilt}(t)\right) + \sqrt{2\alpha D}\,\xi_x(t) \\ \dfrac{dy}{dt} = -\partial_y V(y-x) - k_m(y-z) + \sqrt{2D}\,\xi_y(t) \end{cases} \tag{6.6}$$

In the above for simplicity we omit the notation $\tilde{\bullet}$.

The Fokker-Planck equations corresponding to the normalized systems of Langevin equations (6.5) and (6.6) take the form:

- in the soft device configuration:

$$\begin{aligned} \partial_t P^s(x,y,t) = &\alpha D \partial_x \left[\frac{P^s(x,y,t)}{D}\partial_x G^s(x,y,t) + \partial_x P^s(x,y,t)\right] + \\ &D\partial_y \left[\frac{P^s(x,y,t)}{D}\partial_y G^s(x,y,t) + \partial_y P^s(x,y,t)\right] \end{aligned} \tag{6.7}$$

where $P^s(x,y,t)$ is the probability density. The function $G^s(x,y,t)$ is the energy potential in the soft device

$$G_s(x,y,t) = \Phi(x) + V(y-x) - xf_{tilt}(t) - yf_{ext} \tag{6.8}$$

where f_{ext} is the external conservative load.

- in the hard device configuration:

$$\begin{aligned}\partial_t P^h(x,y,t) =& \alpha D\partial_x \left[\frac{P^h(x,y,t)}{D}\partial_x G^h(x,y,t) + \partial_x P^h(x,y,t)\right] + \\ & D\partial_y \left[\frac{P^h(x,y,t)}{D}\partial_y G^h(x,y,t) + \partial_y P^h(x,y,t)\right]\end{aligned} \tag{6.9}$$

where $P^h(x,y,t)$ is the probability density function, the function $G^h(x,y,t)$ is the energy potential in the hard device:

$$G^h(x,y,t) = \Phi(x) + V(y-x) - xf_{tilt}(t) + \frac{1}{2}k_m(y-z)^2 \tag{6.10}$$

Here z is the control parameter, usually we take $z = 0$.

In the next sections we study this system by performing numerical simulations. To simplify the numerical model we adopted the simplest descriptions of the functions $\Phi(x)$, $V(y-x)$ and $f_{tilt}(t)$. In particular we assumed that

$$\Phi(x) = \begin{cases} \dfrac{V_{max}}{\lambda_1}(x - nL), & \text{for } nL \le x < nL + \dfrac{L+\Delta}{2} \\ \dfrac{V_{max}}{\lambda_2}((n+1)L - x), & \text{for } nL + \dfrac{L+\Delta}{2} \le x < (n+1)L,\ n \in \mathbb{N} \end{cases} \tag{6.11}$$

where $\Delta = \lambda_1 - \lambda_2$ is the parameter, which controls the potential asymmetry. The potential is symmetric when $\Delta = 0$. By construction $\lambda_1 = (L+\Delta)/2$ and $\lambda_2 = (L-\Delta)/2$. A periodic force $f_{tilt}(t)$ with period T is assumed to be a square wave signal with amplitude A

$$f_{tilt}(t) = \begin{cases} +A \quad \text{for,} \quad \text{for } n\dfrac{T}{2} \le t \le (n+1)\dfrac{T}{2}, \\ -A \quad \text{for,} \quad \text{for } (n+1)\dfrac{T}{2} \le t \le nT,\ n \in \mathbb{N} \end{cases} \tag{6.12}$$

. The bistable element is modeled by a piece-wise quadratic function with stiffness k_0 and k_1. The minima are located in the points 0 and a, and the singular barrier is at l.

$$V(y-x) = \begin{cases} \frac{1}{2}k_0\,(y-x)^2 + \varepsilon_0\,(y-x) \leqslant l \\ \\ \frac{1}{2}k_1\,(y-x-a)^2 \qquad (y-x)\ \geqslant l \end{cases} \tag{6.13}$$

As $k_0 \neq k_1$ and $l \neq a/2$ the bistable potential is asymmetric with $\varepsilon_0 = 1/2\left(k_1(l-a)^2 - k_0 l^2\right)$. Usually we associate with phase "0" the well characterized by the stiffness k_0 and with phase "1" – the well characterized by the stiffness k_1. We illustrate the functions $\Phi(x)$, $V(y-x)$ and $f_{tilt}(t)$ in Fig.6.2a). The external force $f_{tilt}(t)$ takes in our model two value $+A$ and $-A$ so we can easy illustrate the action of the tilting on the energy landscape by presenting $G(x,y,t)$ in two configuration associated with positive and negative phases of the rocking. Our Fig.6.2b),c) shows the two-dimensional energy landscape biased by $f_{tilt}(t)$ in positive and negative phases. The motor cycle is defined by the sequence of visited energy minima during different stages of the rocking.

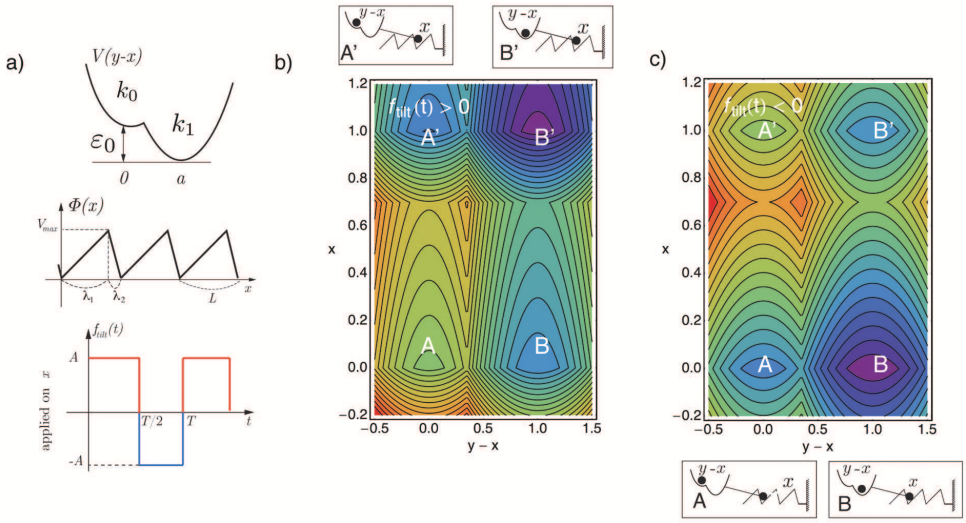

Figure 6.2. The X-tilted ratchet. a)The sketch of potentials used in numeric applications. b)The picture illustrate the action of $f_{tilt}(t)$ on two-dimensional energy landscape in plane $[y-x, x]$. The increasing energy level scale graduated from cold color to hot colors. a) We show unbiased landscape in soft device configuration we identify the occupancy motor state, is intrinsic energy potential. b) The landscape corresponds to positive phase of $f_{tilt}(t) = A$. c) The landscape corresponded to the negative phase of $f_{tilt}(t) = -A$.

6.2 A typical cycle of the X-tilted motor

6.2.1 Soft device

We begin with a series of numerical simulations of our system in the soft device. Assume for determinacy that $\alpha = 1$ and $f_{ext} = 0$. Other parameters are taken to be $k_0 = 1.5,\ k_1 = 0.43,\ l = 0.22,\ a = 1,\ \lambda_1 = 0.35,\ L = 0.5,\ V_{max} = 1.5$. Suppose that applied rocking force has amplitude $A = 2$ and period $T = 16$. We perform computations by using the standard Euler scheme with the time step $\Delta t = 1 \times 10^{-3}$ and perform averaging over $N_r = 1 \times 10^3$ realizations.

In Fig.6.3 we show the average trajectory of the motor. One can see that the system reaches an oscillatory steady state with the average velocity $\langle v_x \rangle = \langle v_y \rangle \equiv \langle v \rangle$. In Fig.6.3b) we show the time evolution of the system in coordinates $[time, y-x]$. We observe the characteristic oscillations between the two wells of the effective bistable potential. Notice that our motor crosses few space periods, see 6.3c). We define one motor cycle as segment of the average trajectory corresponding to one period of the correlated nose $f_{tilt}(t)$. In Fig.6.3d) where we show one cycle of the motor, one can associate the transition $A" \to B'$ with the release of the power stroke mechanism and the transition $B \to A"$ with the recharging of power stroke mechanism. Simultaneously, several attachment-detachment events also take place.

In order to make sure that during each cycle the motor performs only one attachment-detachment step along the potential $\Phi(x)$, we need to modify the parameters of the model. Suppose that $\alpha = 0.2$ (control of the drift of x), take $L = 3$, and, in order to preserve the value of the force acting on the particle, choose $V_{max} = 4.5$. In Fig.6.4 we show the new average trajectory of the motor associate with one cycle of the tilting force. As in the previous case, the system reaches the steady state with a particular value of the average velocity, see Fig.6.3a). The remaining fluctuations can be explained by the relatively small

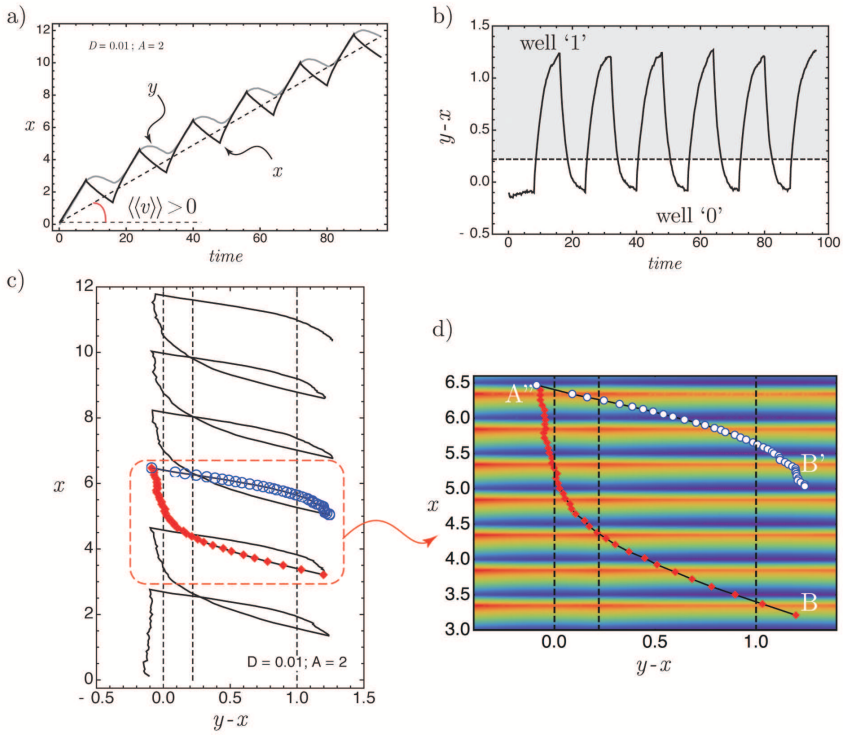

Figure 6.3. The X-tilted ratchet model in soft device configuration, $f_{ext} = 0$. a) The average trajectory x_t (solid black line) and y_t (solid gray line). b) The time evolution of the system in coordinates $[time, y - x]$, note the characteristic oscillations between the two wells of the effective bistable potential. c)The average trajectory in coordinates $[y - x, x]$, note that the motor crosses few space periods. d) One motor cycle as segment of average trajectory during the time period T of the $f_{tilt}(t)$. The red scatters correspond to the positive phase of the rocking $f_{tilt}(t) = +A$ and the blue scatters–to the negative phase of rocking $f_{tilt} = -A$. The colored bands indicate the structure of the energy landscape, the coldest colors indicate the minima and hottest colors indicate the maxima. $k_0 = 1.5$, $k_1 = 0.43$, $l = 0.22$, $a = 1$, $\lambda_1 = 0.35$, $L = 0.5$, $V_{max} = 0.75$, $\alpha = 1$ with the amplitude $A = 2$ and the period $T = 16$.

number of stochastic realization $N_r = 200$.

Once again, we can identify the transition $A' \to B'$ with the motor power stroke, and the transition $B \to A$ with the recharging of the power stroke. We therefore obtain a 2-states cycle (shown in Fig.6.4) where the detachment and re-attachment all take place simultaneously with the recharge of the power stroke. Since the power stroke in this model is passive, the advance of the motor is due exclusively to the asymmetry of the potential $V(y - x)$ and the motor must jump forward along the x axis in order to do the recharging of the power stroke mechanism. Note, that the ratchet must make a sufficiently large step in the forward direction in order to recharge the double well potential mechanically.

To summarize, the motor cycle can be decomposed into the following steps:

- ①→②. First, because of the broken space symmetry, the motor advances in the x direction and crosses the energy barrier associated with the maxima of the periodic potential $\Phi(x)$. While doing the motor recharges the power stroke (performs transition from the lower energy well 1 to the higher energy well 0 in the bistable potential).

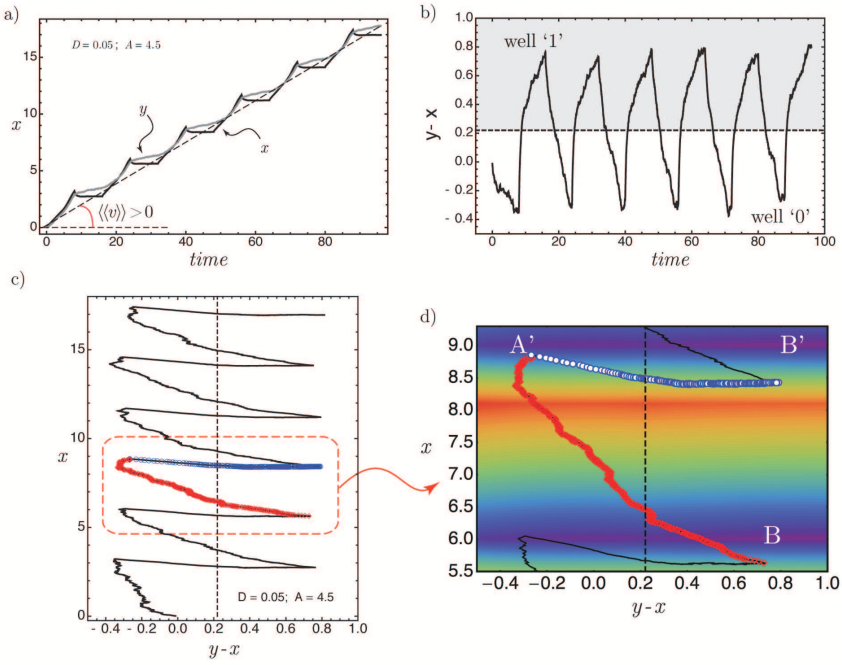

Figure 6.4. The X-tilted ratchet model in soft device configuration, $f_{ext} = 0$. a) The average trajectory x_t (solid black line) and y_t (solid gray line). b) The time evolution of the system in coordinates $[time, y - x]$, note the characteristic oscillations between the two wells of the effective bistable potential. c)The average trajectory in coordinates $[y - x, x]$, note that the motor crosses few space periods. d) One motor cycle as segment of average trajectory during the time period T of the $f_{tilt}(t)$. The red scatters correspond to the positive phase of the rocking $f_{tilt}(t) = +A$ and the blue scatters–to the negative phase of rocking $f_{tilt} = -A$. The coldest colors indicate the minima and hottest colors indicate the maxima. $k_0 = 1.5$, $k_1 = 0.43$, $l = 0.22$, $a = 1$, $\lambda_1 = 2.4$, $L = 3$, $\alpha = 0.2$ with the amplitude $A = 2$ and the period $T = 16$.

- ②→③. As the rocking force changes the sign, the new configuration of the energy landscape drives the motor into backward direction along the x axis. However, the motor is now trapped and instead of going backwards, it just performs the power-stroke. Then the motor cycle starts again.

By varying parameters of the model we can obtain other cycles as well. For instance, the motor step ①→② can be made longer than a simple jump between the two nearest periods. Also, by fine tuning of the parameters we can force the motor to move according to the scheme ①→②'→②, shown in Fig.6.5b). Moreover, the motor can advance few periods along the x axis in the forward direction before accomplishing the power-stroke ②→③ and can also move backward during a few periods following the path ②→③'→③. While both motor positions, ③' and ③, correspond to the same energy well "0" of the bistable element, they are associated with different (nearest) wells of the periodic potential, see Fig.6.3d).

6.2.2 Hard device

Adding to the energy the quadratic term $1/2k_m(y - z_0)^2$ in the hard device changes the energy landscape. To analyze the structure of the ensuing cycle, we fix the values of $z \equiv Const$, $z = 0$. We use a simplified version of the model with $k_0 = k_1$ and we fix

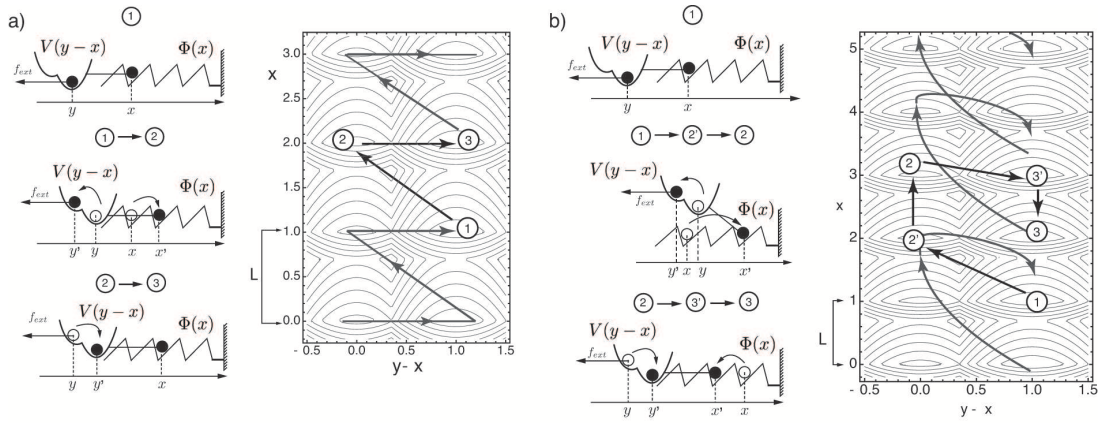

Figure 6.5. The X-tilted ratchet model, the scheme of the motor cycle in the soft device configuration. With the solid gray lines we plot the surface contours of the energy landscape $\Phi(x) + V(y-x)$ for the $f_{ext} = 0$. a) The simplest motor cycle, in the positive phase of rocking the motor advances in the x direction and recharges the power stroke. As the rocking force changes the sign, the motor is trapped and performs the power-stroke. b) By varying parameters the motor step can be made longer, the motor can advance few periods along the x axis in the forward direction before accomplishing the power-stroke and can also move backward during a few periods. On the scheme for simplicity motor cross just one period.

$\alpha = 5$. We also adopt the following values of other relevant parameters: $k_0 = k_1 = 7$, $l = 0.22$, $a = 1$, $L = 2, \lambda_1 = 1.4$, $V_{max} = 5$ and fix the time period of rocking force at $T = 20$.

From Fig.6.4 one can see that the ensuing cycle is trivial showing only two-states oscillations between the well "0" corresponding to larger value of x and the well "1" corresponding to lower value of x axis. We call this regime a diagonal cycling. Note what in the soft device the motor with the same parameters would show a cycle presented in 6.5b), so the obtained path in a hard device is similar to what we have seen in Fig.6.3.

To study the effect of noise on the structure of the mechanical cycle we use direct numerical simulations of our Langevin system and vary the parameter D. For each realization we use the same amplitude of tilting A. In Fig.6.6 we show the average trajectory of our stochastic process during one time period of the force $f_{tilt}(t)$ with $A = 6$. With solid black lines we depict the level set representation of the energy landscape in the positive phase of rocking $(\Phi(x) + V(y-x) + 1/2k_m y^2 - xA)$ and with dashed black lines –the same landscape in the negative phase of rocking $(\Phi(x) + V(y-x) + 1/2k_m y^2 + xA)$. We plot the average trajectory by using different colors depending on the phase of rocking.

The cycle is stabilized after a short transient regime around a particular minimum of the periodic potential ($x = 2$ in this case). At low temperature the stochastic process is localized around only one minimum along the $y-x$ dimension, see Fig.6.6a). The increase of temperature gives to our particle sufficient energy to cross the potential barriers along both $y-x$ and x axes in particular it allows for a transition between the energy wells "0" and "1" of the bi-stable potential, see Fig.6.6b),c). The 3-state cycle is formed if the motor is able to displace itself along x sufficiently far in order to be able to recharge the power stroke element. If we increase the parameter D further, the particle makes larger jumps along the x direction, see 6.6d). At even higher temperature the system looses its the ability to generate force. The increasing of the amplitude A of the correlated noise $f_{tilt}(t)$ influences the motor cycle shape in the similar way (as the increase of D). In particular, one can show that without rocking our system is unable to generate tension in the hard

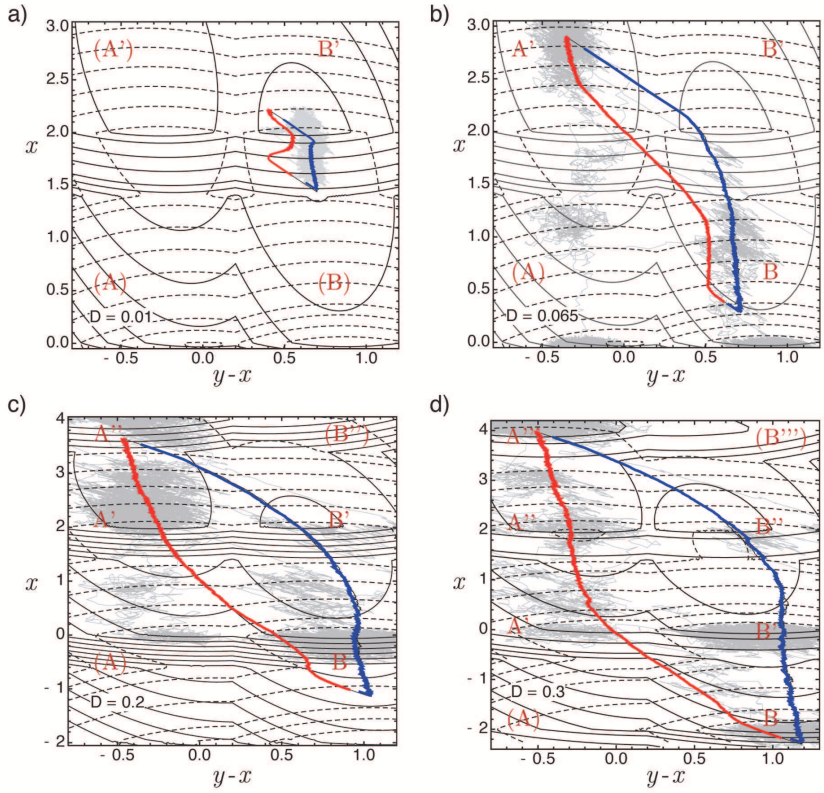

Figure 6.6. The X-tilted ratchet model in hard device configuration, the variation of the motor cycle with the increasing temperature D at the constant amplitude $A = 6$. With solid black lines we depict the level set representation of the energy landscape in the positive phase of rocking and with dashed black lines –the same landscape in the negative phase of rocking. The average motor trajectory plotted by the thick red line during the positive phase of $f_{tilt}(t)$ and by the thick blue line during the negative phase. The light gray lines follow the single stochastic realization during one time period. a) The cycle at $D = 0.01$. b) The cycle at $D = 0.065$. c) The cycle at $D = 0.08$. d) The cycle at $D = 0.3$. The relevant parameters $k_0 = k_1 = 7$, $l = 0.22$, $a = 1$, $L = 2, \lambda_1 = 1.4$, $V_{max} = 5$, $\alpha = 5$ and the time period of the rocking force $T = 20$.

device. By increasing the rocking amplitude we open more and more distant sites for the transition.

In Fig.6.7 we present the schematic explanation of the observed 3-state cycle in the hard device. After a transient stage the motor performs the following cycle in the clockwise direction ①→②→③→①

- Transition ①→2. The average trajectory is shown schematically by black arrows. During the positive phase of $f_{tilt}(t)$, motor crosses the barrier in the forward direction along the saw-tooth actin potential. It drags the bistable element and recharges the power stroke element into the state 0, see Fig.6.6 (phase plotted in red).

- During the negative phase of $f_{tilt}(t)$ the motor makes the transition ②→③→①, see Fig.6.6 (phase plotted in blue). The change of sign of the force $f_{tilt}(t)$ biases the transition in the backward direction along the potential $\Phi(x)$. At the same time, the transition ②→③ takes place (from well "0" to well "1"): it is natural to identify this step with the "power stroke". After the transition ③→① the motor cycle can start

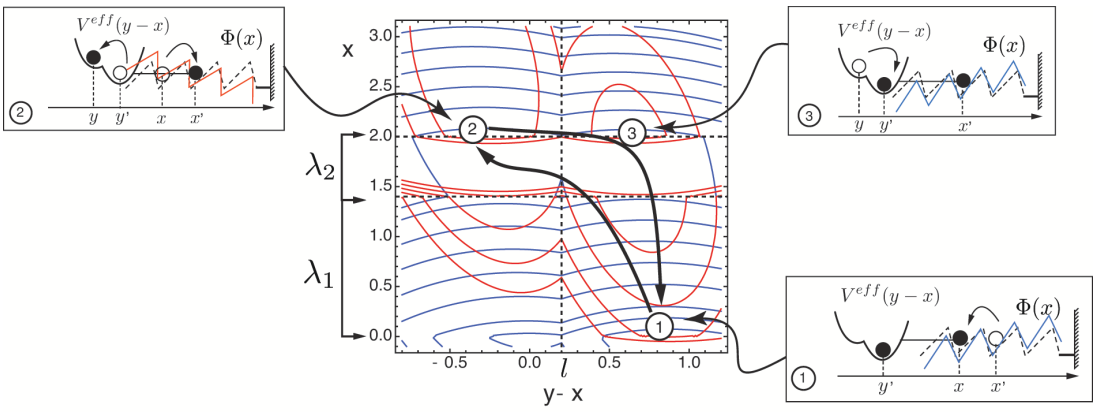

Figure 6.7. The X-tilted ratchet, the scheme of the motor cycle in hard device configuration. With the solid red lines we plot the surface contours of the energy landscape in positive phase of the rocking and with the blue lines –the surface contours of the energy landscape in negative phase of the rocking. The average trajectory is shown schematically by black arrows. During the positive phase of $f_{tilt}(t)$, motor moves in the forward direction along the saw-tooth actin potential and recharges the power stroke. The change of sign of the force $f_{tilt}(t)$ biases the transition in the backward direction along the potential $\Phi(x)$ and at the same time the motor performs the power-stroke.

again.

The main characteristic feature of this model is that the power stroke is recharged together with the advance of the motor along the actin filament. This combines two steps of the Lymn-Taylor cycle into one. The other two steps, the power stroke and the detachment, are represented adequately by this mechanical model.

6.3 Force-Velocity relation

Next we study the force-velocity relation for the X-tilted ratchet placed in the soft device configuration. Due to the presence of the active force $f_{tilt}(t)$ the motor can transform the input energy into the mechanical work.

To characterize this work we adopt the physical definition of the sign of the external load f_{ext} meaning that the positive force is acting in the positive direction along the corresponding coordinate axis (physiological definition of the positive force is opposite to ours). If we now plot the steady state relation between the applied external force and the velocity, $[\langle v\rangle, f_{ext}]$, we obtain the desired force velocity relation.

We define the active work performed by motor against a conservative load as a negative of the energy release rate $f_{ext}\langle v\rangle$. Therefore the active work (energy supply) is positive when the average velocity and the external force have opposite signs. This means what the system is anti-dissipative, the motor uses (instead of dissipating) the external energy and can therefore perform some useful work. The passive regimes correspond to the cases where the average velocity and the external load have the same directions. Such system is dissipative and the energy is released rather than being absorbed. The system is passive and dissipative if the motor follows the direction imposed by the external load rather than acting against the load, see Fig.6.8.

In our numerical experiments we use the following values of the motor parameters: $k_0 = 1.5,\ k_1 = 0.43,\ l = 0.22,\ a = 1,\ L = 1,\ \lambda_1 = 0.7,\ V_{max} = 1.5,$, we fix $\alpha = 1$ and

we again fix the time period of the correlated noise at $T = 20$. In Fig.6.8 we show the force velocity relation at different values of D when $A = 2.5$ and $A = 4.5$. In Fig.6.8a)

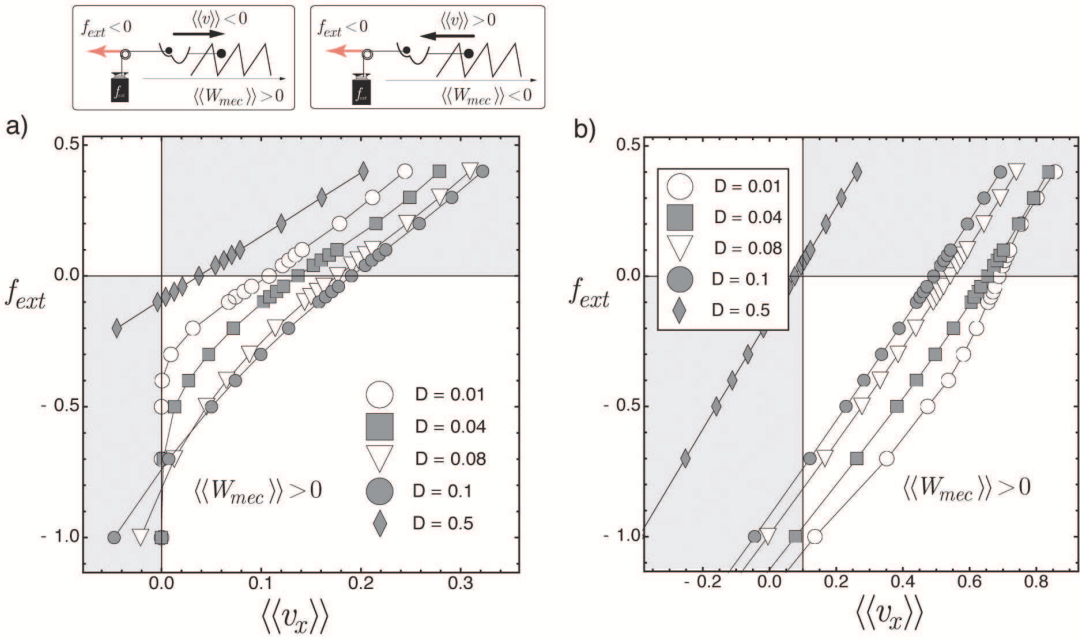

Figure 6.8. The force-velocity relation of X-tilted ratchet. a) The force velocity relation with increasing temperature D at fixed amplitude $A = 2.5$ of $f_{tilt}(t)$. The area limited by force-velocity curve and figure axes increases with D until the threshold value. We are in the thermal ratchet regime. After the temperature threshold the thermal fluctuations perturb the motion generation. b) The force velocity relation with increasing temperature at fixed amplitude $A = 4.5$ of $f_{tilt}(t)$. Note the convex character of force-velocity curve at $D = 0.01$ and compare to force-velocity curve at same temperature on the left picture. We lose the convex character to linear progressively with increase of temperature. Here we are in mechanical ratchet regime, the fluctuation provided by thermal bath perturb the system. The relevant parameters: $k_0 = 1.5$, $k_1 = 0.43$, $l = 0.22$, $a = 1$, $L = 1$, $\lambda_1 = 0.7$, $V_{max} = 1.5$, $\alpha = 1$, we fix $\alpha = 1$ and we again fix the time period of the correlated noise at $T = 20$.

we show the force velocity relation at increasing temperatures D. At $A = 2.5$ we observe the characteristic concave shape. The area limited by the curve and the axes increases with D until the threshold is reached at $D = 0.1$. This shows that unlimited increase of temperature leads eventually to the loss of the performance of the motor. The stall force, defined in soft device as the value of force at zero average velocity, increases with increasing temperature until the threshold value D and decrease afterwards. In Fig.6.8b) we see how the force velocity relation changes at $A = 4.5$. We observe that the curve becomes convex. With the increase of temperature D we progressively approach the linear force velocity relation. Here we are in the mechanical ratchet regime and the presence of thermal bath only diminishes the value of the generated force.

In summary, the performance of this motor system is similar to what we have seen in the case of a simple Magansco ratchet. This means that the power stroke element does not contribute to the overall behavior in a major way.

6.4 Stochastic energetics

To study energetics of the X-tilted ratchet in the soft device we rewrite the equations 6.5 in the form

$$\begin{cases} \partial_x[\Psi(x) + V(y-x)] - f_{tilt}(t) = -\dfrac{1}{\alpha} d_t x + \sqrt{\dfrac{2D}{\alpha}}\ \xi_x(t) \\ \partial_y V(y-x) - f_{ext} = -d_t y + \sqrt{2D}\ \xi_y(t) \end{cases} \tag{6.14}$$

We will go into the energetics along the motor trajectory. Therefore, we then multiply the system by the vector $d\mathbf{X}$ in the Stratonovich sense. After what, using the definition of the heat exchange in each of the processes $\delta Q_i = \left(-\eta d_t x_i + \sqrt{2\eta_i D}\xi_i(t)\right) \circ dx_i$ we can write

$$\begin{cases} \partial_x \left[\Psi(x) + V(y-x)\right] \circ dx - f_{tilt}(t) \circ dx = \delta Q_x \\ \partial_y V(y-x) \circ dy - f_{\text{ext}} \circ dy = \delta Q_y \end{cases} \tag{6.15}$$

We can define the intrinsic two-dimensional landscape in soft device configuration $G_0(x_t, y_t) = \Phi(x_t) + V(y_t - x_t) - y f_{ext}$. By using these definitions we rewrite the energy balance in the form

$$\begin{cases} \partial_x G_0 \circ dx - f_{tilt}(t) \circ dx = \delta Q_x \\ \partial_y G_0 \circ dy = \delta Q_y \end{cases} \tag{6.16}$$

To study the steady state change of the energy of the system we need to average over one time period T, and we can formally write

$$\frac{1}{T} \int\limits_{\mathbf{X}_{t_i}}^{\mathbf{X}_{t_i+T}} dG_0(\mathbf{X}_t) - \frac{1}{T} \int\limits_{x_{t_i}}^{x_{t_i+T}} f_{tilt}(t) dx_t = \frac{1}{T} \int\limits_{\mathbf{X}_{t_i}}^{\mathbf{X}_{t_i+T}} \delta Q_x + \delta Q_y \tag{6.17}$$

where the time moment t_i indicate the duration the transition regime. According to the energetics [100] the input energy per time period R reads

$$R = \frac{1}{T} \int\limits_{x_{t_i}}^{x_{t_i+T}} f_{tilt}(t) dx_t \tag{6.18}$$

while the mechanical work W_{mec} takes the form

$$W_{mec} = \frac{1}{T} \int\limits_{\mathbf{X}_{t_i}}^{\mathbf{X}_{t_i+T}} dG_0(\mathbf{X}_t) \tag{6.19}$$

We can simplify the definition (6.19) observing that

$$\frac{1}{T} \int\limits_{\mathbf{X}_{t_i}}^{\mathbf{X}_{t_i+T}} dG_0(\mathbf{X}_t) = \frac{1}{T} \int\limits_{\mathbf{X}_{t_i}}^{\mathbf{X}_{t_i+T}} d\left(\Phi(\mathbf{X}_t) + V(\mathbf{X}_t)\right) - \frac{1}{T} \int\limits_{y_{t_i}}^{y_{t_i+T}} f_{ext} dy \tag{6.20}$$

Since the internal cycle is periodic we conclude that $\frac{1}{T} \int_{\mathbf{X}_{t_i}}^{\mathbf{X}_{t_i+T}} d\left(\Phi(\mathbf{X}_t) + V(\mathbf{X}_t)\right) \equiv 0$. Then the performed mechanical work W_{mec},

$$W_{mec} = -\frac{1}{T} \int\limits_{y_{t_i}}^{y_{t_i+T}} f_{ext} dy = -f_{ext} \langle v_y \rangle \tag{6.21}$$

By using (6.17),(6.18),(6.21) we obtain the energy balance

$$W_{mec} \equiv R + Q \tag{6.22}$$

where the total heat exchange Q is defined as follows

$$Q = \frac{1}{T} \int_{\mathbf{x}_{t_i}}^{\mathbf{x}_{t_i+T}} \delta Q_x + \delta Q_y \tag{6.23}$$

We can now define the mechanical efficiency of the system as,

$$\epsilon_{mec} = \frac{W_{\text{mec}}}{R} \tag{6.24}$$

In order to measure the efficiency of the motion of an unloaded motor against the viscous drag, we define the useful work as follows

$$W_{\text{Stokes}} = \alpha^{-1} \langle v_x \rangle^2 + \langle v_y \rangle^2 \tag{6.25}$$

Then the Stokes efficiency can be written as

$$\epsilon_{Stokes} = \frac{W_{Stokes}}{R} \tag{6.26}$$

We can also compute the rectifying efficiency–the sum of Stokes and mechanical efficiencies – which can be viewed as the global characteristic of the energy transduction by our ratchet system:

$$\epsilon_{rec} = \frac{W_{mec} + W_{Stokes}}{R} \tag{6.27}$$

The above definition of efficiency works only in the soft device configuration, where we are able to observe the motion of our motor. In the hard device configuration all injected energy R is simply dissipated as heat and the energy balance can be written as follows $R = -Q$. This gives us the value of the maintenance energy/heat which may be used as the energetic measure associated with the stall force conditions.

To illustrate these definitions we apply to our motor the conservative load $f_{ext} = -0.1$ and use the following value of the parameters $k_0 = 1.5,\ k_1 = 0.43,\ l = 0.22,\ a = 1,\ L = 2,\ \lambda_1 = 0.7,\ V_{max} = 1.5$. We also fix $\alpha = 1$ and take $T = 30$. The system is out of the adiabatic regime and we perform direct numerical study of the Langevin equations. We use the Euler scheme with the time step $\Delta t = 0.5 \times 10^{-3}$ and average over $N_3 = 10^4$ stochastic realizations.

In Fig.6.9a) we present the average velocity of the motor as a function of temperature D for several values of the rocking amplitude A. For small amplitudes A the motor shows a maximum of velocity at a finite temperature which we can interpret as the phenomenon of stochastic resonance. At high amplitudes A, the average velocity is a monotonically decreasing function of D which means that for mechanical ratchet thermal fluctuations work as an obstacle. By light green color we identify the region with negative velocity where the motor is dragged backwards by the cargo. At small value of D the average velocity may also be negative at some values of parameters.

In Fig.6.9b.) we show the consumed energy R as a function of D, again for the several values of A. As the level of thermal fluctuations increases the motor needs more in order to rectify the fluctuations and to preform the work. At large temperatures we observe

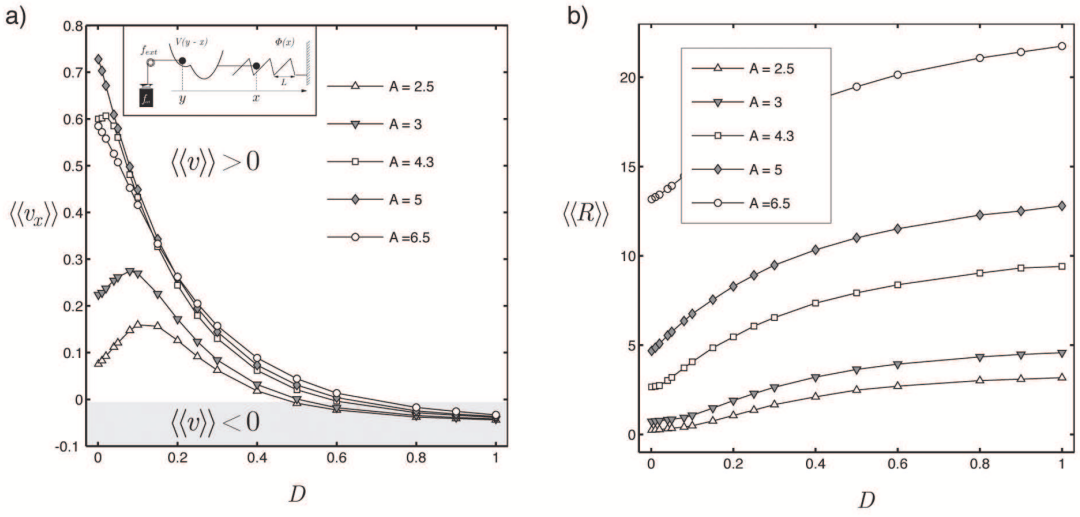

Figure 6.9. The X-tilted model in soft device configuration with the conservative load $f_{ext} = -0.1$. a) The variation of the average velocity $\langle v_y \rangle$ with the increasing temperature D for the different amplitudes A of the rocking force $f_{tilt}(t)$. For small amplitudes A the motor shows a maximum of velocity at a finite temperature. At high amplitudes A, the average velocity is a monotonically decreasing function of D. b) The variation of the consumed energy R with the increasing temperature D for the different amplitudes A of $f_{tilt}(t)$. As the level of thermal fluctuations increases the motor needs more in order to rectify the fluctuations and to preform the work. The relevant parameters $k_0 = 1.5,\ k_1 = 0.43,\ l = 0.22,\ a = 1,\ L = 1,\ \lambda_1 = 0.7,\ V_{max} = 1.5,\ \alpha = 1$ with time period $T = 30$ of the rocking force.

saturation, showing that the motor dragged by the cargo consumes energy with a fixed rate.

In Fig.6.10a) we show the mechanic work as a function of D for increasing A. By color, we mark the region of positive and negative mechanic work. In Fig.6.10b) we show the temperature dependence of the mechanical efficiency defined by (6.24). In the regime of small amplitude A we observe a maximum of efficiency at finite temperature. With increasing amplitude A, the maximum vanished and the efficiency becomes a monotonically decreasing function of D, which is behavior characteristic for mechanic ratchet regime. By light green color we indicate the regime of negative efficiency, where our motor is unable to perform a positive mechanic work against the external force and works instead as an active breaking mechanism.

In Fig.6.10c) we plot the Stokes efficiency as a function of D. By definition this is always a positive function. The rectifying efficiency is shown in Fig.6.10d). The shape of this function is dominated by the quadratic Stokes term. The important observation is that this cumulative efficiency also has a maximum at a finite temperature where the amplitude of the rocking is small and the device works as a Brownian ratchet.

6.5 Conclusions

In this section we presented the simplest arrangement of the motor combined with the power stroke element. In this arrangement, the power stroke is passive and all the activity is concentrated in the actin attachment sites. The working of such device is similar to the mechanism of Magnasco ratchet. By assuming that it is the x variable which consumes

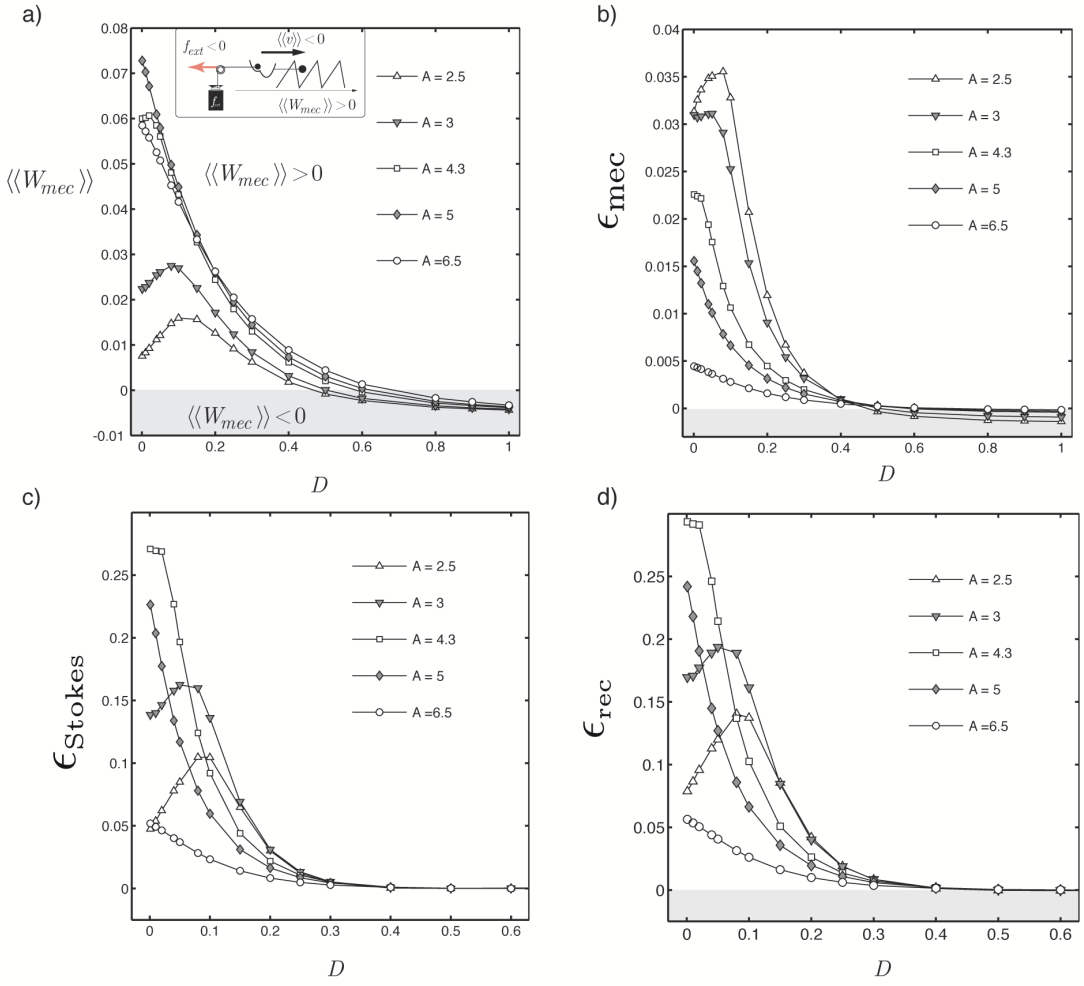

Figure 6.10. The X-tilted model in soft device configuration with the conservative load $f_{ext} = -0.1$. a) The variation of the mechanic work W_{mec} with the increasing temperature D for different amplitudes A. b) The variation of the mechanic efficiency ϵ_{mec} with the increasing temperature D for different amplitudes A. In the regime of small amplitude A we observe a maximum of efficiency at finite temperature. c) The variation of the Stokes efficiency with the increasing temperature D. By definition, this is always positive function. For hight values of D the Stokes efficiency is increasing function of D, because we are in regime there the motor follows the direction imposed by cargo. d) The variation of the rectifying efficiency with the increasing temperature D. The shape of this function is dominated by the quadratic Stokes term. The relevant parameters $k_0 = 1.5,\ k_1 = 0.43,\ l = 0.22,\ a = 1,\ L = 1,\ \lambda_1 = 0.7,\ V_{max} = 1.5,\ \alpha = 1$ with time period $T = 30$ of the rocking force.

the energy provided by the ATP (correlated noise $f_{tilt}(t)$) we assume that all the ATP is spent on detachment and reattachment while the bistable element, modeling the power stroke, does not directly consume the metabolic energy and is largely carried/dragged by such a motor. We have shown that with X-tilted model one cannot simulate the full $4-state$ Lymn-Taylor cycle and that detachment and the recharge of the power stroke are always combined. Therefore, the passive nature of the power-stroke action is apparently incompatible with the the biochemical perspective on muscle contraction and this model must be improved. Essentially we must ensure that the energy provided by the time

periodic (correlated) source and represented in our general scheme by the force $f_{tilt}(t)$, act partially or fully on the internal variable describing the configuration of the bistable element. In the following chapters we present several examples of the systems where the bistable element plays an active role in the contraction cycle.

Chapter 7

Y-tilted ratchet

In this chapter we make the first step in the direction of making the power stroke mechanism active. More specifically, we study the Y-tilted ratchet where the the correlated component of the noise is applied to the y variable. This variable characterizes the power stroke mechanism and is not directly related either to actin fiber, or to attachment-detachment phenomenon. Such activation is therefore possible even in the fully attached state and the corresponding active force will then be entirely due to the power stroke activity. As in the previous chapter we study the motor cycle in the soft in hard device configurations and make connection between mechanical and biochemical intermediate states. In particular, we establish the force-velocity relation and perform its parametric study by varying both the temperature and the amplitude of the correlated noise. We then investigate the energetics of the Y-tilted motor and search for the regimes with maximum rectifying efficiency.

7.1 Preliminaries

The Y-tilted ratchet is a system coupling the bistable potential $V(y-x)$ with the space periodic potential $\Phi(x)$. This mechanical system is exposed to white noise representing thermal reservoir and the correlated noise which takes the form of a force acting on variable y. On the scheme presented in Fig.7.1 we show one period of the two-dimensional energy landscape with four mechanical configurations A, B, A', B' representing local minima of the energy. We drew a fictitious axis around which the rocking is applied. One can see that the tilting acts along the "diagonal" of this landscape and biases periodically either the state B', during the positive phase of rocking, or the state A, during the next negative phase.

As before we study this system in two distinct configurations: isometric or hard device (we fix the length of the system) and isotonic or soft device (we fix the external conservative force). In the soft device configuration the system is described by the following system of coupled overdamped Langevin equations:

$$\begin{cases} \eta_x \dfrac{dx}{dt} = -\partial_x \Phi(x) - \partial_x V(y-x) + \sqrt{2\eta_x D}\,\xi_x(t) \\ \eta_y \dfrac{dy}{dt} = -\partial_y V(y-x) + f_{tilt}(t) + f_{ext} + \sqrt{2\eta_y D}\,\xi_y(t) \end{cases} \tag{7.1}$$

where f_{ext} is the external conservative load. In the hard device the Y-tilted ratchet is

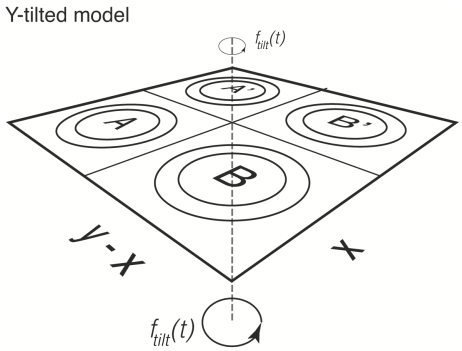

Figure 7.1. Y-tilted ratchet design. We show the two-dimensional landscape biased by $f_{tilt(t)}$ around a fictive axe.

described by the system

$$\begin{cases} \eta_x \dfrac{dx}{dt} = -\partial_x \Phi(x) - \partial_x V(y-x) + \sqrt{2\eta_x D}\ \xi_x(t) \\ \eta_y \dfrac{dy}{dt} = -\partial_y V(y-x) - k_m(y-z) + f_{tilt}(t) + \sqrt{2\eta_y D}\ \xi_y(t) \end{cases} \tag{7.2}$$

where η_x and η_y are viscous drag coefficients and $D = k_B T$. Here z is the external control parameter, which characterizes the stretch in the series linear spring with stiffness k_m. Once again, the $\xi_i(t)$ are Gaussian random variables with

$$\langle \xi_i(t) \rangle = 0, \qquad \langle \xi_i(t)\xi_j(s) \rangle = \delta_{ij}\delta(t-s), \qquad t > s, \quad i,j = x,y$$

It will be convenient to use the dimensionless form of the equations (7.1) and (7.2). We use the following scaling of the parameters (6.3) and the time scale (6.4). The dimensionless system of Langevin equation for the Y-tilted motor in the soft device takes the form

$$\begin{cases} \dfrac{dx}{dt} = -\alpha\left(\partial_x \Phi(x) + \partial_x V(y-x)\right) + \sqrt{2\alpha D}\ \xi_x(t) \\ \dfrac{dy}{dt} = -\partial_y V(y-x) + f_{\text{ext}} + f_{tilt}(t) + \sqrt{2D}\ \xi_y(t) \end{cases} \tag{7.3}$$

In the hard device we obtain accordingly

$$\begin{cases} \dfrac{dx}{dt} = -\alpha\left(\partial_x \Phi(x) + \partial_x V(y-x)\right) + \sqrt{2\alpha D}\ \xi_x(t) \\ \dfrac{dy}{dt} = -\partial_y V(y-x) - k_m(y-z) + f_{tilt}(t) + \sqrt{2D}\ \xi_y(t) \end{cases} \tag{7.4}$$

We introduced the dimensionless parameters $\alpha = \frac{\eta_y}{\eta_x}$ and $\tilde{D} \equiv \frac{D}{k_m a^2}$. In what follows we omit $\tilde{\bullet}$ for simplicity of notations. We observe that parameter α controls the scale of the average velocity for the variable x. Indeed, after averaging the corresponding equation over all realizations, we obtain:$\langle d_t x \rangle = -\alpha\left(\partial_x \Phi(x) + \partial_x V(y-x)\right)$.

The Fokker-Planck equation corresponding to the normalized system of Langevin equations (7.3) and (7.4) takes the similar form mentioned in the previous chapter, the expressions (6.7) and (6.9). In the soft device the Fokker-Planck equation reads with the energy potential

$$G^s(x,y,t) = \Phi(x) + V(y-x) - y f_{tilt}(t) + f_{ext}) \tag{7.5}$$

where f_{ext} is external conservative load. In the hard device the Fokker-Planck equation reads with the energy potential

$$G^h(x,y,t) = \Phi(x) + V(y-x) - yf_{tilt}(t) + \frac{1}{2}k_m(y-z)^2 \tag{7.6}$$

where z is the external control parameter.

In order to simplify the model and preserve the continuity with the X-tilted model we use the same potentials $\Phi(x)$ (6.11), $V(y-x)$ (6.13) and $f_{tilt}(t)$ (6.12) as in previous chapter.

We illustrate the definition of $\Phi(x)$, $V(y-x)$ and $f_{tilt}(t)$ in Fig.7.2a). Since the force $f_{tilt}(t)$ is a simple square wave signal, the tilting has two phases: positive and negative. In Fig.7.2b,c) we show the energy landscape in three configurations: untilted, in positive and in negative phases of rocking. Notice that in this model tilting couples bistable and

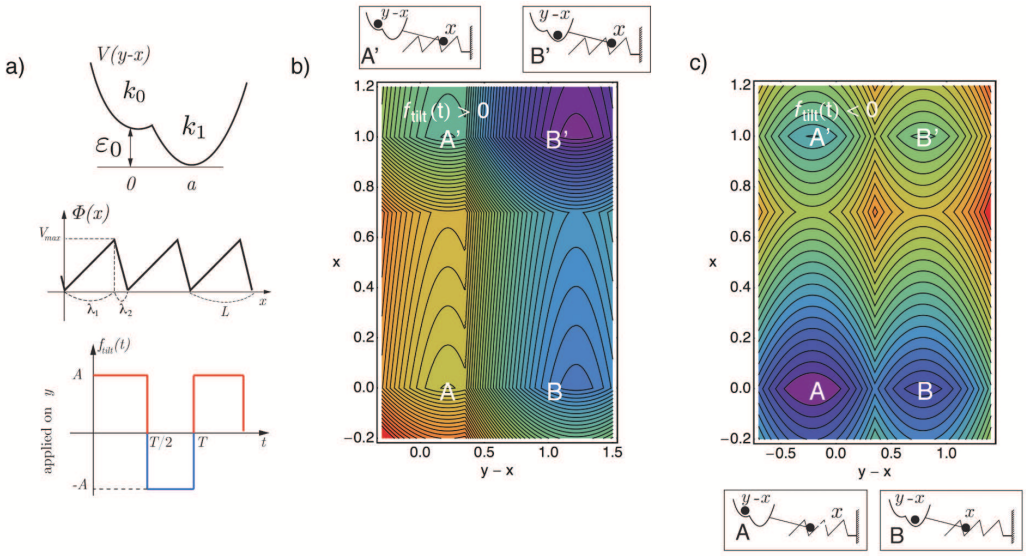

Figure 7.2. The Y-tilted ratchet. a)The sketch of potentials used in numeric applications. b)The picture illustrate the action of $f_{tilt}(t)$ on two-dimensional energy landscape in plane $[y-x, x]$. The increasing energy level scale graduated from cold color to hot colors. a) We show unbiased landscape in soft device configuration we identify the occupancy motor state, is intrinsic energy potential. b) The landscape corresponds to positive phase of $f_{tilt}(t) = A$. c) The landscape corresponded to the negative phase of $f_{tilt}(t) = -A$.

space periodic potentials.

7.2 A typical cycle of the Y-tilted motor

7.2.1 Soft device

In our numerical experiment we fix $\alpha = 1$ and assume that $k_0 = 1.5$, $k_1 = 0.43$, $l = 0.35$, $a = 1$, $L = 1$, $\lambda = 0.7$, $V_{max} = 1.5$. In Fig.7.3 we show the two-dimensional representation of motor trajectory in the case of zero external load, $f_{ext} = 0$. The paths were obtained by using the Euler scheme with time step $\Delta t = 0.5 \times 10^{-3}$ and were averaged over $N_r = 100$ realizations.

Notice that in the steady state regime the average velocity of variables x and y are the same. The variable $y_t - x_t$ describes the configuration of the bistable element at moment

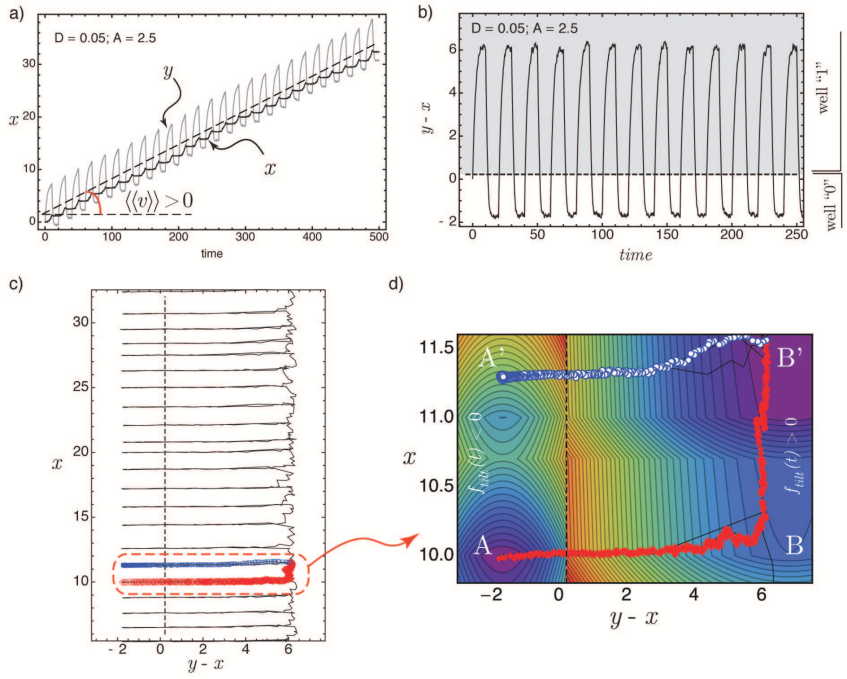

Figure 7.3. The Y-tilted ratchet model in soft device configuration, $f_{ext} = 0$. a) The average trajectory x_t (solid black line) and y_t (solid gray line). b) The time evolution of the system in coordinates $[time, y - x]$, note the characteristic oscillations between the two wells of the effective bistable potential. c)The average trajectory in coordinates $[y - x, x]$, note that the motor crosses few space periods. d) One motor cycle as segment of average trajectory during the time period T of the $f_{tilt}(t)$. The red scatters correspond to the positive phase of the rocking $f_{tilt}(t) = +A$ and the blue scatters–to the negative phase of rocking $f_{tilt} = -A$. The colored bands indicate the structure of the energy landscape, the coldest colors indicate the minima and hottest colors indicate the maxima. The relevant parameters $k_0 = 1.5$, $k_1 = 0.43$, $l = 0.35$, $a = 1$, $L = 1$, $\lambda_1 = 0.7$, $V_{max} = 1.5$, $\alpha = 1$ with the amplitude $A = 2.5$ and the time period $T = 16$ of rocking at temperature $D = 0.06$.

t, see Fig.7.3b). In Fig.7.3c) we show the averaged trajectory in the coordinate plane $[y-x, x]$. By colored scatters we indicate one motor cycle during time period T. In Fig.7.3d) we show the motor cycle on top of the energy landscape contour plot in positive and negative phases of the rocking. We use red scatters to identify the part of the cycle associated with the positive phase of f_{tilt}, and blue scatters to show the path associated with the negative phase of f_{tilt}. From these figures we can see that our Y-tilted motor is able to reproduce a four-states functional cycle $A \to B \to B' \to A'$, see Fig.7.3d). This cycle is much more realistic than what we have seen in the X-tilted model and can be directly compared with the biochemical theory behind the Lymn-Taylor cycle.

The schematic representation of the obtained mechanical cycle is shown in Fig.7.4. The "power stroke" is clearly associated with the transition ①→② (or $A \to B$) and the switch from positive to negative phase of the tilting force $f_{tilt}(t)$ recharges the power stroke during the transition ③→④. In more detail, the obtained mechanical cycle in the soft

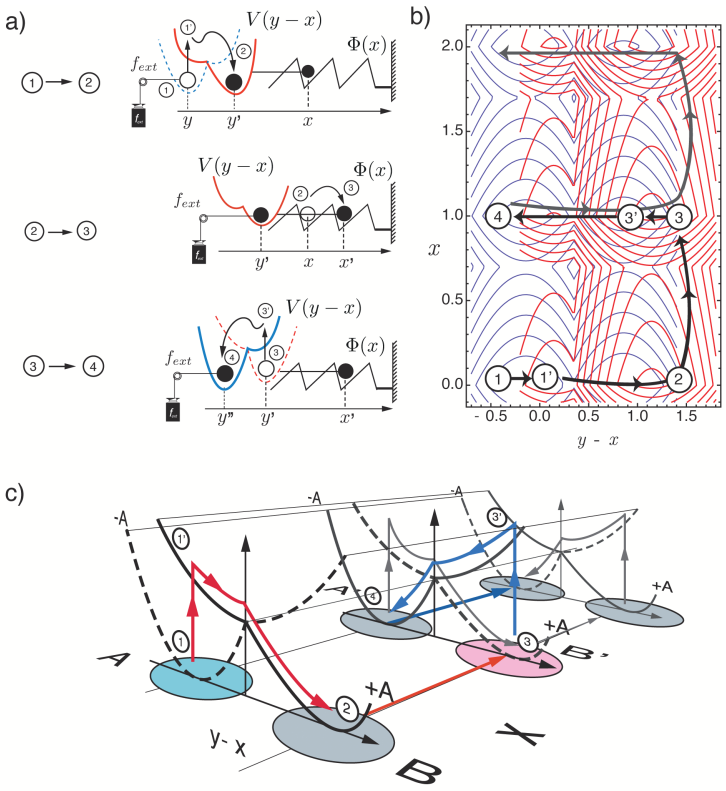

Figure 7.4. The mechanical cycle of Y-tilted ratchet model in soft device configuration. a) The simple, step by step, mechanical representation of the motor cycle. b) The average trajectory path superposed with the surface contours of energy landscape $(\Phi(x) + V(y-x) - yA$ by solid red contours and $\Phi(x) + V(y-x) + yA$ by solid blue contours). c) We start at the end of negative phase of $f_{tilt}(t)$, then $f_{tilt}(t)$ changes the phase to positive, the bi-stable element goes through the major transition which we identify with the power stroke. While we remain in the positive phase of tilting $f_{tilt}(t)$ the motor makes a step along x direction from state B to state B'. The correlated force changes its sign and the energy landscape becomes tilted in the opposite direction. Following an immediate transition the power stroke is getting recharged and the cycle can start again.

device can be characterized as follows:

- ①→①'→②. We start at the end of negative phase of $f_{tilt}(t)$ when our Brownian

particle explores the well "0" (or state A). Then $f_{tilt}(t)$ changes the phase to positive, the energy landscape is now $\Phi(x) + V(y-x) - yA$. After an immediate advance ① →①', the bi-stable element goes through the major transition ①'→② which we identify with the power stroke.

- ②→③. While we remain in the positive phase of tilting $f_{tilt}(t)$ the motor makes a step along x direction from state B to state B'. This advance along the actin filament is the direct consequence of the power stroke which is a driving force behind the corresponding detachment and reattachment.

- ③→③'→④. We now are in state ③ (or state B'), see Fig.7.3d). The correlated force changes its sign and the energy landscape becomes tilted in the opposite direction $\Phi(x) + V(y-x) + yA$. Following an immediate transition ③→③' the power stroke is getting recharged by making the transition ③'→④. Because of space asymmetry of the actin potential $\Phi(x)$ the Brownian particle with coordinate x gets trapped and does not move in the backward direction. Therefore the advance along the actin filament has taken place and the cycle can start again.

Depending on the amplitude of the correlated noise term, the motor step ②→③ can be longer or shorter. In particular, the system can jump over several periods of the potential $\Phi(x)$. The length of such 'step' is influenced by the fine structure of the energy landscape and also depends on the stiffness of the bi-stable spring.

7.2.2 Hard device

To study the system in the isometric case, we fix $z = 0$ and use the following values for the remaining parameters $k_0 = 7,\ k_1 = 7,\ l = 0.22,\ a = 1,\ L = 2,\ \lambda = 1.4,\ V_{max} = 5$. The computations are again performed by using Euler scheme with constant time step $\Delta t = 0.5 \times 10^{-3}$ and the averaging is performed over $N_3 = 100$ realizations. We increase progressively the temperature D at fixed values of the amplitude $A = 6$ and the time period $T = 20$.

The results are summarized in Fig.7.5. One can see that after a short transient regime the motor performs a stable cycle. With solid lines we plot the energy level contours in the positive phase ($\Phi(x) + V(y-x) + 1/2k_m y^2 - yA$) and with dashed lines – in the negative phase ($\Phi(x) + V(y-x) + 1/2k_m y^2 + yA$). By dashed thick line we indicate the separation between two wells of the bistable potential. The average motor trajectory is plotted by thick red line during the positive phase of $f_{tilt}(t)$ and by thick blue line during the negative phase. The light gray line shows a single stochastic realization during one time period. On the bottom picture we show the averaged trajectory y_t. We recall that the variable y_t is related directly to the tension

$$f_{h.d.} = k_m \left(\langle \langle y \rangle \rangle - z \right) \tag{7.7}$$

where we must use $z = 0$ and $k_m = 1$. Therefore the averaged value $\langle \langle y \rangle \rangle$ gives directly the averaged tension in the system.

At small temperature $D = 0.01$ we observe oscillations between the conformational states A and B inside the same space period of the actin potential ($x = 0$), see Fig.7.5a). This behavior can be interpreted as a power-stroke (red path) followed by the recharging (blue path) in the attached state. The little loop around the state B is a consequence of the distorted landscape in the hard device. We can therefore speak here about a two state cycle. With the increase of temperature the Brownian particle is able to explore larger

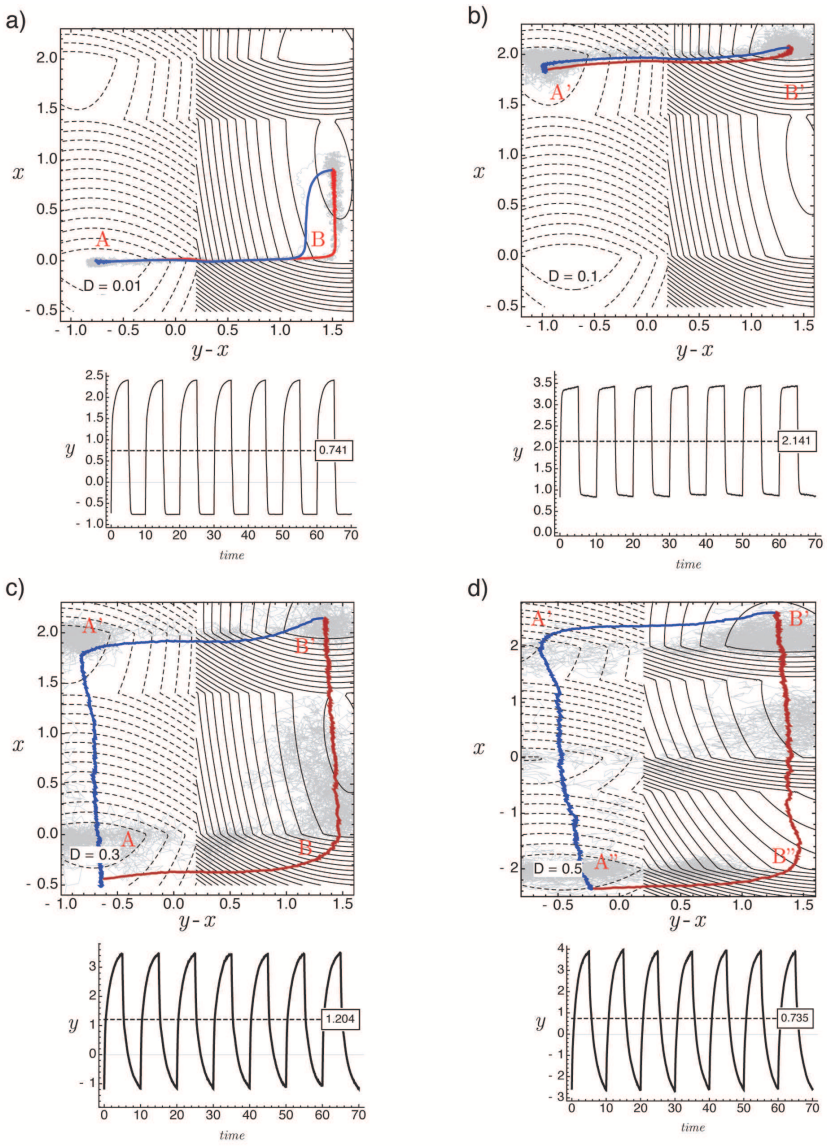

Figure 7.5. The Y-tilted ratchet model in hard device configuration, the variation of the motor cycle with the increasing temperature D at the constant amplitude $A = 6$. With solid black lines we depict the level set representation of the energy landscape in the positive phase of rocking and with dashed black lines –the same landscape in the negative phase of rocking. The average motor trajectory plotted by the thick red line during the positive phase of $f_{tilt}(t)$ and by the thick blue line during the negative phase. The light gray lines follow the single stochastic realization during one time period. a) The motor cycle and generated average tension at $D = 0.01$. b) The motor cycle and average tension at $D = 0.1$. c) The motor cycle and average tension at $D = 0.3$. d) The motor cycle and average tension at $D = 0.8$. The relevant parameters $k_0 = k_1 = 7,\ l = 0.22,\ a = 1,\ L = 2, \lambda_1 = 1.4,\ V_{max} = 5,\ \alpha = 5$ and the time period of the rocking force $T = 20$.

areas of the two-dimensional landscape and at $D = 0.1$ we can stabilize the oscillations between the state A' and B', see 7.5b). In this case the system reattached to a new cite on the actin filament and stretched the spring. As the result the motor generates much larger average tension, however, the cycle is still composed of only two states.

By increasing the temperature further, we are able to force the system to exhibit a four

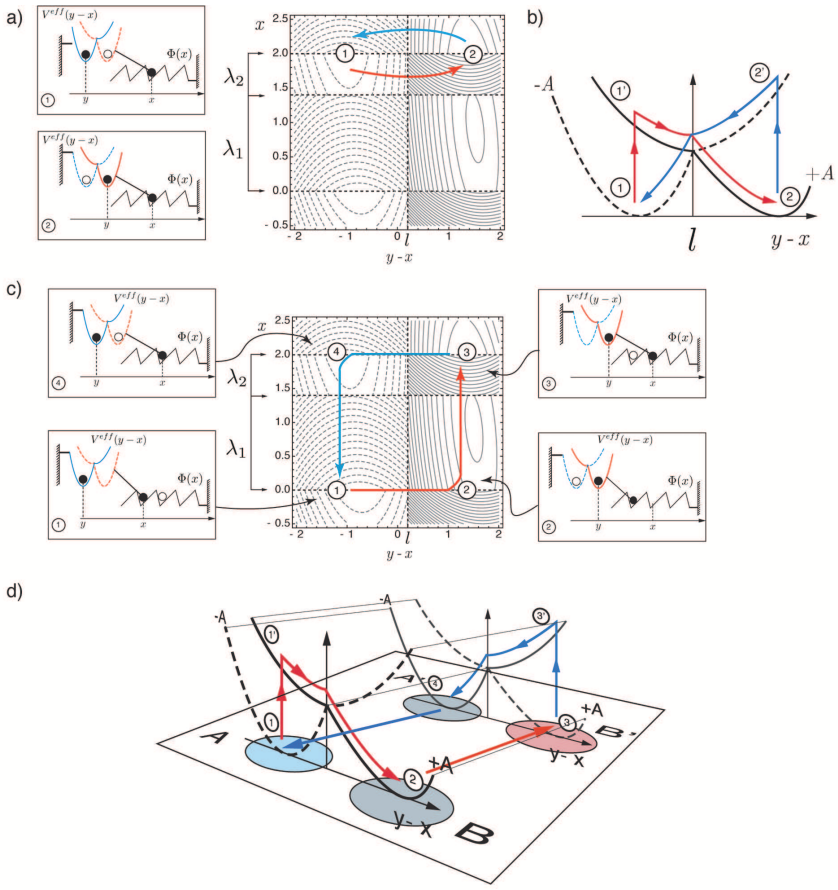

Figure 7.6. The Y-tilted ratchet model, the motor cycle in hard device configuration. With solid gray lines we plot the energy level contours in positive phases of rocking ($\Phi(x)+V(y-x)+1/2k_m y^2-yA$) and with dashed gray lines we plot the energy level contours in negative phase of rocking ($\Phi(x)+V(y-x)+1/2k_m y^2+yA$). a) The two-state motor cycle, the average trajectory is shown schematically by red arrows in positive phase of rocking and by blue arrows in negative phase of rocking. b) The schematic explanations of the observed two-states cycle. c) The four-state motor cycle, the average trajectory is shown schematically by red arrows in positive phase of rocking and by blue arrows in negative phase of rocking. d) The schematic explanations of the observed four-states cycle. For more details see the description in the text.

state motor cycle, see Fig.7.5c). The motor first goes through mechanical configurations A, B and then through the configurations B', A'. Interestingly, in this regime the motor generates smaller tension when in the regime of slightly lower temperature $D = 0.1$ when the cycle consists of two states only. For even higher values of D we preserve the 4 states cycle but we authorize the disadvantageous transitions in the backward direction long the actin potential, see Fig.7.5d).

In Fig.7.6 we give schematic explanations of the observed two-states and four-states cycles in the hard device configuration. With red arrows we sketch transitions in the positive phase of rocking and with blue arrows – in the negative phase of rocking. More specifically, in the 'two- state cycle' we observe the following stages:

- ①→①'→②. We start at the end of the phase of $f_{tilt}(t)$ with negative tilt. The Brownian particle explores the state A (well "0" of the bistable element), see Fig.7.6b).

The correlated noise changes the tilt to positive and the particle makes the immediate transition ①→①'. From this new configuration the Brownian particle performs the power stroke 1'→2. The motor then remain in the state B (well "1" of bistable element).

- 2 → 2' → 1. While the system is in the state B (well "1"), see Fig.7.6b), the correlated noise term $f_{tilt}(t)$ changes sign, creating again the negative tilt of the energy landscape. The system undergoes an immediate transition 2→2'. Because of the spatial asymmetry of the actin potential the system remains trapped in the same period of the periodic potential $\Phi(x)$ while the power stroke is recharged which amounts to a transition 2'→1. Afterwards the cycle can start again.

In the 'four-state cycle' the stages are the following:

- 1 → 1' → 2. We start again at the end of the negative phase of the rocking. The Brownian particle explores the state A (well "0"). As the correlated noise term $f_{tilt}(t)$ changes the value from negative to positive, the system makes an immediate transition 1→1', see Fig.7.6d). from this new configuration the particle performs the power stroke 1'→2.

- 2→3. While in the positive phase of $f_{tilt}(t)$, the motor makes a jump into the next nearest well in the positive x direction which is of course still a consequence of the power stroke.

- 3→3'→4. The system is now in the state ③ and the corresponding energy well is B' (well "1"), see Fig.7.6d). The correlated noise term changes the sign to negative configuration, and the system undergoes immediate transition 3→3'. Then the instability causes the particle to perform the transition 3'→4, which we identify with recharging of the power stroke mechanism.

- 4→1 From the state A' always following the phase space asymmetry, the motor jumps in backward direction making the transition 4→1. The system returns into the initial state and the cycle can start again.

In summary, we obtain two types of cyclic motion simulating isometric muscle contraction. In the two-state regime the system is residing in a distant, force generating well of the periodic potential while performing periodic oscillations between the two conformational states of the power stroke element. The level of the generate force is high because the cross bridge is firmly attached throughout the cycle. In the four-state regime, the system is periodically reaching the distant well of the periodic potential but remains there only for a limited time before returning back to the original attachment site. In this regime the average force is smaller, however the mechanical cycle is closer to its biochemical analog. Below we show how such difference in the structure of the cycle manifests itself in terms of force velocity relation and the efficiency of the energy transduction.

7.2.3 Parametric study in the soft device setting

We now investigate more systematically the influence of the level of noise, both correlated and uncorrelated, on the performance of the Y-tilted motor. As an example, we consider the soft device setting and focus our attention on the behavior of the average velocity as a function of temperature (parameter D), amplitude of the correlated noise A and its period T. For simplicity we fix the external load at zero $f_{ext} = 0$.

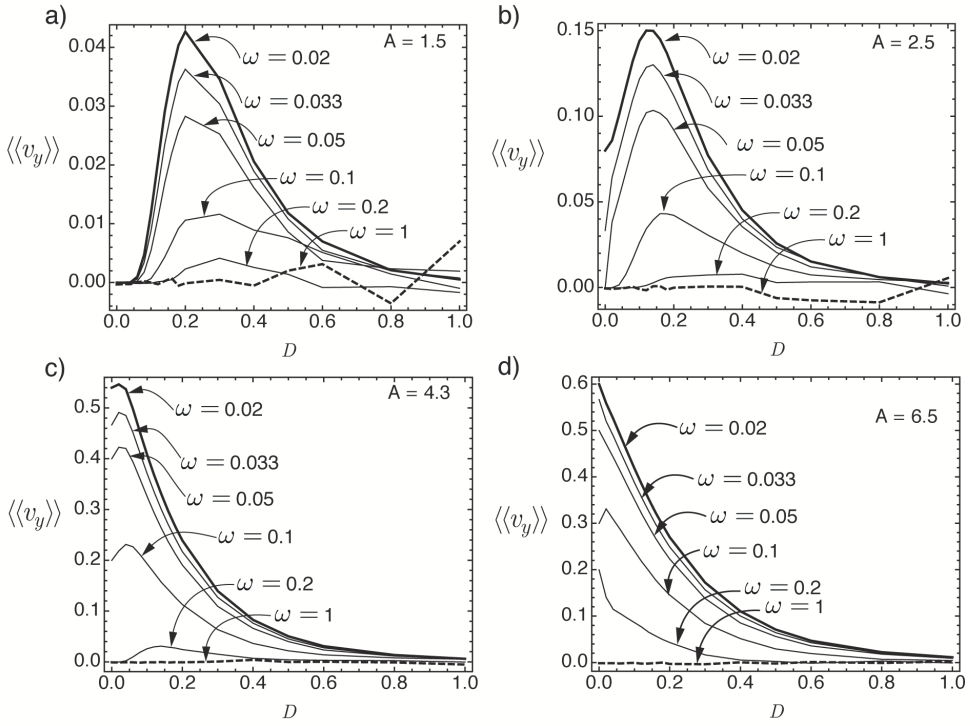

Figure 7.7. The Y-tilted model in soft device with zero load $f_{ext} = 0$. The variation of the average velocity with increasing temperature D computed at different frequencies $\omega = 1/T$ of rocking force $f_{tilt}(t)$. a) At small amplitude $A = 1.5$ we observe the presence of a velocity maximum at finite value temperature. b) The results of the measurements at the amplitude $A = 2.5$. c) The results of the measurements at the amplitude $A = 4.3$. d) The results of the measurements at the amplitude $A = 6.5$. In the regimes with high amplitudes of rocking the stochastic resonance disappears and the average velocity becomes a monotonically decreasing function of D.

In Fig.7.7a) we show the average velocity as a function of D, at different values of the frequency ω characterizing the $f_{tilt}(t)$. At small amplitude $A = 1.5$ we observe the presence of a velocity maximum at finite value temperature which characterizes the stochastic resonance. The maximum shifts to larger values of temperature as we increase ω (decrease the period T) until the maximum disappears at $\omega < 0.0034$. To interpret these observations we recall that stochastic resonance takes place when the Kramers time of barrier crossing which is increasing function of temperature is comparable to the characteristic period of imposed oscillations. Therefore the two must increase along the velocity maximum which what we see in our numerical experiments.

In Fig.7.7b),c),d) we show our experimental results at larger values of the amplitude $A = 2.5$, $A = 4.3$, $A = 6.5$. One can see that in the regimes with high amplitudes of rocking the stochastic resonance disappears and the average velocity becomes a monotonically decreasing function of D. This means that the nature of the ratchet changes from Brownian to purely mechanical and as a result the thermal noise changes its role from assisting motor activity to being detrimental.

In Fig.7.8 we show the average velocity as a function of the driving period T. We observe saturation at hight values of T when the time scale of the correlated noise becomes much larger that the Kramers time in the bi-stable problem. From Fig.7.8a) we see that the average velocity first grows at fixed T with increasing D but then starts to decrease.

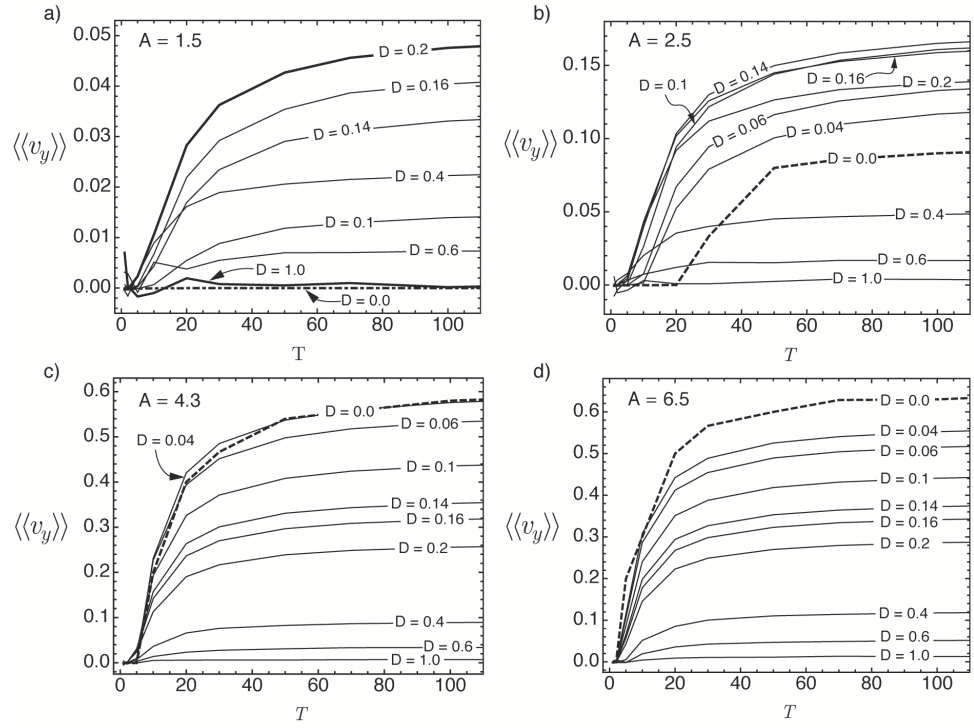

Figure 7.8. The Y-tilted model in soft device with zero load $f_{ext} = 0$. The variation of the average velocity with the increasing time period T of $f_{tilt}(t)$ computed at different temperatures D. a) The results of the measurements at the amplitude $A = 1.5$, note that the average velocity first grows at fixed T with increasing D but then starts to decrease. b) The results of the measurements at the amplitude $A = 2.5$, we are always in thermal ratchet regime. c) The results of the measurements at the amplitude $A = 4.3$. d) The results of the measurements at the amplitude $A = 6.5$, note that the average velocity decreases with increasing D, meaning that the white noise interferes negatively with the force generation process.

This means that we are in the thermal ratchet regime whose optimal performance requires finite temperature instead, in Fig.7.8d), the average velocity decreases with increasing D, meaning that the white noise interferes negatively with the force generation process, which is characteristic for the mechanical ratchet regime. While we did not try to resolve with sufficient accuracy the behavior at low values of T, there is probably always a local maximum of performance sufficiently close to the origin, see Fig.7.8a),b).

7.3 Force-Velocity relation

The introduction of a non zero load f_{ext} in the soft device experiments opens a possibility to recover the force-velocity curve. We recall that in the presence of active force $f_{tilt}(t)$ the motor can transform the input energy into mechanical work. Once again we adopt the physical definition of the sign of the external load in the plots $[\langle v \rangle, f_{ext}]$, see the scheme in Fig.7.9. Then the mechanic work is negative (energy is dissipated) if the motor moves in the direction imposed by the load.

In Fig.7.9a) we show the computed force-velocity relation while varying D at fixed amplitude of rocking $A = 2.5$. We observe that the force velocity relation is concave at $D = 0.01$. With the increase of temperature the area under the force-velocity curve

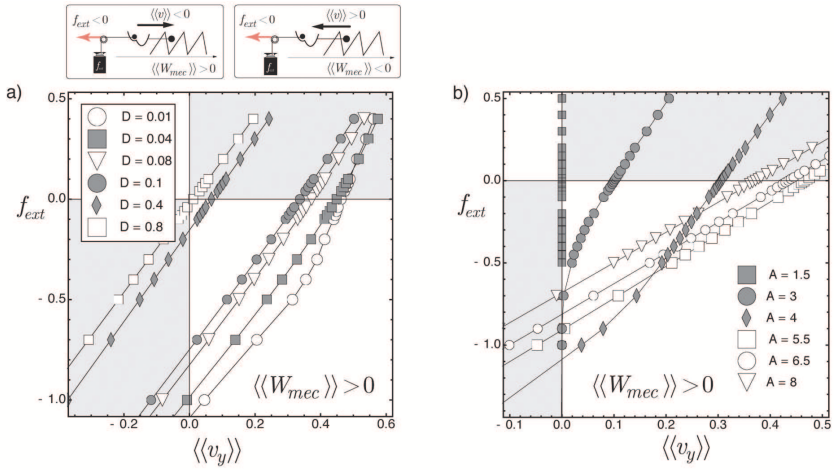

Figure 7.9. The Y-tilted ratchet model. a) The variation of the force-velocity relation with increasing temperature D at the amplitude $A = 2.5$, note the characteristic concave shape at $D = 0.01$. With the increase of temperature the area under the force-velocity curve decreases and the system generates smaller average velocity at zero load and smaller stall force at zero velocity. b) The variation of the force-velocity relation with increasing amplitude A at the temperature $D = 0.01$. We observe the characteristic concave shape of the force-velocity curve in the interval $\approx 1.5 < A \leq \approx 3$

decreases and the system generates smaller average velocity at zero load and smaller stall force at zero velocity. Recall that we observed similar behavior for the X-tilted ratchet in this almost mechanical (vs thermal) ratchet regime, see Fig.6.8. However, we observe that our Y-tilted motor is less efficient in rectification of noise fluctuations, in comparison with the X-tilted motor.

In Fig.7.9b) we show how the force-velocity relation changes when we vary the amplitude of rocking A at the fixed temperature $D = 0.01$. We observe the characteristic concave shape of the force-velocity curve in the interval $\approx 1.5 < A \leq \approx 3$, where we expect that the system works as a thermal ratchet.

7.4 Stochastic energetics

In this section we study the temperature dependence of the energetics for the Y-tilted ratchet. We again define the heat as $\delta Q_i = \left(-\eta d_t x_i + \sqrt{2\eta_i D}\xi_i(t)\right) \circ dx_i$ and write the energy balance in the form

$$\begin{cases} (\partial_x \Psi(x) + \partial_x V(y-x)) \circ dx = \delta Q_x \\ \partial_y V(y-x) \circ dy - f_{tilt}(t) \circ dy - f_{\text{ext}} \circ dy = \delta Q_y \end{cases} \tag{7.8}$$

Introduce the averaged intrinsic energy $G_0(x_t, y_t) = \Phi(x_t) + V(y_t - x_t) - y f_{ext}$ over a period

$$\frac{1}{T} \int\limits_{\mathbf{X}_{t_i}}^{\mathbf{X}_{t_i+T}} dG_0(\mathbf{X}_t) - \frac{1}{T} \int\limits_{x_{t_i}}^{x_{t_i+T}} f_{tilt}(t) dy_t = \frac{1}{T} \int\limits_{\mathbf{X}_{t_i}}^{\mathbf{X}_{t_i+T}} \delta Q_x + \delta Q_y \tag{7.9}$$

where the time moment t_i indicate the duration the transition regime. According to the energetics [100] the input energy per time period R reads

$$R = \frac{1}{T} \int_{x_{t_i}}^{x_{t_i+T}} f_{tilt}(t) dy_t \tag{7.10}$$

Now since the variation of the $\Phi(x) + V(y-x)$ over one period is equal to zero, the mechanical work W_{mec} takes the form

$$W_{mec} = \frac{1}{T} \int_{\mathbf{X}_{t_i}}^{\mathbf{X}_{t_i+T}} dG_0(\mathbf{X}_t) = -f_{ext}\langle v_y \rangle \tag{7.11}$$

Then

$$W_{mec} \equiv R + Q \tag{7.12}$$

where

$$Q = \frac{1}{T} \int_{\mathbf{X}(t=t_i)}^{\mathbf{X}(t=t_i+T)} \delta Q_x + \delta Q_y \tag{7.13}$$

This allows us to define the mechanical efficiency

$$\epsilon_{mec} = \frac{W_{\text{mec}}}{R} \tag{7.14}$$

Similarly we introduce the Stokes work

$$W_{\text{Stokes}} = \alpha^{-1}\langle v_x \rangle^2 + \langle v_y \rangle^2 \tag{7.15}$$

and define the Stokes efficiency as

$$\epsilon_{Stokes} = \frac{W_{Stokes}}{R} \tag{7.16}$$

Finally we can define the total rectifying efficiency

$$\epsilon_{rec} = \frac{W_{mec} + W_{Stokes}}{R} \tag{7.17}$$

These definitions make sense in the soft device configuration. In the hard device configuration we simply have $R = -Q$.

In Fig.7.10a) we show the average velocity as a function of temperature at different values of the amplitude A. For small amplitude A (Brownian ratchet) the motor exhibits a maximum of velocity at finite temperature. At higher amplitude A (mechanical ratchet) the average velocity decreases monotonically with D. Overall the Y-tilted model is generating smaller average velocities than the X-tilted model at the same values of parameters. In Fig.7.10b) we plot the consumed energy R as a function of D and use the same range of amplitudes A. One can see that as the temperature increases, the motor consumes more and more energy in order rectify the fluctuations and preform a useful work. We also again observe a saturation at high temperatures meaning that there is a limit of how much thermal energy the motor can rectify.

In Fig.7.11b) we show the temperature dependence of mechanical efficiency, (7.14), for increasing values of A. In the regime of small amplitudes A we again observe a maximum of

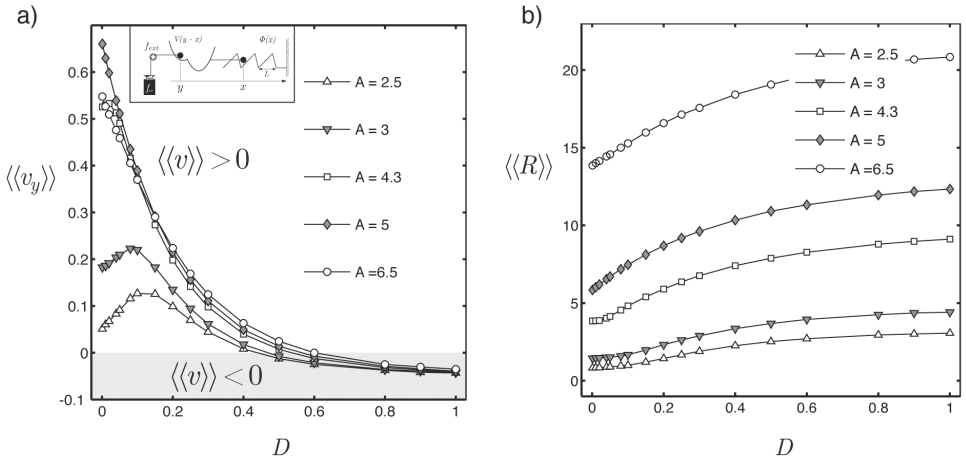

Figure 7.10. The Y-tilted model in the soft device configuration with the conservative load $f_{ext} = -0.1$. a) The variation of the average velocity $\langle v_y \rangle$ with the increasing temperature D for different amplitudes A of $f_{tilt}(t)$. For small amplitude A (Brownian ratchet) the motor exhibits a maximum of velocity at finite temperature. At higher amplitude A (mechanical ratchet) the average velocity decreases monotonically with D. b) The variation of the consumed energy R with increasing temperature D for different amplitudes A of $f_{tilt}(t)$, note that the motor consumes more and more energy in order rectify the fluctuations and preform a useful work. The relevant parameters $k_0 = 1.5,\ k_1 = 0.43,\ l = 0.22,\ a = 1,\ L = 1,\ \lambda_1 = 0.7,\ V_{max} = 1.5,\ \alpha = 1$ with time period $T = 60$ of rocking force.

mechanical efficiency at finite temperature. In the regime of high amplitudes the efficiency becomes a monotonically decreasing function of D, which characterizes such system as a mechanical ratchet. By light green color we indicate the regime with negative efficiency, when the motor is unable to perform a positive mechanical work and can only resist (drags) the imposed external load.Overall the Y-tilted ratchet is less efficient when the X-tilted ratchet. We can explain this difference by the design of the active mechanism: the consumed metabolic energy is partially consumed by the bi-stable element and partially for forward steps long x.

In Fig.7.11c) we present the parametric study of the Stokes efficiency (7.15) and in Fig.7.11d) of the rectifying efficiency (7.17). The qualitative behavior of these functions is basically the same as in the case of X-tilted ratchet.

7.5 Conclusions

In this section we have shown that muscle contraction can be driven by the correlated noise acting on an internal variable inside the power stroke mechanism. The system performs 4-state cycle in the soft device configuration and either 2-state or 4-state cycle in the hard device. We have shown that the maximal isometric tension is generated in the 2-state motor cycle implying strongly bound actin-myosin configuration. Although the proposed framework is sufficient to describe the complete Lymn-Taylor cycle the ensuing motor is slightly less efficient than in the X-tilted model. Overall this model is of intermediate nature while in the next section we study the fully power-stroke driven contraction mechanism.

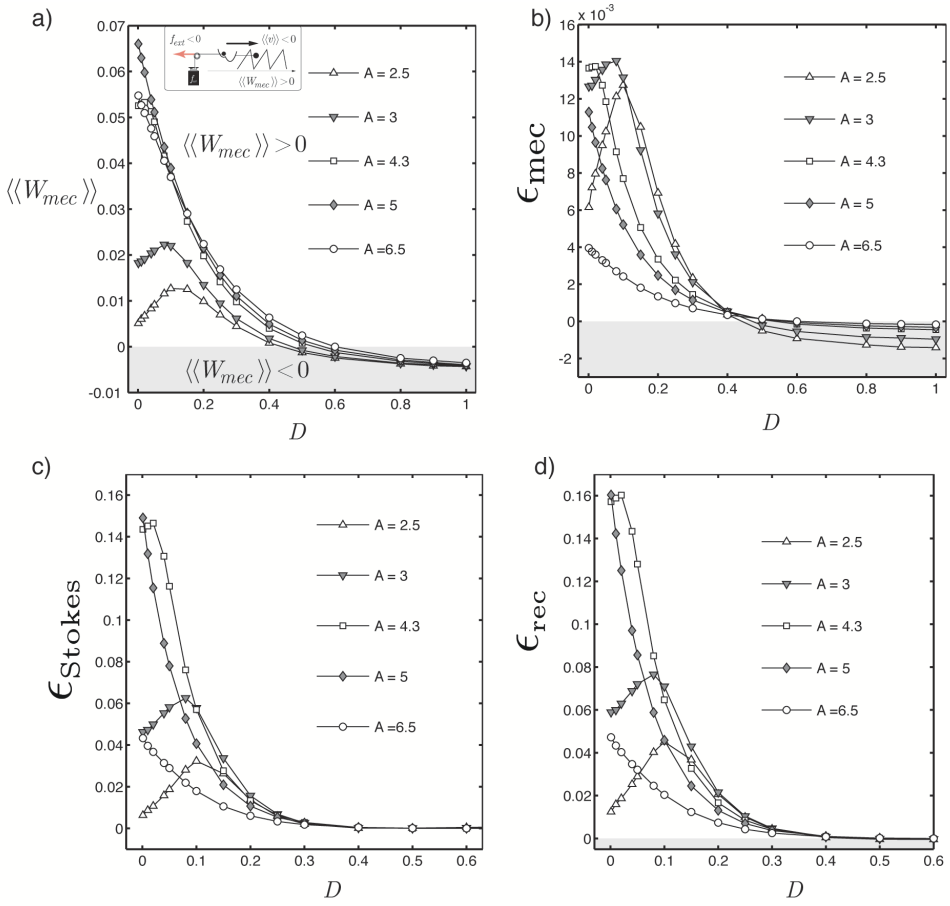

Figure 7.11. The Y-tilted model in the soft device configuration with the conservative load $f_{ext} = -0.1$. a) The variation of the mechanic work W_{mec} with the increasing temperature D for different amplitudes A of $f_{tilt}(t)$. b) The variation of the mechanic efficiency ϵ_{mec} with the increasing temperature D for different amplitudes A of $f_{tilt}(t)$. In the regime of small amplitudes A we again observe a maximum of mechanical efficiency at finite temperature. In the regime of high amplitudes the efficiency becomes a monotonically decreasing function of D. c) The variation of the Stokes efficiency ε_{Stokes} with the increasing temperature D for different amplitudes A. By definition, this is always positive function. For hight values of D the Stokes efficiency is increasing function of D, because we are in regime there the motor follows the direction imposed by cargo. d) The variation of the rectifying efficiency ε_{rec} with the increasing temperature D. The shape of this function is dominated by the quadratic Stokes term. The relevant parameters $k_0 = 1.5$, $k_1 = 0.43$, $l = 0.22$, $a = 1$, $L = 1$, $\lambda_1 = 0.7$, $V_{max} = 1.5$, $\alpha = 1$ with time period $T = 60$ of rocking force.

Chapter 8

XY-tilted thermal ratchet

In this chapter we consider a XY-tilted ratchet model where the biasing force is acting directly on the $y - x$ coordinate. This means that we are rocking/tilting the bi-stable element proper. In this formulation, the model resembles the Brownian ratchet description of kinesin where ATP acts on an internal bi-stable device forcing two legs to move along the actin filament modeled by the spatial potential with periodically spaced preferred attachment sites. In this sense the model considered in this chapter can be viewed as a 'single-leg' analog of the kinesin motor. What is important, in both models the motor is driven through a power stroke element. To characterize the proposed design we use the direct Langevin-based numerical simulations. As in the two previous sections we first explore the fine structure of the averaged trajectories of the system in the phase space in soft in hard device configurations and study the consistency of these mechanical cycles with the prevailing biochemical cycle of muscle contraction. We then establish force-velocity relations in the soft device case and study its parametric dependence by varying temperature the amplitude/ frequency of the correlated component of the noise. Finally we study elementary energetics of the ensuing motors and look for the regimes with maximum efficiency. We show what the XY-tilted ratchet can partially reproduce all four stages in the Lymn-Taylor cycle. We also presented evidence that this ratchet can optimize its behavior by taking advantage of the phenomenon of stochastic resonance.

8.1 Preliminaries

As we have already mentioned, in the XY-tilted thermal ratchet the correlated force $f_{tilt}(t)$ acts on the combination of variables $y - x$, which can be identified with an internal displacement inside the bistable element. This means that the rocking force affects the power stroke mechanism directly instead of implicitly modifying the internal state of this device through other external degrees of freedom. In Fig.8.1 we illustrate the mechanical action of the rocking force on our two dimensional energy landscape showing that in the case of XY-tilted ratchet the ATP activity is fully decoupled from the actin filament.

We begin by formulating the model in our two standard cases, the isometric setting where we fix the total length of the system and the isotonic case where we fix the externally applied force. We again refer to these two settings as hard device and soft device configurations, respectively. In the soft device the model is described by the following

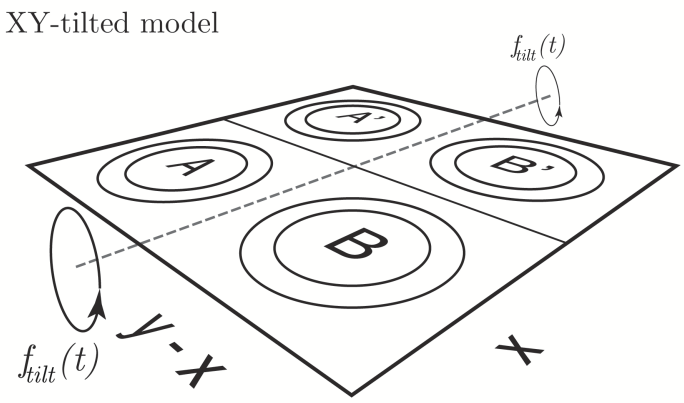

Figure 8.1. XY-tilted ratchet model. The schematic sketch of the mechanical action of rocking force on energy landscape. We show one period of energy landscape in coordinates plane $[y-x, x]$, the landscape wells noted A, B, A', B', we drew a fictive axe on each the correlated noise is applied.

system of coupled overdamped Langevin equations:

$$\begin{cases} \eta_x \dfrac{dx}{dt} = -\partial_x \Phi(x) - \partial_x V(y-x) - f_{tilt}(t) + \sqrt{2\eta_x D}\,\xi_x(t) \\ \eta_y \dfrac{dy}{dt} = -\partial_y V(y-x) + f_{tilt}(t) + f_{ext} + \sqrt{2\eta_y D}\,\xi_y(t) \end{cases} \tag{8.1}$$

In the hard device the XY-tilted ratchet is described by the system:

$$\begin{cases} \eta_x d_t x = -\partial_x \Phi(x) - \partial_x V(y-x) - f_{tilt}(t) + \sqrt{2\eta_x D}\,\xi_x(t) \\ \eta_y d_t y = -\partial_y V(y-x) - k_m(y-z) + f_{tilt}(t) + \sqrt{2\eta_y D}\,\xi_y(t) \end{cases} \tag{8.2}$$

In both cases η_x and η_y are viscous drag coefficients and $D = k_B T$. Here again z is external control parameter, which prescribes the stretch of the linear spring with stiffness k_m, and f_{ext} is the applied conservative load.

It will be convenient to introduce the nondimensional variables, we use the following scaling of the parameters (6.3) and the time scale (6.4). Applying the normalization we are left with the following dimensionless parameters $\tilde{D} \equiv \frac{D}{k_m a^2}$ and $\alpha = \frac{\eta_y}{\eta_x}$. In the nondimensional parameters the main system for the soft device case takes the form

$$\begin{cases} \dfrac{dx}{dt} = -\alpha\left(\partial_x \Phi(x) + \partial_x V(y-x) + f_{tilt}(t)\right) + \sqrt{2\alpha D}\,\xi_x(t) \\ \dfrac{dy}{dt} = -\partial_y V(y-x) + f_{\text{ext}} + f_{tilt}(t) + \sqrt{2D}\,\xi_y(t) \end{cases} \tag{8.3}$$

In the hard device configuration we obtain accordingly

$$\begin{cases} \dfrac{dx}{dt} = -\alpha\left(\partial_x \Phi(x) + \partial_x V(y-x) + f_{tilt}(t)\right) + \sqrt{2\alpha D}\,\xi_x(t) \\ \dfrac{dy}{dt} = -\partial_y V(y-x) - k_m(y-z) + f_{tilt}(t) + \sqrt{2D}\,\xi_y(t) \end{cases} \tag{8.4}$$

In both cases we omit $\tilde{\bullet}$ for simplicity of notations.

The Fokker-Planck equation, corresponding to the normalized system of Langevin equations in the soft device and hard device configuration, takes the similar form as

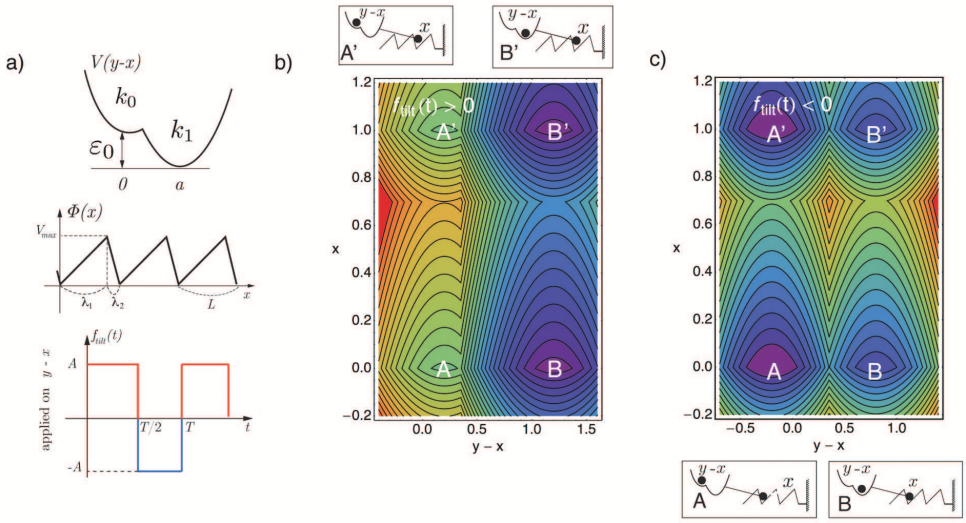

Figure 8.2. The XY-tilted ratchet. a)The sketch of potentials used in numeric applications. b)The picture illustrate the action of $f_{tilt}(t)$ on two-dimensional energy landscape in plane $[y-x, x]$. The increasing energy level scale graduated from cold color to hot colors. a) We show unbiased landscape in soft device configuration we identify the occupancy motor state, is intrinsic energy potential. b) The landscape corresponds to positive phase of $f_{tilt}(t) = A$. c) The landscape corresponded to the negative phase of $f_{tilt}(t) = -A$.

the expressions (6.7) and (6.9). In soft device the Fokker-Planck equation reads with $G_s(x, y, t) = \Phi(x) + V(y-x) - (y-x)f_{tilt}(t) - yf_{ext}$ where f_{ext} is the external control parameter. In the hard device configuration the corresponding Fokker-Planck equation reads with $G^h(x, y, t) = \Phi(x) + V(y-x) - (y-x)f_{tilt}(t) + \frac{1}{2}k_m(y-z)^2$ and z is the external control parameter. In our numerical simulations we use the same choices for the functions $\Phi(x)$ (6.11), $V(y-x)$ (6.13) and $f_{tilt}(t)$(6.12) as in the previous chapters, see Fig.8.2.

We notice that a somewhat related model of two coupled rocking ratchets moving on the same periodic potential has been recently used for the description of kinesin [76]. The corresponded two dimensional system of over-damped Langevin equation has the form:

$$\begin{cases} \dfrac{dx}{dt} = -\partial_x\Phi(x) - \partial_x V(x-y) - f_{tilt}(t) + \sqrt{2D}\,\xi_x(t) \\ \dfrac{dy}{dt} = -\partial_y\Phi(y) - \partial_y V(x-y) + f_{tilt}(t) + \sqrt{2D}\,\xi_y(t) \end{cases} \tag{8.5}$$

where $\Phi(x)$ and $\Phi(y)$ are two identical ratchet potentials. The $V(x-y)$ is the bistable potential describing the interaction between the two legs of the kinesin, whose positions are given by x and y. Here as in our model the time periodic rocking signal with zero average $f_{tilt}(t)$ acts on the coordinate $x-y$, meaning that the activity is concentrated inside the bistable potential. In contrast to this 'two-legged' model, our model can be interpreted as 'one-legged' which underlines the difference between processive and non-processive motors. However, the fact that both types of motors are driven not through the actin filament but through the bi-stable element opens the possibility for the unified description inside a single framework.

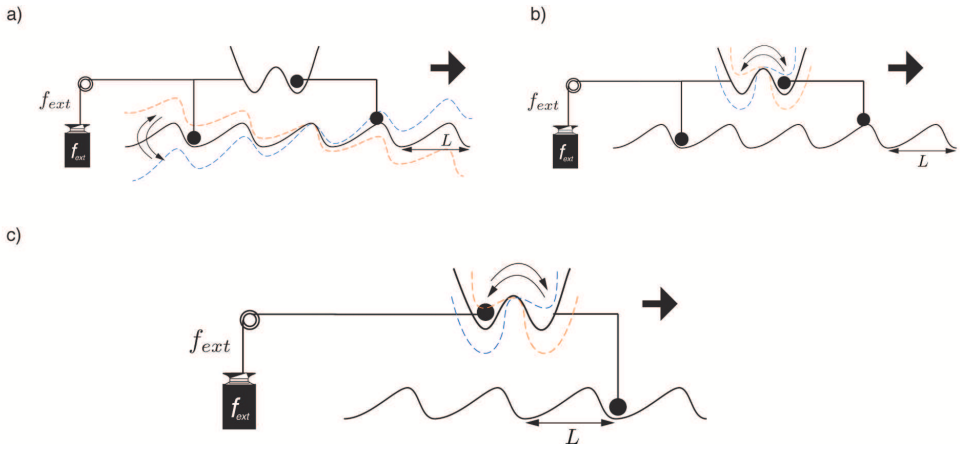

Figure 8.3. The scheme of kinesin-like mollecular motor in soft device configuration. a) The concept of Brownian motor with two leg, developed in the works of L.Schimansky-Geier [79]. The rocking force applied on space periodic ratchet potential, see the details in Chapter 2. b) The concept of Brownian motor with two leg developed in works of J.L. Mateos and F.R. Alatriste, [76]. The rocking force applied on bistable potential. c) The molecular motor developed in our work. The one-leg "mutant kinesin" jumping along space periodic potential. The motion driven by the active bistable potential.

8.2 The XY-tilted motor cycles

In this section we perform a series on numerical experiments whose goal is to identify the nature of the steady state cyclic motion.

8.2.1 Soft device

We use the following values of parameters: $k_0 = 1.5,\ k_1 = 0.43,\ l = 0.35,\ a = 1$. For the periodic potential we use two sets of parameters $\lambda_1 = 0.35,\ L = 0.5,\ V_{max} = 1,\ \alpha = 1$. In Fig.8.4 we show the averaged trajectory of the XY-tilted ratchet exposed to square-wave rocking force with amplitude $A = 0.6$ and the period $T = 16$ and also subjected to thermal noise with $D = 0.02$. The simulation of the Langevin system was performed by Euler scheme with $\Delta t = 10^{-3}$ and the results were averaged over $N_r = 10^3$ realizations. The ensuing trajectory is surprising, because the motion takes place along the untilted periodic potential and all external forces have zero average. The only non-equilibrium entry in this model is a correlated tilting of the bi-stable potential associated with an internal degree of freedom inside the motor mechanism.

We recall that the variable $y_t - x_t$ describes the configuration of the bistable element at moment t. In Fig.8.4c) we show the trajectory of the system in coordinates $[y - x, x]$. With colored scatters we represent one motor cycle during time period T, see Fig.8.4d). By the red scatters we plot the average path of motor cycle during the positive phase of f_{tilt}, and by the blue scatters – the path associated with the negative phase of $f_{tilt}(t)$.

One can see that the XY-tilted motor performs a three-state functional cycle passing through sites $A \to B \to B' \to A'$, see Fig.8.4d). First this motor device performs a power-stroke while being attached to one particular state on the periodic landscape $\Phi(x)$ and after that it moves in forward direction long $\Phi(x)$, while in same time recharging the power-stroke mechanism. The overall behavior is very similar to what we have seen in the X-tilted ratchet. The change of sign of the tilting force $f_{tilt}(t)$ both re-activates the power-stroke

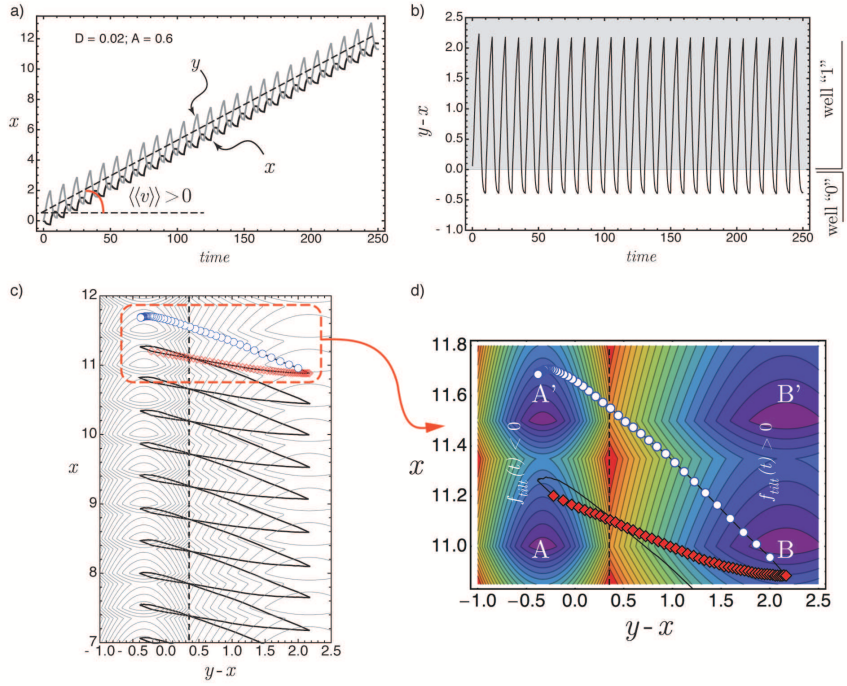

Figure 8.4. The XY-tilted ratchet model in soft device configuration, $f_{ext} = 0$. a) The average trajectory x_t (solid black line) and y_t (solid gray line). b) The time evolution of the system in coordinates $[time, y - x]$, note the characteristic oscillations between the two wells of the effective bistable potential. c)The average trajectory in coordinates $[y - x, x]$, note that the motor crosses few space periods. d) One motor cycle as segment of average trajectory during the time period T of the $f_{tilt}(t)$. The red scatters correspond to the positive phase of the rocking $f_{tilt}(t) = +A$ and the blue scatters–to the negative phase of rocking $f_{tilt} = -A$. The coloured bands indicate the structure of the energy landscape, the coldest colors indicate the minima and hottest colors indicate the maxima. The relevant parameters $k_0 = 1.5$, $k_1 = 0.43$, $l = 0.35$, $a = 1$, $\lambda_1 = 0.35$, $L = 0.5$, $V_{max} = 1$, $\alpha = 1$ with time period $T = 16$ of the rocking force.

mechanism and causes the directional motion of the motor. The value of the amplitude of tilting strongly influences the shape of the energy landscape in tilted configurations. In each phase, positive and negative, the intrinsic bi-stability of the potential in $y - x$ direction may be either preserved or not.

In Fig.8.5 we present a schematic mechanical illustration showing the states visited by the motor pass during one functional cycle. More specifically, the motor cycle in the soft device can be described as follows:

- ①→①'→②. We start the cycle at the very end of the negative phase of f_{tilt}, see Fig.8.5. Our Brownian particle exploits the well "0", or state A. As the force $f_{tilt}(t)$ changes from negative to positive, the energy becomes $\Phi(x) + V(y - x) - (y - x)A$ and the particle makes an immediate transition ①→①'. During the positive phase of the force f_{tilt} the system further undergoes a transition from well 0 to well 1 in the bistable element ①'→② which we identify with the power stroke.

- ②→③'→③. We are now in state ② corresponding to well "1", state B, see Fig.8.4. The correlated noise changes the sign and the energy becomes $\Phi(x) + V(y - x) + (y - x)A$. The system makes the step ②→③', and since the bistable potential now

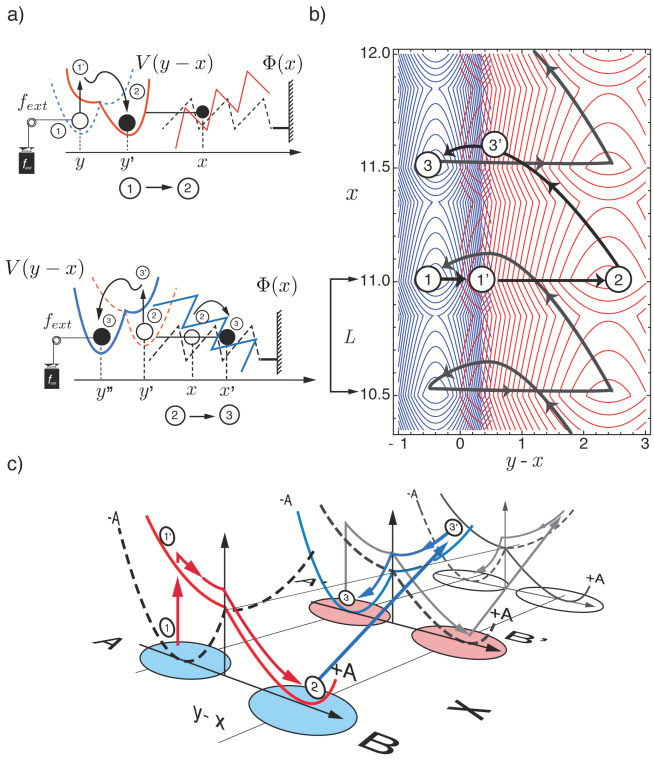

Figure 8.5. The mechanical cycle of XY-tilted ratchet model in soft device configuration. a) The simple, step by step, mechanical representation of the motor cycle. b) The corresponded average trajectory path superposed with the surface contours of energy landscape $(\Phi(x) + V(y-x) - (y-x)A$ by solid red contours and $\Phi(x) + V(y-x) + (y-x)A$ by solid blue contours). c) We start the cycle at the very end of the negative phase of f_{tilt}, as the force $f_{tilt}(t)$ changes from negative to positive, the energy becomes $\Phi(x) + V(y-x) - (y-x)A$ and during the positive phase of the force f_{tilt} the system further undergoes a transition from well 0 to well 1 in the bistable element which we identify with the power stroke. The correlated noise changes the sign and the energy becomes $\Phi(x) + V(y-x) + (y-x)A$. The system makes the step forward x, and since the bistable potential now biases the well "0", the motor finalizes the recharging of the power stroke element. Then the cycle can start again.

biases the well "0", the motor performs an additional transition ③'→③, finalizing the recharging of the power stroke element. Because of the spatial asymmetry the periodic potential the attachment site does not change during such recharging. Then the cycle can start again.

We observe that depending on the amplitude of the rocking, the motor cycle during one time period T, can occur over one or several spatial periods of the actin potential.

In summary, we observed a clear evidence of the 3 step cycle. Here again the motor advance and the recharging of the power stroke take place simultaneously. Those are two stages where external energy supply is necessary and as we see, they cannot be separated in the soft device setting.

8.2.2 Hard device

The XY-tilted ratchet in a hard device is a complex system, where the correlated and the white noise terms show an interesting interplay. In our experiments we fix the total displacement at $z = 0$ and vary both the temperature and the amplitude of the correlated noise. At zero temperature and weak amplitude of rocking the motor is unable to generate a force and the configuration particle remains practically frozen in the original well. The system exhibits the temperature and the amplitude thresholds whose crossing allows the motor to form a cycle utilizing both the thermal fluctuations and the correlated noise.

In Fig.8.6 we show the simplest motor cycle exhibited by the average trajectory during one time period of $f_{tilt}(t)$ in the hard device. The energy contours for the potential $\Phi(x) + V(y-x) + 1/2k_m y^2 - (y-x)A$ are plotted with solid lines, and for the potential $\Phi(x) + V(y-x) + 1/2k_m y^2 + (y-x)A$ – with dashed lines. The red color corresponds to positive phase of rocking and the blue color – to the negative phase. Below each cycle diagram we show the averaged trajectory $y(t)$ during several time period where by dashed line we indicate the observed average tension

$$f_h = k_m \left(\langle \langle y \rangle \rangle - z \right) \tag{8.6}$$

Since $z = 0$ and $k_m = 1$ the quantity $\langle \langle y \rangle \rangle$ can be used as the measure of tension in the hard device.

One can see that at low temperatures our effective particle moves only between the wells "0" (state A) and "1" (state B), see Fig.8.6a) for $D = 0.01$ and $A = 2.4$. This means that the cross bridge is attached to a particular site of the actin potential while performing random oscillations between two states of the power stroke element. In this regime the system works as our bi-stable element in the hard device considered in Chapter 4.

With the increase of temperature D the motor eventually crosses the energy barrier (detaches) and then stabilizes (attaches) in the next site on the actin filament. In this new attached position the motor continue to perform periodically first the power stroke and then recharging of the power stroke (transitions between state A' and state B'), see 8.6b) for $D = 0.065$ and $A = 2.4$. Observe that now the attachment site is distant from the reference position, the spring is stretched and the motors shows two time higher level of tension comparing to what we saw in Fig.8.6a).

By increasing the temperature and amplitude of colored noise further, we force the motor to visit more sites on the energy landscape. Thus in Fig.8.6c) the motor periodically changes the attachment site: the cycle is performed between the state A' and the state B, corresponding to different attachment sites along the potential $\Phi(x)$. In this regime the motor is able to generate the highest level of average tension. The two states can be interpreted as follows: first motor detachment and advance accompanied by the recharging of the power stroke device and then the power stroke combined with re-attachment to the original site. One can see that the two pairs of the biochemical steps are un-separable in this mechanical setting.

The slanted two-state shape of the cycle is preserved also at higher values of D, see Fig.8.6d). The fine structure of the cycle, however, looks a bit different because higher level of noise authorizes supplementary transitions inside the landscape, see light gray trajectory. After reach the optimal combination of the temperature D and the amplitude value A the motor starts to generate less and less tension, see Fig.8.7. Eventually the ratchet effect vanishes because the device progressively looses its ability to rectify thermal fluctuations. Note also that at high temperature the motor changes the direction in which the motor cycle is performed. Thus in Fig.8.7a) and b) the cycle is performed in the clockwise direction (red line above blue line).

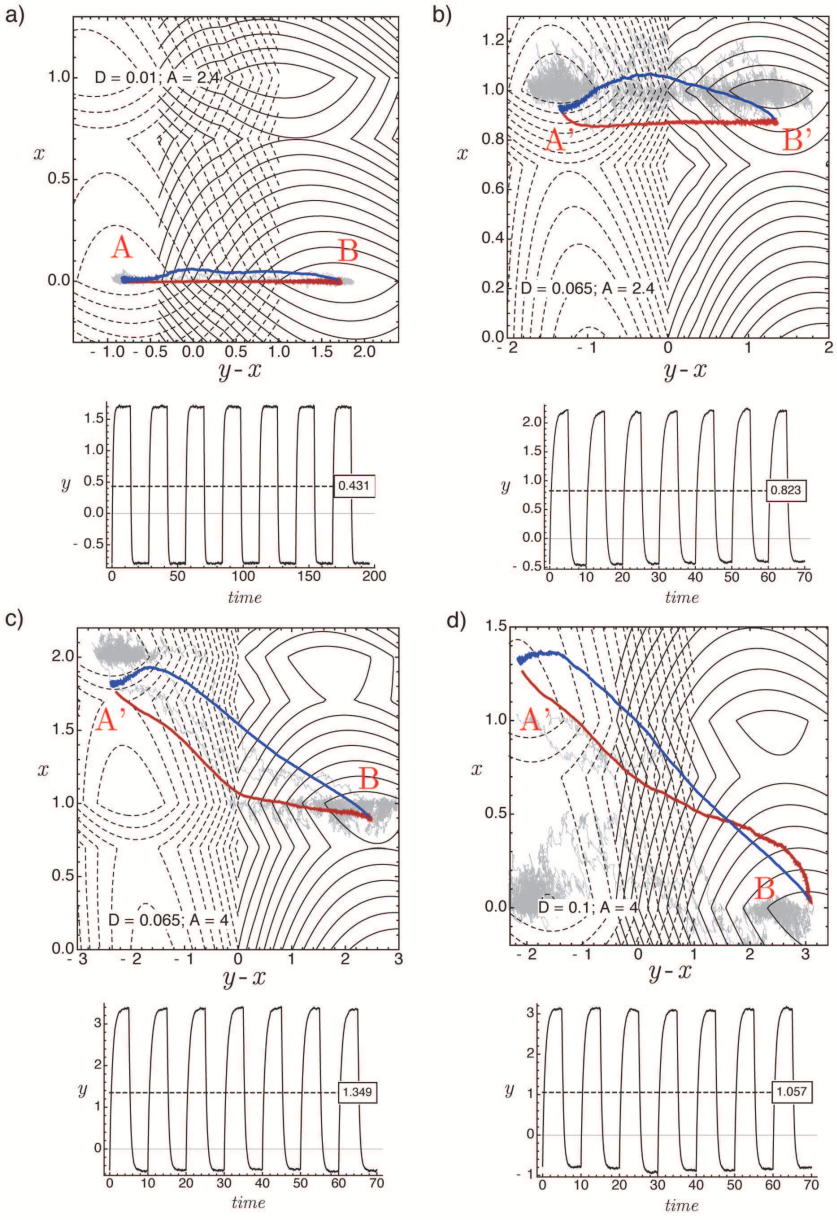

Figure 8.6. The XY-tilted ratchet model in hard device configuration with $z = 0$. The variation of the motor cycle shape with the increasing temperature D and amplitude A. With solid lines we plot the surface contours of energy landscape in positive phase of $f_{tilt}(t)$ and by red thick line we report the associated average trajectory path. With dashed lines we show the surface contours of energy landscape in the negative phase $f_{tilt}(t)$ and by blue thick line we report the associated average trajectory path. The light gray lines follow the single stochastic realization during one time period. The cycle drives in the trigonometric sense. a) The motor cycle at $D = 0.01$, $A = 2.4$ and the generated average tension. b) The cycle at $D = 0.065$, $A = 2.4$ and the generated average tension. c) The cycle at $D = 0.08$, $A = 4$ and the generated average tension. d)The cycle at $D = 0.1$, $A = 4$ and the generated average tension. The relevant parameters $k_0 = 1.5$, $k_1 = 0.43$, $l = 0.35$, $a = 1$, $\lambda_1 = 0.7$, $L = 1$, $V_{max} = 1.5$, $\alpha = 1$ with the time period $T = 10$ of the $f_{tilt}(t)$, performed by Euler scheme with $\Delta t = 10^{-3}$ and over $N_r = 10^3$ realizations.

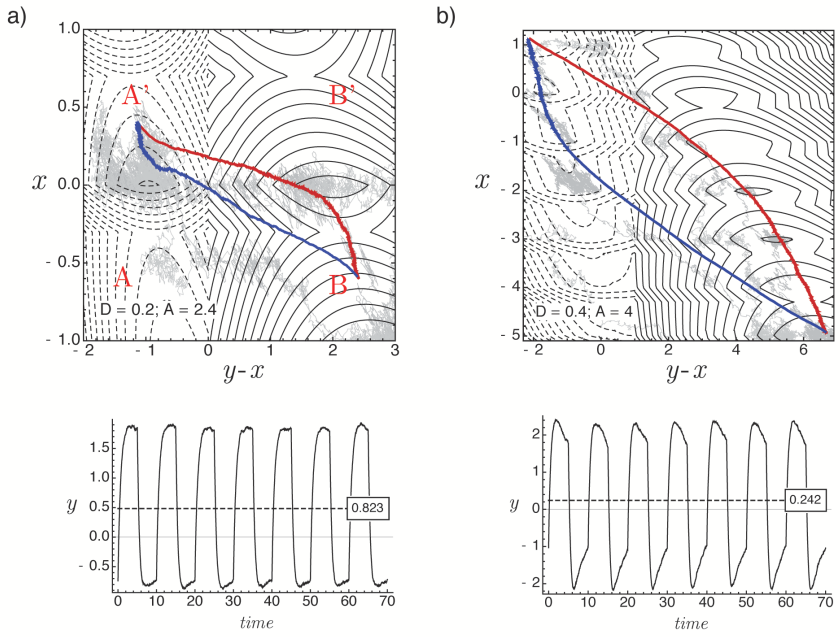

Figure 8.7. The XY-tilted ratchet model in hard device configuration with $z = 0$. The variation of the motor cycle shape with the increasing temperature D and amplitude A. With solid lines we plot the surface contours of energy landscape in positive phase of $f_{tilt}(t)$ and by red thick line we report the associated average trajectory path. With dashed lines we show the surface contours of energy landscape in the negative phase $f_{tilt}(t)$ and by blue thick line we report the associated average trajectory path. The light gray lines follow the single stochastic realization during one time period. The motor cycles are driven in clockwise sense. a) The motor cycle at $D = 0.2,\ A = 2.4$ and the generated average tension. b) The cycle at $D = 0.4;\ A = 4$ and the generated average tension. The relevant parameters $k_0 = 1.5,\ k_1 = 0.43,\ l = 0.35,\ a = 1,\ \lambda_1 = 0.7,\ L = 1,\ V_{max} = 1.5$, performed by Euler scheme with $\Delta t = 10^{-3}$ and over $N_r = 10^3$ realizations.

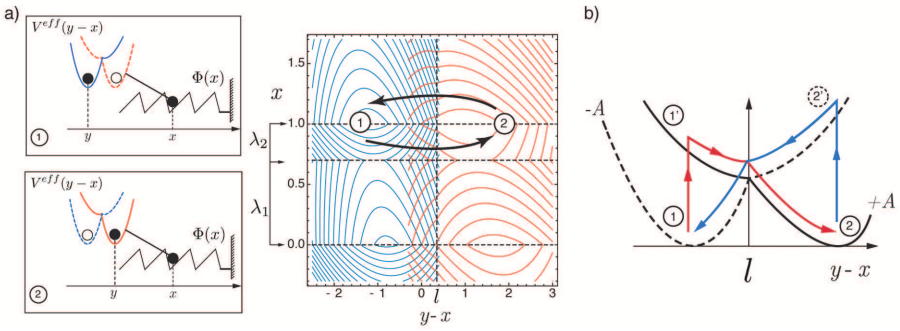

Figure 8.8. The XY-tilted ratchet model in hard device. The scheme of the motor cycle corresponded to the trajectory Fig.8.6a). With solid gray lines we plot the energy level contours in positive phases of rocking $(\Phi(x) + V(y-x) + 1/2k_m y^2 - (y-x)A)$ and with dashed gray lines we plot the energy level contours in negative phase of rocking $(\Phi(x)+V(y-x)+1/2k_m y^2 + (y+x)A)$. a) The two-state motor cycle. b) The schematic explanations of the observed two-states cycle, the average trajectory is shown schematically by red arrows in positive phase of rocking and by blue arrows in negative phase of rocking.

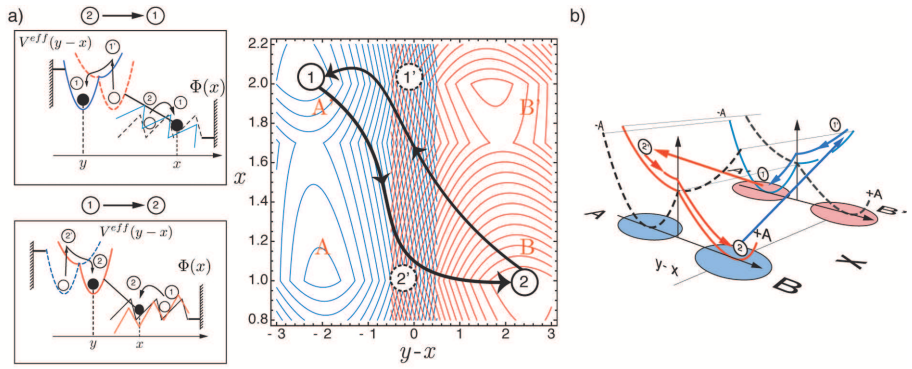

Figure 8.9. The XY-tilted ratchet model in a hard device. The scheme of the motor cycle corresponded to the trajectory on Fig.8.6d). With solid gray lines we plot the energy level contours in positive phases of rocking ($\Phi(x)+V(y-x)+1/2k_m y^2-(y-x)A$) and with dashed gray lines we plot the energy level contours in negative phase of rocking ($\Phi(x)+V(y-x)+1/2k_m y^2+(y+x)A$). a) The four-state motor cycle. b) The schematic explanations of the observed four-states cycle, the average trajectory is shown schematically by red arrows in positive phase of rocking and by blue arrows in negative phase of rocking.

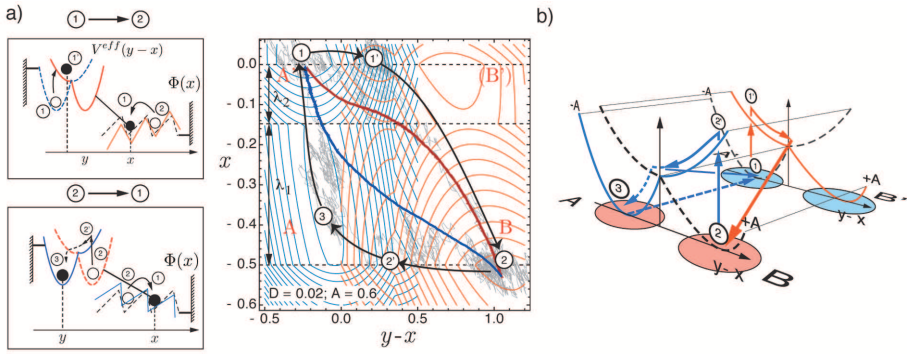

Figure 8.10. The scheme XY-tilted ratchet model in hard device configuration. The detailed scheme of four-states clockwise motor cycle. With solid gray lines we plot the energy level contours in positive phases of rocking ($\Phi(x)+V(y-x)+1/2k_m y^2-(y-x)A$) and with dashed gray lines we plot the energy level contours in negative phase of rocking ($\Phi(x)+V(y-x)+1/2k_m y^2+(y+x)A$). a) The four-state motor cycle , the average trajectory is shown by red line in positive phase of rocking and by blue line in negative phase of rocking. By examining a single stochastic realization, we observe that it is natural to introduce an intermediate state (3) b) The schematic explanations of the observed four-states cycle.

The schematic representation of the simplest two-state hard device cycle is shown in Fig.8.8.

- ①→①'→②. We start again at the end of the negative phase of f_{tilt}. The configurational particle explores the state A (well "0"). Then f_{tilt} changes sign and the energy becomes tilted $\Phi(x)+V(y-x)+\frac{1}{2}k_m(y)^2-(y-x)A$. The particle makes the immediate transition ①→①'. During the positive phase of f_{tilt} the particle performs a transition ①'→②, which we associate with the power stroke.

- ②→②'→①. We are now in the state B (well "1"). The correlated force changes the sign and the energy landscape tilts in the opposite direction $\Phi(x)+V(y-x)+$

$\frac{1}{2}k_m(y)^2 + (y-x)A$. The motor makes instantaneous transition ②→②'. Because of the spatial asymmetry of the periodic potential, the system remains trapped in the 'distant minimum' of $\Phi(x)$ while performing the transition ②'→①, which we interpret as recharging of the power stroke mechanism. Now the cycle can start again.

In Fig.8.9 we present schematic representation of the 'slanted' cycle corresponding to what we have seen in Fig.8.6d). We recall that this cycle ensures the maximum average tension. Formally, the motor visits two sites corresponding to the stable states A' (well "0") and B', see Fig.8.9a). However, because of the peculiar shape of the cycle we can distinguish two additional intermediate states denoted ①' and ②'. The nature of the additional states is clear from our schematic explanations in Fig.8.9b). We notice what in our schematic figures we can show only the average trajectory while the the trajectories corresponding to single stochastic realizations may demonstrate much more complex shapes.

With the additional states taken into consideration we can interpret our periodic trajectory as the following four-states cycle:

- ①→②'→②. We start again at the very end of the negative phase of f_{tilt}. The configurational particle explores the state A' (well "0"). Then f_{tilt} changes the sign from negative to positive and the particle makes a transition ①→②' 'moving back' along the x coordinate. During the positive phase of f_{tilt} the particle performs additional transition ②'→② and finds itself in the state B (well "1"). We interpret the transition ②'→② as the power stroke.

- ②→①'→①. We now are in the state ②, point B. The correlated force changes its sign again to negative. The particle detaches and makes a 'forward jump' to the next site along the actin filament performing transition ②→①'. Subsequently the particle continues with the transition ①'→① which we interpret as recharging of the power stroke mechanism. Now, the cycle can start again.

In Fig.8.10 we illustrate the motor cycle performed in the clockwise direction, see Fig.8.7a). In this figure, in order to make intermediate states more visible we utilized a slightly modified potential with parameters:$k_0 = 1.5$, $k_1 = 0.43$, $l = 0.35$, $a = 1$, $\lambda_1 = 0.35$, $L = 0.5$, $V_{max} = 1$. With red lines we show the energy contours during the positive phase of $f_{tilt}(t)$ and with blue color –the energy contours corresponding to the negative phase of f_{tilt}. By examining a single stochastic realization, we observe that it is natural to introduce an intermediate state ③, marked by letter A, despite the fact that the average cycle remains similar as in Fig.8.9.

Here a general comment is in order. So far, throughout three chapters devoted to X,Y and XY-tilted ratchets we have always used the same potentials $\Phi(x)$ and $V(y-x)$. Both potential were asymmetric, and we controlled the asymmetry of $Phi(x)$ through the parameter $\Delta = \lambda_1 - \lambda_2$, and the asymmetry of $V(y-x)$ through the ratio of the stiffnesses k_0/k_1 and through the position of the barrier between the wells l. In fact, to ensure the directional motion of the motor in Y-tilted and XY-tilted designs there is no necessity to keep both potential asymmetric. Thus, we could have also used a symmetric bistable potential $V(y-x)$ together with an asymmetric spatially periodic potential $\Phi(x)$, or we could have chosen to use the asymmetric bistable potential $V(y-x)$ together with symmetric spatially periodic potential $\Phi(x)$. It is important that the symmetry is broken but the exact place of the asymmetry is not essential for the drift itself. More generally our configurational space is two dimensional and the absence of the asymmetry in the

'periodic dimension' will be generically compensated by the asymmetry in the 'bistable dimension'. The resulting drift, however, may be more or less efficient, for instance the Peclet number measuring the relative efficiency of drift vs diffusion may be very different for different designs.

8.3 Force-velocity relation

We begin our analysis of the macroscopic performance of the XY-tilted ratchet with the study of the average velocity of an unloaded system in the soft device as a function of D (temperature associated with the white noise term) and of the time period T (time scale associated with the correlated noise term). In Fig.8.11 we present the results of numerical computations for the amplitudes $A = 1.5,\ A = 2.5,\ A = 3,\ A = 4.5$. Instead of T we use as a parameter the frequency of the correlated noise term $\omega = 1/T$.

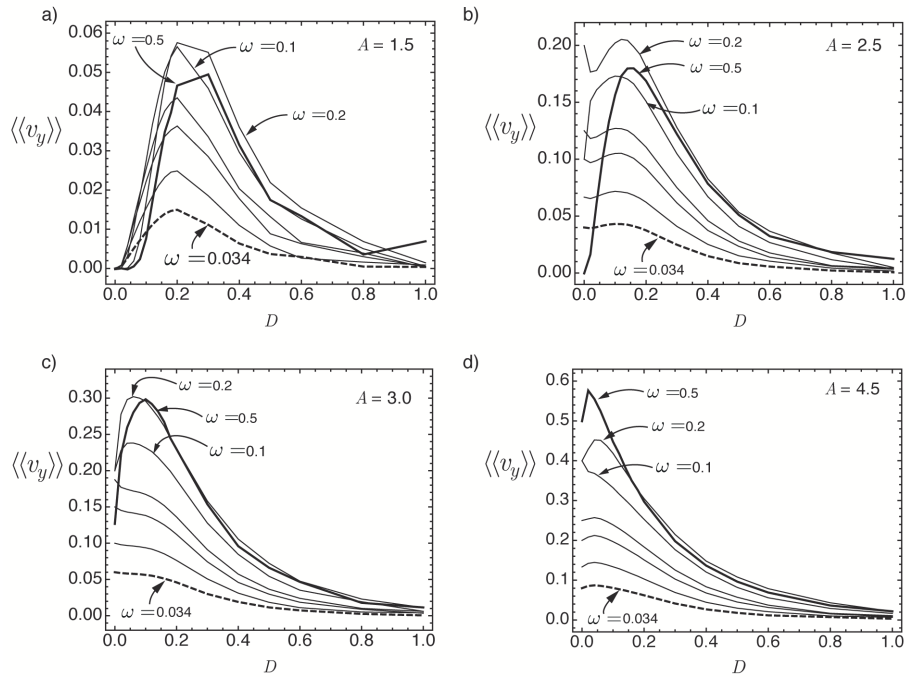

Figure 8.11. The XY-tilted model in soft device configuration with zero load. The variation of the average velocity with the increasing temperature D computed for the different frequencies $\omega = 1/T$ of rocking force $f_{tilt}(t)$. a) The results of computation at the amplitude $A = 1.5$. b) The results of computation at the amplitude $A = 2.5$. We observe a clear maximum of the average motor velocity at finite value D which indicates that we are encounting here the phenomenon of stochastic resonance. The growth of frequency leads to an increase in the value of the velocity maximum until a certain limit ($\omega = 0.2$ in the graph) after which the the maximum value starts to decrease with frequency. c) The results of computation at the amplitude $A = 3$. d) The results of computation at the amplitude $A = 4.5$. At high values of the amplitudes the ratchet becomes purely mechanical and the maximum of velocity disappears. The relevant parameters $k_0 = 1.5,\ k_1 = 0.43,\ l = 0.35,\ a = 1,\ \lambda_1 = 0.7,\ L = 1,\ V_{max} = 1.5$, performed by Euler scheme with $\Delta t = 0.5 \times 10^{-3}$ and over $N_r = 10^4$ realizations.

Quite expectedly we observe a clear maximum of the average motor velocity at finite value D which indicates that we are encounting here the phenomenon of stochastic reso-

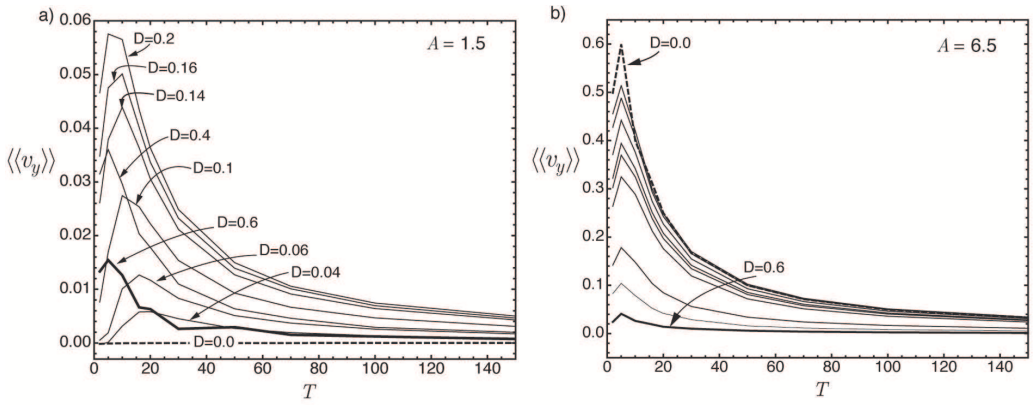

Figure 8.12. The XY-tilted model in soft device configuration with zero load. The variation of the average velocity with the increasing time period T of rocking $f_{tilt}(t)$ computed at the different temperatures D. a) The amplitude $A = 1.5$, we observe peaked distribution of velocity. The average velocity vanishes at large T as the system leaves the resonance regime. At fixed low value of T the average velocity grows with increasing D until the limit value is reached after which the drift rapidly disappears. b) The amplitude $A = 6.5$. The maximum of velocity is achieved at $D = 0$ which means that we are dealing here with a classical mechanical resonance. At fixed low T the average velocity decreases with increasing D. The relevant parameters $k_0 = 1.5,\ k_1 = 0.43,\ l = 0.35,\ a = 1,\ \lambda_1 = 0.7,\ L = 1,\ V_{max} = 1.5$, performed by Euler scheme with $\Delta t = 0.5 \times 10^{-3}$ and over $N_r = 10^4$ realizations.

nance. The growth of frequency leads to an increase in the value of the velocity maximum until a certain limit ($\omega = 0.2$ in the graph) after which the the maximum value starts to decrease with frequency, see Fig.8.11a),b). The observed phenomenon of stochastic resonance is characteristic only for sufficiently low values of the amplitude A. At high values of the amplitudes the ratchet becomes purely mechanical and the maximum of velocity disappears, see Fig.8.11c),d). In the interval of low amplitudes of rocking the system behaves as Brownian ratchet and the origin of directional motion lies in delicate interaction between white and colored components of the noise.

In Fig.8.12 we show the averaged velocity as a function of the period T for increasing values of D. For $A = 1.5$, we observe peaked distribution of velocity which first gets more localized with increasing D but eventually flattens out. The average velocity vanishes at large T as the system leaves the resonance regime. At fixed low value of T the average velocity grows with increasing D until the limit value is reached after which the drift rapidly disappears. The reason is that sufficiently strong thermal noise destroys correlations kills the directed motion. All these features suggest that at $A = 1.5$ we are dealing with a real Brownian ratchet. At higher amplitude of the correlated noise $A = 6.5$ the behavior of the average velocity is markedly different, see Fig.8.12b) where we show the average velocity as a function of T at different values of D. The maximum of velocity is achieved at $D = 0$ which means that we are dealing here with a classical mechanical resonance. At fixed low T the average velocity decreases with increasing D meaning that mechanical resonance is being corrupted by thermal fluctuations and there is no positive interference between random and correlated noises. This suggests that we are in the classical mechanical ratchet regime.

The introduction of a non zero cargo f_{ext} in the soft device configuration opens the possibility to recover the complete force-velocity relation. In Fig.8.13a) we study the effect of the variation of temperature at low amplitude of rocking $A = 2.5$ on the force-velocity

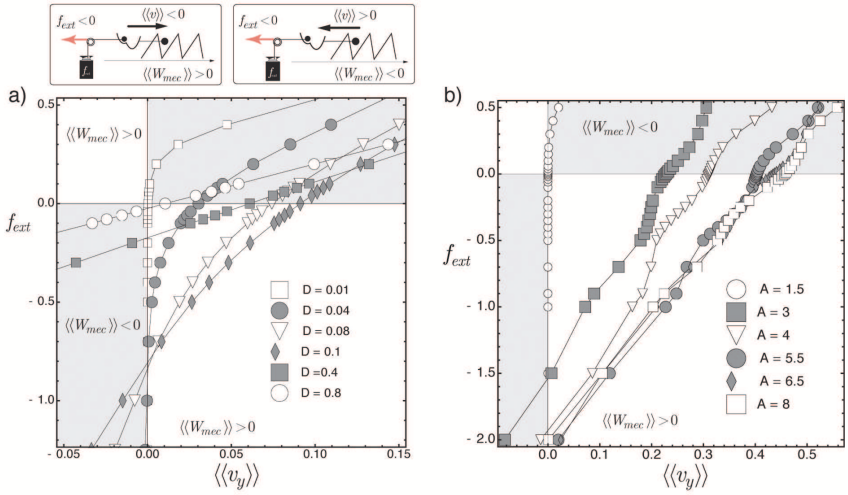

Figure 8.13. The XY-tilted ratchet in soft device configuration. a) The variation of the force-velocity relation with the increasing temperature D at the fixed amplitude $A = 2.5$ of rocking. b) The variation of the force-velocity relation with the increasing amplitude A of rocking at the fixed temperature $D = 0.02$. The model parameters are $k_0 = 1.5$, $k_1 = 0.43$, $l = 0.35$, $a = 1$, $\lambda_1 = 0.7$, $L = 1$, $V_{max} = 1.5$ $T = 20$. The direct Langevin simulations performed with Euler scheme for time step $\Delta T = 0.5 \times 10^{-3}$ and $N_r = 10 \times 10^4$ stochastic realisations.

relation. At zero temperature the system exhibits purely mechanical behavior without any 'anti-dissipation' (no entrance into the white quadrants). The increase of temperature D progressively increases the area between the force-velocity curve and the axes in the domain of anti-dissipative behavior. We observe the pronounced concave character of the force-velocity relation at sufficiently low temperatures. After the threshold in D the concavity progressively vanishes and the profile becomes linear, while the motor loses its ability to carry the cargo.

In Fig.8.13b) we illustrate the dependence of the force-velocity relation on the amplitude A at fixed $D = 0.02$. At small amplitudes of rocking the motor follows closely the external force f_{ext} and does not perform useful mechanical work. Only after a certain threshold in amplitude the motor starts to generate active transport against the load. In this regime the system acts as a purely mechanical ratchet.

8.4 Stochastic energetics

We now turn to the energetics of the XY-tilted ratchet at fixed value of the external load. He we use the same landscape parameter as in the previous section, and throughout this section adopt the value of conservative load $f_{ext} = -0.3$ and time period of rocking force $T = 16$. The direct Langevin simulations were performed by using Euler scheme with the time step $\Delta T = 1.0 \times 10^{-4}$ and the results were averaged over $N_r = 10 \times 10^4$ realizations.

According to the energetics [100], we again define the heat $\delta Q_i = \left(-\eta d_t x_i + \sqrt{2\eta_i D}\xi_i(t)\right) \circ dx_i$ and the consumption of energy $dR = f_{tilt}(t)(dy - dx)$. Then the energy balance can be written as

$$\begin{cases} (\partial_x \Phi(x) + \partial_x V(y-x)) \circ dx - dR_x = \delta Q_x \\ \partial_y V(y-x) \circ dy - f_{ext} \circ dy - dR_y = \delta Q_y \end{cases} \tag{8.7}$$

We are interested in system behavior averaged over one time period T. We write the system intrinsic energy $G_0(x_t, y_t) = \Phi(x) + V(y-x) - yf_{ext}$, since the variation of $\Phi(x) + V(y-x)$ over a period is equal to zero we can define the mechanical work

$$W_{mec} = \frac{1}{T} \int_{\mathbf{X}_{t_i}}^{\mathbf{X}_{t_i+T}} dG_0(\mathbf{X}_t) = -f_{ext}\langle v_y \rangle \tag{8.8}$$

and

$$R = \frac{1}{T} \int_{y_{t_i}}^{y_{t_i+T}} f_{tilt}(t)dy_t - \frac{1}{T} \int_{x_{t_i}}^{x_{t_i+T}} f_{tilt}(t)dx_t \tag{8.9}$$

Then the energy balance is

$$W_{mec} \equiv R + Q \tag{8.10}$$

where

$$Q = \frac{1}{T} \int_{\mathbf{X}_{t_i}}^{\mathbf{X}_{t_i+T}} \delta Q_x + \delta Q_y \tag{8.11}$$

The mechanical efficiency is then

$$\epsilon_{mec} = \frac{W_{\text{mec}}}{R} \tag{8.12}$$

The work of translation against viscous friction (Stokes term) can be written as

$$W_{\text{Stokes}} = \alpha^{-1}\langle v_x \rangle^2 + \langle v_y \rangle^2 \tag{8.13}$$

which allows us to define the stokes efficiency

$$\epsilon_{Stokes} = \frac{W_{Stokes}}{R} \tag{8.14}$$

Finally we can define the rectifying efficiency–the sum of the Stokes and the mechanical efficiency

$$\epsilon_{rec} = \frac{W_{mec} + W_{Stokes}}{R} \tag{8.15}$$

In Fig.8.14a) we plot the average velocity as a function of temperature D for increasing value of amplitude of rocking A. Observe a characteristic maximum at finite a temperature for $A = 1.5$ and $A = 2.5$. At higher values of the amplitude A, the average velocity is a decreasing function of D and in this range we are dealing with purely mechanical ratchet. By light green color we mark the region with negative average velocity, where the motor loses the ability to carry the external load and is instead being dragged by the load while contributing some active resistance.

In Fig.8.14b). we show the consumed energy R_x and in Fig.8.14c)– the consumed energy R_y. Notice that the former is an increasing function of temperature while the latter is a decreasing function of temperature. In Fig.8.14d) we show the total energy consumed by motor which appear to be temperature independent which is an interesting property of XY tilted ratchet.

In Fig.8.15a) we show the mechanical work as a function of D at different amplitudes of rocking A. we observe two regimes: with positive and with negative mechanic work. In Fig.8.15b) we present the mechanical efficiency. At small amplitudes A we observe a maximum of efficiency at finite temperature. With increasing A the maximum vanishes

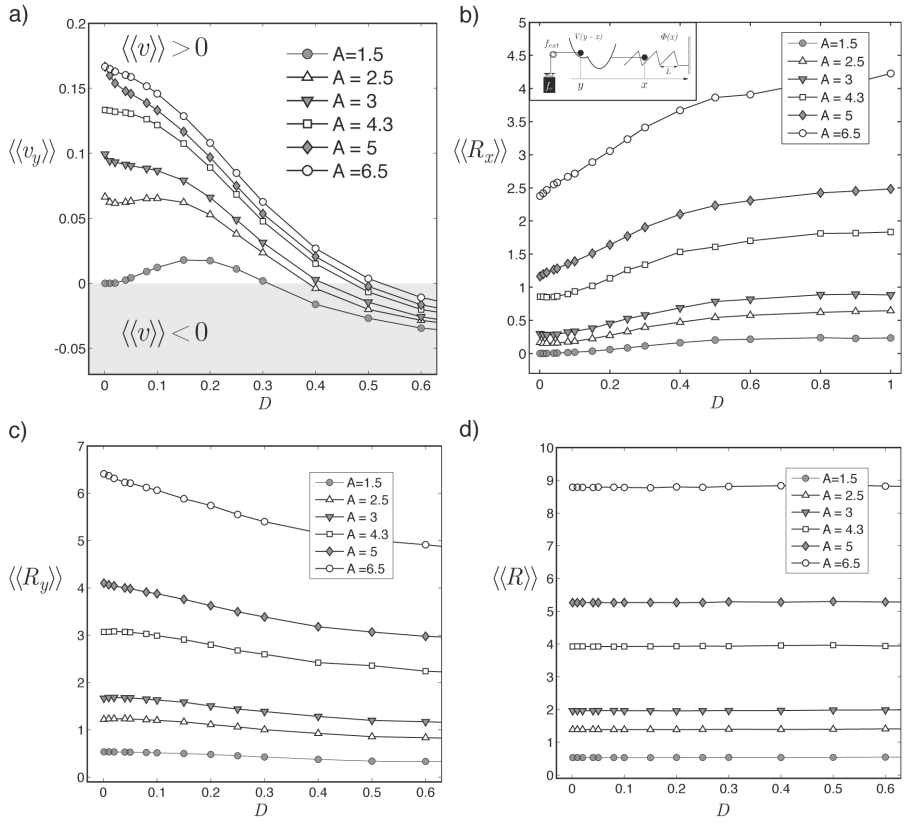

Figure 8.14. The XY-tilted model in the soft device configuration with the conservative load $f_{ext} = -0.1$. a) The variation of the average velocity $\langle v_y \rangle$ with the increasing temperature D for different amplitudes A of $f_{tilt}(t)$. For small amplitude A (Brownian ratchet) the motor exhibits a maximum of velocity at finite temperature. At higher amplitude A (mechanical ratchet) the average velocity decreases monotonically with D. b) The variation of the consumed energy R_x with increasing temperature D for different amplitudes A of $f_{tilt}(t)$, note that the motor consumes more and more energy in order rectify the fluctuations and preform a useful work. c) The variation of the consumed energy R_y with increasing temperature D for different amplitudes A of $f_{tilt}(t)$, see (8.9), note what the level of consumed energy decreases with D. d) The variation of the consumed energy R with increasing temperature D for different amplitudes A of $f_{tilt}(t)$. The function appear to be temperature independent which is an interesting property of XY tilted ratchet.The relevant parameters $k_0 = 1.5,\ k_1 = 0.43,\ l = 0.22,\ a = 1,\ L = 1,\ \lambda_1 = 0.7,\ V_{max} = 1.5,\ \alpha = 1$ with time period $T = 30$ of rocking force.

and the efficiency becomes a monotonically decreasing function of D, as one can expect in a purely mechanic ratchet. By light green color we indicated the regimes with negative efficiency, where dissipation prevails. If we make the comparison between the efficiencies of X-tilted, Y-tilted and XY-tilted ratchets we find that the XY device is least efficient.

In Fig.8.15c) we present the Stokes efficiency as a function of D. We observe maxima at finite temperatures for low amplitude regimes and see that at high temperatures the Stokes efficiency may increase with temperature. The rectifying efficiency is shown in Fig.8.15d). Once again, at small amplitude of rocking we see thermal ratchet behavior with a maximum of efficiency at finite temperature while at high rocking amplitudes we see the mechanical ratchet behavior with efficiency decreasing with temperature.

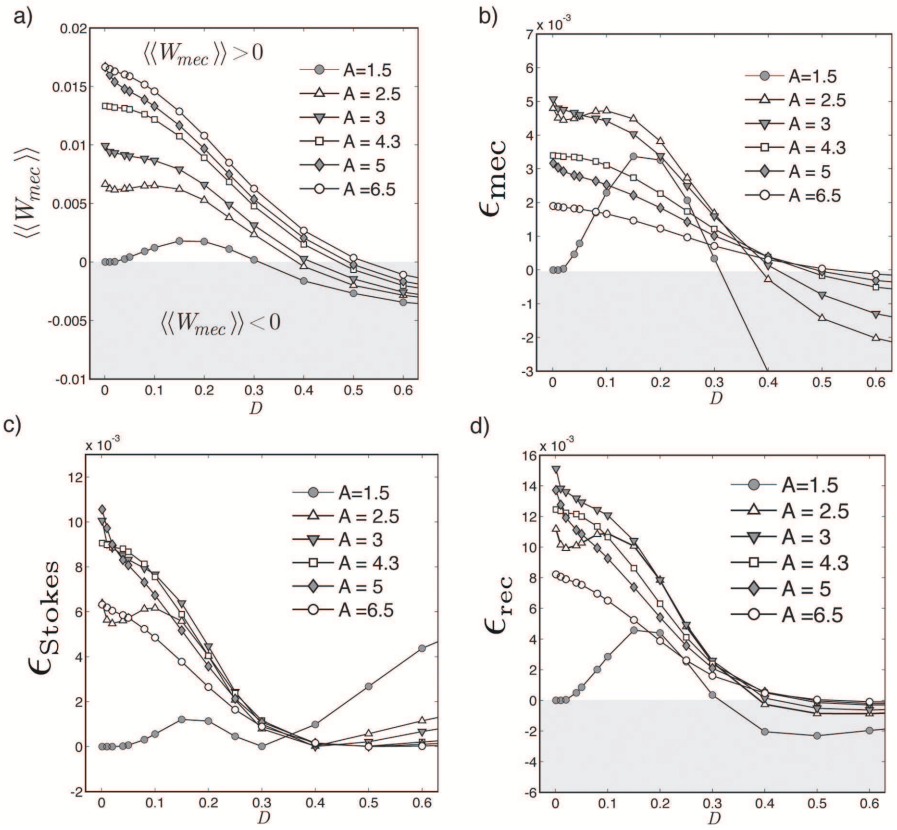

Figure 8.15. The XY-tilted model in the soft device configuration with the conservative load $f_{ext} = -0.1$. a) The variation of the mechanic work W_{mec} with the increasing temperature D for different amplitudes A of $f_{tilt}(t)$. b) The variation of the mechanic efficiency ϵ_{mec} with the increasing temperature D for different amplitudes A of $f_{tilt}(t)$. In the regime of small amplitudes A we again observe a maximum of mechanical efficiency at finite temperature. c) The variation of the Stokes efficiency ε_{Stokes} with the increasing temperature D for different amplitudes A. By definition, this is always positive function. For hight values of D the Stokes efficiency is increasing function of D, because we are in regime there the motor follows the direction imposed by cargo. d) The variation of the rectifying efficiency ε_{rec} with the increasing temperature D. The shape of this function is dominated by the quadratic Stokes term. The relevant parameters $k_0 = 1.5,\ k_1 = 0.43,\ l = 0.22,\ a = 1,\ L = 1,\ \lambda_1 = 0.7,\ V_{max} = 1.5,\ \alpha = 1$ with time period $T = 30$ of rocking force.

8.5 Conclusions

The association of the ATP activity with the power stroke element is motivated by the dominating physiological perception that it is the power stroke which drives the muscle contraction. In the XY-tilted model we attempted to quantitatively examine the most radical mechanical implementation of this idea. We have shown that the corresponding functional element driven by rocking bi-stable device can rectify thermal noise and ensure directional advance of a molecular motor. More specifically, by remaining in purely mechanical framework we were able to obtain a stable cycle in both soft and hard devices which converts colored noise into directional motion and structurally resembles the biochemical Lymn-Taylor cycle. In the proposed XY device the primary agent is the power stroke while the attachment detachment is a secondary structure which is necessary in view of translational character of the motion. We have shown that average velocity is

maximized at finite temperatures correlated to particular frequencies associated with external supply of energy. This suggest that the physical mechanism behind the activity of the XY-tilted ratchet is associated with the phenomenon of stochastic resonance. The proposed XY tilted ratchet can perform a positive mechanical work, however it is less efficient than X-tilted and Y-tilted ratchets. To understand why such seemingly inefficient device may be selected by evolution as the main driving force of muscle contraction, it is important to remember that alternative more efficient strategies include mechanical activity of actin filaments which may be imposable to ensure locally in a real muscle (nonprocessive) setting.

While we can conclude that the XY tilted ratchet is a viable candidate as a mechanical analog of the Lymn-Taylor cycle, we still have ambiguity of the interpretation of the detached state which is not explicitly present in the proposed model. To deal with this conceptual deficiency we consider in the next chapter a more complex model where the XY tilted ratchet mechanism is augmented by taking into consideration the explicit steric separation of thick and thin filaments.

Chapter 9

Synthetic model

We have developed in the previous chapters a mechanical framework allowing one to describe muscle contraction as a power stroke driven mechanism. The advantage of the proposed formalism is its transparency and analytical simplicity. However, the price of such simplicity (reduction of the system to a set of interacting points moving along one line) is a neglect of geometrical complexity, in particular, the omission of steric effects. In this sense, the weakest point of the proposed model is the over schematic description of the detached configuration which was described as a discrete set of points on the actin filament corresponding to the maxima of the periodic potential. In reality, the detached state is most probably continuous or at least spread over due to the geometrical separation of the myosin head and the actin filament. In this chapter we formulate a synthetic model which is set in the XY-titled framework but allows the actin potential to be stronger (closer) or weaker (far) depending on the conformational state of the myosin head. By introducing this additional coupling we assume that our bistable myosin head controls the degree of detachment through steric separation from the actin filament. In some sense the mechanism proposed in this chapter can be viewed as blend of flashing and rocking thermal ratchets.

9.1 Detached state as a shallow minim of the energy

We recall that myosin II is a non-processive system which means that for each cross-bridge the time spent in the detached state is much longer than the time of the attachment. Such motors can operate only in groups and cooperation of different force producing units is essential. In particular, we may conclude that while some of the cross bridges are attached and produce forces, other cross bridges are detached and are simply carried along. This suggests that the detached state cannot consist of discrete set of isolated points.

The simplest way of creating extended detached states in our two parametric framework is to replace the maxima of the periodic potential by broad plateaus. For instance, we can modify the saw-tooth potential $\Phi(x)$ by replacing the maxima of $\Phi(x)$ by the horizontal segments. We can also insert shallow parabolas at the maxima of $\Phi(x)$, associating their minima with the detached states. In this model we introduce the subdivision of the minima of the periodic potential into attached and detached states. We may now associate the detached time with the time spent in the detached energy well. Our computations show that unless the new well is sufficiently deep, this time is small because the particle passes quickly from one minimum to another. Therefore we were not able to obtain the desired motor cycle in this setting.

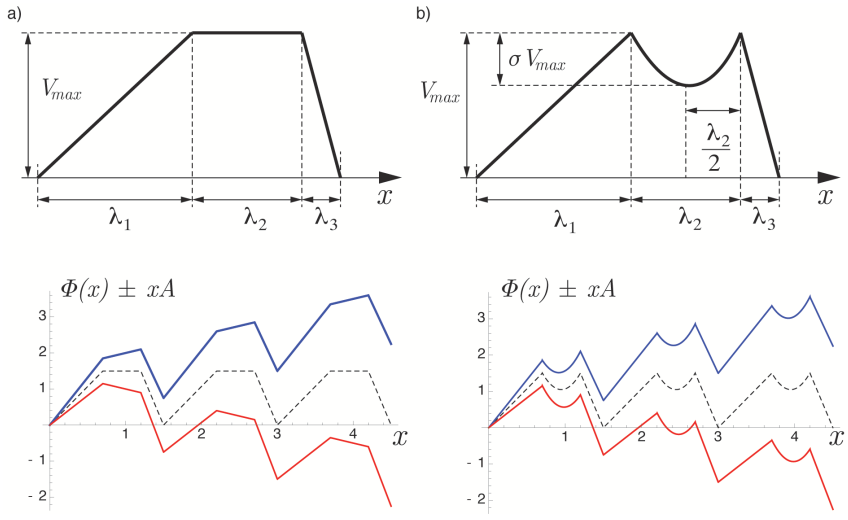

Figure 9.1. The simplest form of modified space periodic ratchet potential with introduced detached state.

9.2 Control mechanisms

Recall that after the execution of the power stroke, the cross bridge detaches which simplifies recharging of the power stroke mechanism. To capture this effect we can introduce the control function $\Psi(y-x)$ which depends on the state of the power stroke mechanism but acts on the spatially periodic potential. The action results in switching it on and off depending on the state of the bi-stable unit. When the periodic potential is on, the actin potential is present which facilitates the attachment. When it is off, the actin filament is far away and the attachment is impossible. This means that the myosin head is detached. In geometrical terms turning the potential off means that the head moves away from actin filament and turning it on means that the head again approaches the actin filament. This can be interpreted as a steric effect when the power stroke results in displacement of the myosin head away from the actin filament. Instead, the recharging makes the myosin head again close to the actin filament.

To implement this idea we write the general energy potential $G(x,y,z,t)$ in the form:

$$G(x,y,t) = \Psi(y-x)\Phi(x) + V(y-x) - xf^x_{tilt}(t) - yf^y_{tilt}(t) - yf_{ext} \tag{9.1}$$

where the term $\Psi(y-x)\Phi(x)$ describes the coupling between the configuration of the power stroke and the state of the attachment. The simplest function $\Psi(y-x)$ would be

$$\Psi(y-x) \sim \frac{1}{2}\left(1 + \tanh\frac{y-x-l}{e}\right) \tag{9.2}$$

where e is a small parameter, which define the maximum slope of the control function. One can see that the spatially periodic potential is 'on' when the configurational particle is in well B of the bistable potential (post-power stroke). As we show in Fig.9.2c) one can replace the smooth function (9.2) by its piece-wise linear approximation.

In the soft device the XY-model with the coupling introduce above is described by the

following system of over-damped Langevin equations:

$$\begin{cases} \eta_x \dfrac{dx}{dt} = -\partial_x \left[\Psi(y-x)\Phi(x)\right] - \partial_x V(y-x) - f_{tilt}(t) + \sqrt{2\eta_x D}\ \xi_x(t) \\ \eta_y \dfrac{dy}{dt} = -\partial_y V(y-x) - \Phi(x)\partial_y \Psi(y-x) + f_{ext} + f_{tilt}(t) + \sqrt{2\eta_y D}\ \xi_y(t) \end{cases} \tag{9.3}$$

In the hard device we can similarly write:

$$\begin{cases} \eta_x \dfrac{dx}{dt} = -\partial_x \left[\Psi(y-x)\Phi(x)\right] - \partial_x V(x,y) - f_{tilt}(t) + \sqrt{2\eta_x D}\ \xi_x(t) \\ \eta_y \dfrac{dy}{dt} = -\partial_y V(y-x) - \Phi(x)\partial_y \Psi(y-x) - k_m(y-z) + f_{tilt}(t) + \sqrt{2\eta_y D}\ \xi_y(t)) \end{cases} \tag{9.4}$$

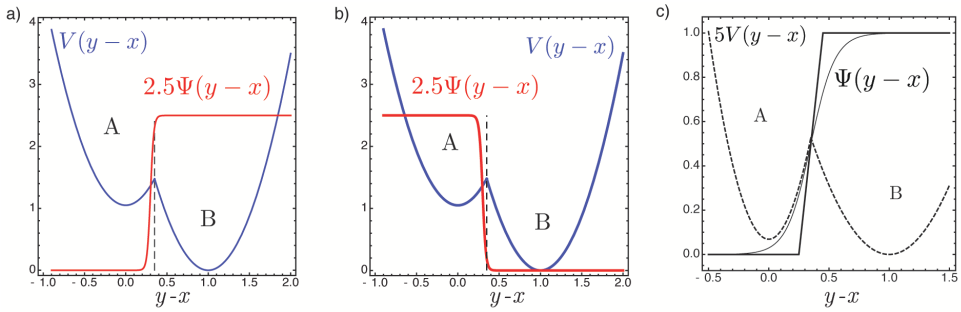

Figure 9.2. The graphic representation of control function $\Psi(y-x)$. a) The control function defined in way to activate the space periodic potential when the Brownian particle explores the well B of bistable potential $V(y-x)$. b) The control function define in way activate the space periodic potential when the Brownian particle explores the well A of bistable potential $V(y-x)$. c) The piece-wise linear simplification of control function.

It will be convenient to introduce the nondimensional variables, we use the following scaling of the parameters (6.3) and the time scale (6.4). Applying the normalization we are left with the following dimensionless parameters $\tilde{D} \equiv \frac{D}{k_m a^2}$ and $\alpha = \frac{\eta_y}{\eta_x}$. The dimensionless system of Langevin equations in the soft device reads:

$$\begin{cases} \dfrac{dx}{dt} = -\alpha\left(\partial_x \left[\Psi(y-x)\Phi(x)\right] + \partial_x V(y-x) + f_{tilt}(t)\right) + \sqrt{2\alpha D}\ \xi_x(t) \\ \dfrac{dy}{dt} = -\partial_y V(y-x) - \Phi(x)\partial_y \Psi(y-x) + f_{\text{ext}} + f_{tilt}(t) + \sqrt{2D}\ \xi_y(t) \end{cases} \tag{9.5}$$

In the hard device we obtain similarly:

$$\begin{cases} \dfrac{dx}{dt} = -\alpha\left(\partial_x \left[\Psi(y-x)\Phi(x)\right] + \partial_x V(y-x) + f_{tilt}(t)\right) + \sqrt{2\alpha D}\ \xi_x(t) \\ \dfrac{dy}{dt} = -\partial_y V(y-x) - \Phi(x)\partial_y \Psi(y-x) - k_m(y-z) + f_{tilt}(t) + \sqrt{2D}\ \xi_y(t) \end{cases} \tag{9.6}$$

The corresponding Fokker-Planck equations have the similar structure as the expressions (6.7) and (6.9) with in the soft device setting

$$G^s(x,y,t) = \Psi(y-x)\Phi(x) + V(y-x) - (y-x)(f_{tilt}(t) + f_{ext}) \tag{9.7}$$

where f_{ext} is external load; in the hard device setting:

$$G^h(x,y,t) = \Psi(y-x)\Phi(x) + V(y-x) - (y-x)f_{tilt}(t) + \frac{1}{2}k_m(y-z)^2 \tag{9.8}$$

where z is the external control parameter.

We use again the piece-wise linear approximation for $\Phi(x)$ (6.11), the square-wave function for periodic tilting force $f_{tilt}(t)$ (6.12) and we define the bistable element $V(y-x)$ as usually by the formulas (6.13). Finally the control function $\Psi(y-x)$ will be defined either by (9.2) or by the corresponding piecewise linear approximation:

$$\Psi(y-x) = \begin{cases} 0 & \text{for } (y-x) < l - \frac{e}{2} \\ \frac{1}{e}(y-x) + \frac{e-2l}{2e} & \text{for } l - \frac{e}{2} \leqslant (y-x) \leqslant l + \frac{e}{2} \\ 1 & \text{for } (y-x) > l + \frac{e}{2} \end{cases} \tag{9.9}$$

To illustrate the positive and negative phases of the tilting in the hard and soft device settings we compute the corresponding stationary probability distributions. We define $P_{st}(x, y-x, A)$ in the soft device by :

$$P_{st}(x,y,A) = \begin{cases} Z_+^{-1} \exp\left(-\dfrac{G^s(x,y,A)}{D}\right), & \text{for} \quad f_{tilt}(t) > 0 \\ Z_-^{-1} \exp\left(-\dfrac{G^s(x,y,A)}{D}\right), & \text{for} \quad f_{tilt}(t) < 0 \end{cases} \tag{9.10}$$

where Z_+ and Z_- are the normalization factors. To simplify the picture we can take $f_{ext} = 0$ and then

$$G^s(x,y,A) = \begin{cases} \Psi(y-x)\Phi(x) + V(y-x) - (y-x)A, & \text{for} \quad f_{tilt}(t) > 0 \\ \Psi(y-x)\Phi(x) + V(y-x) + (y-x)A, & \text{for} \quad f_{tilt}(t) < 0 \end{cases} \tag{9.11}$$

Similarly we define $P_{st}(x, y, A \parallel z)$ in the hard device, by assuming that $z = 0$:

$$P_{st}(x,y,A \parallel z) = \begin{cases} Z_+^{-1} \exp\left(-\dfrac{G^h(x,y,z,A)}{D}\right) & \text{for} \quad f_{tilt}(t) > 0 \\ Z_-^{-1} \exp\left(-\dfrac{G^h(x,y,z,A)}{D}\right) & \text{for} \quad f_{tilt}(t) < 0 \end{cases} \tag{9.12}$$

Here again Z_+ and Z_- are the normalization factors and

$$G^h(x,y,z,A) = \begin{cases} \Psi(y-x)\Phi(x) + V(y-x) - (y-x)A + \dfrac{1}{2}k_m(y-z)^2 & \text{for } f_{tilt}(t) > 0 \\ \Psi(y-x)\Phi(x) + V(y-x) + (y-x)A + \dfrac{1}{2}k_m(y-z)^2 & \text{for } f_{tilt}(t) < 0 \end{cases} \tag{9.13}$$

In Fig.9.3 we show the location of the maxima of the ensuing equilibrium probability distribution in soft and hard devices.

9.3 Motor cycle in the soft device

To find the direction of the drift of our motor in the soft device configuration we need to solve numerically the following system of equations:

$$\begin{cases} \dfrac{dx}{dt} = -\alpha\left(\partial_x\left[\Psi(y-x)\Phi(x)\right] + \partial_x V(y-x) + f_{tilt}(t)\right) + \sqrt{2\alpha D}\ \xi_x(t) \\ \dfrac{dy}{dt} = -\partial_y V(y-x) - \Phi(x)\partial_y\Psi(y-x) + f_{tilt}(t) + f_{\text{ext}} + \sqrt{2D}\ \xi_y(t) \end{cases} \tag{9.14}$$

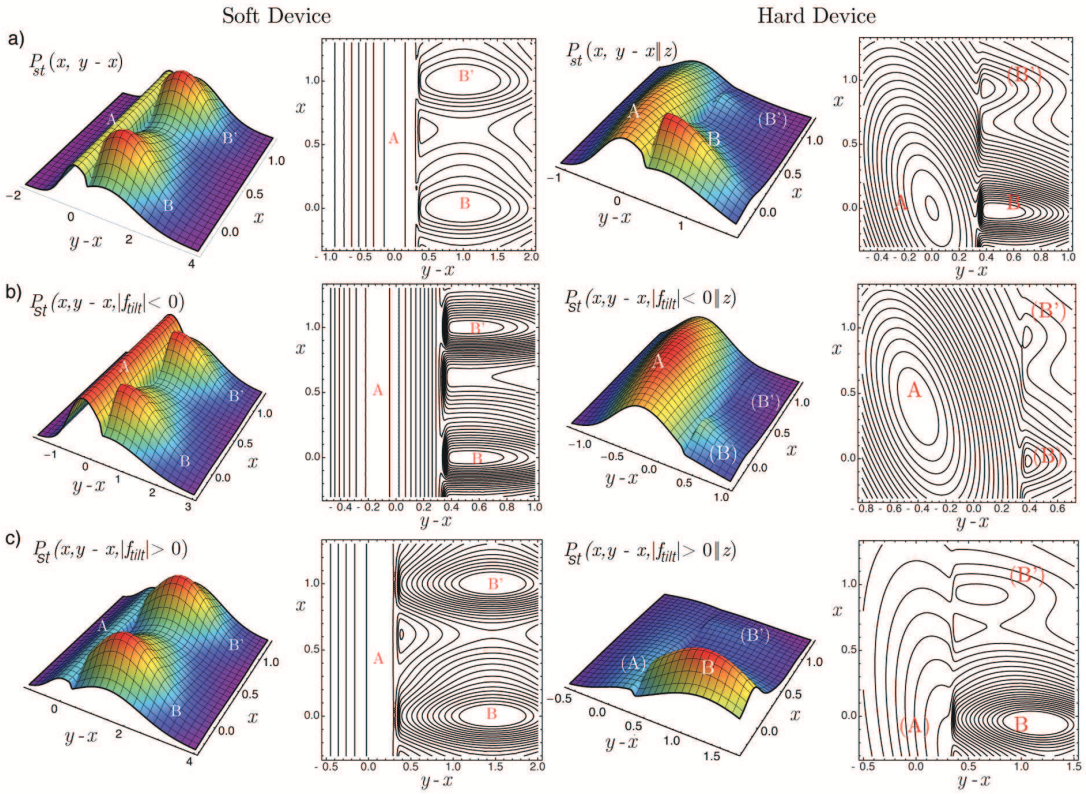

Figure 9.3. The XY-tilted model with control parameter in soft and hard device configurations. The plot of the stationary probability distribution function and of corresponding contour surface plot. For best graphic representation we replaced the saw-tooth potential $\Phi(x)$ by equivalent sum of two sinus. a) The plot of functions $P_{st}(x, y)$ and $P_{st}(x, y, |f_{tilt}| = 0 \parallel z)$ with the corresponded surface contour plots in untitled configuration. b) The surface plot of function $P_{st}(x, y, |f_{tilt}| < 0)$ and $P_{st}(x, y, |f_{tilt}| < 0 \parallel z)$ with the corresponded surface contour plots in negative phase of tilting force. c) The plot of functions $P_{st}(x, y, |f_{tilt}| > 0)$ and $P_{st}(x, y, |f_{tilt}| > 0 \parallel z)$ with the corresponded contour plots in positive phase of tilting.

First, we illustrate the delicate interplay of the asymmetry of both the periodic potential and the bistable potential in the ultimate selection of the direction of motion. In Fig.9.4 we show how the average velocity depends on $\Delta = \lambda_1 - \lambda_2$ at different values of D.

In particular we observe non zero average flux at $\Delta = 0$, which means that motor can move even on a symmetric periodic potential. Moreover we see that due to the asymmetry of the bistable potential the motion is always biased towards positive values of x . To emphasize the active role of the bistable potential in the following we shall only use the symmetric spatially periodic potential $\Phi(x)$.

We fix the following values of parameters: $\alpha = 1$, $k_0 = 1.5$, $k_1 = 0.43$, $a = 1$, $l = 0.35$, $L = 1$, $V_{max} = 1.5$. The control function will be $\Psi(x, y)$ taken in the form (9.2) with $e = 0.01$. The correlated component of the noise will be characterized by the amplitude $A = 2.5$ and the period $T = 20$. The white noise characterised by the temperature $D = 0.02$.

In Fig.9.5 we show the averaged position of the system in the soft device configuration with zero load. The averaged internal configuration $y - x$ shown in Fig.9.5b) illustrates characteristic oscillations between the two configurational states. In Fig.9.5c) we show the shape of the averaged trajectory in coordinates $[y - x, x]$. Finally in Fig.9.5d) we

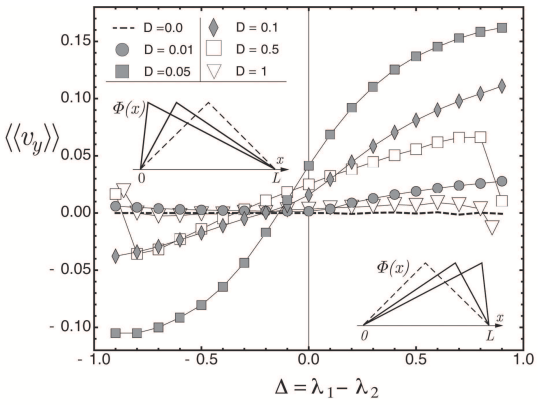

Figure 9.4. The XY-tilted model with control function. The variation of the average velocity with $\Delta = \lambda_1 - \lambda_2$ at different D. Note the presence of non zero average flux at $\Delta = 0$. The relevant parameters $k_0 = 1.5,\ k_1 = 0.5,\ a = 1,\ l_0 = 0.2,\ L = 1,\ V_{max} = 1.5,\ \alpha = 1,$ the control function $\Psi(y - x)$ defined by (9.2) with $e = 0.01$.We apply the correlated noise with the amplitude $A = 2.5$ and the time period $T = 3$. The numeric computation done by simple Euler scheme with time step $\Delta t = 10^{-4}$ and for $N_r = 10^4$ number of realizations.

superimpose the motor cycle on the energy landscape in corresponding phases of the tilting. By red scatters we show the averaged path in the positive phase of f_{tilt}, and with the blue scatters - in the negative phase of f_{tilt}. The contour plot for the energy landscape has a cut at point l.

We can identify the state A which corresponds to the valley in the energy landscape describing the detached configuration. We can also identify the wells B, B' corresponding to different states of the power stroke element in the attached configuration. We conclude that our XY-tilted motor performs a two-three state functional cycle passing through sites $A \to B \to B' \to A$, which is similar to what we have seen in the XY-tilted model without control.

In Fig.9.6 we show the averaged trajectory in the case of non-zero load, $f_{ext} = -0.02$. We see that the general structure of the cycle is preserved, however the motor is surely less efficient because of the periodic sliding in the direction of the load which is opposite to the direction of motion. Notice the presence of the characteristic shift induced by the load in the detached state, see the region selected by the dashed yellow line in Fig.9.6d).

In Fig.9.7 we present schematic representation of the ensuing cycle. We vaguely identify three steps:

- ① → ①' → ② . We start at the end of the negative phase of f_{tilt}, see Fig.9.7a) and e). The configurational particle is in the state A described by a valley of the energy landscape which we identify with the detached state ($\Psi(y - x) = 0$). As we see the detached particle is being dragged backwards by the load, see transition ① → ①'. Then $f_{tilt}(t)$ changes phase from negative to positive, favoring post power stroke configuration of the bistable potential. The system performs the power stroke which prevents the sliding moreover, as soon as the particle crosses the barrier in the bistable element, it gets attached attached ($\Psi(y - x) = 1$), see 9.7b) and e). The transition ①'→② can be identified with the power stroke in the attached state. We can also say that the attachment and the power stroke take place simultaneously.

- ②→③'→③. We start in the attached post power stroke state ②, see 9.7c) and e). The external force changes sign, favoring now the pre-power stroke state. As a result

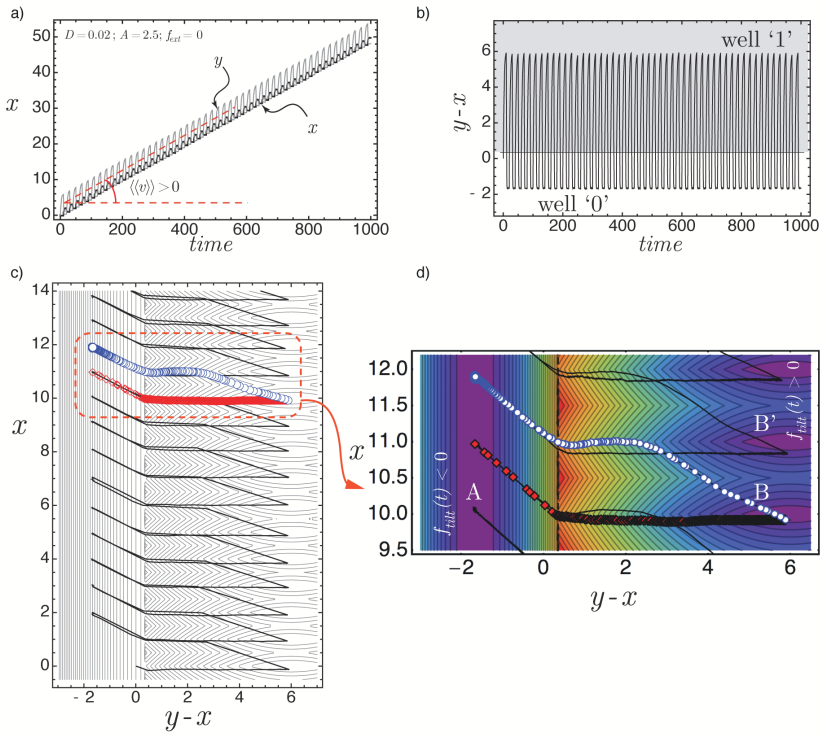

Figure 9.5. The XY-tilted ratchet with control function in soft device configuration with $f_{ext} = 0$ and at temperature $D = 0.02$. a) The average trajectory x_t (solid black line) and y_t (solid gray line). b) The time evolution of the system in coordinates $[time, y - x]$. c)The average trajectory in coordinates $[y - x, x]$, note that the motor crosses few space periods. d) One motor cycle as segment of average trajectory during the time period T of the $f_{tilt}(t)$. The red scatters correspond to the positive phase of the rocking $f_{tilt}(t) = +A$ and the blue scatters–to the negative phase of rocking $f_{tilt} = -A$. The colored bands indicate the structure of the energy landscape, the coldest colors indicate the minima and hottest colors indicate the maxima. The relevant parameters $k_0 = 1.5$, $k_1 = 0.43$, $l = 0.35$, $a = 1$, $\lambda_1 = 0.5$, $L = 1$, $V_{max} = 1$, $\alpha = 1$ with time period $T = 20$ and amplitude $A = 2.5$ of the rocking force.

the motor makes a step forward in the x direction, see transition ②→③'. As soon as the configurational particle crosses the barrier between the two wells, we motor detaches ($\Psi(y - x) = 0$), see 9.7d) and e). The motor continues to move forward in the detached state, see transition ③'→③ which finally recharges the power stroke mechanism. Here one can say that recharging leads to the detachment which in turn facilitates this energy demanding stage. Then the cycle starts again.

In summary, we clearly identified a two state cycle. However, it can also be interpreted as a four state cycle if we consider transition ①→①' as attachment, transition ①'→② as the power stroke in the attached state, transition ②→③' as detachment and finally transition ③'→③ as the recharging of the power stroke in the detached state.

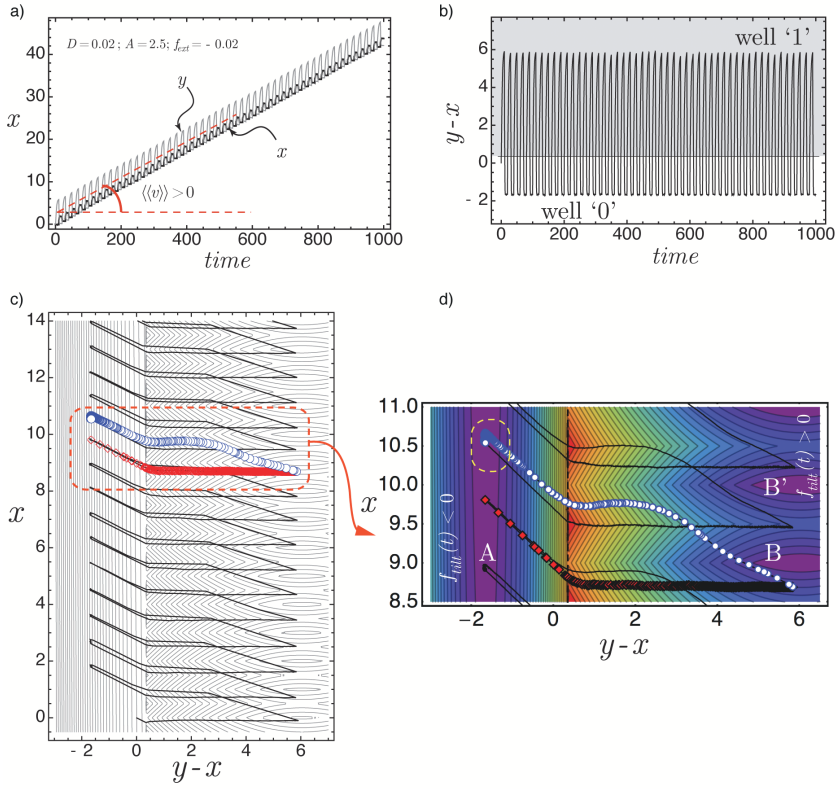

Figure 9.6. he XY-tilted ratchet with control function in soft device configuration with $f_{ext} = -0.02$ and at temperature $D = 0.02$. a) The average trajectory x_t (solid black line) and y_t (solid gray line). b) The time evolution of the system in coordinates $[time, y - x]$. c)The average trajectory in coordinates $[y - x, x]$, note that the motor crosses few space periods. d) One motor cycle as segment of average trajectory during the time period T of the $f_{tilt}(t)$. The red scatters correspond to the positive phase of the rocking $f_{tilt}(t) = +A$ and the blue scatters–to the negative phase of rocking $f_{tilt} = -A$. The colored bands indicate the structure of the energy landscape, the coldest colors indicate the minima and hottest colors indicate the maxima. Note the presence of the shift induced by the load in the detached state, the region selected by the dashed yellow line. The relevant parameters $k_0 = 1.5$, $k_1 = 0.43$, $l = 0.35$, $a = 1$, $\lambda_1 = 0.5$, $L = 1$, $V_{max} = 1$, $\alpha = 1$ with time period $T = 20$ and amplitude $A = 2.5$ of the rocking force.

9.4 Motor cycle in the hard device

For convenience, we repeat here the Langevin equations describing the system in the hard device

$$\begin{cases} \dfrac{dx}{dt} = -\alpha\left(\partial_x\left[\Psi(y-x)\Phi(x)\right] + \partial_x V(y-x) + f_{tilt}(t)\right) + \sqrt{2\alpha D}\,\xi_x(t) \\ \dfrac{dy}{dt} = -\partial_y V(y-x) - \Phi(x)\partial_y\Psi(y-x) - k_m(y-z) + f_{tilt}(t) + \sqrt{2D}\,\xi_y(t) \end{cases} \tag{9.15}$$

We fix $z = 0$, $\alpha = 1$ and assume that $k_0 = 1.5$, $k_1 = 0.5$, $a = 1$, $l_0 = 0.2$, $L = 1$, $V_{max} = 1.5$. The control function $\Psi(y - x)$ will be taken in the form (9.2) with either $e = 0.02$ or in few cases –$e = 0.2$. We apply the same tilting force characterized by variable amplitude A and a constant period $T = 20$.

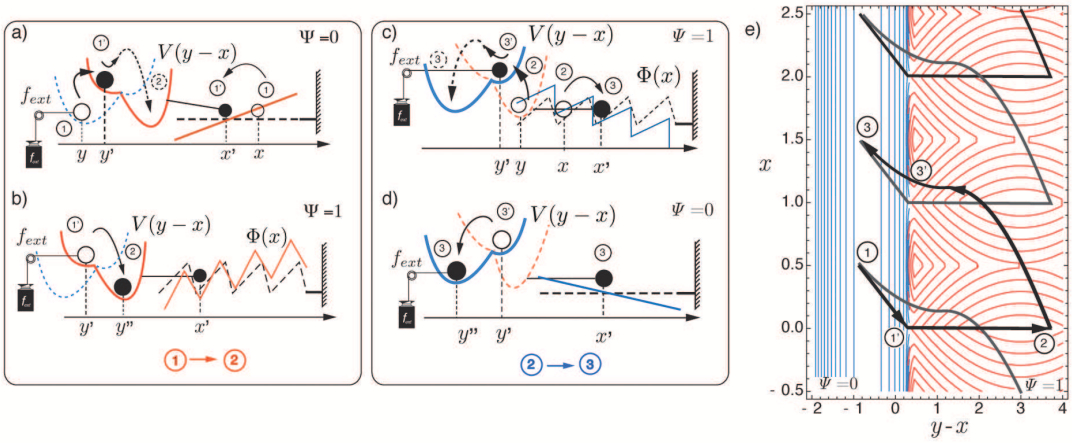

Figure 9.7. The schematic representation of the ensuing cycle of XY-tilted model with control term in absence of external load. Through the picture a),b),c),d) we illustrate step by step one motor cycle using very simplified sketch of energy landscape configurations. Note that we does not represent the characteristic shift along x in detached states, $\Psi(y-x)=0$. e) The scheme of average trajectory path in soft device configuration.

For convenience we also recall here the definition of average tension:

$$f_{h.d.} = k_m\left(\langle\langle y\rangle\rangle - z\right) \tag{9.16}$$

Since $z=0$ and $k_m=1$ the quantity $\langle\langle y\rangle\rangle$ gives us directly the tension.

In Fig.9.8 we show the average configurational trajectory in the hard device during one cycle at several values of A. With the red thick line we show the average trajectory during the positive phase of the tilting force $f_{tilt}(t)$, and with blue line – during the negative phase of $f_{tilt}(t)$. The light gray line shows a single stochastic realisation during one motor cycle. Below each cycle we plot the averaged trajectory y_t which characterizes the mean tension measured in the hard device configuration. We show with red lines the energy levels of the two-dimensional landscape in the positive phase $\Psi(y-x)\Phi(x) + V(y-x) + 1/2k_m y^2 - (y-x)A$ (attached state) and with blue lines – the energy levels of $\Psi(y-x)\Phi(x) + V(y-x) + 1/2k_m y^2 + (y-x)A$ (detached state).

One can see that at low amplitudes A the configurational particle is trapped in a single well of the bistable system corresponding to post power stroke configuration, see Fig.9.8a). Note that the system nevertheless generates positive tension (bottom picture) because the system constantly attempts to perform the power stroke. However, after passing the (degenerate) saddle point of the bistable potential the system does not have enough energy to reach the second well of the bistable potential.

At higher amplitudes A, the motor is able to cross the energy barrier and to perform the power stroke, see Fig.9.8b) - d). In Fig.9.9 we show the average trajectory in the hard device while increasing temperature D. At the intermediate temperatures D we obtain the motor cycle incorporating attached and detached states as well as pre and post power stroke configurations. The growth of temperature D increases generated tension till a threshold is reached after which the tension decreases as thermal fluctuations progressively destroy the correlations in the system. Note the numerical value of the generated tension in Fig.9.9a) and d): the system generates the same low tension at two very different values of the temperatures. In between this two values of D, the value of the generated force passes through a maximum.

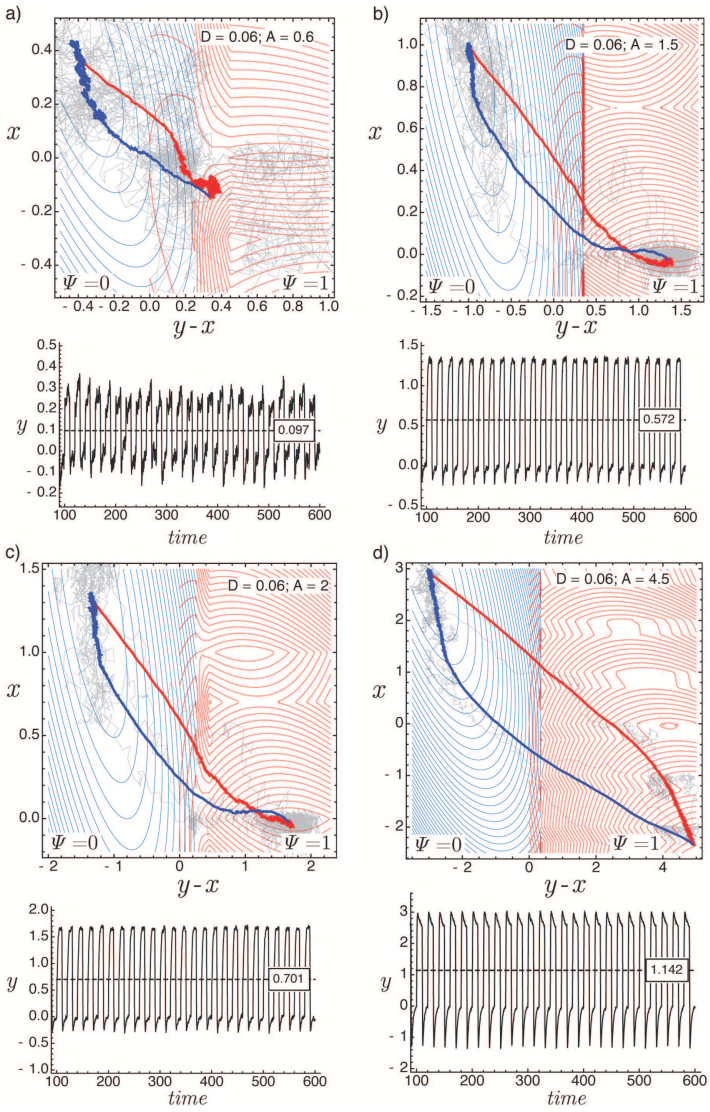

Figure 9.8. The XY-tilted model with control function in hard device configuration. The variation of the motor cycle with the increasing amplitude A of rocking at constant temperature $D = 0.06$. With the dark red lines we plot the surface contours of energy landscape in positive phase of $f_{tilt}(t)$ and by red thick line we report the associated average trajectory path. With the dark blue lines we show the surface contours of energy landscape in the negative phase $f_{tilt}(t)$ and by blue thick line we report the associated average trajectory path. The light gray lines follow the single stochastic realization during one time period. The cycle drives in the trigonometric sense. a) The motor cycle at $A = 0.6$ and the generated average tension (e=0.2). b) The cycle at $A = 1.5$ and the generated average tension (e=0.02). c) The cycle at $A = 2$ and the generated average tension (e=0.2). d)The cycle at $A = 4.5$ and the generated average tension (e=0.02). The relevant parameters $k_0 = 1.5$, $k_1 = 0.43$, $l = 0.35$, $a = 1$, $\lambda_1 = 0.7$, $L = 1$, $V_{max} = 1.5$, $\alpha = 1$ with the time period $T = 20$ of the $f_{tilt}(t)$, performed by Euler scheme with $\Delta t = 10^{-3}$ and over $N_r = 10^3$ realizations.

We conclude that the motor visits at less 2 different states, detached and attached. In Fig.9.10 we show schematic trajectory of the motor cycle. The motor performs a stable cyclic motion in the clockwise direction after a short transient. Below we interpret the

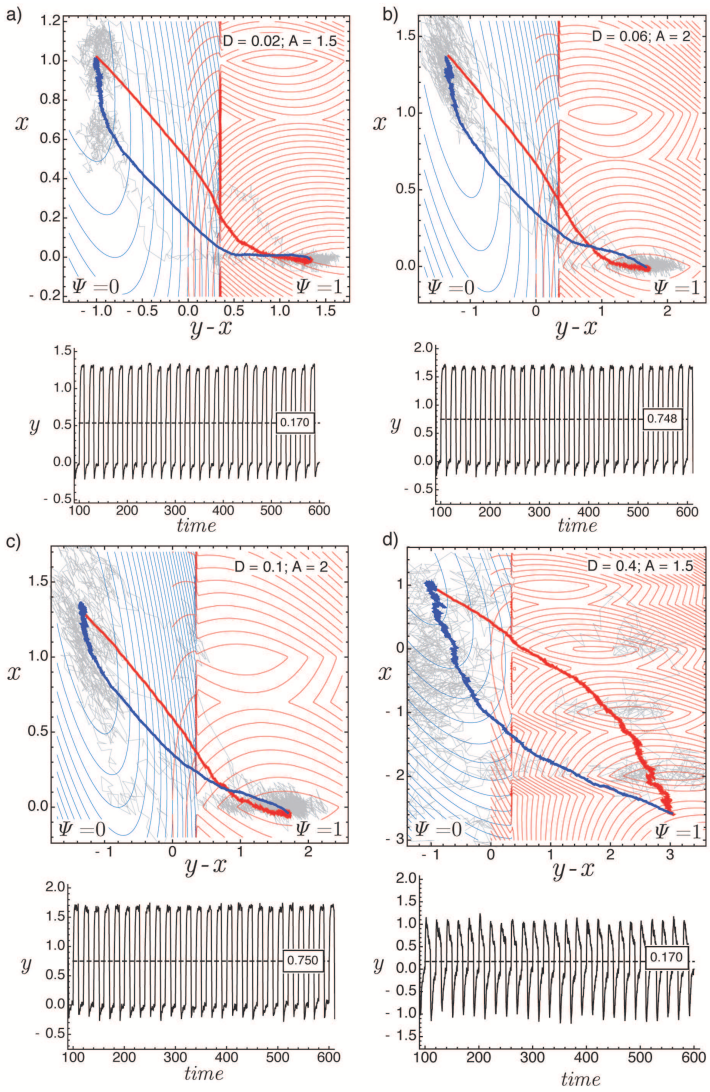

Figure 9.9. The XY-tilted model with control function in hard device configuration. The variation of the motor cycle with the increasing temperature D. With the dark red lines we plot the surface contours of energy landscape in positive phase of $f_{tilt}(t)$ and by red thick line we report the associated average trajectory path. With the dark blue lines we show the surface contours of energy landscape in the negative phase $f_{tilt}(t)$ and by blue thick line we report the associated average trajectory path. The light gray lines follow the single stochastic realization during one time period. The cycle drives in the trigonometric sense. a) The motor cycle at $D = 0.02,\ A = 1.5$ and the generated average tension. b) The cycle at $D = 0.06,\ A = 2$ and the generated average tension. c) The cycle at $D = 0.1,\ A = 2$ and the generated average tension. d)The cycle at $D = 0.4,\ A = 1.5$ and the generated average tension. The relevant parameters $k_0 = 1.5,\ k_1 = 0.43,\ l = 0.35,\ a = 1,\ \lambda_1 = 0.7,\ L = 1,\ V_{max} = 1.5,\ \alpha = 1,\ e = 0.02$ with the time period $T = 20$ of the $f_{tilt}(t)$, performed by Euler scheme with $\Delta t = 10^{-3}$ and over $N_r = 10^3$ realizations.

motor steps in the following way:

- ①→①'→②. We start as usually at the very end of the negative phase of the tilting force $f_{tilt}(t)$. The motor is in detached state ① (the valley "0", $\Psi(y-x)=0$). Then the force $f_{tilt}(t)$ changes sign, and the configurational particle makes the transition

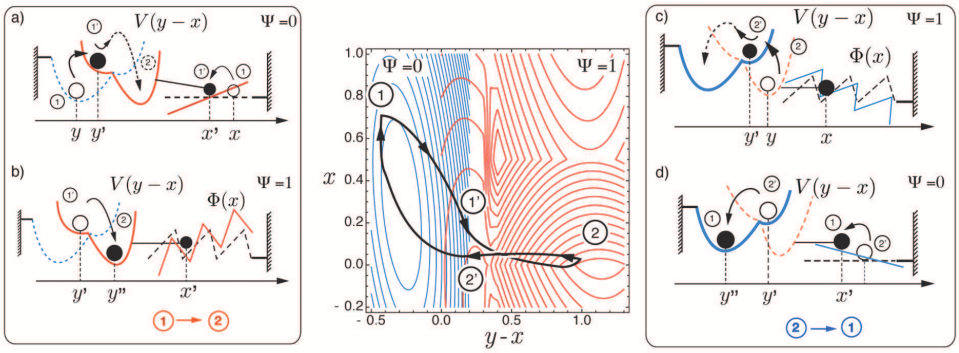

Figure 9.10. The XY-tilted ratchet with control function. The detailed scheme of motor cycle in hard device configuration.The scheme XY-tilted ratchet model in hard device configuration. With red lines we show the surface contours of energy landscape in positive phase of rocking $(\Psi(y-x)\Phi(x)+V(y-x)+1/2k_m y^2-(y-x)A)$ and with the blue lines–the surface contours of energy landscape in negative phase of rocking $(\Psi(y-x)\Phi(x)+V(y-x)+1/2k_m y^2+(y-x)A)$. a)-b) The motor is in detached state. Then the force $f_{tilt}(t)$ changes sign, and the configurational particle makes the transition which can be interpreted as attachment. During the positive phase the particle crosses the energy barrier between the two wells of the bistable potential performing the power stroke. c)-d) The motor now is attached. The $f_{tilt}(t)$ changes sign again, the motor performs a step which can be interpreted as detachment. The subsequent transition in bi-stable element can be interpreted as the recharging of the power stroke in the detached configuration.

①→①' which can be interpreted as attachment, see Fig.9.10a). During the positive phase of $f_{tilt}(t)$ the particle crosses the energy barrier between the two wells of the bistable potential performing the power stroke ①'→②.

- ②→②'→①. We are now in state ② corresponding to the conformation "1" in the attached state. The correlated noise changes sign again, and due to the asymmetry of the bi-stable potential, the motor performs a step ②→②' which can be interpreted as detachment, see Fig.9.10c). The subsequent transition ②'→① can be interpreted as the recharging of the power stroke in the detached configuration, see Fig.9.10d). Then the cycle starts again.

In summary, the XY-tilted device with internal control (coupling) exhibits dynamics which may be interpreted in two different ways: either as a two state cycle or as a four state cycle. In the two site interpretation the attachment is accompanied by the power stroke while the detachment comes together with recharging of the power stroke mechanism. In the four site interpretation the mechanical cycle resembles the biochemical cycle of Lymn and Taylor, however, the identification of different (transient) mechanical states with stable chemical states remains ambiguous.

9.5 Force-Velocity relation

By applying a non zero load f_{ext} in the soft device setting we can recover the force-velocity relation for the coupled model. As usually, we adopt a physical definition of the direction for the external force when we plot the response in the axis $[\langle v\rangle, f_{ext}]$. By green color area we indicate the region of anti-dissipation where the average velocity and the external force have opposite defections, see Fig.9.11. We recall that in such anti-dissipative regimes

the motor uses the input energy to performs useful work. The passive dissipative regime corresponds to the cases where the average velocity and the external load have the same direction. That means that the motor is dragged by the external load and the input energy can at most contribute to enhanced drug force.

To solve the Langevin equations we apply the Euler scheme with time step $\Delta t = 1 \times 10^{-4}$ and average over $N_r = 10^4$ numerical realizations. We fix $\alpha = 1$ and use the following parameters of the potential: $k_0 = 1.5,\ k_1 = 0.43,\ a = 1,\ l = 0.35,\ L = 1,\ V_{max} = 1.5$. The control function $\Psi(x, y)$ is given by (9.2) with $e = 0.01$. The periodic component of the noise has always a period $T = 20$.

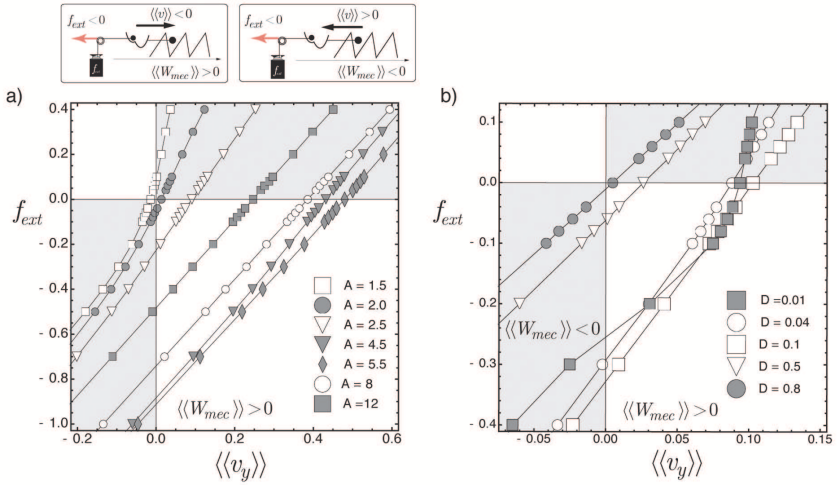

Figure 9.11. The XY-tilted ratchet with control function in soft device configuration. a) The variation of the force-velocity relation with the increasing amplitude A of rocking at the fixed temperature $D = 0.02$. b) The variation of the force-velocity relation with the increasing temperature D at the fixed amplitude $A = 2.5$ of rocking. The relevant parameters $k_0 = 1.5,\ k_1 = 0.43,\ l = 0.35,\ a = 1,\ \lambda_1 = 0.7,\ L = 1,\ V_{max} = 1.5\ e = 0.01,\ T = 20$. The direct Langevin simulations performed with Euler scheme for time step $\Delta T = 0.5 \times 10^{-3}$ and $N_r = 10 \times 10^4$ stochastic realisations.

In Fig.9.11a) we show the computed force-velocity relation at several values of A and fixed temperature temperature $D = 0.02$. One can see that the ratchet device with internal control can indeed performs a positive mechanical work against an external load (can carry a cargo). As in other models, the force velocity relation is concave at small values of A (thermal ratchet) and concave at large values of A (mechanical ratchet). In Fig.9.11b) we show the sensitivity of the force-velocity relation to increasing temperature D at fixed amplitude $A = 2.5$. Notice almost linear behavior except when the temperature is small ($D = 0.01$). With increase of temperature D the system passes through the optimum regime, and then the performance of the motor eventually degrades.

In Fig.9.12a) we plot the average velocity as a function of amplitude A at different values of the temperature D. The computation was performed in the presence of conservative load, $f_{ext} = -0.1$. The system shows a maximum at a finite value of A, see the curve corresponding to temperature $D = 0.1$. For higher amplitudes A the average velocity decreases. Notice the interval where the average velocity is negative and the motor is dragged by the load because the energy input is not sufficient to reverse the direction of motion. In Fig.9.12b) we show the average velocity as a function of temperature D at different values of the rocking amplitude A. Here the computations were performed without

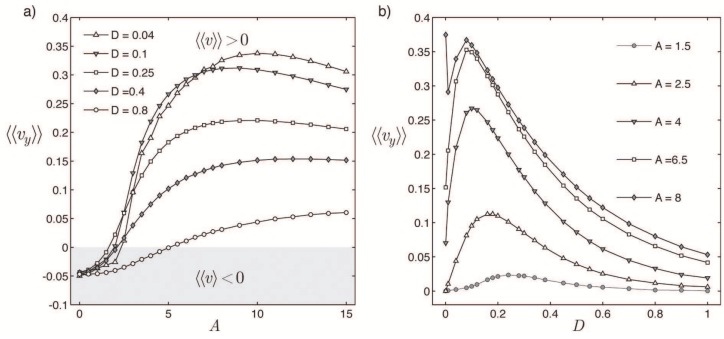

Figure 9.12. The XY-tilted model with control function in soft device. a) The variation of the average velocity with the increasing amplitude A of $f_{tilt}(t)$, the computation performed with conservative load $f_{ext} = -0.01$ for different values of D. The negative average velocity is consequence of load. b) The variation of the average velocity with the increasing temperature D for different values of amplitude A, the computation performed without external load. The relevant parameters $k_0 = 1.5,\ k_1 = 0.43,\ l = 0.35,\ a = 1,\ \lambda_1 = 0.7,\ L = 1,\ V_{max} = 1.5\ e = 0.01,\ T = 20$. The direct Langevin simulations performed with Euler scheme for time step $\Delta T = 0.5 \times 10^{-3}$ and $N_r = 10 \times 10^4$ stochastic realisations.

any load, $f_{ext} = 0$. The motor performance shows a maximum at finite value of D which is a manifestation of stochastic resonance. Here we clearly deal with thermal (rather than mechanical) ratchet system and the motor velocity is optimized at finite temperature.

9.6 Stochastic energetics

To study the energetics of our system we apply by now familiar procedure. We first rewrite the system 9.5 in the form

$$\begin{cases} \left(\partial_x \left[\Psi(y-x)\Phi(x)\right] + \partial_x V(y-x)\right) \circ dx + f_{tilt}(t) \circ dx = \delta Q_x \\ \partial_y V(y-x) \circ dy + \Phi(x)\partial_y \Psi(y-x) \circ dy - f_{tilt}(t) \circ dy - f_{\text{ext}} \circ dy = \delta Q_y \end{cases} \tag{9.17}$$

where we defined the heat by using Sekimoto formula $\delta Q_i = \left(-\eta \frac{dx_i}{dt} + \sqrt{2\eta_i D}\xi_i(t)\right) \circ dx_i$, see [100]. The all expressions have the similar form as for previously studied XY-tilted ratchet model. We can define the mechanical work

$$W_{mec} = \frac{1}{T} \int_{\mathbf{X}_{t_i}}^{\mathbf{X}_{t_i+T}} dG_0(\mathbf{X}_t) = -f_{ext}\langle v_y \rangle \tag{9.18}$$

where $G_0 = \Psi(y_t - x_t)\Phi(x_t) + V(y_t - x_t) - y_t f_{ext}$. And the energy input R

$$R = R_y - R_x = \frac{1}{T} \int_{y_{t_i}}^{y_{t_i+T}} f_{tilt}(t)dy_t - \frac{1}{T} \int_{x_{t_i}}^{x_{t_i+T}} f_{tilt}(t)dx_t \tag{9.19}$$

The energy balance finally written

$$W_{mec} = R + Q \tag{9.20}$$

The mechanical efficiency can then be written as

$$\epsilon_{mec} = \frac{W_{\text{mec}}}{R} \tag{9.21}$$

The stokes efficiency is again

$$\epsilon_{Stokes} = \frac{W_{Stokes}}{R} \tag{9.22}$$

where

$$W_{\text{Stokes}} = \alpha^{-1}\langle v_x\rangle^2 + \langle v_y\rangle^2 \tag{9.23}$$

Finally, the rectifying efficiency–the sum of Stokes and mechanical efficiencies, which can be viewed as the global characteristic of the energy transformation in the ratchet system, takes the form

$$\epsilon_{rec} = \frac{W_{mec} + W_{Stokes}}{R} \tag{9.24}$$

In Fig.9.13a) we present the results of numerical computations at a given value of the applied load $f_{ext} = -0.1$. We first show the average velocity as a function of temperature D at different values of the amplitude A. As expected the motor exhibits maxima at performance at finite temperature for small amplitudes $A = 2.5$, $A = 3$, $A = 4$ and $A = 5.5$. At higher amplitudes A, the average velocity is a monotonically decreasing function of D. By light green color we indicate the region with negative velocity, where the motor moves backwards. For instance, one can see that at $A = 1.5$ the motor consumes energy but does not produce positive mechanical work.

In Fig.9.13d) we show the period averaged energy R consumed by the motor. With increasing temperature D, the motor consumes more energy in order to perform a forward motion along the actin filament, see Fig.9.13b). Interestingly, the part of the consumed energy through y variable decreases with temperature D, see Fig.9.13c), exactly as we have seen in the decoupled XY-tilted ratchet system.

In Fig.9.14b) we show the parametric dependence of mechanical efficiency. At small amplitudes A we again see maxima of the energetic performance at finite temperatures. With increasing A the maxima vanish and the efficiency becomes a monotonically decreasing function of D, which is characteristic for the mechanical ratchet regime. Notice the peculiar behavior at small energy input $A = 1.5$, see Fig.9.14a) and Fig.9.14b). In Fig.9.14c) we show the variation of Stokes efficiency with increasing temperature D. At small amplitudes of the rocking and high temperatures D the Stokes efficiency, (9.22), is an increasing function of D, because we are in regime where the motor is dragged by the cargo, see Fig.9.14a). In Fig.9.14d) we study the variation of rectifying efficiency with temperature D The behavior of this function is mostly controlled by the Stokes efficiency.

9.7 Conclusions

In this section we presented a synthetic ratchet model where rocking is combined with flashing in a synchronized way. In this way we introduced the internal coupling which imitates steric effects and regulates the distance of the myosin head from the actin filament depending on the conformational state of the power stroke mechanism. This allowed us to make the detachment state more integrated into the mechanical cycle. By introducing the special multiplicative control function $\Psi(y - x)$, we could associate the pre-power stroke with a detached state (no interaction with the spatial periodic potential $\Phi(x)$) and the post power stroke – with the attached state (the system interacts strongly with the space periodic potential $\Phi(x)$). As the result the proposed model reproduces all four states

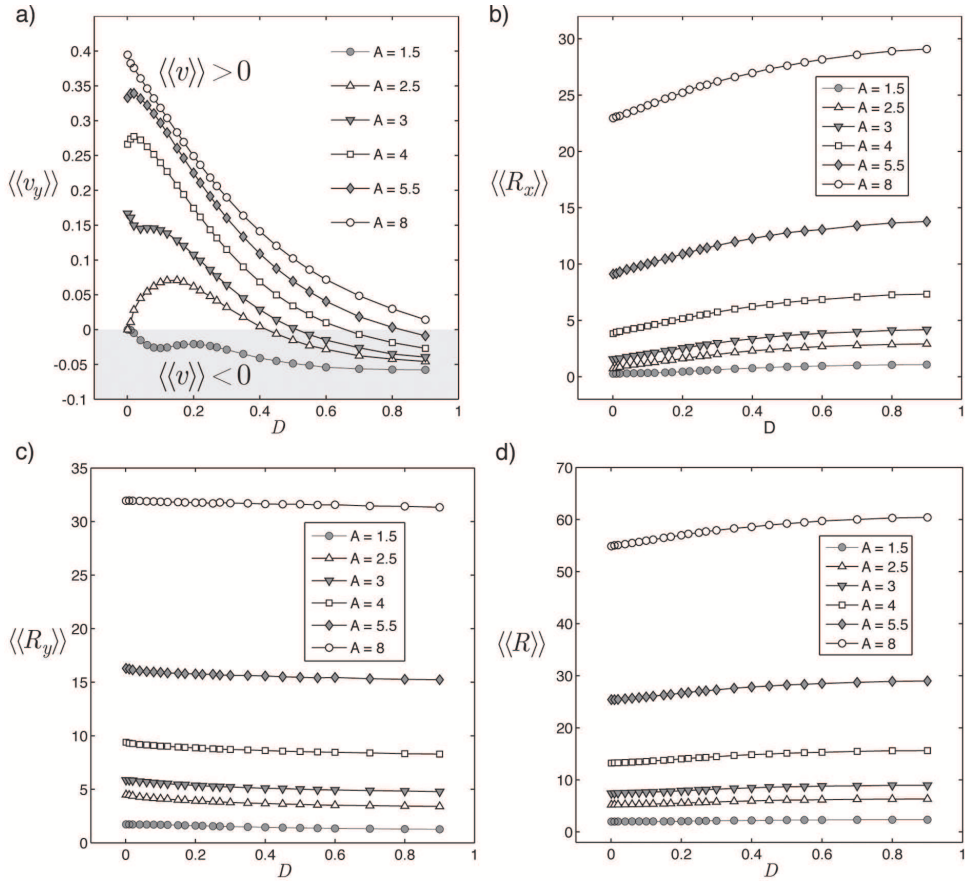

Figure 9.13. The XY-tilted model with control function in soft device configuration with $f_{ext} = -0.1$. a) The variation of the average velocity $\langle v_y \rangle$ with the increasing temperature D at different amplitude A of rocking. b) The variation of consumed energy R_x with the increasing temperature D at different amplitude A of rocking, see (9.19). c) The variation of consumed energy R_y with the increasing temperature D at different amplitude A, see (9.19). d) We show the variation of function R (the resulted energy consumed by motor) with the increasing temperature D at different amplitude A. The relevant parameters $k_0 = 1.5$, $k_1 = 0.43$, $l = 0.35$, $a = 1$, $\lambda_1 = 0.7$, $L = 1$, $V_{max} = 1.5$ $e = 0.1$, $T = 6$. The direct Langevin simulations performed with Euler scheme for time step $\Delta T = 0.5 \times 10^{-3}$ and $N_r = 10 \times 10^4$ stochastic realisations.

of the Lymn-Taylor cycle even though the individual states are interpreted as transient mechanical configurations.

The schematic structures of the ensuing cycles in the hard and soft devices are presented in Fig.9.15.

Most importantly, the proposed ratchet device is able to generate the directional motion in the presence of a cargo and can produce force in isometric conditions. Interestingly, the ratchet effect here is due to the asymmetry of the bistable potential while the actin filament with its periodically located attachment sites is symmetric and passive. The force-velocity curves and the motor energetics are similar to what we have seen in the uncoupled XY-tilted model. However, the coupled model is preferable because it presents the design with mechanically explicit detached state. Although our aim is to obtain a model of a non-processive motor, the proposed mechanism is capable of working alone in the absence of collective effects (kind of 'one-legged kinesin'). We expect that the most

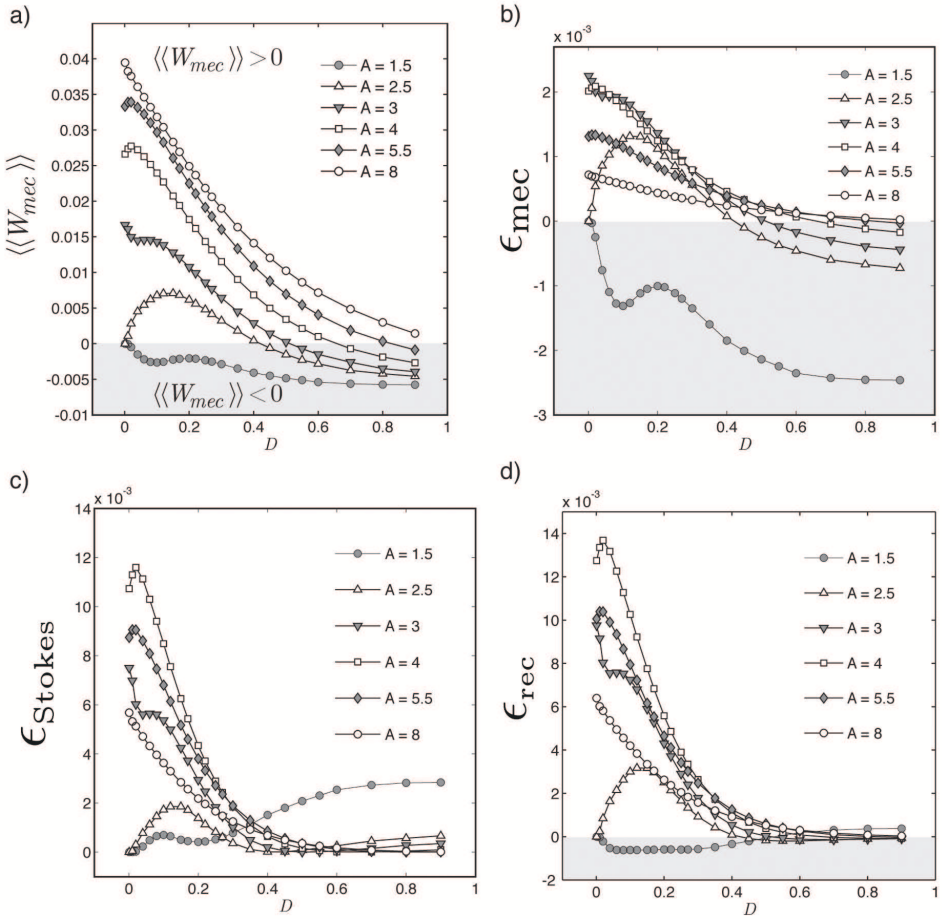

Figure 9.14. The XY-tilted ratchet with control function in soft device configuration with $f_{ext} = -0.1$. a) The variation of mechanical work W_{mec} with the increasing temperature D at different amplitude A. b) The variation of mechanical efficiency ε_{mec} (9.21) with the increasing temperature D at different amplitude A. c) The variation of Stokes efficiency ε_{Stokes} (9.22) with the increasing temperature D at different amplitude A. d) The variation of rectifying efficiency ε_{rec} (9.24) with the increasing temperature D at different amplitude A of rocking. The relevant parameters $k_0 = 1.5$, $k_1 = 0.43$, $l = 0.35$, $a = 1$, $\lambda_1 = 0.7$, $L = 1$, $V_{max} = 1.5$ $e = 0.1$, $T = 6$. The direct Langevin simulations performed with Euler scheme for time step $\Delta T = 0.5 \times 10^{-3}$ and $N_r = 10 \times 10^4$ stochastic realisations.

important consequences of the coupled model will be seen when the collective effects are taken into consideration. This subject however is outside the limited scope of this Thesis.

Finally, we observe that while the proposed model offers a particular mechanical interpretation of the detachment in the power stroke driven framework, other formulations are possible as well. Thus, in the next chapter we continue working with the idea of a control function but introduce a different type of control with a hysteretic memory which allows one to reproduce the four states of the Lymn-Taylor cycle with even more certainty.

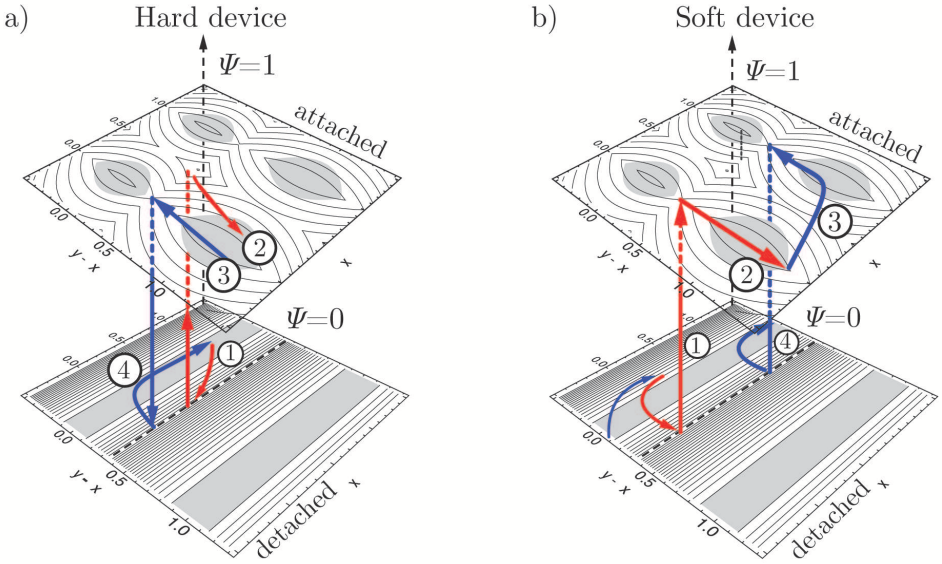

Figure 9.15. The XY-tilted ratchet with control parameter. a) A simplified scheme of motor cycle in hard device configuration. b) A simplified scheme of motor cycle in soft device.

Chapter 10

Synthetic model with hysteretic control

We introduce a generalization of the synthetic model studied in the last chapter where the feedback operator, coordinating the state of the attachment with the conformational state of the power stroke element, has a hysteretic nature. This allows us to build a mechanical device which has four distinct mechanical states that can be associated with the biochemical states constituting the Lymn-Taylor cycle. The new model is formulated in the same framework as our other models under the assumption that the actin filament is passive and may not even be polar so that both the symmetry breaking and the activity come from the power stroke element. The main new assumption is that the relative displacement of the myosin head and the actin filament is a multi-valued function of the internal configuration of the power stroke element which contain some elements of an elementary history dependence. Behind such phenomenological assumption is the idea of internal micro meta-stability which has to be studied at the molecular scale.

More specifically, the coupled model studied in the previous section has an obvious shortcoming: the detachment takes place when the bistable element is in the spinodal state meaning that it is just about to leave the energy well corresponding to pre-power stroke state. As result, the power stroke remains incomplete because the detachment prevents the system of reaching the second well of the bi-stable potential. This means that the detachment must be delayed and should take place when the power stroke has been already completed. Similarly, attachment must take place only after the power stroke element has been recharged. This means that the control function must switch 'on' and 'off' the periodic potential at different values of the variable $y - x$ depending of the conformational state of the bistable element. The model must implicitly contain some history dependence which we implement in this chapter by using conventional Preisach operators.

10.1 Preliminaries

We recall that the main goal of this thesis was to construct a mechanical model of a Brownian ratchet which is driven through the power stroke element and is fully compatible with Lymn-Taylor cycle. As we have seen, the models presented in the previous chapters reproduce the desired cycle only partially. The weak point of X-tilted, Y-tilted and XY-tilted ratchet models was the ambiguous interpretation of the detached state. By using a multiplicative control function we resolved this problem, however, the resulting model can only be interpreted as a four state motor if transient states are interpreted as station-

ary. In this chapter we follow the ideas pioneered by J.Prost, F.Jülicher and J.F.Joanny [3, 52] and make the coordination between the power stroke mechanism and the attachment/detachment mechanism more subtle. More specifically we assume that flashing is not instantaneously coupled to the conformational state but instead takes place with a delay.

We begin with writing a dimensionless system of the over-damped Langevin equations for the case of general time depending control $\Psi(t)$:

$$\begin{cases} \dfrac{dx}{dt} = -\Psi(t)\partial_x\Phi(x) - \partial_x V(y-x) - f_{tilt}(t) + \sqrt{2D}\,\xi_x(t) \\ \dfrac{dy}{dt} = -\partial_y V(y-x) + f_{tilt}(t) + \sqrt{2D}\,\xi_y(t) \end{cases} \tag{10.1}$$

Here $\Phi(x)$ is the periodic potential, $V(x-y)$ is an asymmetric bistable potential and $f_{tilt}(t)$ is time periodic rocking force $f_{tilt}(t)$ with zero average. The parameter D is the intensity of the white noise. Suppose first that the function $\Psi(t)$ takes two values 0 and 1 depending on the sign of the correlated component of the noise $f_{tilt}(t)$:

$$\Psi(t) = \begin{cases} 1, & \text{for } f_{tilt}(t) \geq 0 \\ 0, & \text{for } f_{tilt}(t) < 0 \end{cases} \tag{10.2}$$

In this setting the motor cycle follows the scheme:

- The configurational particle makes a transition between the two wells of the bistable potential: pre-power stroke→ post-power stroke in the attached configuration, as $\Psi(t) = 1$ and $f_{tilt}(t) \geq 0$. During the power stroke the myosin head is attached.
- The configurational particle makes a reverse transition between the two wells of the bistable potential: post-power stroke → pre-power stroke in the detached configuration, as $\Psi(t) = 0$ and $f_{tilt}(t) < 0$. During such recharging of the power stroke mechanism the particle remains detached.

In Fig.10.1 we show a schematic graphic presentation of the resulting motor cycles in hard and soft devices. One can see that in this way we have obtained a hybrid of rocking and flashing ratchet devices. Thus, we may completely eliminate the rocking from the bi-stable element and define the switch between the two configurations of the actin filament: with periodic and with flat energies. In this way we obtained a conventional flashing ratchet [3, 52]. If instead we eliminate the time dependent multiplicative term in front of the periodic energy, we obtain the XY tilted rocking ratchet studied in Chapter 8.

The main problem with a purely flashing ratchet is that it defies simple mechanical interpretation because it can not be formulated directly in terms of applied forces. Therefore we prefer to stay in the framework of rocking ratchet approach and replace explicit excitation of the actin potential by the (steric) coupling between the power stroke and the attachment devices.

In the previous chapter we have already described a prototypical ratchet device with internal control depending on the state of the bistable element. The corresponding set of dimensionless overdamped Langevin equations was written in the form:

$$\begin{cases} \dfrac{dx}{dt} = -\partial_x[\Psi(y-x)\Phi(x)] - \partial_x V(y-x) - f_{tilt}(t) + \sqrt{2D}\,\xi_x(t) \\ \dfrac{dy}{dt} = -\Phi(x)\partial_y\Psi(y-x) - \partial_y V(y-x) + f_{tilt}(t) + \sqrt{2D}\,\xi_y(t) \end{cases} \tag{10.3}$$

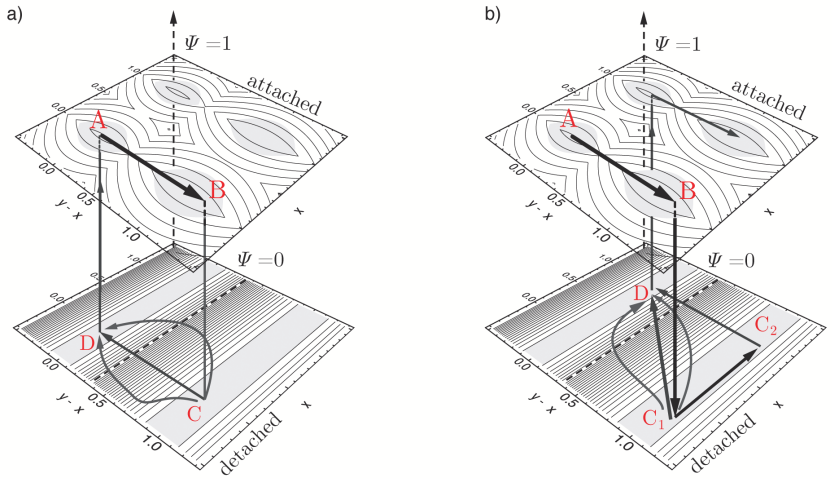

Figure 10.1. The flashing multidimensional motor. The schematic graphic presentation of motor cycle in isometric and isotonic regime. a) The hard device motor cycle. b) The soft device motor. In the detached configuration, the Brownian particle diffuses and can take a different paths to recharge the power-stroke.

where the control parameter was taken in the form:

$$\Psi(y-x) \sim \frac{1}{2}\left(1+\tanh\frac{y-x-l}{e}\right) \tag{10.4}$$

As we have seen, the ensuing device can work as a motor and can carry cargo , moreover it partially reproduces all four states representing the bio-chemical Lymn-Taylor cycle. However, the post power stroke state was only transient because of the detachment and the pre-power stroke was only transient because of the attachment.

To overcome these shortcomings we can delay both the attachment and the detachment and introduce a memory dependence in the multiplicative term $\Psi(y-x)$. To this end we first define two control functions: $\Psi_+(y-x)$ and $\Psi_-(y-x)$, where we recall that $y-x$ is the variable characterizing the state of the bistable element described by the potential $V(y-x)$:

- The function $\Psi_+(y-x)$ affects the space periodic potential $\Phi(x)$ when the bi-stable element switches from well A (pre-power stroke) to well B (post-power stroke).
- The function $\Psi_-(y-x)$ affects the space periodic potential $\Phi(x)$ when the bi-stable element switches from well B (post-power stroke) to well A (pre-power stroke)

In Fig.10.2a) we shows the exact meaning of the two functions $\Psi_+(y-x)$ and $\Psi_-(y-x)$. One can see that they associate attachment/detachment with reaching exactly the minima of the corresponding wells. Another important feature of such model is that these two functions have overlapping domains of definition.

The next step is to superpose these two control functions and incorporate the resulting functional of the history of the process into the Brownian ratchet framework based on the two-dimensional energy landscape $\Psi_\pm(y-x)\Phi(x)+V(y-x)-(y-x)f_{tilt}(t)$. In practice, we need to define the operative branch which depends not only on the current value of the variable $y-x$ but also on its history $y(\tau)-x(\tau), \tau \le t$. In other words we need to introduce a memory into our mechanical system.

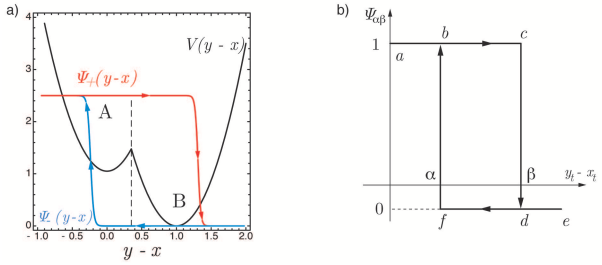

Figure 10.2. The schematic construction of the memory operator. a) The exact meaning of the two control functions $\Psi_+(y-x)$ and $\Psi_-(y-x)$, which control attachment / detachment. The control function $\Psi_+(y-x)$ (red solid line) must be applied during the power stroke when the particle moves from well A (pre-power stroke) into well B (post-power stroke). The function $\Psi_-(y-x)$ (blue solid line) must be applied during the recovery power stroke when the particle moves from the well B (post-power stroke) into the well A (pre-power stroke). b) The hysteresis loop corresponding to the simplest memory control operator $\widehat{\Psi}_{\alpha\beta}$. Numbers α and β correspond to "up" and "down" switching value of input signal. Note that we assume $\alpha \leq \beta$, the operator interacts only with the displacement $y_t - x_t$.

The construction presented below was inspired by the Preisach model of hysteresis in magnetic systems [78]. First, we introduce an operator $\widehat{\Psi}_{\alpha\beta}$ which models the relay switching between the attached and the detached state. This operator acts on the displacement history $y(t) - x(t)$ and the output $\Psi_{\alpha\beta} = \widehat{\Psi}_{\alpha\beta}[y(t) - x(t)]$ constitutes the multiplicative term in front of the periodic potential. Now the energy of the system is: $G(x, y, t) = \Psi_{\alpha\beta}\Phi(x) + V(y - x) - (y - x)f_{tilt}(t)$, where for simplicity we omit the terms identifying soft or hard device configurations. The resulting ratchet device is described by the following system of dimensionless overdamped Langevin equations:

$$\begin{cases} \dfrac{dx}{dt} = -\Psi_{\alpha\beta}\partial_x\Phi(x) - \partial_x V(y-x) - f_{tilt}(t) + \sqrt{2D}\,\xi_x(t) \\ \dfrac{dy}{dt} = -\partial_y V(y-x) + f_{tilt}(t) + \sqrt{2D}\,\xi_y(t) \end{cases} \tag{10.5}$$

The operator $\widehat{\Psi}_{\alpha\beta}$ in (10.5) is the simplest hysteresis-like operator. Numbers α and β define the "up" and the "down" switching values of the input signal, see Fig.10.2b). We limit the output of the operator $\Psi_{\alpha\beta}$ only to two values 1 and 0. The operator has therefore only two-positions, $\widehat{\Psi}_{\alpha\beta}[y_t - x_t] = 1$ and $\widehat{\Psi}_{\alpha\beta}[y_t - x_t] = 0$, which ultimately control the proximity of the space periodic potential $\Phi(x)$. We can illustrate the action of our Preisach operator as follows:

- Suppose that we start in the state with $y_t - x_t < \alpha$. Then the output of the operator is 1 or "up". As the displacement $y_t - x_t$ is increased, the descending branch *abcde* is followed and the output of operator remains 1. When the displacement $y_t - x_t$ reaches the threshold β, the output switches to 0, or "down". Further increase of the displacement $y_t - x_t$ does not change the state of the operator.

- Suppose now that we reverse the process so that the displacement $y_t - x_t$ is decreasing as we follow the ascending branch *edfba*. The output of the operator does not change (remains 0, or "down") until the threshold α is reached where the output switches to 1, or "up". Further decreasing of the displacement $y_t - x_t$ does not change the output.

One can see that the value of the operator's output at time t depends on the past history of the variable $y_t - x_t$, in particular on the state of the system in the moment $t - \delta t$. In our numeric algorithm we express the output of the operator $\Psi_{\alpha\beta}$ at the time moment t as follows:

$$\Psi_{\alpha\beta} = \begin{cases} 1, & \text{for } [y_{t-\delta t} - x_{t-\delta t}] < \alpha \\ 0, & \text{for } [y_{t-\delta t} - x_{t-\delta t}] > \beta \\ \Psi_{\alpha\beta} \text{ remains unchanged if } \alpha \leq [y_{t-\delta t} - x_{t-\delta t}] \leq \beta \end{cases} \tag{10.6}$$

Here α and β define the "up" and the "down" switching values of the input signal $y_{t-\delta t} - x_{t-\delta t}$.

We emphasize that our system (10.5) does not represent a conventional flashing ratchet, because the output of the hysteresis operator $\Psi_{\alpha\beta}$ cannot be given by an explicit function of time. We can rather define the output of our operator as $\Psi_{\alpha\beta}(y_{t-\delta t} - x_{t-\delta t})$. By this representation we emphasize the fundamental short memory structure of this operator: at moment t the ratchet device remembers its state at time $t - \delta t$ where δt may be arbitrary small.

We can fix the parameters α and β rather freely respecting the rule $\alpha \leq \beta$, however, the amplitude of the oscillations $y - x$ under the action of the rocking force $f_{tilt}(t)$ must be strictly larger than the difference $\beta - \alpha$. For instance, in the case of zero load soft device, we can choose the numbers α and β in the interval

$$\alpha, \beta \in \left\{ min[\frac{f_{tilt}(t)}{k_0}, 1 + f_{tilt}(t)/k_1],\ max[\frac{f_{tilt}(t)}{k_0}, 1 + f_{tilt}(t)/k_1] \right\} \tag{10.7}$$

10.2 Cycle structure in soft and hard devices

In our numerical simulations we use the symmetric (!) piece-wise linear saw-tooth potential $\Phi(x)$ ($V_{max} = 1.5,\ L = 1,\ \lambda_1 = \lambda_2 = 0.5$) , and the symmetric (!) bistable potential $V(y - x)$ formed by two parabolas with equal stiffness ($k_0 = k_1 = 1.5,\ l = 0.5$) We apply square wave rocking signal with time period $T = 10$ and amplitude $A = 3$. We fix the "up" and "down" thresholds to $\alpha = 0$ and $\beta = 2$ and this is the only place the asymmetry enters the problem. We perform our numerical simulations by using a simple Euler scheme with a constant time step $\Delta t = 0.5 \times 10^{-3}$ and average the results over $N_r = 10^3$ stochastic realizations.

Despite the symmetry of both potentials, the motor shows directional movement (backwards) along the x axis. In Fig.10.3 we show the average trajectory of a configurational particle in the soft device configuration. In Fig.10.3b) we show the average motion with a constant speed is accompanied by characteristic oscillations between the two distinct wells of the bistable potential. In Fig.10.3c) we show the averaged trajectory reported in the phase plane $[y - x, x]$. By colored scatters we indicate one motor cycle during time period T. In Fig.10.3d) we juxtapose the motor cycle with the energy landscape in positive and negative phases of the rocking. We use red scatters to identify the part of the cycle associated with the positive phase of $f_{tilt}(t)$, and blue scatters to show the part of the path associated with the negative phase of $f_{tilt}(t)$. In Fig.10.4 we show the computed motor cycle in hard device. Here the rocking force was chosen to have a period $T = 20$ and amplitude $A = 3.5$ and we fixed the "up" and "down" thresholds at $\alpha = 1$ and $\beta = 2$.

In Fig.10.5 we present schematic illustrations of the obtained motor cycles in hard and soft devices. From these figures we see that our ratchet system is able to reproduce a four-states functional cycle which can be directly compared with the biochemical theory

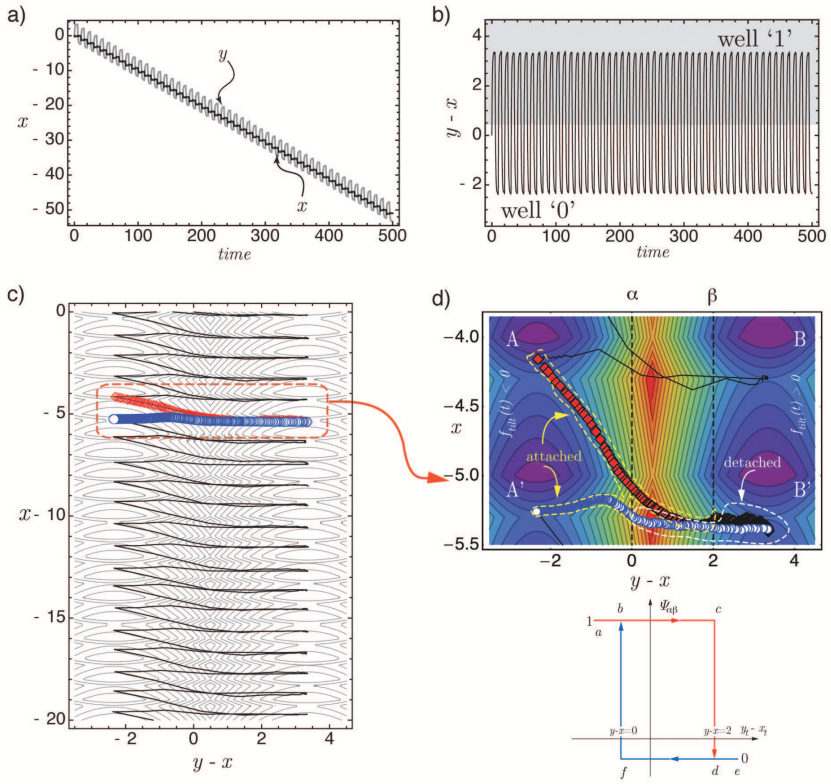

Figure 10.3. The average trajectory of XY-tilted model with memory control operator in the soft device configuration at zero load. a) The average trajectory x_t (solid black line) and y_t (solid gray line). b) The time evolution of the system in coordinates $[time, y-x]$. c)The average trajectory in coordinates $[y-x, x]$, note that the motor crosses few space periods. d) One motor cycle as segment of average trajectory during the time period T of the $f_{tilt}(t)$. The red scatters correspond to the positive phase of the rocking $f_{tilt}(t) = +A$ and the blue scatters–to the negative phase of rocking $f_{tilt} = -A$. The colored bands indicate the structure of the energy landscape, the coldest colors indicate the minima and hottest colors indicate the maxima. The relevant parameters $k_0 = k_1 = 1.5$, $l = 0.5$, $\lambda_1 = 0.5$, $L = 1$, $V_{max} = 1$, $\alpha = 0$, $\beta = 2$ with time period $T = 10$ and amplitude $A = 3$ of the rocking force.

behind the Lymn-Taylor cycle. Indeed, the obtained mechanical cycle in the soft device can be described as follows:

- ①→①'→②. As before we start at the very end of the negative phase of the rocking $f_{tilt}(t)$ when our configurational particle explores the energy well "0". The system is in the attached state and $\Psi_{\alpha\beta} = 1$. Then the value of $f_{tilt}(t)$ changes from negative to positive. After an immediate advance ①→①' (in the backward direction long x), the bi-stable element goes through the major transition ①'→② which we identify with the power stroke, see Fig.10.5b).

- ②→③. As soon as the variable $y_t - x_t$ reaches the threshold β, the motor gets detached and we get $\Psi_{\alpha\beta} = 0$. While we remain in the positive phase of the tilting $f_{tilt}(t)$ the motor finishes the power stroke ending up in the well "1".

- ③→④. We are now in state ③ (energy well "1"), see Fig.10.5b). The periodic external force changes its sign with the memory operator output $\Psi_{\alpha\beta} = 0$. Following

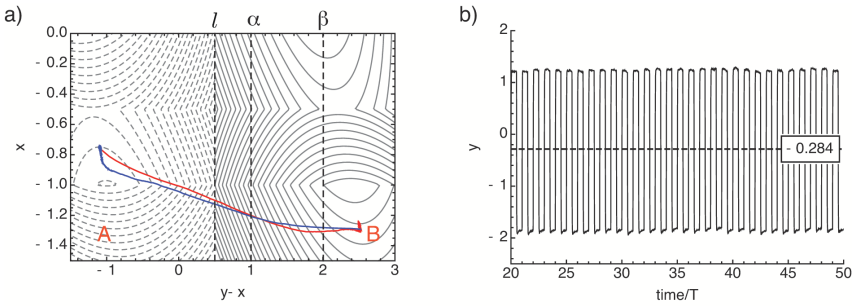

Figure 10.4. The XY-tilted model with memory control operator in the hard device configuration with $z = 0$. a) With solid black lines we depict the level set representation of the energy landscape in the positive phase of rocking and with dashed black lines –the same landscape in the negative phase of rocking. The average motor trajectory plotted by the thick red line during the positive phase of $f_{tilt}(t)$ and by the thick blue line during the negative phase. b) The average tension measured by hard device. The relevant parameters $k_0 = k_1 = 1.5$, $l = 0.5$, $\lambda_1 = 0.5$, $L = 1$, $V_{max} = 1$, $\alpha = 1$, $\beta = 2$ with time period $T = 20$ and amplitude $A = 3.5$ of the rocking force.

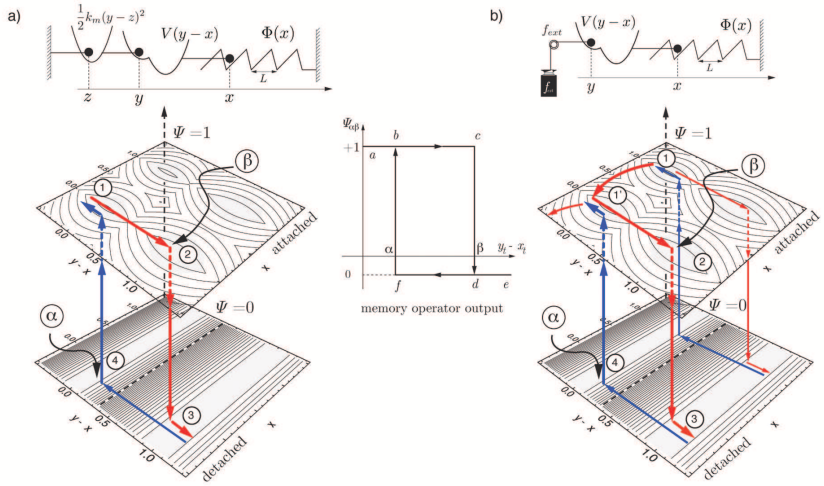

Figure 10.5. The XY-tilted ratchet device with memory control operator. The scheme of the 4-states motor cycle in hard and soft device configurations. a) The motor cycle in the hard device configuration, we can identify the power-stroke in the attached configuration ①→② and the recharging of power stroke in the detached configuration ③→④. We associate each states ①,②,③,④ to the four states of Lymn-Taylor cycle. b) The motor cycle in the soft device configuration. The motor moves in the backward direction along x axe. We identify as the motor forward step with following power-stroke the transition ①→② in the attached configuration, we identify as the recharging of power stroke the transition③→④ in the detached configuration.

the change in the energy landscape the power stroke gets recharged. As soon as the displacement $y_t - x_t$ becomes equal to α, the system passes into the attached state $\Psi_{\alpha\beta} = 1$. This means that the motor returns into the initial configuration and the cycle can start again.

Similar mechanical cycle in the hard device can be described as follows:

- ①→②. We start at the end of the negative phase of the tilting $f_{tilt}(t)$ when our

configurational particle explores the energy well "0". The system is in the attached state and $\Psi_{\alpha\beta} = 1$. Then $f_{tilt}(t)$ changes the sign to positive. The bi-stable element goes through a transition ①→② which we identify with the power stroke Fig.10.5a) .

- ②→③. As soon as the displacement $y_t - x_t$ reaches the threshold β, the system passes into the detached state with $\Psi_{\alpha\beta} = 0$. During the positive phase of tilting $f_{tilt}(t)$ the motor finishes the power stroke advancing into the well "1".
- ③→④. We now are in state ③ (energy well "1"), see Fig.10.5a). The periodic force changes sign again and the energy landscape becomes tilted in the opposite direction with the memory operator output equal to $\Psi_{\alpha\beta} = 0$. In response to the new driving force the power stroke mechanism is getting recharged.
- ④→① As soon as the displacement $y_t - x_t$ becomes equal to α, the system passes into the attached state $\Psi_{\alpha\beta} = 1$. Therefore during the negative phase of tilting $f_{tilt}(t)$ the motor finishes the recharging of the power stroke ending up in the well "1". Therefore the motor returns into its initial configuration and the cycle can start again.

We observe that in the conventional Brownian ratchet we need to brake spatial symmetry in order to obtain a directional motion. The system introduced in this chapter is different: it advances on a fully symmetric two-dimensional energy landscape. Here the phase space symmetry is broken by the presence of a memory operator, see Fig.10.6. In fact the defined hysteresis loop id closely related to the displacement $y_t - x_t$ in the effective bi-stable potential, but the mechanics of bi-stable element controlled by the correlated noise term $f_{tilt}(t)$. Notice that by definition, the correlated noise acts in opposite phase on y_t and x_t, see (10.5). In this way the memory loop not implicitly correlated with rocking mechanism $f_{tilt}(t)$. Why we obtain the paradoxical situation, in the system characterized by symmetric potentials $\Phi(x)$ and $V(y-x)$ the direction of the average motion is defined by the particular configuration of the hysteresis loop.

In fact, we can define two symmetric hysteresis operators: in the first case the attached state is associated with the well A of the bistable potential and in the second case the attached state is associated with the well B. We can then select the thresholds in a symmetric way $\alpha = -\beta$. In the ratchet system with the memory operator of the first type, see the top trajectory in Fig.10.6c), the motor moves in the forward direction along x axis. Instead, in the ratchet system with the memory operator of the second type, see the bottom trajectory in Fig.10.6c), the motor moves in the backward direction. This shows that the configuration of the memory operator output fully determines the direction of the averaged motion. Note what the four-state structure of the motor cycle is preserved in both types of hysteretic coupling.

10.3 Conclusions

By introducing a hysteretic coupling between the power stroke element and the attachment mechanism we obtained a model of molecular motor whose direction of motion is controlled solely by the orientation of the hysteretic loop. This idea may be useful outside the domain of muscle mechanics because the proposed mechanism of the rectification of thermal noise appear to be new.

In the muscle context, the strong point of the new approach is that it allows one to explicitly introduce into the mechanical model all for distinct chemical states constituting

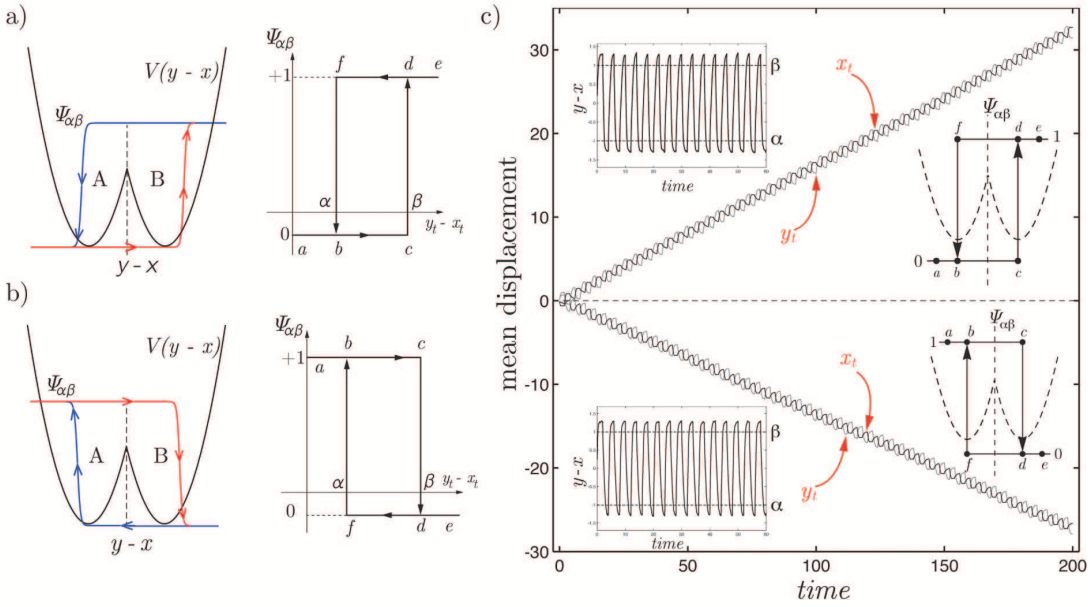

Figure 10.6. The nature of asymmetry introduced by operator $\widehat{\Psi}_{\alpha\beta}$. a) The particle moves from the well A into the well B (solid blue arrows) during the detached configuration, which now associated to positive phase of rocking. The motor moves from the well B into the well A (solid red arrows) during the attached configuration, which now associated to negative phase of rocking. b) The Brownian particle moves from the well A into the well B (the solid red arrows) during the attached configuration, which associated to the positive phase of rocking. The motor moves from the well B into the well A (the solid blue arrows) during the detached configuration, which associated to the negative phase of rocking. c) The system characterized by symmetric space periodic potential $\Phi(x)$ and symmetric double well potential $V(y-x)$. We define the output of hysteresis operator $\Psi_{\alpha\beta}$ by symmetric values $\alpha = -\beta$. Numbers α and β correspond to "down" and "up" switching value of input signal. We assume two distinct choices of output of hysteresis operator. The relevant parameters $k_0 = k_1 = 1.5$, the minima of bistable element in $-0.5,\ 0.5$ so $l = 0$ and $\lambda_1 = 0.5,\ L = 1,\ V_{max} = 1,\ \alpha = -1,\ \beta = 1$ with time period $T = 5$ and amplitude $A = 2.5$ of the rocking force.

the basic biochemical Lymn-Taylor cycle. Such chemo-mechanical identification opens new perspectives in the physical understanding of the fundamental mechanics hidden behind the existing chemo-mechanical models.

The memory operator, introduced in this chapter, can be viewed as an attempt of a $1\mathbb{D}$ description of the most elementary steric effect associated with myosin /actin interaction. The origin of this effect lies in the fact that the power stroke is accompanied by the separation of the actin myosin from the myosin head while the recharging of the power stroke element leads to the myosin head coming closer to the actin filament. The hysteretic nature of such effective coupling originates from the fact that not only the current state of the power stroke matters but also whether it is in the phase of the strike or in the phase of the recharging. This may mean that in realistic $3\mathbb{D}$ settings the two processes, the strike and the recharge, are not exactly symmetric which is difficulty to represent explicitly in the $1\mathbb{D}$ projection.

General discussion and conclusions

In this Thesis, we developed a new mathematical model simulating force-generating mechanical behavior of myosin II in skeletal muscles. The proposed model provides the first purely mechanical description of both the power-stroke and the attachment-detachment process. It reproduces all four main stages of the biochemical Lymn-Taylor cycle without any reference to chemical states. To evaluate mechanical efficiency of the resulting engines we used a simple methodology of stochastic energetics allowing one to analyse the energy transduction associated with different motor designs. This approach is complementary to the more conventional biochemical energetics which is commonly used to evaluate efficiency of the myosin cycle.

We first suppressed the power stroke and presented a thorough study of the rocking ratchet model adapted to the modeling of the myosin/actin interaction. We focused on the important difference between the soft and hard device loading configurations which remained undervalued in the purely biochemical models. We then suppressed the attachment-detachment and developed a separate theory of the power stroke driven contractions in soft and hard device configurations. As a biproduct of this analysis we developed a new understanding of the tension-length curve for a tetanized sarcomere in isometric conditions.

To model the full cross-bridge mediated actin-myosin interaction we proposed a general three dimensional phase space framework coupling a periodic potential with a bistable potential. In this framework the periodic potential represents myosin/actin interaction; the conformational change responsible for the power stroke is described by a double-well potential. The internal driving, which represents the ATP activity, is represented as a time periodic force with zero average. The correlations associated with this signal reflects the nonequilibrium nature of the external reservoir.

Depending on the particular subunit where the external correlated force is applied, we defined three archetypal designs of our thermal ratchet machinery. By localizing the effect of the periodic rocking in these three different settings on a single internal degree of freedom, we obtained X-tilted, Y-tilted and XY-tilted models:

- The X-tilted motor is the simplest arrangement where the external activity is concentrated in the actin filament. We have shown that with X-tilted design one cannot simulate the full $4-state$ Lymn-Taylor cycle because the detachment and the recharge of the power stroke element are always combined. This model undermines the role of the power stroke by treating it as a passive component of the contraction mechanism. In addition, this model does not treat adequately the detached state of the acto-myosin system.

- In the Y-tilted model the correlated noise acts on the internal variable located inside the power stroke mechanism making both the power stroke and the actin filament

active. The resulting ratchet performs 4-state cycle in the soft device and either 2-state or 4-state cycle in the hard device. This means that the proposed framework is capable of mimicking the complete Lymn-Taylor cycle however the interpretation of such internal solicitation in term of the molecular structure of the cross-bridges remains ambiguous.

- XY-tilted model can be viewed as a ratchet system which is driven entirely through the activity concentrated in the power stroke element while the actin filament is treated as passive. This interpretation is compatible with the physiological perception that it is the power stroke which is the active element behind muscle contraction. By treating the power stroke as the primary agent we view the attachment detachment is a secondary process ensuring the translational character of the motion. This model generates 3-state cycle which remain only partially compatible with the existing biochemical models.

While the XY tilted ratchet is a viable mechanical analog of the Lymn-Taylor cycle, we still have an ambiguity in the interpretation of the detached state which is not explicitly present in the proposed model. In all discussed models the detached state is represented as a maximum of the periodic and therefore the detachment is always associated with a horizontal displacement and takes place very quickly. Therefore we proposed two synthetic models where the XY tilted ratchet mechanism is augmented by taking into consideration the explicit steric separation of thick and thin filaments:

- In the first model a multiplicative ramp type control $\Psi(y-x)$ is applied to space-periodic potential $\Phi(x)$. We associated the pre-power stroke with a detached state (no interaction with the spatial periodic potential $\Phi(x)$) and the post power stroke – with the attached state (the system interacts strongly with the space periodic potential $\Phi(x)$). In this way the detached state is fully integrated into the mechanical cycle. As the result the proposed model reproduces all four states of the Lymn-Taylor cycle even though the individual states are interpreted as transient mechanical configurations. Most importantly, in this model the conformational state of the power stroke mechanism regulates the distance of the myosin head form actin filament.

- In the second model we introduced a ratchet system with a hysteretic memory control operator which allows one to associate particular mechanical configurations with all four states of the Lymn-Taylor cycle with full confidence. By introducing such delayed coupling between the power stroke element and the attachment mechanism we obtained a model of molecular motor whose directional of motion is controlled solely by the orientation of the hysteretic loop. The memory operator can be viewed as an attempt of a $1\mathbb{D}$ description of the most elementary steric effect associated with myosin /actin or kinesin/microtubule interaction. The origin of this effect lies in the fact that the power stroke is accompanied by the separation of the actin myosin from the myosin head while the recharging of the power stroke element leads to the myosin head coming closer to the actin filament. The hysteretic nature of such effective coupling originates from the fact that the actin potential feels not only the current state of the power stroke matters but also whether it is in the phase of the strike or in the phase of the recharging.

In summary, we have shown that a very simple mechanical system is able to generate complex stochastic motion, which is close to what is observed during muscle contractions. Starting from the existing approach of rocking ratchets and reinventing it in the

framework of the power stroke activity , we were able to unify the description of a single processive molecular motor such as kinesin, with the description of the collectively operating non-processive molecular motors such as myosin. In this way we built a bridge between theoretical description myosin and kinesin motors that have so far been treated as completely different. One can say that our "kinesin-like" myosin is a mutant one-leg ratchet device jumping under strong power-stroke pushes from one attached site to another while transporting cargo. The next stage of the modeling should include a study of the collectively operating myosin motors, see Fig.10.7

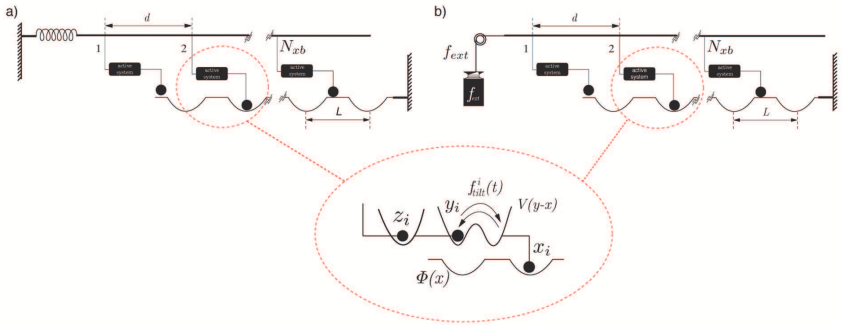

Figure 10.7. The scheme of collective model in hard and soft device incorporating N_{xb} single cross-bridge each based on the power stroke driven thermal ratchet framework. Probably, the one possible way describe the functional half-sarcomere. a) The hard device configuration. b) The soft device configuration.

Using the proposed framework we can explore the possibility to match the real experimental measurements done in vitro. This requires filtres the values of the parameters using the experimental data and in this way we should be able obtain not only qualitative but also quantitative results. Most importantly, given the purely mechanical nature of our modeling, one can consider building the actual artificial molecular size devices based on the principles developed in this work.

Appendix A

Theoretical background

In this section we review several important technical tools from the theory of stochastic differential equations which we later use to study particular models of the power stroke. In particular, we discuss the interpretation of solutions of a Langevin equation, the formalism of Fokker-Plank equation, the numerical methods for solving stochastic differential equations, the energetics of a stochastic system and the basics of the theory of Brownian ratchets. This prepares us for the study of the power stroke element which we view is a mechanical system with few degrees of freedom subjected to a thermal noise and described by a system of stochastic differential equations. In contrast to white noise a molecular motor is also subjected to correlated noise which characterizes the nonequilibrium nature of the environment and allows the motor to extract useful energy from this environment.

A.1 Langevin equation

Langevin equation was originally proposed for the description of free Brownian motion. More recently it is viewed as a universal way to describe the mechanics of a small object in contact with a large system in thermal equilibrium. There are particular situations where the Langevin equation can be derived rigorously from a microscopic model, for instance when a heavy particle interacts with an infinite number of light particles and there is a clear separation of time scales. More often this equation is simply postulated without any reference to the particular Hamiltonian system at a smaller scale.

A general Langevin equation in multidimensional case with a configuration described by a vector $\mathbf{q} = q_1, q_2 \ldots, q_n$ can be written as :

$$\frac{dq_i}{dt} = F_i(\mathbf{q}) + \Gamma_i(t) \tag{A.1}$$

where $\mathbf{F} = F_1, F_2 \ldots, F_n$ is the deterministic force. The stochastic Langevin force is expressed as an additive white noise $\mathbf{\Gamma}(t) = \Gamma_1(t), \Gamma_2(t), \ldots, \Gamma_n(t)$ where

$$\begin{aligned} \langle \Gamma_i(t) \rangle &= 0, \\ \langle \Gamma_i(t)\Gamma_j(s) \rangle &= D_{ij}\delta(t-s). \end{aligned} \tag{A.2}$$

Instead of following stochastic trajectories directly one can instead study the evolution of the probability density function $P(\mathbf{q}, t)$ which is described by the Fokker-Planck equation

$$\frac{\partial P(\mathbf{q},t)}{\partial t} = -\sum_i \frac{\partial}{\partial q_i}\left[F_i P(\mathbf{q},t)\right] + \frac{1}{2}\sum_{ij} D_{ij}\frac{\partial^2 P(\mathbf{q},t)}{\partial q_i \partial_j q}. \tag{A.3}$$

The equation (A.1) simplifies if the Langevin force has only diagonal term, $D_{ij} \sim 2D_i\delta_{ij}$. Then we can write

$$\frac{dq_i}{dt} = F_i(\mathbf{q}) + \sqrt{2D_i}\ \xi_i(t) \tag{A.4}$$

where we used the standard Gaussian white noise $\xi(t)$ with the properties

$$\begin{aligned} \langle \xi_i(t) \rangle &= 0, \\ \langle \xi_i(t)\xi_j(s) \rangle &= \delta_{ij}\delta(t-s) \end{aligned} \tag{A.5}$$

Consider an inertial system subjected to the potential $V(x_1, x_2, \ldots, x_N)$. The corresponding Langevin equation reads:

$$\begin{cases} \dfrac{dx_i}{dt} = v_i, \quad i = 1, 2, \ldots, d \\ m\dfrac{dv_i}{dt} = -\eta_i v_i - \dfrac{\partial V(x_1, \ldots, x_N)}{\partial x_i} + \sqrt{2D_i}\ \xi_i(t) \end{cases} \tag{A.6}$$

where the state vector consists of d components of displacement x_i and d components of velocity v_i and η_i are the coefficient of viscous friction. The diffusion coefficients D_i must satisfy the fluctuation-dissipation relationships

$$D_i = \eta_i k_B T, \tag{A.7}$$

where T is the temperature. For a single particle we can rewrite

$$\frac{dv}{dt} = -\frac{\eta}{m}v + \frac{\eta}{m}\sqrt{\frac{2k_BT}{\eta}}\xi(t) \tag{A.8}$$

Here we made apparent the inertial time scale

$$\tau_0 = \frac{m}{\eta} \tag{A.9}$$

After direct integration and taking the average we can express the mean value of velocity as:

$$\langle v(t) \rangle = v(0)\exp(-\frac{t}{\tau_0}) \tag{A.10}$$

where $v(0)$ is defined by the initial conditions. For large t, the velocity distribution converges to Maxwell distribution with time scale τ_0. Using the known Stokes relation from fluid mechanics, see [65], we can estimate the value of this time scale. For simplicity, we consider the colloidal particle of radius r, with density ρ and assume that the viscosity of fluid is η. Trough simple geometric consideration, we express the drag coefficient $\eta = 6\pi\zeta r$ and the mass $m = \frac{4}{3}\pi\rho r^3$. From these relations we can find that

$$\tau_0 = \frac{2}{9}\frac{\rho}{\zeta}r^2 \tag{A.11}$$

Notice that τ_0 is proportional to the square of particle radius which lowers τ_0 significantly when we leave the macroscopic word. Thus, at $r = 100nm$, comparable to myosin, we take the water viscosity at $20°C$ approximatively equal to one centipoise, $\zeta_{water} = 10^{-9}g/(nm\ s)$, and using the density of latex $960kg/m^3$ for $\rho_{latex} \approx 10^{-21}g/nm^3$,we estimate the inertial time scale to be $\approx 2,2 \times 10^{-9}s$ which is much smaller than the time scale of motor reaction cycle $\approx 10^{-3}s$.

Consider now a particle under the action of the potential $V(x)$. The provided demonstration was performed by H.Wang, [125].

We are interested, typically, in the time scale of chemical reaction. Let us show the consequences of the limit $\tau_0 \to 0$ on Langevin equation with inertia. To generalize our case we introduce in the Langevin equation with inertial term and we introduce the potential $V(x)$, have,

$$\frac{dv}{dt} = -\frac{1}{\tau_0}\left[v + \frac{D}{k_B T}\partial_x V(x) - \sqrt{2D}\xi(t)\right] \tag{A.12}$$

we consider a model equation for velocity

$$\frac{dv}{dt} = -\frac{1}{\tau_0}\left[v - g(t)\right] \tag{A.13}$$

taking the limit of exact solution for $\tau_0 \to 0$

$$v(t) = g(t) + \exp\left(-\frac{t}{\tau_0}\right)[v(0) - g(0)] + \frac{1}{\tau_0}\int_0^t \exp\left(-\frac{t-s}{\tau_0}\right)[g(s) - g(t)]dt \tag{A.14}$$

ans the term with exponential goes to zero at the limit $\tau_0 \to 0$

$$\lim_{\tau_0 \to 0} v(t) = g(t) \tag{A.15}$$

we can identify the function $g(t)$ by

$$g(t) = -\frac{D}{k_B T}\partial_x V(x) + \sqrt{2D}\xi(t) \tag{A.16}$$

we see that for limit $\tau_0 \to 0$ the solution of equation (A.12) satisfy the relation

$$v = \frac{dx}{dt} = -\frac{D}{k_B T}\partial_x V(x) + \sqrt{2D}\xi(t) \tag{A.17}$$

or we can rewrite the equation in familiar form:

$$\frac{dx}{dt} = \frac{1}{\eta}\left(-\partial_x V(x) + \sqrt{2k_B T\eta}\xi(t)\right) \tag{A.18}$$

which is the overdamped Langevin equation. The limit $\tau_0 \to 0$ called Einstein-Smoluchowski, and the time scale τ_0 is a Smoluchowski limit. This equation signify that If we interested in the behavior for the time scales much larger than τ_0, we can safely ignored the effect of inertia – the high-friction. This will be our main modeling tool in what follows.

A.2 Stochastic differential equations

Notice that in our Langevin equation (A.18), the white noise term can be viewed as a derivative of a Wiener process [23]. It is then natural to rewrite (A.18) as the Stochastic Differential Equation (noted SDE):

$$dX_t = \frac{1}{\eta}\left(-\partial_x V(X_t)dt + \sqrt{2k_B T\eta}dB_t\right) \tag{A.19}$$

where dB_t is an increment of a Wiener process with variance dt. For numerical application we use $dB_t \sim N(0,1)$.

The task now is to define the stochastic process X_t. For a free particle we have $X_t \sim N(0,1)$ which means that the probability density of X is a normal distribution with zeros mean and variance equal to 1, or in other terms that $P(x) = \sqrt{2\pi}\exp(-t^2/2)$. For a given initial condition $X_0 = x_0$, the solution of (A.19) can be written as

$$X_t = X_0 + \frac{1}{\eta}\left(\int_0^t -\partial_x V(X_t)dt + \sqrt{2k_B T\eta}\int_0^t dB_t\right) \tag{A.20}$$

where, we first interpret the second term as an Itô stochastic integral. It is defined on the interval $[0,t]$ with a given partition $t_1,\ldots,t_n$ as follows

$$\int_0^t f(t)dB_t = m.s.\lim_{n\to\infty}\left[\sum_{i=1}^{n} f(t_{i-1})(B_{t_i} - B_{t_{i-1}})\right] \tag{A.21}$$

where the essential properties of the increment dB^t are:

$$\int_{t_i}^{t_{i+1}} (dB_t)^2 = t_{i+1} - t_i; \quad \int_{t_i}^{t_{i+1}} (dB_t)^{n+2} = 0, \quad n > 0 \tag{A.22}$$

We can also consider a more general form of SDE:

$$dX_t = a(X_t,t)dt + b(X_t,t)dB_t \tag{A.23}$$

whose formal solution can be written in the form:

$$X_t = X_0 + \int_0^t a(X_t,t)dt + \int_0^t b(X_t,t)dB_t \tag{A.24}$$

The integral in the last term can also be defined following either Stratonovich as

$$\int_0^t b(X_t,t)\circ dB_t \backsimeq \sum_n \left(\frac{b(X_{t_{n+1}},t_{n+1}) + b(X_{t_n},t_n)}{2}\right)\left(B_{t_{n+1}} - B_{t_n}\right) \tag{A.25}$$

and following Itô as

$$\int_0^t b(X_t,t)\cdot dB_t \backsimeq \sum_n b(X_{t_n},t_n)\left(B_{t_{n+1}} - B_{t_n}\right). \tag{A.26}$$

The difference of two schemes is the choice of a point, where we define the value of the function $b(X_t,t)$. In the Itô approach we take the left point of interval and in the Stratonovich– the middle point of interval. To understand the difference we can compute the integral of a known function, for example of a Brownian motion W_t. The Stratonovich integral gives

$$\begin{aligned}\int_0^\tau B_t\circ dB_t &\backsimeq \sum_{n=0}^{N-1}\left(\frac{B_{t_{n+1}} + B_{t_n}}{2}\right)\left(B_{t_{n+1}} - B_{t_n}\right) = \\ &= \frac{1}{2}\sum_{n=0}^{N+1} {B^2}_{t_{n+1}} - {B^2}_{t_n} = \frac{1}{2}{B^2}_{\tau}\end{aligned} \tag{A.27}$$

The Itô integral gives a different result

$$\begin{aligned}\int_0^\tau B_t \cdot dB_t \backsimeq \sum_{n=0}^{N-1} B_{t_n}\left(B_{t_{n+1}} - B_{t_n}\right) = \\ = \frac{1}{2}\sum_{n=0}^{N-1}\left(\left({B^2}_{t_{n+1}} - {B^2}_{t_n}\right) - \left(B_{t_{n+1}} - B_{t_n}\right)^2\right) = \\ = \frac{1}{2}\left({B^2}_\tau - {B^2}_0\right) - \frac{1}{2}\sum_{n=0}^{N-1}\left(B_{t_{n+1}} - B_{t_n}\right)^2\end{aligned} \tag{A.28}$$

Here we can interpret the term under the sum as $B_{t_{n+1}} - B_{t_n} = \sqrt{\Delta t} G_n$, where with G_n we denote the Gaussian distribution. Then the second term in the left hand side of the last equation takes the form $\frac{\tau}{2}\frac{1}{N}\sum_{n=0}^{N-1} {G^2}_n$. As we know the limit $\lim_{N\to\infty}\frac{1}{N}\sum_{n=0}^{N-1}{G^2}_n \to 1$ and therefore

$$\int_0^\tau B_t \cdot dB_t \backsimeq \sum_{n=0}^{N-1} B_{t_n}\left(B_{t_{n+1}} - B_{t_n}\right) = \frac{1}{2}{B^2}_\tau - \frac{\tau}{2} \tag{A.29}$$

The use of these two different integration schemes is not just a mathematical trick to solve a particular SDE, but it can also emerge naturally in the modeling of physical phenomena,[62]. For instance, in same physical systems, white noise processes is usually used as a limit of a correlated or colored noise. In those cases the Stratonovich interpretation may be appropriate for limiting stochastic differential equation obtained by replacing the real noise by the Wiener process. On the other hand, real processes are often discrete: the events may be happening at discrete time moments and the system can be spatially discrete as well. In those cases Itô integral provides more natural approximation of the real process. In this Thesis, all stochastic differential equation will be interpreted as Itô stochastic differential equations. Even if Stratonovich interpretation is used to do the computations which are easier in this case, the final expressions will be always given in the Itô's formulation.

To build a link between the two formulations we can use a result known as Itô formula or Itô lemma . Consider an arbitrary function f of a stochastic variable X^t interpreted as a solution of a general SDE. The Itô formula describes the change of variables in the context of stochastic differential equations:

$$df(X_t) = \left[a(X_t,t)\frac{\partial}{\partial_x}f(X_t) + \frac{1}{2}[b(X_t,t)]^2\frac{\partial^2}{\partial_{x^2}}f(X_t)\right]dt + b(X_t,t)\frac{\partial}{\partial_x}f(X_t)dB_t \tag{A.30}$$

By applying this formula one can show that, see [23]:

- If we use the Itô SDE:

$$dX_t = a(X_t,t)dt + b(X_t,t)dB_t \tag{A.31}$$

  the corresponding Stratonovich SDE is:

$$dX_t = \left[a(X_t,t) - \frac{1}{2}b(X_t,t)\partial_X b(X_t,t)\right]dt + b(X_t,t)\circ dB_t \tag{A.32}$$

- If we use the Stratonovich SDE

$$dX_t = a(X_t,t)dt + b(X_t,t)\circ dB_t \tag{A.33}$$

the corresponding Itô SDE is:

$$dX_t = \left[a(X_t,t) + \frac{1}{2}b(X_t,t)\partial_X b(X_t,t)\right]dt + b(X_t,t)dB_t \tag{A.34}$$

Usually,a stochastic process X_t can be describe either by a stochastic differential equation , say the Langevin equation, or by the Fokker-Planck formalism based on the description of the probability distribution for the process X_t. Let's us associate with random variable X_t at each time t, the probability density $P(x,t) > 0$ with normalization $\int P(x,t) = 1$. We can write

$$\frac{d}{dt}\langle f(X_t)\rangle = \int_x f(x)\frac{dP(x,t)}{dt}dx = \int_x \frac{1}{\eta}\left[-\partial_x V(x)f(x) + k_B T\partial_{xx}f(x)\right]P(x,t)dx \tag{A.35}$$

which after integration by parts and discarding the surface terms gives:

$$\int_x f(x)\frac{dP(x,t)}{dt} = \int_x f(x)\frac{1}{\eta}\left[\partial_x[V(x)p(x,t)] + k_B T\partial_{xx}P(x,t)\right]dx \tag{A.36}$$

Since this equality is true for arbitrary $f(x)$, we obtain the (forward) Fokker-Planck equation:

$$\frac{d}{dt}P(x,t) = \frac{1}{\eta}\left[\frac{\partial}{\partial x}\left[V(x)P(x,t)\right] + k_B T\frac{\partial^2}{\partial x^2}P(x,t)\right] \tag{A.37}$$

with the initial condition $P(x, t = t_0) = P_0(x)$.

The two problems (A.19) and (A.37) are equivalent under the condition that $\partial_x V(x)$ is Lipschitzian and that there exist $C \in \mathbb{R}$ such that $\partial_x V(x) \leq C(1 + |x|)$. There exists a number of numerical methods to solve the problem of finding $P(x,t)$ by using both approaches [62]. Once the solution of (A.37) is found we can express the average as:

$$\langle x(t)\rangle = \int_x xP(x,t)dx \tag{A.38}$$

where $P(x,t)$ is the solution of (A.37).

A.3 Numerical solution of SDEs

Through the direct numerical simulation of the Langevin equation we can find the time series recording motor positions. In numerical simulation we need to consider a time-discretized version of the stochastic equation by introducing a time step Δt. This step has to be much shorter than the characteristic time scale of dynamics. We begin with now classical Milstein scheme, which in one-dimensional case takes the form

$$\begin{aligned} X_{n+1} =& X_n + \left(a(X_n,n) - \frac{1}{2}b(X_n,n)\partial_x b(X_n,n)\right)\Delta t + \\ &+ b(X_n,n)\Delta B + \frac{1}{2}b(X_n,n)\partial_x b(X_n,n)\Delta B^2 \end{aligned} \tag{A.39}$$

where ΔB is an increment of the Wiener process and is therefore a Gaussian random variable which we denote $N(0,\Delta t)$. In our case $b(X_n,n) = Const$ and the Milstein scheme reduces to a simple Euler-Maruyama scheme:

$$X_{n+1} = X_n + a(X_n,n)\Delta t + b\Delta B \tag{A.40}$$

We are interested in computing the average position of our random variable in discrete moments t_i :

$$\langle x(t_i)\rangle = \frac{1}{N_\mathrm{r}} \sum_{j=1}^{j=N_\mathrm{r}} x_{t_i}^j \tag{A.41}$$

where N_r is the number of realizations, with each realization starting from the same initial conditions; t_i is the discrete numerical time:

$$t \in [0, \Delta t, 2\Delta t, ..., N\Delta t] \tag{A.42}$$

where N is number of time step of numerical simulation.

The direct Langevin simulations give us access to the characteristics of the single motor trajectory-path. Instead we could also solve numerically the Fokker-Planck equation by using, for instance, the finite element method. In the finite elements method, the numerical cost increases exponentially with the dimension d of the phase space (the dimension of the discretization grid), thus they are not adapted for solving problems with $d > 3$. In our case $d \approx 3$ and therefore in most cases we had to deal directly with stochastic dynamics. However, were it is necessary we also show the results obtained by the Fokker Plank method and in fact all principal results have been verified by both methods.

In most of the cases, where the drift and diffusions are sufficiently smooth, the convergence of the Euler scheme for Langevin dynamics with the order 0.5 is guaranteed. In our case, we achieved a good numerical convergence and good interval confidence with $\Delta = 1.0 \times 10^{-4} - 1.0 \times 10^{-3}$ and with $N_r \approx 10^3 - 10^4$. In some cases it is advantageous to use higher order schemes, for instance, Runge-Kutta scheme, which give more stable results and have same other advantages [57]. This scheme is preferred in the case of non constant drift coefficient or if we need to achieve high precision around extrema of the potentials, however, in our case we found the simplest algorithm fully adequate.

Through numerical simulations we have access to the detailed behavior of the motor at a given instant t_i. One of the most important mechanical quantities what we need to characterize is the average velocity of the motor. Several numerical definition of the instantaneous velocity can be given. For instance, it can be viewed as a numerical derivative:

$$v_i = \frac{X_{t_{i+1}} - X_{t_i}}{t_{i+1} - t_i} \tag{A.43}$$

where X_{t_i} is the position of the motor at time t_i of obtained by the numeric approximation of stochastic process X_t. In fact, we are interested in the average value in stationary regime over different realizations and we must therefore also average along the trajectory

$$\langle v\rangle = \frac{1}{N-1}\sum_{i=1}^{N-1} v_i = \frac{1}{N-1}\frac{1}{N_r}\sum_{i=1}^{N-1}\sum_{j=1}^{N_r} \frac{x_{t_{i+1}}^j - x_{t_i}^j}{t_{i+1} - t_i} \tag{A.44}$$

As we use the numerical scheme with a constant time step Δt, we can give an alternative definition of motor velocity:

$$\langle v^\star\rangle = \frac{\sum_{i=1}^{N} X_{t_i}}{\sum_{i=1}^{N} t_i} = \frac{2\sum_{i=1}^{N} X_{t_i}}{N(N+1)\tau} = \frac{l^\star}{\tau^\star} \tag{A.45}$$

were we introduced an apparent characteristic length, $l^\star \equiv \frac{2}{N(N+1)} \sum_{i=1}^{N} X_{t_i}$, traveled by the motor during the time interval τ. In this way we defined the average velocity relatively

to the "center of mass" of a generated set of trajectories. In this Thesis we retained the definition based on the average instantaneous velocity which is better adopted to mechanical interpretation . In the steady state this definition exhibits the following useful property:

$$\langle v \rangle = \frac{X_{t_f} - X_{t_i}}{t_f - t_i} \tag{A.46}$$

where X_{t_f} is the motor position at the final time instant t_f, and X_{t_i} the motor position at initial time instant t_i.

A.4 The typical problem

A typical stochastic problem which we address in our study is characterized by the following ingredients:

- A random source of fluctuations modeled as a Gaussian noise,and representing the action of a thermal bath.
- Spacial and temporal periodicity, which reflects cycling functionality of our system. Either space or time symmetry must be broken in order to generate the ratchet effect.
- All acting forces vanish after averaging over space, time, or corresponded statistical ensembles.
- The detailed balance symmetry must be a broken which positions the system out of equilibrium.

The spatial symmetry breaking is the central concept in the understanding of the motion generation in ratchet systems [97] and we illustrate it by considering a simple one dimensional overdamped Langevin equation

$$\frac{dx}{dt} = -\partial_x V(x) + f_{tilt}(t) + \sqrt{2D}\xi(t) \tag{A.47}$$

where $V(x)$ is a periodic potential, the term $\sqrt{2D}\xi(t)$, modeling thermal fluctuations, is a Gaussian white noise with zero average and time correlations $\langle \xi(t)\xi(s) \rangle \equiv 2D\delta(t-s)$, for $t > s$. We recall that in thermal equilibrium, a Brownian particle cannot exhibit a systematic drift in one preferential direction, due to the second law of thermodynamics and therefore we added a correlated tilting force $f_{tit}(t)$ which places the system out of thermal equilibrium. This function may be a fully deterministic periodic signal in time or a stochastic process. The tilting force is zero if averaged over time averaging or over the corresponding ensemble. The space periodic potential with the period L is symmetric if

$$V(x) = V(-x). \tag{A.48}$$

Similarly, the periodic tilting force of period T is symmetric if

$$-f_{tilt}(t) = f_{tilt}(t + \frac{T}{2}) \tag{A.49}$$

Consider a steady state defined by (A.47) for a symmetric potential $V(x)$ and a symmetrical periodic force $f_{tilt}(t)$. We are interested in the average particle velocity over a long time and consider only a stationary process. We therefore define the average velocity by

$$\langle \frac{dx}{dt} \rangle = \langle \dot{x} \rangle = \lim_{t_f - t_0 \to \infty} \frac{x(t_f) - x(t_0)}{t_f - t_i} \tag{A.50}$$

Introduce the new variable $z(t)$

$$z(t) = -x(t + \frac{T}{2}) \tag{A.51}$$

Taking in consideration the definition (A.50) we find that the time average current $\langle \dot{z(t)} \rangle$ satisfy

$$\langle \dot{z(t)} \rangle = -\langle \dot{x(t)} \rangle \tag{A.52}$$

On the other hand if we consider (A.47) for $x(t)$ we can see that $z(t)$ satisfies the same equation. Therefore

$$\langle \dot{z(t)} \rangle = \langle \dot{x(t)} \rangle \tag{A.53}$$

and it view of the previous line

$$\langle \dot{x(t)} \rangle = 0 \tag{A.54}$$

We conclude what if both the space periodic potential and the periodic driving force are symmetric, there is no ratchet effect. The same conclusion can be reached if both the space periodic potential and the driving force are supersymmetric meaning that $-V(x) = V(x + \frac{L}{2}), \quad -f_{tilt}(t) = f_{tilt}(-t)$ [97]. The non zero current can be therefore expected if either the space periodic potential or the driving force break the symmetry. Moreover, even in the case of a symmetric potential $V(x)$ and a supersymmetric driven force $f_{tilt}(t)$ the nonzero particle current can take place.

The simplest example of a system with an asymmetric potential and symmetric driven force is the saw-tooth like ratchet with time periodic square wave driving proposed by Magnasco [72], which we study in full detail in the next section.

A.5 Stochastic energetics

In this section we present several concepts that are necessary to analyze energetics of various Brownian ratchets. The associated stochastic thermodynamics was developed only in the last decades [100, 86, 101, 67].

We define R as the work done on a system by external forces; negative work $R < 0$ mean that the system does work itself. Suppose that a is an external control parameter affecting the system potential $V(x, a)$ meaning that the system can be manipulated externally trough the variation of a. Then we can write

$$\delta R = \frac{\partial V(x, a)}{\partial a} da \tag{A.55}$$

In addition to work, we can define the energy obtained from the thermal bath which we call heat Q. Since the heat is a form of energy exchange with the thermal bath represented by the two forces $-\eta \frac{dx}{dt} + \sqrt{2\eta k_B T}\, \xi(t)$ we can define the heat as the work that these forces exerts upon the particle advance $dx(t)$. Then we obtain

$$\delta Q \equiv \left(-\eta \frac{dx}{dt} + \sqrt{2\eta k_B T}\, \xi(t) \right) \circ dx(t) \tag{A.56}$$

Here the symbol $\circ$ denotes multiplication in the Stratonovich sense, because the Stratonovich formulation preserves the usual rules of differential calculus. Since the heat is not an exact differential and depends on the trajectory X^t, we use δ instead of d. Now the energy balance can be written as

$$\frac{dG}{dt} = \frac{\delta R}{dt} + \frac{\delta Q}{dt} \tag{A.57}$$

If there is a conservative force applied to the system, it performs the mechanical work

$$dW_{mec} = -f_{ext} \circ dx. \tag{A.58}$$

Then the energy balance can be rewritten as

$$\frac{dU}{dt} + \frac{dW_{\text{mec}}}{dt} = \frac{\delta R}{dt} + \frac{\delta Q}{dt} \tag{A.59}$$

where dU/dt is the derivative of the internal energy of the system.

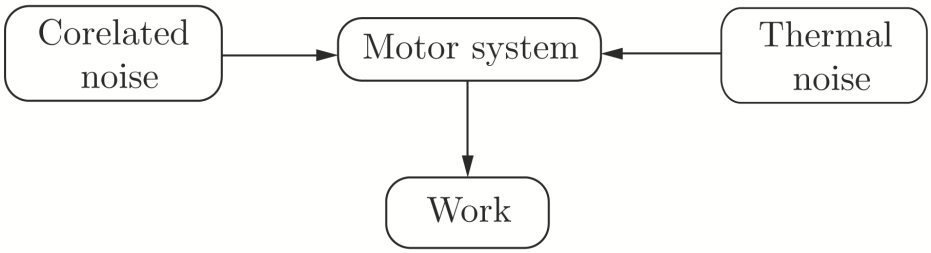

Figure A.1. Energy flow in a thermal Brownian motor in contact with a thermal bath and a color noise bath–the external input of energy

To illustrate these notions consider first a particle described by the inertial Langevin equation:

$$m\frac{dv}{dt} = -\partial_x V(x,t) - \eta v + \sqrt{2\eta k_{\text{B}} T}\xi(t). \tag{A.60}$$

To obtain the energy balance we need to first rewrite (A.60) in the form:

$$dv = \frac{1}{m}\left(-\partial_x V(x,t)dt - \eta v dt\right) + \frac{\sqrt{2\eta k_B T}}{m}\xi(t)dt \tag{A.61}$$

Then using the Itô's formula (A.30) we obtain

$$dv^2 = \frac{1}{m}\left(-\left[\eta v + \partial_x V(x,t)\right]2v + \frac{1}{m^2}\left[\sqrt{2\eta k_{\text{B}} T}\right]^2\right)dt + 2\frac{v}{m}\sqrt{2\eta k_{\text{B}} T}dB(t) \tag{A.62}$$

If we now complete the total differential of the potential $V(x,t)$ we obtain the desired expression of the energy balance:

$$\begin{aligned} m\frac{dv^2}{2} + dV(x,t) = \\ = -\frac{2\eta}{m}\left(\frac{mv^2}{2} - \frac{k_{\text{B}}T}{2}\right)dt + v\sqrt{2\eta k_{\text{B}} T}dB(t) + \partial_t V(x,t)dt. \end{aligned} \tag{A.63}$$

Here we can identify $\delta R = \partial_t V(x,t)dt$ as the work produced externally on the system. If we define the change of total energy of the system as

$$dG = m\frac{dv^2}{2} + dV(x,t) \tag{A.64}$$

we can write

$$\begin{aligned} dG &= -\frac{2\eta}{m}\left(\frac{mv^2}{2} - \frac{k_{\text{B}}T}{2}\right)dt + v\sqrt{2\eta k_{\text{B}} T}\, dB(t) + \partial_t V(x,t)dt \\ &= \delta Q + \delta R \end{aligned} \tag{A.65}$$

Here we identified δQ with

$$\frac{2\eta}{m}\left(\frac{mv^2}{2}-\frac{k_{\mathrm{B}}T}{2}\right)dt+v\sqrt{2\eta k_{\mathrm{B}}T} \tag{A.66}$$

which can be also justified based on the definition (A.56). To this end, we need to replace $-\eta\frac{dx}{dt}+\sqrt{2\eta k_{\mathrm{B}}T}$ by $m\frac{dv}{dt}+\partial_x V(x,t)$ and use the formulas $dx=vdt$ and $\frac{d(v^2)}{2}=v\circ dv$. Then by passing from Stratonovich to Itô calculus and using the we find:

$$\delta Q=-\frac{2\eta}{m}\left(\frac{mv^2}{2}-\frac{k_{\mathrm{B}}T}{2}\right)dt+v\sqrt{2\eta k_{\mathrm{B}}T}\,dB(t) \tag{A.67}$$

if we now take the average over the realization of the white noise we obtain

$$\langle\delta Q\rangle=-\frac{2\eta}{m}\left(\frac{m\langle v^2\rangle}{2}-\frac{k_{\mathrm{B}}T}{2}\right)dt \tag{A.68}$$

This formula shows that the loss or the gain of heat take place only if the velocity distribution is out of equilibrium.

Consider now much larger time scales where one can use an overdamped Langevin description and simply drop the inertia term:

$$\eta\frac{dx}{dt}=-\partial_x V(x,t)+\sqrt{2\eta k_{\mathrm{B}}T}\xi(t) \tag{A.69}$$

If we multiply the left and the right hand sides by dx in the sense of Stratonovich, we obtain

$$\left(-\eta\frac{dx}{dt}+\sqrt{2\eta k_{\mathrm{B}}T}\xi(t)\right)\circ dx(t)=dV(x,t)-\partial_t V(x,t)\circ dt \tag{A.70}$$

Now we can directly write the energy balance of system in the form

$$\begin{aligned}\left(-\eta\frac{dx}{dt}+\sqrt{2\eta k_{\mathrm{B}}T}\xi(t)\right)\circ dx(t)+\partial_t V(x,t)\circ dt&=dV(x,t)\\&=\delta Q+\delta R\end{aligned} \tag{A.71}$$

The total change of energy of system is now

$$dG=dV(x,t) \tag{A.72}$$

To find a different expression for the heat term we replace $-\eta\frac{dx}{dt}+\sqrt{2\eta k_{\mathrm{B}}T}\,\xi(t)$ by $\partial_x V(x,t)$, and we rewrite the dx using the expression (A.69):

$$\delta Q=-\frac{1}{\eta}\left(\left(\partial_x V(x,t)\right)^2dt+\sqrt{2\eta^{-1}k_{\mathrm{B}}T}\partial_x V(x,t)\circ dB(t)\right) \tag{A.73}$$

Now, by applying the Itô formula to the term $\partial_x V(x,t)\circ dB(t)$, we obtain

$$\delta Q=-\frac{1}{\eta}\left(\left(\partial_x V(x,t)\right)^2-k_{\mathrm{B}}T\partial_x^2 V(x,t)\right)dt+\sqrt{2\eta^{-1}k_{\mathrm{B}}T}\,\partial_x V(x,t)dB(t) \tag{A.74}$$

Finally by taking the average over all realizations of the stochastic process, we can write

$$\langle\delta Q\rangle=-\frac{1}{\eta}\left[\langle\left(\partial_x V(x,t)\right)^2\rangle-k_{\mathrm{B}}T\langle\partial_x^2 V(x,t)\rangle\right]dt \tag{A.75}$$

We can now generalize the obtained expressions for the system with d degrees of freedom. Consider the vectorial Langevin system:

$$\boldsymbol{\eta}\frac{d\mathbf{X}}{dt} = -\nabla G(\mathbf{X},t) + \boldsymbol{\sigma}\boldsymbol{\xi}(t) \tag{A.76}$$

where $\mathbf{X}$ and $\boldsymbol{\xi}(t)$ are d-dimensional vectors, $\boldsymbol{\eta}$ and σ are positive definite matrices and $\boldsymbol{\xi}(t)$ is the stochastic vector function with the properties

$$\langle \xi_i(t)\rangle = 0, \qquad \langle \xi_i(t)\xi_j(s)\rangle = \delta_{ij}\delta(t-s), \qquad t > s, \quad i,j = 1,2,..,d \tag{A.77}$$

Then the energy lost in the interaction with the thermostat can be written as

$$\delta\mathbf{Q} \equiv \left(-\boldsymbol{\eta}\frac{d\mathbf{X}}{dt} + \boldsymbol{\sigma}\boldsymbol{\xi}(t)\right) \circ d\mathbf{X}(\mathbf{t}) \tag{A.78}$$

while the external energy supply rate takes the form

$$\delta R = \nabla_a G(\mathbf{X},t) \circ d\mathbf{a}. \tag{A.79}$$

A.6 Second Law

In this section we go beyond the energy balance and consider a way to generalize the second law of thermodynamics for our stochastic system which for simplicity we assume to be overdamped. It is natural to define the entropy by the relation

$$S(t) = -k_B \int_\Omega p(x,t)\ln p(x,t)dx, \quad \{x\} \in \Omega \tag{A.80}$$

where $p(x,t)$ is the probability density. The corresponding Fokker-Planck equation can be written in the form:

$$\partial_t p = -\partial_x J(x,t) \tag{A.81}$$

where the function $J(x,t)$ is the probability current:

$$J(x,t) = -\frac{1}{\eta}p(x,t)\left[\partial_x V(x,t) + k_B T\partial_x \ln p(x,t)\right] \tag{A.82}$$

We assume that the functions $p(x,t)$ and $J(x,t)$ haves the appropriate boundary condition so that all surface integral vanish. Then taking the time derivative of (A.90) we obtain

$$\frac{\partial S(t)}{\partial t} = -k_B \int_\Omega J(x,t)\partial_x\left(\ln p(x,t)\right)dx - k_B\int_\Omega p(x,t)\partial_t\left(\ln p(x,t)\right)dx \tag{A.83}$$

we used that $\int_\Omega \partial_t p \ln p dx = \int_\Omega J\partial_x(\ln p)dx$. The second integral in the right side is zero and we can write

$$\frac{\partial S}{\partial t} = -k_B \int_\Omega J(x,t)\partial_x\left(\ln p(x,t)\right)dx \tag{A.84}$$

The time derivative of the average heat flux in the overdamped system reads

$$\frac{\langle \delta Q\rangle}{dt} = \int_\Omega \partial_x V(x,t)J(x,t)dx \tag{A.85}$$

which allows us to write

$$\frac{\partial S(t)}{\partial t} - \frac{1}{T}\frac{\langle \delta Q\rangle}{dt} = \frac{\eta}{T}\int_\Omega \frac{1}{p(x,t)}\left(J(x,t)\right)^2 dx \tag{A.86}$$

To make a connection with the second law of thermodynamics we observe that the right hand side is non negative

$$\frac{\partial S(t)}{\partial t} - \frac{1}{T}\frac{\langle \delta Q \rangle}{dt} \geq 0 \tag{A.87}$$

Similar analysis can be done in the case of inertial Langevin equation. The corresponding Fokker-Planck equation can be written as

$$\frac{\partial p(x,v,t)}{\partial t} = -\partial_x J_x - \partial_v J_v \tag{A.88}$$

where J_x and J_v are the associated probability fluxes

$$\begin{aligned} J_x &= \partial_x (v p(x,v,t)) \\ J_v &= -\frac{1}{m}\left(\partial_x V(x,t) + \eta v + \frac{\eta k_B T}{m}\partial_v \ln p(x,v,t)\right) p(x,v,t) \end{aligned} \tag{A.89}$$

The entropy in phase space $[x, v]$ can be defined as follows

$$S = -k_B \int_\Omega (p \ln p) dx dv, \quad \{x, v\} \in \{\Omega\} \tag{A.90}$$

By computing the time derivative of the average heat flux we obtain

$$\frac{\langle \delta Q \rangle}{dt} = \int_\Omega ((\partial_x E(x,v,t)) J_x + \partial_v E(x,v,t) J_v) dx dv \tag{A.91}$$

and after some manipulation the use of an identity

$$\int_\Omega \left(\partial_x V \partial_v \ln p - v \partial_x p\right) p dx dv = 0$$

we find that

$$\frac{dS}{dt} - \frac{1}{T}\frac{\langle \delta Q \rangle}{dt} = \frac{\eta}{T}\int_\Omega p(x,v,t)\left[v + \frac{k_B T}{m}\partial_v \ln p(x,v,t)\right]^2 dx dv \tag{A.92}$$

Once again, the right side of this expression is not negative and can be associated with dissipation

$$\frac{\partial S(t)}{\partial t} - \frac{1}{T}\frac{\langle \delta Q \rangle}{dt} \geq 0 \tag{A.93}$$

As an application of these results we mention that in such system with constant temperature, we can define the analogue of the Helmholtz free energy F

$$F = \langle G \rangle - TS \tag{A.94}$$

where G is the internal energy. Then the associated second law of thermodynamics can be written as

$$\frac{dF}{dt} - \langle \partial_t V(x,t) \rangle = -T\left(\frac{dS}{dt} - \frac{1}{T}\frac{\langle \delta Q \rangle}{dt}\right) \leq 0 \tag{A.95}$$

where $\langle \partial_t V(x,t) \rangle$ is the rate of energy supply by the external system containing all the ATP related sources.

A.7 Efficiency

In this section we study the efficiency of the energy transformation during one functional cycle of an externally driven Brownian motor. We assume that the motor works in a stationary regime and that the energy balance can be averaged over a cycle. If a motor works against a conservative force then the energy the energy output is the potential energy increase or the mechanical work done against the loads. The input energy is the chemical energy consumed by the motor. Then we can define the mechanical efficiency as follows

$$\epsilon_{mec} = \frac{\langle W_{\text{mec}} \rangle}{\langle R \rangle} \tag{A.96}$$

where the averaging is over one cycle.

The definition (A.96) does not take into consideration that if the motor advances directionally against viscous drag it is also producing useful output. That is why one can also define Stokes efficiency in the case when the cargo is absent as follows [127, 126]

$$\epsilon_{Stokes} = \frac{\eta \langle v \rangle \langle v \rangle}{\langle R \rangle} \tag{A.97}$$

where $\langle v \rangle$ is the average velocity of the motor. Indeed, in this case $R = -Q$. Introduce

$$A = \eta \langle v \rangle^2 \tag{A.98}$$

as the "useful' work of the motor against viscous resistance averaged over a motor time cycle. We can now rewrite the energy balance as

$$0 = R + A + Q - A \tag{A.99}$$

where $Q^\star = Q + A$, can be reinterpreted as the new dissipated heat (with directional component removed) [108, 71]. Then the energy balance can be written as

$$A = R + Q^\star \tag{A.100}$$

which justifies the definition (A.97). Now if the motor system performers a mechanical work, (A.58) against a conservative external load f_{ext} we can rewrite the energy balance as:

$$W_{mec} + A = R + Q^\star \tag{A.101}$$

In this case the full rectifying efficiency takes the form

$$\begin{aligned} \epsilon_{rec} &= \frac{W_{mec} + A}{R} \\ &= \frac{W_{mec} + A}{W_{mec} + A - Q^\star} \end{aligned} \tag{A.102}$$

which is the sum of Stokes efficiency and the mechanical efficiency [108]

$$\epsilon_{rec} = \epsilon_{mec} + \epsilon_{Stokes} \tag{A.103}$$

These definitions will be repeatedly used in this work as the way to access the efficiency of the energy transduction by different motor designs proposed in the Thesis.

A.8 The approximation $2\mathbb{D} \to 1\mathbb{D}$

We look for more light description, for example in soft device, witch consist to use the one-dimensional description instead the two-dimensional, inspiring by the works of T.C. Elston and C.S. Peskin on the motor-cargo system,[19]. The one dimensional form is sufficient complex to presented all proprieties of the model. We can write the general form of the model based on overdamped Langevin equation (5.1) in two dimensional form:

$$\begin{cases} \eta_x \dfrac{dx}{dt} = -\partial_x G(x,y,t) + \sqrt{2\eta_x D}\ \xi_x t \\ \eta_y \dfrac{dy}{dt} = -\partial_y G(x,y,t) + \sqrt{2\eta_y D}\ \xi_y t \end{cases} \tag{A.104}$$

A.8.1 The limit $\gamma_y \to \infty$

We assume that the diffusion of the motor part corresponding to the dynamics in bistable element is a fast process. The stochastical processes y_t comes to equilibrium very fast before the x associate processes has a time to move. So the system can by replaced by the effective dynamics in x coordinate. we can write the associated Fokker-Planck equation to the (A.104)

$$\begin{aligned} \partial_t P(x,y,t) =& \gamma_x\ D\partial_x \left[\frac{P(x,y,t)}{D}\partial_x G + \partial_x P(x,y,t)\right] + \\ & \gamma_y D\partial_y \left[\frac{P(x,y,t)}{D}\partial_y G + \partial_y P(x,y,t)\right] \end{aligned} \tag{A.105}$$

the limit $\gamma_y \to \infty$ get as the possibility associate to stochastical process X_t the probability for any fixed x

$$P(y,t \parallel x) = Z_t^{-1} P_{eff}(x,t) \exp\left(-\frac{G(x,y,t)}{D}\right) \tag{A.106}$$

with normalization factor Z_t

$$Z_t = \int_{-\infty}^{+\infty} \exp\left(-\frac{G(x,y,t)}{D}\right) dy \tag{A.107}$$

This means what, we are associated to the process y_t the measure of probability density

$$y_t \sim Z_t^{-1} \exp\left(-\frac{G(x,y,t)}{D}\right) dy = \mu_{X_t} dy \tag{A.108}$$

in presence we can build the effective dynamics associated to the motor with equilibrated stochastic process corresponded to x variable:

$$dx_{eff} = -\gamma_x \left[b(x^{eff}(x,t),t)\right] dt + \sqrt{2\gamma_x D} dW_t^{x^{eff}} \tag{A.109}$$

where

$$\begin{aligned} b(x^{eff},t) &= \int_{-\infty}^{+\infty} \partial_x G(x,y,t)\mu_{x_t} dx \\ &= \frac{\int_{-\infty}^{+\infty} \partial_x G(x,y,t) e^{-\frac{G(x,y,t)}{D}} dy}{\int_{-\infty}^{+\infty} e^{-\frac{G(x,y,t)}{D}} dy} \end{aligned} \tag{A.110}$$

we can introduce the effective potential Φ_{eff} define as:

$$\phi_{eff}(x,t) = -D \ln \left(\int_{-\infty}^{+\infty} e^{-\frac{G(x,y,t)}{D}} dy \right) \tag{A.111}$$

and the equation (A.109) can be expressed on the form

$$dx = -\gamma_x \partial_x \left[\Phi^{eff}(x,t) \right] dt + \sqrt{2\gamma_x D} dW_t^x \tag{A.112}$$

The equation (A.112) is equivalent to the corresponding Fokker-Planck equation:

$$\begin{aligned} \partial_t P_{eff}(x,t) &= -\partial_x J_{eff}(x,t) \\ J_{eff}(x,t) &= -\gamma_x D \left[\partial_x P_{eff}(x,t) + \frac{P_{eff}(x,t)}{D} \partial_x (\Phi_{eff}(x,t)) \right] \end{aligned} \tag{A.113}$$

This the resulting effective diffusion equation that governs the motion of motor head with averaged rapidly diffusing double-well part dynamics.
In present we can solve by direct numerical simulation the equation (A.112) and deduce form them the characteristic of the system or find numerically the probability distribution function for process y_t from equation (A.113).

A.8.2 The stationary solution

Let us look for stationary solution of (A.113). We can see that the effective potential $\phi^{eff}(x,t)$ satisfies the periodic condition

$$\Phi_{eff}(x + nL, t) = \Phi_{eff}(x) + n\Delta\phi^{eff}, \qquad n \in N \tag{A.114}$$

with

$$\Delta\Phi_{eff} = -f_{ext} L \tag{A.115}$$

So we can see the dynamics (A.113) has the standard form, this is precisely the equation for a particle moving in a tilted periodic potential Φ^{eff}. The stationary probability distribution of (A.113) is periodic in x with period L. Because of the periodicity and after normalization of stationary distribution in the periodicity interval we can express constant probability flux of such system as:

$$J_{eff} = \frac{\gamma_x D}{\alpha \int_0^L e^{\frac{\Phi_{eff}(x)}{D}} dx \int_0^L e^{-\frac{\Phi_{eff}(x)}{D}} dx - \int_0^L e^{-\frac{\Phi_{eff}(x)}{D}} \int_0^x e^{\frac{\Phi_{eff}(x')}{D}} dx' dx} \tag{A.116}$$

where

$$\alpha = \frac{\exp\left(-\frac{\Delta\Phi_{eff}}{D}\right)}{\exp\left(-\frac{\Delta\Phi_{eff}}{D}\right) - 1} \tag{A.117}$$

from (A.116) we can express the average velocity associated to the effective dynamics as:

$$\langle v \rangle = L \int_0^T J_{eff} dt \tag{A.118}$$

A.9 Conclusions

In this section we reviewed several important theoretical concepts [101, 77] which we applied in our analysis. We defined the stochastic process, introduced the concept of stochastic differential equation (Langevin equation) and showed how it can be solved numerically. We also presented an alternative way of analyzing the behavior of stochastic system by studying the corresponding equation for probability density distribution (Fokker-Plank equation). Then we introduced important definitions of of the different energy contributions to the power balance including the outside sources and the heat exchange with a thermostat.

Appendix B

Energetics in $3\mathbb{D}$

In this section we extend the essential results on energetics obtained for the models with $2\mathbb{D}$ energy landscape to the full three-dimensional models describing X-tilted, Y-tilted and XY-tilted ratchets with attached cargo. We show what there is no major differences between the behavior of two-dimensional and three-dimensional models of this type.

In Fig.B.1 we present the general $3\mathbb{D}$ model of a motor placed in the soft loading device. To introduce cargo we need to modify the energy potential by adding a new variable z:

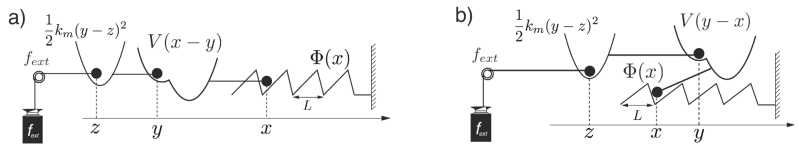

Figure B.1. The sketch of simple $3\mathbb{D}$ soft device, the model of one single cross-bridge adopted as element of collective model used a big number of coupled cross-bridges.

- X-tilted ratchet :

$$G(x,y,z,t) = \Psi(x) + V(y-x) + 1/2k_m(y-z)^2 - xf_{tilt} - zf_{ext} \tag{B.1}$$

- Y-tilted ratchet :

$$G(x,y,z,t) = \Psi(x) + V(y-x) + 1/2k_m(y-z)^2 - yf_{tilt} - zf_{ext} \tag{B.2}$$

- XY-tilted ratchet :

$$G(x,y,z,t) = \Psi(x) + V(y-x) + 1/2k_m(y-z)^2 - (y-x)f_{tilt} - zf_{ext} \tag{B.3}$$

The corresponding system of the coupled Langevin equations can be written in the following general form:

$$\begin{cases} \eta_x \dfrac{dx}{dt} = -\partial_x G(x,y,z,t) + \sqrt{2\eta_x D}\ \xi_x(t) \\ \eta_y \dfrac{dy}{dt} = -\partial_y G(x,y,z,t) + \sqrt{2\eta_y D}\ \xi_y(t) \\ \eta_z \dfrac{dz}{dt} = -\partial_z G(x,y,z,t) + \sqrt{2\eta_y D}\ \xi_z(t) \end{cases} \tag{B.4}$$

where η_x and η_y are the viscous drag coefficients and $D = k_B T$. The $\xi_i(t)$ are a Gaussian random variables characterized by the standard conditions:

$$\langle \xi_i(t) \rangle = 0, \qquad \langle \xi_i(t)\xi_j(s) \rangle = \delta_{ij}\delta(t-s), \qquad t > s, \quad i,j = x,y,z$$

In our simulations we deal with the dimensionless form of (B.4) by using the scaling (6.3) and (6.4). We obtain

$$\begin{cases} \dfrac{dx}{dt} = -\,\alpha\,[\partial_x G(x,y,z,t)] + \sqrt{2\alpha D}\;\xi_x(t) \\ \dfrac{dy}{dt} = -\,\partial_y G(x,y,z,t) + \sqrt{2D}\;\xi_y(t) \\ \dfrac{dz}{dt} = -\,\beta\,[\partial_z G(x,y,z,t)] + \sqrt{2\beta D}\;\xi_z(t) \end{cases} \tag{B.5}$$

Here we introduced the following dimensionless parameters $\alpha = \frac{\eta_y}{\eta_x}$, $\beta = \frac{\eta_y}{\eta_z}$. The normalized $\xi_i(t)$ variable is now characterized by:

$$\langle \xi_i(t) \rangle = 0, \qquad \langle \xi_i(t)\xi_j(s) \rangle = \delta_{ij}\delta(t-s), \qquad i,j = x,y,z$$

We observed no major differences in the behavior of the 3𝔻 model comparing to the behavior of the analogous 2𝔻 model. The averaged trajectories and the motor cycles look similar. The parametric dependence of the force-velocity relations with D and A are also similar in 3𝔻 and 2𝔻 models.

More care need to be devoted to the 3𝔻 energetics. First we define the heat over the period

$$Q = \frac{1}{T} \int_{\mathbf{X}(t=t_i)}^{\mathbf{X}(t=t_i+T)} \delta Q_x + \delta Q_y + \delta Q_z \tag{B.6}$$

where $\delta Q_i = \left(-\eta \frac{dx_i}{dt} + \sqrt{2\eta_i D}\xi_i(t)\right) \circ dx_i$. Then we define the mechanical work W_{mec} over the period as

$$W_{mec} = \frac{1}{T} \int_{\mathbf{X}_{t_i}}^{\mathbf{X}_{t_i+T}} dG_0(\mathbf{X}_t) = -f_{ext}\langle v_z \rangle \tag{B.7}$$

where $G_0(x_t, y_t, z_t) = \Phi(x_t) + V(y_t - x_t) + \frac{1}{2}k_m(y_t - z_t)^2 - z f_{ext}$. Finally, the input energy consumed over one period is defined in same way as for the previously studied 2𝔻 systems, see (6.18) (X-tilted),(7.10) (Y-tilted), (8.9)(XY-tilted). Then the energy balance for the whole system can be written as:

$$W_{mec} \equiv R + Q. \tag{B.8}$$

Now we can define the mechanical efficiency

$$\epsilon_{mec} = \frac{W_{\text{mec}}}{R} \tag{B.9}$$

and the Stokes efficiency

$$\epsilon_{Stokes} = \frac{W_{Stokes}}{R} \tag{B.10}$$

where

$$W_{\text{Stokes}} = \alpha^{-1}\langle v_x \rangle^2 + \langle v_y \rangle^2 + \beta^{-1}\langle v_z \rangle^2 \tag{B.11}$$

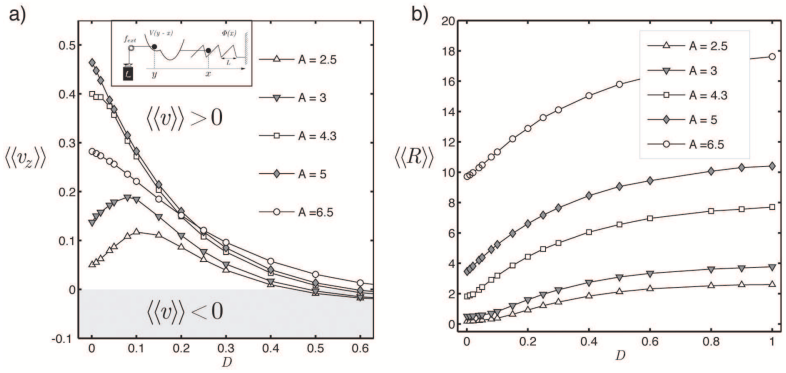

Figure B.2. The X-tilted model in soft device configuration with conservative load $f_{ext} = 0.1$. a) The plot of the average velocity $\langle v_z \rangle$ versus the temperature$D$ for the increasing value of amplitude A rocking force f_{tilt}. b) The consumed energy by the motor system R versus temperature D for the increasing value of amplitude A.

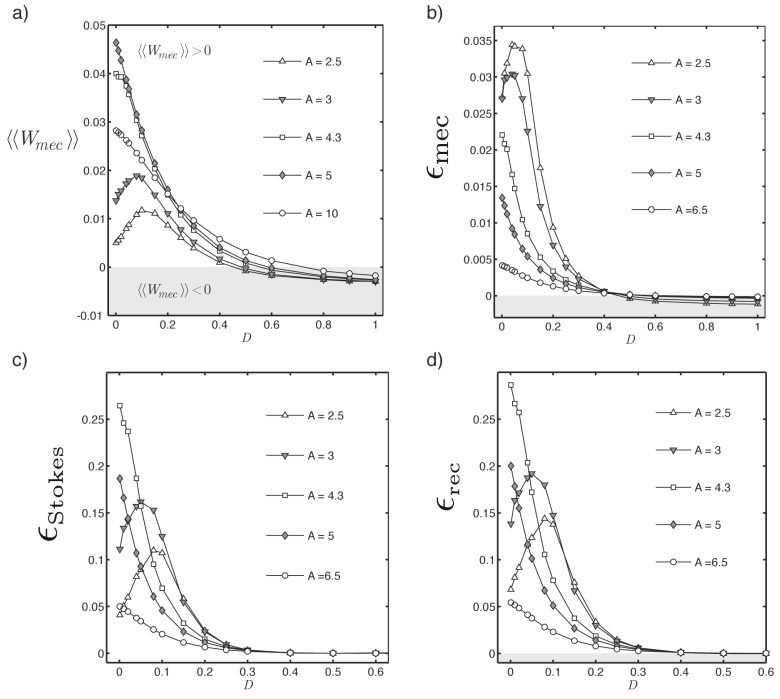

Figure B.3. The X-tilted ratchet in soft device with the conservative load fixed $f_{ext} = -0.1$. a) The mechanic work W_{mec} versus D for the increasing amplitude A. b) The mechanic efficiency ϵ_{mec} versus D for the increasing amplitude A. c) The Stokes efficiency ε_{Stokes} versus temperature D for the increasing amplitude A, by definition this is a positive function. d) The rectifying efficiency ε_{rec} versus temperature D for the increasing amplitude A. The function reflects the transformation of energy input of energy into the global motion.

Finally, we introduce the rectifying efficiency as

$$\epsilon_{rec} = \frac{W_{mec} + W_{Stokes}}{R} \tag{B.12}$$

The system of the Langevin equations in the case of the X-tilted ratchet in the soft

device can be written as:

$$\begin{cases} \dfrac{dx}{dt} = -\alpha\left[\partial_x\Phi(x) + \partial_x V(y-x) - f_{tilt}(t)\right] + \sqrt{2\alpha D}\,\xi_x(t) \\ \dfrac{dy}{dt} = -\partial_y V(y-x) - k_m(t)(y-z) + \sqrt{2D}\,\xi_y(t) \\ \dfrac{dz}{dt} = \beta k_m(y-z) + \beta f_{ext} + \sqrt{2\beta D}\,\xi_z(t) \end{cases} \tag{B.13}$$

The parameters of the bi-stable potential are:$k_0 = 1.5$, $k_1 = 0.43$, $l = 0.22$, $a = 1$ and $k_m = 1$. We use asymmetric saw-tooth ratchet potential with parameters $V_{max} = 1.5$, $L = 1$, $\lambda_1 = 0.7$ and $\lambda_2 = 0.3$. The rocking square wave signal is characterized by the period $T = 30$. All numerical computations were performed with the constant time step $\Delta t = 0.5 \times 10^{-3}$ and the results were averaged over $N_r = 1 \times 10^{-4}$ realizations. In all stationary regimes we observed that $\langle v_x\rangle = \langle v_y\rangle = \langle v_z\rangle$.

In Fig.B.2a) we present the average velocity of the motor as a function of temperature D for several values of the rocking amplitude A. For small amplitudes A the motor shows a maximum of velocity at a finite temperature which we can interpret as the manifestation of stochastic resonance. At high amplitudes A, the average velocity is a monotonically decreasing function of D which means that system works as a mechanical ratchet with thermal fluctuations playing the role of obstacles. Notice that at small values of D the average velocity may be negative. In general the 3𝔻 system shows similar behavior as the 2𝔻 system with slightly smaller average velocity.

In Fig.B.3a) we show the mechanical work as a function of D at increasing A. By color, we identify the regions of positive and negative mechanical work. In Fig.B.3b) we show the temperature dependence of the mechanical efficiency. In the regime of small amplitude A we observe a maximum of efficiency at finite temperature. With increasing amplitude A, the maximum vanishes and the efficiency becomes a monotonically decreasing function of D, which is behavior characteristic of a mechanical ratchet regime. By light green color we indicate the regime of negative efficiency, where our motor is unable to perform positive mechanic work against the external force and works instead as an active breaking mechanism.

Finally, in Fig.B.3c) we plot the Stokes efficiency as a function of D. By definition this is always a positive function. The rectifying efficiency is shown in Fig.B.3d). The shape of this function is dominated by the quadratic Stokes term. The important observation is that this cumulative efficiency also has a maximum at a finite temperature where the amplitude of the rocking is small and the device works as a Brownian ratchet. Once again, the general behavior of the 3𝔻 ratchet system is similar to what we have obtained for the 2𝔻 ratchet system.

Next we consider the system of Langevin equations describing the 3𝔻 version of the Y-tilted ratchet in the soft device:

$$\begin{cases} \dfrac{dx}{dt} = -\alpha\left[\partial_x\Phi(x) + \partial_x V(y-x)\right] + \sqrt{2\alpha D}\,\xi_x(t) \\ \dfrac{dy}{dt} = -\partial_y V(y-x) - k_m(t)(y-z) + f_{tilt}(t) + \sqrt{2D}\,\xi_y(t) \\ \dfrac{dz}{dt} = \beta k_m(y-z) + \beta f_{ext} + \sqrt{2\beta D}\,\xi_z(t) \end{cases} \tag{B.14}$$

In Fig.B.4a) we show the average velocity as a function of temperature at different values of the amplitude A. For small amplitude A (Brownian ratchet) the motor exhibits

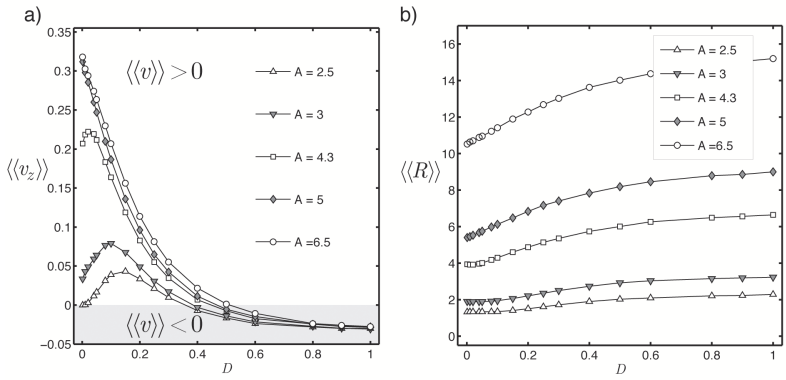

Figure B.4. The Y-tilted model in the soft device configuration with the conservative load $f_{ext} = -0.1$. For simplicity we fix $\alpha = \beta = 1$. a) The variation of the average velocity $\langle v_z \rangle$ with the increasing temperature D for different amplitudes A of $f_{tilt}(t)$. For small amplitude A (Brownian ratchet) the motor exhibits a maximum of velocity at finite temperature. At higher amplitude A (mechanical ratchet) the average velocity decreases monotonically with D. b) The variation of the consumed energy R with increasing temperature D for different amplitudes A of $f_{tilt}(t)$, note that the motor consumes more and more energy in order rectify the fluctuations and preform a useful work.

a maximum of velocity at finite temperature. At higher amplitude A (mechanical ratchet) the average velocity decreases monotonically with D. In Fig.B.4b) we plot the consumed energy R as a function of D and use the same range of amplitudes A. One can see that as the temperature increases, the motor needs more energy in order rectify the fluctuations and preform a useful work. We again observe a saturation at high temperatures meaning that there is a limit of how much thermal energy the motor can rectify. The $3\mathbb{D}$ system shows again the same qualitative behavior as the $2\mathbb{D}$ system but with smaller average velocity.

In Fig.B.5b) we show the temperature dependence of the mechanical efficiency at increasing values of A. In the regime of small amplitudes A we again observe a maximum of mechanical efficiency at finite temperatures. In the regime of high amplitudes the efficiency becomes a monotonically decreasing function of D, which characterizes such system as a mechanical ratchet. In Fig.B.5c) we present the parametric study of the Stokes efficiency and in Fig.B.5d) of the rectifying efficiency. The qualitative behavior of these functions is basically the same as in the case of $2\mathbb{D}$ Y-tilted ratchet.

Notice that the variation of β changes the ratio $\frac{\eta_y}{\eta_z}$ and that in Y-tilted ratchet the rocking force acts on the y coordinate. To check the role of the asymmetry of viscosity we fix $\alpha = 1$ and perform computations for two different values of β. In Fig.B.6 we show the variation of the average velocity with the increasing temperature D for $\alpha = 1,\ \beta = 8$ and for $\alpha = 1,\ \beta = 0.2$. We can compare the results with the simple case $\alpha = \beta = 1$ shown in Fig.B.4a). At constant temperature, the increase of β makes the value of the average velocity larger while preserving the general behavior. In Fig.B.7 we report the dependence of the efficiency on D in both cases. The influence of β studied in this section for Y-tilted ratchet is similar for all other ratchet models: X-titled, and XY-tilted.

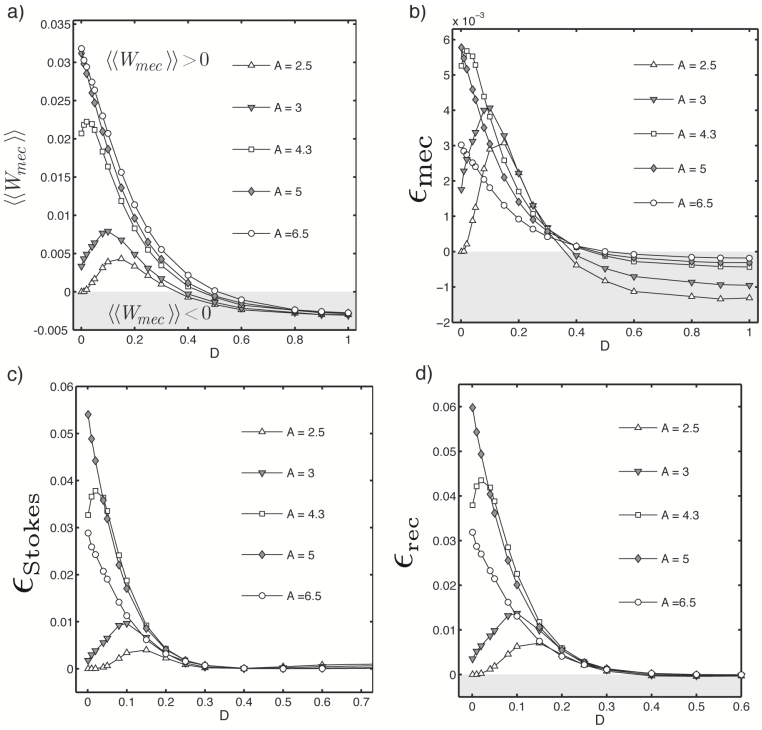

Figure B.5. The Y-tilted ratchet model energetics, the conservative load is fixed to $f_{ext} = 0.1$. For simplicity we fix $\alpha = \beta = 1$. a) The mechanic work W_{mec} versus the temperature D for the increasing amplitude A of $f_{tilt}(t)$. b) The mechanic efficiency ϵ_{mec} versus the temperature D for the increasing amplitude A of $f_{tilt}(t)$. In the regime of small amplitudes A we again observe a maximum of mechanical efficiency at finite temperature. In the regime of high amplitudes the efficiency becomes a monotonically decreasing function of D. c) The Stokes efficiency ε_{Stokes} versus the temperature D for the increasing amplitude A. By definition, this is always positive function. For hight values of D the Stokes efficiency is increasing function of D, because we are in regime there the motor follows the direction imposed by cargo. d) The rectifying efficiency ε_{rec} versus the temperature D for the increasing amplitude A. The shape of this function is dominated by the quadratic Stokes term..

Now we turn our attention to the 3𝔻 version of the XY-tilted ratchet in the soft device:

$$\begin{cases} \dfrac{dx}{dt} = -\alpha\left[\partial_x\Phi(x) + \partial_x V(y-x) + f_{tilt}(t)\right] + \sqrt{2\alpha D}\ \xi_x(t) \\ \dfrac{dy}{dt} = -\partial_y V(y-x) - k_m(t)(y-z) + f_{tilt}(t) + \sqrt{2D}\ \xi_y(t) \\ \dfrac{dz}{dt} = \beta k_m(y-z) + \beta f_{ext} + \sqrt{2\beta D}\ \xi_z(t) \end{cases} \tag{B.15}$$

In Fig.B.8a) we plot the average velocity as a function of temperature D for increasing values of the amplitude of rocking A. We again observe the characteristic maximum at finite temperature for $A = 1.5$ and $A = 2.5$. At higher values of A, the average velocity is a decreasing function of D and in this range we are dealing with a purely mechanical ratchet. By light green color we mark the region with negative average velocity, where the motor loses its ability to carry the external load and is instead being dragged by the load while contributing some active resistance.

In Fig.B.8b) we show the consumed energy R_x and in Fig.B.8c)– the consumed energy

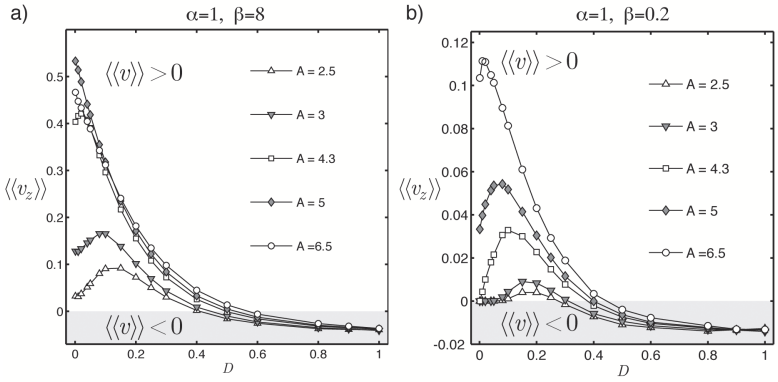

Figure B.6. The 3𝔻 Y-tilted model in soft device configuration with conservative load fixed at $f_{ext} = -0.1$. a) The plot of average velocity $\langle v_y \rangle$ versus D for the increasing values of amplitude A of $f_{tilt}(t)$ in the case $\alpha = 1,\ \beta = 8$. The average velocity is highest than in the case $\alpha = \beta = 1$, see Fig.B.4a). The general behavior is preserved. b) The plot of average velocity $\langle v_y \rangle$ versus D for the increasing values of amplitude A of f_{tilt} in the case $\alpha = 1,\ \beta = 0.2$. The value of the average velocity is smaller then in the case $\alpha = \beta = 1$, see Fig.B.4a). Note that we are not more able distinguish a monotonically decreasing regimes of average velocity.

R_y. Notice that the former is an increasing function of temperature while the latter is a decreasing function of temperature. In Fig.B.8d) we show the total energy consumed by the motor which appear to be temperature independent which is an interesting feature of the XY-tilted ratchet.

In Fig.B.9a) we show the mechanical work as a function of D at different amplitudes of rocking A. We observe two regimes with the system producing positive and negative mechanical work. In Fig.B.9b) we present the mechanical efficiency. At small amplitudes A we observe a maximum of efficiency at finite temperature. With increasing A the maximum vanishes and the efficiency becomes again a monotonically decreasing function of D.

In Fig.B.9c) we present the Stokes efficiency as a function of D. We observe maximum at finite temperatures for low amplitude regimes and see that at high temperatures the Stokes efficiency may even increase with temperature. The rectifying efficiency is shown in Fig.B.9d). Once again, at small amplitudes of rocking we see thermal ratchet behavior with a maximum of efficiency at finite temperature while at high rocking amplitudes we see the mechanical ratchet behavior with efficiency decreasing with temperature.

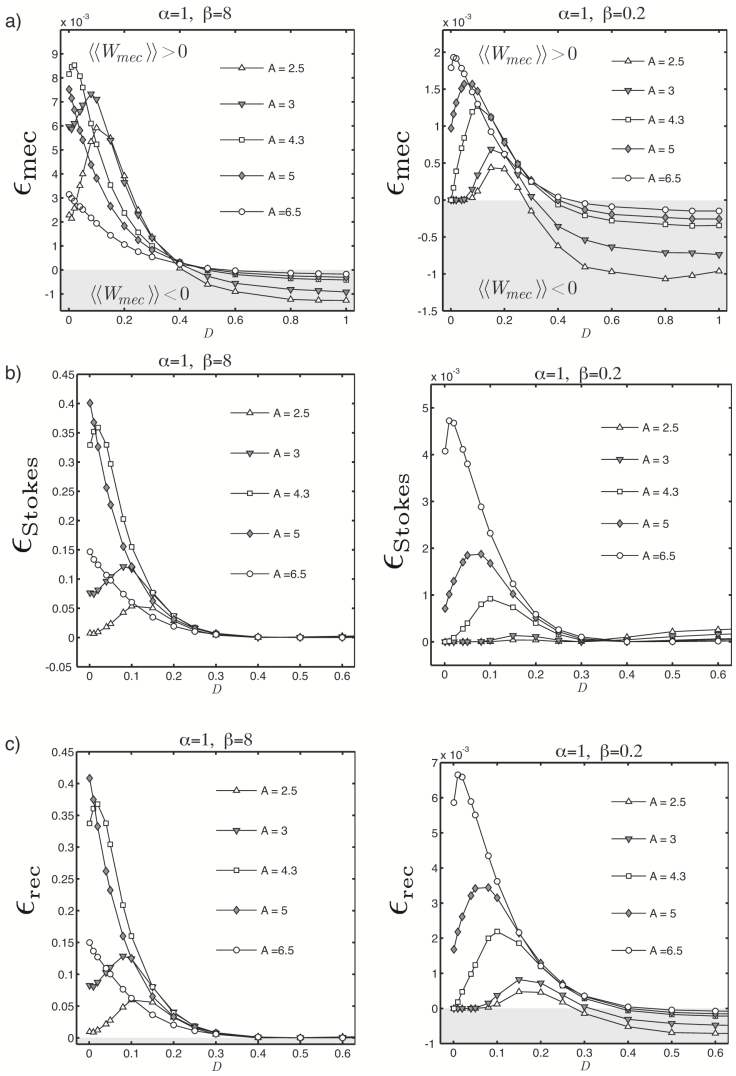

Figure B.7. The Y-tilted ratchet model energetics for $\beta = 8$ and $\beta = 0.2$, the conservative load $f_{ext} = -0.1$ and coefficient $\alpha = 1$. a) The mechanic efficiency ϵ_{mec} versus D. b) The Stokes efficiency ε_{Stokes} versus temperature D. c) The rectifying efficiency ε_{rec} versus D.

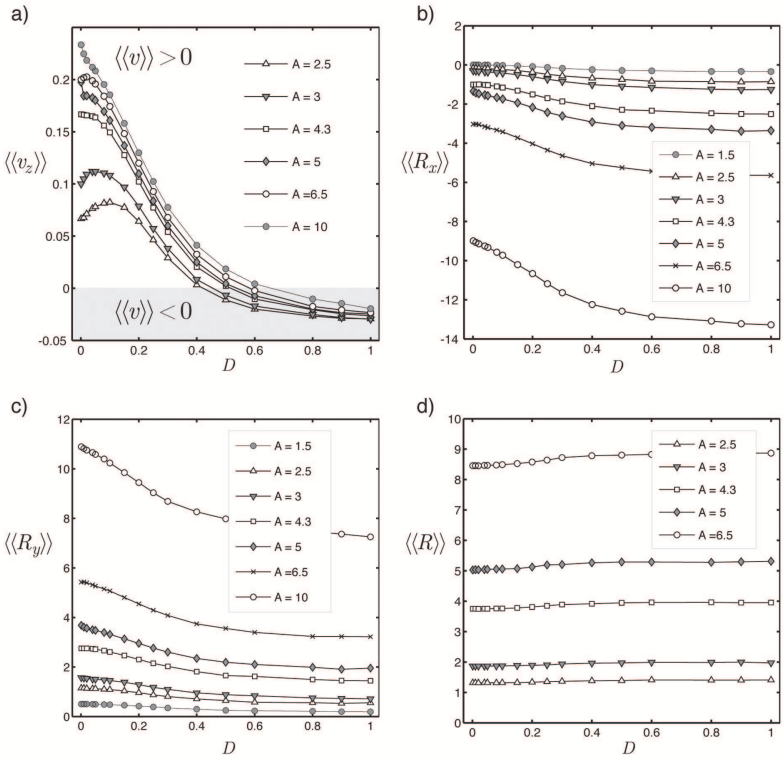

Figure B.8. The XY-tilted model in the soft device configuration with the conservative load is fixed to $f_{ext} = -0.1$. For simplicity we fix $\alpha = \beta = 1$. a) The variation of the average velocity $\langle v_y \rangle$ with the increasing temperature D for different amplitudes A of $f_{tilt}(t)$. For small amplitude A (Brownian ratchet) the motor exhibits a maximum of velocity at finite temperature. At higher amplitude A (mechanical ratchet) the average velocity decreases monotonically with D. b) The variation of the consumed energy R_x with increasing temperature D for different amplitudes A of $f_{tilt}(t)$, note that the motor consumes more and more energy in order rectify the fluctuations and preform a useful work. c) The variation of the consumed energy R_y with increasing temperature D for different amplitudes A of $f_{tilt}(t)$, see (8.9), note what the level of consumed energy decreases with D. d) The variation of the consumed energy R with increasing temperature D for different amplitudes A of $f_{tilt}(t)$. The function appear to be temperature independent which is an interesting property of XY tilted ratchet.

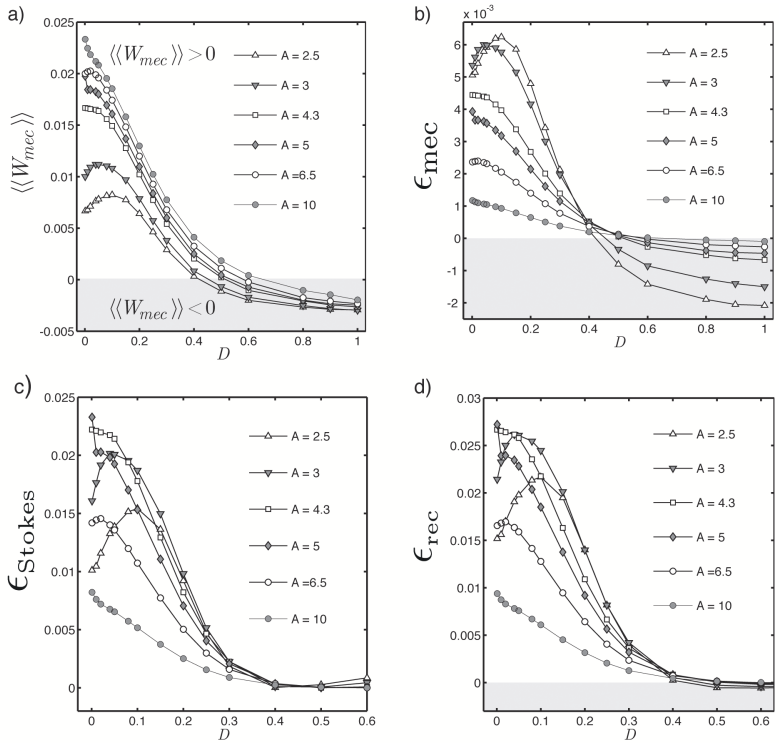

Figure B.9. The XY-tilted ratchet model in soft device with the conservative load $f_{ext} = 0.1$. For simplicity we fix $\alpha = \beta = 1$. a) The variation of the mechanic work W_{mec} with the increasing temperature D for different amplitudes A of $f_{tilt}(t)$. b) The variation of the mechanic efficiency ϵ_{mec} with the increasing temperature D for different amplitudes A of $f_{tilt}(t)$. In the regime of small amplitudes A we again observe a maximum of mechanical efficiency at finite temperature. c) The variation of the Stokes efficiency ε_{Stokes} with the increasing temperature D for different amplitudes A. By definition, this is always positive function. For hight values of D the Stokes efficiency is increasing function of D, because we are in regime there the motor follows the direction imposed by cargo. d) The variation of the rectifying efficiency ε_{rec} with the increasing temperature D. The shape of this function is dominated by the quadratic Stokes term.

Bibliography

[1] A. Agarwal and H. Hess. Biomolecular motors at the intersection of nanotechnology and polymer science. *Progress in Polymer Science*, 35(1-2, SI):252–277, Jan-Feb 2010.

[2] B.Q. Ai, L.Q. Wang, and L.G. Liu. Brownian micro-engines and refrigerators in a spatially periodic temperature field: Heat flow and performances. *Physics Letters A*, 352(4-5):286–290, Apr 3 2006.

[3] A. Ajdari and J. Prost. Drift induced by a spatially periodic potential of low asymmetry - pulsed dielectrophoresis. *Comptes rendus de L'Académie des Sciences Série II*, 315(13):1635–1639, Dec 17 1992.

[4] B. Alberts. *Molecular Biology of the Cell*. Garland Science, 5 edition, 2007.

[5] C.R. Bagshaw and D.R. Trentham. The characterization of myosin-product complexes and of product-release steps during the magnesium ion-depended adenosine triphosphatase reaction. *Biochemical Journal*, 141:331–349, 1974.

[6] J. Berna, D.A. Leigh, M. Lubomska, S.M. Mendoza, E.M. Perez, P. Rudolf, G. Teobaldi, and F. Zerbetto. Macroscopic transport by synthetic molecular machines. *Nature Materials*, 4(9):704–710, Sep 2005.

[7] A.D. Bershadsky and J.M. Vasiliev. *Cytoskeleton*. 1989.

[8] W.R. Browne and B.L. Feringa. Making molecular machines work. *Nature Nanotechnology*, 1(1):25–35, Oct 2006.

[9] M. Büttiker. Transport as a consequence of state-dependent diffusion. *Zeitschrift fur Physik B-Condensed Matter*, 68(2-3):161–167, 1987.

[10] M. Capitanio, M. Canepari, P. Cacciafesta, V. Lombardi, R. Cicchi, M. Maffei, F.S. Pavone, and R. Bottinelli. Two independent mechanical events in the interaction cycle of skeletal muscle myosin with actin. *Proceedings of The National Academy of Sciences of The United States of America*, 103(1):87–92, Jan 3 2006.

[11] G. Cappello, P. Pierobon, C. Symonds, L. Busoni, J. Christof M. Gebhardt, M. Rief, and J. Prost. Myosin V stepping mechanism. *Proceedings of The National Academy of Sciences of The United States of America*, 104(39):15328–15333, Sep 25 2007.

[12] M. Caruel. *Mechanics of fast force recovery in striated muscles*. PhD thesis, École Polytechnique de Paris, 2011.

[13] J.-P. Collin, C. Dietrich-Buchecker, P. Gavìna, M.C. Jiminez-Molero, and J.-P. Sauvage. Shuttles and muscles: linear molecular machines based on transition metals. *Accounts of Chemical Research*, 34(6):477–487, 2001.

[14] I. Derényi and T. Vicsek. The kinesin walk: A dynamic model with elastically coupled heads. *Proceedings of The National Academy of Sciences of The United States of America*, 93(13):6775–6779, Jun 25 1996.

[15] R. Dominguez and K.C. Holmes. Actin structure and function. *Annual Review of Biophysics*, 40(1):169–186, 2011.

[16] T.A.J. Duke. Molecular model of muscle contraction. *Proceedings of The National Academy of Sciences of The United States of America*, 96(6):2770–2775, Mar 16 1999.

[17] K.A.P. Edman. Double-hyperbolic force velocity relation in frog-muscle fibers. *Journal of Physiology - London*, 404:301–321, Oct 1988.

[18] E. Eisenberg and T.L. Hill. A cross-bridge model of muscle contraction. *Progress in Biophysics & Molecular Biology*, 33:55–82, 1978.

[19] T.C. Elston and C.S. Peskin. The role of protein flexibility in molecular motor function: Coupled diffusion in a tilted periodic potential. *SIAM Journal on Applied Mathematics*, 60(3):842–867, Mar 21 2000.

[20] T. Fischer, A. Agarwal, and H. Hess. A smart dust biosensor powered by kinesin motors. *Nature Nanotechnology*, 4(3):162–166, Mar 2009.

[21] L.E. Ford, A.F. Huxley, and R.M. Simmons. Tension transients during steady shortening of frog-muscle fibers. *Journal of Physiology - London*, 361:131–150, Apr 1985.

[22] L. Gammaitoni, P. Hänggi, P. Jung, and F. Marchesoni. Stochastic resonance. *Reviews of Modern Physics*, 70(1):223–287, Jan 1998.

[23] C. Gardiner. *Handbook of Stochastic Methods: for Physics, Chemistry and the Natural Sciences (Springer Series in Synergetics)*. Springer, 3rd edition, 2004.

[24] M.A. Geeves and K.C. Holmes. The molecular mechanism of muscle contraction. In *Fibrous Proteins: Muscle and Moleclar Motors*, volume 71 of *Advances in Protein Chemistry*, pages 161+. Elsevier Academic Press Inc, 2005.

[25] A. Goel and V. Vogel. Harnessing biological motors to engineer systems for nanoscale transport and assembly. *Nature Nanotechnology*, 3(8):465–475, Aug 2008.

[26] L.S.B. Goldstein. With apologies to scheherezade – tails of 1001 kinesin motors. *Review of Genetics*, 27:319–351, 1993.

[27] L.S.B. Goldstein. Kinesin molecular motors: transport pathways, receptors, and human disease. *Proceedings of The National Academy of Sciences of The United States of America*, 98(13):6999–7003, 2001.

[28] A.M. Gordon, A.F. Huxley, and F.J. Julian. Variation in isometric tension with sarcomere length in vertebrate muscle fibres. *Journal of Physiology - London*, 184(1):170+, 1966.

[29] L.M. Griffith, S.M. Downs, and J.A. Spudich. Myosin light chain kinase and myosin light chain phospatase from dictyostelium – effects of reversible phosphorylation on myosin structure and function. *Journal of Cell Biology*, 104(5):1309–1323, May 1987.

[30] T. Guérin, J. Prost, and J. F. Joanny. Bidirectional motion of motor assemblies and the weak-noise escape problem. *Physical Review E*, 84(4, Part 1), Oct 3 2011.

[31] T. Guérin, J. Prost, and J. F. Joanny. Dynamical behavior of molecular motor assemblies in the rigid and crossbridge models. *European Physical Journal E*, 34(6), Jun 2011.

[32] P. Hänggi, P. Talkner, and M. Borkovec. Reaction-rate theory – 50 years after Kramers. *Reviews of Modern Physics*, 62(2):251–341, Apr 1990.

[33] J. Hanson and H.E. Huxley. Structural basis of the cross-striations in muscle. *Nature*, (172):530–532, 1953.

[34] T.L. Hill. Theoretical formalism for the sliding filament model of contraction of striated muscle. part i. *Progress in Biophysics & Molecular Biology*, 28:267–340, 1974.

[35] N. Hirokawa, Y. Noda, H. Tanaka, and S. Niwa. Kinesin superfamily proteins and intracellular transport. *Nature Reviews Molecular Cell Biology*, 10(10):682–696, Oct 2009.

[36] K.C. Holmes. The actomyosin interaction and its control by tropomysoin. *Biophysical Journal*, 68(4, Suppl. S):S2–S7, Apr 1995.

[37] K.C. Holmes. The actin-myosin interaction. *FASEB Journal*, 11(9, Suppl. S):40, Jul 31 1997.

[38] K.C. Holmes. Actin in a twist. *Nature Structural Biology*, 457(7228):389–390, JAN 22 2009.

[39] K.C. Holmes and M.A. Geeves. The structural basis of muscle contraction. *Philosophical Transactions of The Royal Society of London Series B-Biological Sciences*, 355(1396):419–431, Apr 29 2000.

[40] K.C. Holmes, R.R. Schroder, H.L. Sweeney, and A. Houdusse. The structure of the rigor complex and its implications for the power stroke. *Philosophical Transactions of The Royal Society of London Series B-Biological Sciences*, 359(1452):1819–1828, Dec 29 2004.

[41] A.M. Houdusse, V.N. Kalbokis, D. Himmel, A.G. Szent-Gyorgyi, and C. Cohen. Atomic structure of scallop myosin subfragment $s1$ complex with mgadp: A novel conformation of the myosin head. *Cell*, 97(4):459–470, May 1999.

[42] J. Howard. *Mechanics of motor proteins and the cytoskeleton*. Sinauer Associates Inc.-Publishers Sunderland, Massachusetts, 2001.

[43] T.J. Huang, B. Brough, C.-M. Ho, A.H. Liu, Y. Flood, P.A. Bonvallet, H.-R. Tseng, J.F. Stoddart, M. Baller, and S. Magonov. A nanomechanical device based on linear molecular motors. *Applied Physics Letters*, 85(22):5391–5393, Nov 29 2004.

[44] A.F. Huxley. Muscle structure and the theories of contraction. *Progress in Biophysics and Biophysical Chemistry*, (7):255–318, 1957.

[45] A.F. Huxley and R. Niedergerke. Structural changes in muscle during contraction. interference microscopy of living muscle fibres. *Nature*, 4412(173):971–973, 1954.

[46] A.F. Huxley and R.M. Simmons. Proposed mechanism of force generation in striated muscle. *Nature*, (233):533–538, 1971.

[47] H.E. Huxley. Electron microscope studies on the structure of natural and synthetic protein filaments from striated muscle. *Journal of Molecular Biology*, 7(3):281–308, 1963.

[48] H.E. Huxley. Mechanism of muscular contraction. *Science*, (164):1356–1366, 1969.

[49] H.E. Huxley. The crossbridge mechanism of muscular contraction. *Journal of Experimental Biology*, (115):17–30, 1985.

[50] A. Ishijima, H. Kojima, H. Tanaka, T. Funatsu, H. Higuchi, M. Tokunaga, and T. Yanagida. Simultaneous observation of individual ATPase and mechanical events by a single myosin molecule during interaction with actin. *Biophysical Journal*, 74(2, Part 2):A265, Feb 1998.

[51] F. Jülicher. Statistical physics of active processes in cells. *Physica A-Statistical Mechanics and Its Applications*, 369(1):185–200, Sep 1 2006.

[52] F. Jülicher, A. Ajdari, and J. Prost. Modeling molecular motors. *Reviews of Modern Physics*, 69(4):1269–1281, Oct 1997.

[53] F. Jülicher and J. Prost. Cooperative molecular motors. *Physical Review Letters*, 75(13):2618–2621, Sep 25 1995.

[54] F. Jülicher and J. Prost. Spontaneous oscillations of collective molecular motors. *Physical Review Letters*, 78(23):4510–4513, Jun 9 1997.

[55] F. Jülicher and J. Prost. Molecular motors: From individual to collective behavior. *Progress of Theoretical Physics Suplement*, (130):9–16, 1998.

[56] H. Kamegawa, T. Hondou, and F. Takagi. Energetics of a forced thermal ratchet. *Physical Review Letters*, 80(24):5251–5254, Jun 15 1998.

[57] N.J. Kasdin. Discrete simulation of colored noise and stochastic-processes and $1/f^{\alpha}$ power-law noise generation. *Proceedings of the IEEE*, 83(5):802–827, May 1995.

[58] K. Kawaguchi and S. Ishiwata. Temperature dependence of force, velocity, and processivity of single kinesin molecules. *Biochemical and Physical Research Communications*, 272(3):895–899, Jun 16 2000.

[59] M. Kawai and H.R. Halvorson. 2 step mechanism of phosphate release and the mechanism of force generation in chemically skinned fibers of rabbit psoas muscle. *Biophysical Journal*, 59(2):329–342, Feb 1991.

[60] K. Kitamura, M. Tokunaga, S. Esaki, A.H. Iwane, and T. Yanagida. Mechanism of muscle contraction based on stochastic properties of single actomyosin motors observed in vitro. *Biophysics*, 1:1–19, 2005.

[61] K. Kitamura, M. Tokunaga, A.H. Iwane, and T. Yanagida. A single myosin head moves along an actin filament with regular steps of 5.3 nanometres. *Nature*, 397(6715):129–134, Jan 14 1999.

[62] P. Kloeden and E. Platen. *Numerical Solution of Stochastic Differential Equations (Applications of Mathematics)*. Springer, 1997.

[63] R. Krishnan, J. Chacko, M. Sahoo, and A. M. Jayannavar. Stokes efficiency of temporally rocked ratchets. *Journal of Statistical Mechanics-Theory and Experiment*, Jun 2006.

[64] R. Krishnan, S. Roy, and A.M. Jayannavar. Enhanced thermodynamic efficiency in time asymmetric ratchets. *Journal of Statistical Mechanics-Theory and Experiment*, Apr 2005.

[65] P. Kundu and I. Cohen. *Fluid Mechanics, Second Edition*. Academic Press, 2 edition, 2001.

[66] R. Landauer. Motion out of noisy states. *Journal of Statistical Physics*, 53(1-2):233–248, Oct 1988.

[67] T. Lelievre, G. Stoltz, and M. Rousset. *Free Energy Computations: A Mathematical Perspective*. Imperial College Press, 1 edition, 2010.

[68] D.S. Lemons and A. Gythiel. Paul langevin's 1908 paper "On the Theory of Brownian Motion". *American Association of Physics Teachers*, 65(11):1079–1081, 1997.

[69] V. Lombardi and G. Piazzesi. The contractile response during steady lengthening of stimulated frog-muscle fibers. *Journal of Physiology - London*, 431:141–171, Dec 1990.

[70] R.W. Lymn and E.W. Taylor. Mechanism of adenosine triphosphate hydrolysis by actomyosin. *Biochemistry*, 10(25):4617–4624, 1971.

[71] L. Machura, M. Kostur, P. Talkner, J. Łuczka, F. Marchesoni, and P. Hänggi. Brownian motors: Current fluctuations and rectification efficiency. *Physical Review E*, 70(6, Part 1), Dec 2004.

[72] M.O. Magnasco. Forced thermal ratchets. *Physical Review Letters*, 71(10):1477–1481, Sep 6 1993.

[73] A. Mansson, M. Sundberg, R. Bunk, M. Balaz, I.A. Nicholls, P. Omling, J.O. Tegenfeldt, S. Tagerud, and L. Montelius. Actin-based molecular motors for cargo transportation in nanotechnology - Potentials and challenges. *IEEE Transactions on Advanced Packaging*, 28(4):547–555, Nov 2005.

[74] L. Marcucci and L. Truskinovsky. Mechanics of the power stroke in myosin II. *European Physical Journal E*, 81(9):915–922, May 2010.

[75] L. Marcucci and L. Truskinovsky. Muscle contraction: A mechanical perspective. *European Physical Journal E*, 32(4):411–418, Aug 2010.

[76] J. L. Mateos and F.R. Alatriste. Brownian motors and stochastic resonance. *Chaos*, 21(4), Dec 2011.

[77] M. Matsuo and S. Sasa. Stochastic energetics of non-uniform temperature systems. *Physica A*, 276(1-2):188–200, Feb 1 2000.

[78] I.D. Mayergoyz. *Mathematical Models of Hysteresis*. Springer-Verlag, 1991.

[79] J. Menche and L. Schimansky-Geier. Two particles with bistable coupling on a ratchet. *Physics Letters A*, 359(2):90–98, Nov 13 2006.

[80] E. Meyhöfer and J. Howard. The force generated by a single kinesin molecule against an elastic load. *Proceedings of The National Academy of Sciences of The United States of America*, 92(2):574–578, Jan17 1995.

[81] D. Mitrossilis, J. Fouchard, A. Guiroy, N. Desprat, N. Rodriguez, B. Fabry, and A. Asnacios. Single-cell response to stiffness exhibits muscle-like behavior. *Proceedings of The National Academy of Sciences of The United States of America*, 106(43):18243–18248, Oct 27 2009.

[82] J.E. Molloy, J.E. Burns, J. Kendrick-Jones, R.T. Tregear, and D.C.S. White. Movement and force produced by a single myosin head. *Nature*, 378(6553):209–212, Nov 9 1995.

[83] T. Nishizaka, R. Seo, H. Tadakuma, K. Kinosita, and S. Ishiwata. Characterization of single actomyosin rigor bonds: Load dependence of lifetime and mechanical properties. *Biophysical Journal*, 79(2):962–974, Aug 2000.

[84] T. Oda, M. Iwasa, T. AIhara, Y. Maeda, and A. Naritas. The nature of the globular-to-fibrous actin transition. *Nature*, 457(7228):209–212, Jan 22 2009.

[85] A. Parmeggiani, F. Jülicher, A. Ajdari, and J. Prost. Energy transduction of isothermal ratchets: Generic aspects and specific examples close to and far from equilibrium. *Physical Review E*, 60(2, Part B):2127–2140, Aug 1999.

[86] J.M.R. Parrondo and B.J. De Cisneros. Energetics of Brownian motors: a review. *Applied Physics A-Materials Science & Processing*, 75(2):179–191, Aug 2002.

[87] E. Pate, G.J. Wilson, M. Bhimani, and R. Cooke. Temperature-dependence of the inhibitory of effects on orthovanadate on shortening velocity in fast skeletalimuscle. *Biophysical Journal*, 66(5):1554–1562, May 1994.

[88] F. Patolsky, Y. Weizmann, and I. Willner. Actin-based metallic nanowires as bio-nanotransporters. *Nature Materials*, 3(10):692–695, Oct 2004.

[89] G. Piazzesi and V. Lombardi. A cross-bridge model that is able to explain mechanical and energetic properties of shortening muscle. *Biophysical Journal*, 68(5):1966–1979, May 1995.

[90] G. Piazzesi, L. Lucii, and V. Lombardi. The size and the speed of the working stroke of muscle myosin and its dependence on the force. *Journal of Physiology - London*, 545(1):145–151, Nov 15 2002.

[91] G. Piazzesi, M. Reconditi, M. Linari, L. Lucii, Y.B. Sun, T. Narayanan, P. Boesecke, V. Lombardi, and M. Irving. Mechanism of force generation by myosin heads in skeletal muscle. *Nature*, 415(6872):659–662, Feb 7 2002.

[92] J. Prost, J.F. Chauwin, L. Peleti, and A. Ajdari. Asymmetric pumping of particles. *Physical Review Letters*, 72(16):2652–2655, Apr 18 1994.

[93] I. Rayment, H.M. Holden, M. Whittaker, C.B. Yohn, M. Lorenz, K.C. Holmes, and R.A. Milligan. Structure of the actin-myosin complex and its implications for muscle-contraction. *Science*, 261(5117):58–65, Jul 2 1993.

[94] I. Rayment, W.R. Rypniewski, K. Schmidtbase, R. Smith, D.R. Tomchick, M.M. Benning, D.A. Winkelmann, G. Wesenberg, and H.M. Holden. 3-dimensional structure of myosin subfragment-1 – a molecular motor. *Science*, 261(5117):50–58, Jul 2 1993.

[95] M. Reconditi, N. Koubassova, M. Linari, I. Dobbie, T. Narayanan, O. Diat, G. Piazzesi, V. Lombardi, and M. Irving. The conformation of myosin head domains in rigor muscle determined by X-ray interference. *Biophysical Journal*, 85(2):1098–1110, Aug 2003.

[96] M. Reconditi, M. Linari, L. Lucii, A. Stewart, Y.B. Sun, P. Boesecke, T. Narayanan, R.F. Fischetti, T. Irving, G. Piazzesi, M. Irving, and V. Lombardi. The myosin motor in muscle generates a smaller and slower working stroke at higher load. *Nature*, 428(6982):578–581, Apr 1 2004.

[97] P. Reimann. Supersymmetric ratchets. *Physical Review Letters*, 86(22):4992–4995, May 28 2001.

[98] H. Risken and T. Frank. *The Fokker-Planck Equation: Methods of Solutions and Applications (Springer Series in Synergetics)*. Springer, 2nd ed. 1989. 3rd printing edition, 1996.

[99] C. Ruegg, C. Veigel, J.E. Molloy, S. Schmitz, J.C. Sparrow, and R.H.A. Fink. Molecular motors: Force and movement generated by single myosin II molecules. *News in Physiological Sciences*, 17:213–218, Oct 2002.

[100] K. Sekimoto. Kinetic characterization of heat bath and the energetics of thermal ratchet models. *Journal of The Physical Society of Japan*, 66(5):1234–1237, May 1997.

[101] K. Sekimoto. *Stochastic Energetics*. Lecture Notes in Physics. Springer, 1st edition. edition, 2010.

[102] J.R. Sellers. Myosins: a diverse superfamily. *Biochemica and Biophysica Acta I - Molecular Cell Research*, 1496(1):3–22, Mar 17 2002.

[103] D. A. Smith, M. A. Geeves, J. Sleep, and S. M. Mijailovich. Towards a unified theory of muscle contraction. I: Foundations. *Annals of Biomedical Engineering*, 36(10):1624–1640, Oct 2008.

[104] D. A. Smith and S. M. Mijailovich. Toward a unified theory of muscle contraction. II: Predictions with the mean-field approximation. *Annals of Biomedical Engineering*, 36(8):1353–1371, Aug 2008.

[105] J.M. Squire, H.A. Al-Khayat, J.J. Harford, L. Hudson, T.C. Irving, C. Knupp, N.S. Mok, and M.K. Reedy. Myosin filament structure and myosin crossbridge dynamics in fish and insect muscles. In Sugi, H., editor, *Molecular and Cellular Aspects of Muscle Contraction*, volume 538 of *Advances in Experimental Medecine and Biology*, pages 251–266. Kluwer Academic/Plenium Publ, 2003.

[106] J.M. Squire, C. Knupp, M. Roessle, H.A. Al-Khayat, T.C. Irving, F. Eakins, N.S. Mok, J.J. Harford, and M.K. Reedy. X-ray diffraction studies of striated muscles. In Sugi, H., editor, *Sliding Filament Mechanism in Muscle Contraction: Fifty Years of Research*, volume 565 of *Advances in Experimental Medecine and Biology*, pages 45–60. Springer, 2005.

[107] W. Steffen, D. Smith, R. Simmons, and J. Sleep. Mapping the actin filament with myosin. *Proceedings of The National Academy of Sciences of The United States of America*, 98(26):14949–14954, Dec 18 2001.

[108] D. Suzuki and T. Munakata. Rectification efficiency of a Brownian motor. *Physical Review E*, 68(2, Part 1), Aug 2003.

[109] H. Tanaka, A. Ishijima, M. Honda, K. Saito, and T. Yanagida. Orientation dependence of displacements by a single one-headed myosin relative to the actin filament. *Biophysical Journal*, 75(4):1886–1894, Oct 1998.

[110] E.W. Taylor. Transient phase of adenosine-triphosphate hydrolysis by myosin, heavy-meromyosin and subfragment-1. *Biochemistry*, 16(4):732–740, 1977.

[111] G. Tortora, G. Tortora, and B. Roesch. *Principles of Anatomy And Physiology*. John Wiley & Sons Inc, 12 edition, 2009.

[112] M.J. Tyska, D.E. Dupuis, W.H. Guilford, J.B. Patlak, G.S. Waller, K.M. Trybus, D.M. Warshaw, and S. Lowey. Two heads of myosin are better than one for generating force and motion. *Proceedings of The National Academy of Sciences of The United States of America*, 96(8):4402–4407, Apr 13 1999.

[113] M.J. Tyska and D.M. Warshaw. The myosin power stroke. *Cell Motility and The Cytoskeletons*, 51(1):1–15, Jan 2002.

[114] R.D. Vale and R.A. Milligan. The way things move: lookking under the hood of molecular motor proteins. *Science*, 288(5463):88–95, Apr 7 2000.

[115] R.D. Vale, T.S. Reese, and M.P. Sheetz. Identification of a novel force-generating protein, kinesin, involved in microtubule-based motility. *Cell*, 42(1):39–50, 1985.

[116] M.G.L. Van den Heuvel and C. Dekker. Motor proteins at work for nanotechnology. *Science*, 317(5836):333–336, Jul 20 2007.

[117] C. Veigel, L.M. Coluccio, J.D. Jontes, J.C. Sparrow, R.A. Milligan, and J.E. Molloy. The motor protein myosin-I produces its working stroke in two steps. *Nature*, 398(6727):530–533, Apr 8 1999.

[118] C. Veigel, J.E. Molloy, S. Schmitz, and J. Kendrick-Jones. Load-dependent kinetics of force production by smooth muscle myosin measured with optical tweezers. *Nature Cell Biology*, 5(11):980–986, Nov 2003.

[119] A. Vilfan and T. Duke. Instabilities in the transient response of muscle. *Biophysical Journal*, 85(2):818–827, Aug 2003.

[120] A. Vilfan, E. Frey, and F. Schwabl. Elastically coupled molecular motors. *European Physical Journal B*, 3(4):535–546, Jun 1998.

[121] A. Vilfan, E. Frey, and F. Schwabl. Force-velocity relations of a two-state crossbridge model for molecular motors. *Europhysics Letters*, 45(3):283–289, Feb 1 1999.

[122] S. Walcott, P.M. Fagnant, K.M. Trybus, and D.M. Warshaw. Smooth muscle heavy meromyosin phosphorylated on one of Its two heads supports force and motion. *Journal of Biological Chemistry*, 284(27):18244–18251, Jul 3 2009.

[123] S. Walcott and S.X. Sun. Hysteresis in cross-bridge models of muscle. *Physical Chemistry Chemical Physics*, 11:4871–4881, 2009.

[124] M.L. Walker, S.A. Burgess, J.R. Sellers, F. Wang, J.A. Hammer, J. Trinick, and P.J. Knight. Two-headed binding of processive myosin to f-actin. *Nature*, 405(6788):804+, Jun 15 2000.

[125] H. Wang. A robust mathematical formulation for studying elastically coupled motor-cargo systems. *Journal of Computational and Theoretical Nanoscience*, 3(6):922–932, Dec 2006.

[126] H. Wang. Stokes efficiency of molecular motors with inertia. *Applied Mathematics Letters*, 22(1):79–83, Jan 2009.

[127] H. Wang and G. Oster. The Stokes efficiency for molecular motors and its applications. *Europhysics Letters*, 57(1):134–140, Jan 2002.

[128] J.Z. Xi, J.J. Schmidt, and C.D. Montemagno. Self-assembled microdevices driven by muscle. *Nature Materials*, 4(2):180+, Feb 2005.

[129] T. Yanagida, T. Arata, and F. Oosawa. Sliding distance of actin filament induced by a myosin crossbridge during one atp hydrolysis cycle. *Nature*, 316(6026):366–369, 1985.

[130] T. Yanagida, M. Iwaki, and Y. Ishii. Single molecule measurements and molecular motors. *Philosophical Transactions of The Royal Society of London Series B-Biological Sciences*, 363(1500):2123–2134, Jun 27 2008.

[131] T. Yanagida, H. Tanaka, K. Kitamura, T. Wazawa, M. Nishiyama, S. Esaki, Y. Sako, T. Ide, A.H. Iwane, and Y. Ishii. Single molecule techniques in biophysics. In Taniguchi, K. and Kaya, S., editor, *Na/K-ATPase and Related ATPases*, volume 1207 of *International Congress Series*, pages 71–85. Elsevier Science Bv, 2000.

[132] A. Yildiz, M. Tomishige, R.D. Vale, and P.R. Selvin. Kinesin walks hand-over-hand. *Science*, 303(5658):676–678, Jan 30 2004.

Résumé:

Cette thèse est consacrée à la modélisation du fonctionnement mécanique de l'interaction myosine II / actine, qui est responsable de la génération de force active dans les muscles squelettiques à l'échelle nanométrique. Les unités contractiles du muscle contiennent les filaments d'actine et de myosine, les derniers sont formés par un assemblage des myosines II. La myosine II est un moteur moléculaire qui s'attache et se détache périodiquement au filament d'actine en présence d'ATP. Afin de comprendre le phénomène de la contraction musculaire d'un point de vue mécanique, nous suivons l'approche développée par la communauté de cliquets Browniens, qui remplace l'interprétation chimique traditionnelle de génération de force active par une étude de la dynamique de Langevin des systèmes mécaniques avec des paysages énergétiques bien définis. Nous mettons l'accent sur le rôle du changement conformationnel, ou « power stroke », dans le fonctionnement de la myosine II. Nous indentifions le « power stroke » comme le principal moteur de la contractilité, ce qui reflète la réalité biologique. Nous proposons un modéle mécanique innovant et, en mettant l'accent sur le rôle actif de « power stroke », nous établissons un lien entre les moteurs processifs et nonprocessifs. Dans cette thèse, nous présentons les premiers exemples de modèles de moteur moléculaire nonprocessif actionnés exclusivement par « power stroke » et exploitant le phénomène de la résonance stochastique.

Abstract:

This thesis is devoted to the modeling of mechanical functioning of myosin II/actin interaction, responsible for active force generation in skeletal muscles at nanometer scale. The muscle contractile units contain actin filament and myosin II filaments formed by an assembly of myosins II. The myosin II is molecular motor that periodically attaches and detaches to the actin filament in presence of ATP. In order to understand the phenomenon of muscle contraction from mechanical point of view, we follow the approach developed by the Brownian ratchets community, which replaced the conventional chemistry-based interpretation of active force generation by a study of Langevin dynamics of mechanical systems with well defined energy landscapes. We focus on the role of the conformational change known as power stroke in the functioning of myosin II. We identify the power stroke as the main driver of contractility. The attribution of active role to power stroke reflects the biological reality imprinted in the molecular motor functional cycle. We propose an innovative mechanical model and by emphasizing the active role of the power stroke we are therefore building a bridge between processive and nonprocessive motors. In this Thesis we present the first examples of models of nonprocessive motors driven exclusively by the power stroke and exploiting the well known phenomenon of stochastic resonance.